Optimization-Based and Distributed Control for Digital Fabrication

Author(s):
Stürz, Yvonne R.

Publication Date:
2019

Permanent Link:

https://doi.org/10.3929/ethz-b-000405809 →

DISS. ETH NO. 26175

Optimization-Based and Distributed Control for Digital Fabrication

A thesis submitted to attain the degree of

DOCTOR OF SCIENCES of ETH ZURICH

(Dr. sc. ETH Zurich)

presented by

Yvonne Rebecca Stürz

Master of Science, TU Munich
Diplôme d'Ingénieur, EC Paris
born on 27. April 1989
citizen of Leonberg, Germany

accepted on the recommendation of

Prof. Dr. Roy S. Smith, examiner (ETH Zurich, Switzerland)
Prof. Dr. Manfred Morari, co-examiner (University of Pennsylvania, USA)
Prof. Dr. Florian Dörfler, co-examiner (ETH Zurich, Switzerland)
Prof. Dr. Giancarlo Ferrari Trecate, co-examiner (École Polytechnique Fédérale de Lausanne, Switzerland)

2019

ISBN 978-3-906916-82-8
DOI 10.3929/ethz-b-000405809

Meinen Eltern

Acknowledgements

I was lucky to meet and interact with many excellent people during the course of my PhD, who have supported me, contributed to the results in this thesis, and who have made the past years truly rewarding and enjoyable.

First and foremost, I would like to express my deepest gratitude to my advisor Prof. Roy Smith, for giving me the opportunity to pursue my PhD at the Automatic Control Laboratory (IfA) at ETH Zurich. I am grateful for all the support, trust and freedom he has given me. His passion for science and research, his broad knowledge of control systems and his innovative ideas for numerous applications have been truly inspiring. I am also indebted to Prof. Manfred Morari for having been a co-advisor in my PhD project, and a member of my examination committee. I am sincerely grateful for his valuable advice not only on research but also on career questions. My thanks further go to Prof. Florian Dörfler and to Prof. Giancarlo Ferrari-Trecate for having acted as referees in my PhD examination and for their valuable feedback on my work. It was Giancarlo's EECI course in Paris which first sparked my interest in the topic of distributed control.

It was a privilege to engage in research on digital fabrication as one of the first scientists within the NCCR Digital Fabrication project at ETH Zurich, which allowed me to learn and benefit from inspiring interdisciplinary collaborations. I thank Prof. Philippe Block for introducing me to the topic of flexible formwork and for the collaboration. I would also like to thank Prof. Sébastien Guillaume for our joint work, for his measurements during the experimental validation of the developed control methods and for keeping up the good spirit throughout the project.

My gratitude is extended to the other professors at IfA for creating the excellent environment of the institute. I thank Prof. John Lygeros for our fruitful collaborations on research and teaching. I enjoyed assisting in his Signals and Systems course as well as being part of the new Projects and Seminars teaching project on quadcopter control. I also thank Prof. Maryam Kamgarpour for stimulating discussions in the lab and for having me as a teaching assistant in her Linear Systems Theory course.

I feel very fortunate to have been a part of IfA, and I would like to thank all my brilliant colleagues, in particular my collaborators: Annika Eichler for our joint work on the topic of interconnected systems; Paul Beuchat for the collaboration, together with Angel Romero, on approximate dynamic programming, for jointly supervising numerous student projects, and developing the crazyfly teaching project from its very beginnings; Mohammad Khosravi and Andrea Iannelli for further developing ideas on learning-based

and robust control in digital fabrication; Lukas Affolter for successfully applying my research to a robotic arm; and Henrik Hesse, Alisa Rupenyan and Angeliki Kamoutsi for joint student project supervision.

I had amazing office mates over the past years. My thanks go to: Marcello Colombino for organizing fun glacier tours; Damian Frick for many discussions and for initiating our bike-to-work team; Andreas Hempel for making K11 a great office; Basilio Gentile for his home parties and quizzes; Mohammad Khosravi for many enriching conversations about work and life in general; Maria Vrakopoulou for her idea of moving into the nice lake-view office; Samuel Balula for his cheerful way and for making our office comfortable.

Thanks to all colleagues at IfA for creating such a uniquely enjoyable atmosphere, both in terms of a great work environment, and also during social activities such as IfA ski weekends, lake BBQs or the SOLA relay race. My gratitude goes to: Tony Wood for helping me to submit my first paper, for sharing many laughs and for making IfA a fun place; Eva Ahbe for nice conference and workshop trips, and together with Suli Zou for giving me refuge in their cool office during the hot phase of writing this thesis; Francesca Parise for being my roommate at many conferences; Ben Flamm for organizing lab events and home parties; Felix Rey for many enriching conversations; Alex Liniger for fun IfA ski weekends and coffee break discussions; Sandro Merkli for sharing the coffee talk duties at the very beginning of our time at IfA; Georgios Darivianakis for the fun trip to Paris; Bala Kameshwar Poolla and Paul Beuchat for smoothly organizing the IfA Open House with me, and to Lukas Ortmann, Andrea Martinelli and Yimeng Lu for taking over our duties; Xiaojing (George) Zhang for his valuable tips for eventually obtaining a US visa; Lukas Ortmann for his positive attitude towards everything and for many reassuring discussions; Mathias Hudoba De Badyn, Jeremy Coulson, Goran Banjac, Miguel Picallo and Saverio Bolognani for the fun CDC trip; and to my other great colleagues: Tobias Sutter, Dario Paccagnan, Adrian Hauswirth, Juan Jerez, Alexander Domahidi, Tyler Summers, Peyman Mohajerin Esfahani, Nicolò Pagan, Luca Furieri, Orcun Karaca, Dominik Groß, Ahmed Aboudonia, Pier Giuseppe Sessa, Wenjun Mei, Anil Parsi, Sandeep Menta, Irina Subotic, Ilnura Usmanova.

I would like to thank Sabrina Baumann and Tanja Turner, and also Martine Wassmer, Alain Bolle and Markus Thierer for their great jobs solving all possible administrative issues before they even exist and for running IfA so smoothly.

Finally, I would like to thank my family and friends, in particular my parents, Irene and Manfred, and my brother Marcel, for all their love and support throughout my life, and for organizing a great defense apéro for me. Special thanks go to Mario for his great support, for (not giving up on) teaching me Swiss German, and for all the great adventures together.

Zurich, June 2019,
Yvonne Rebecca Stürz

Abstract

In the past years technological advances and the availability of inexpensive hardware with sensing, communication and computational capacities have favored a trend of digitization and automation in many industries. The fields of architecture, construction and civil engineering, however, have hardly been affected by this trend so far. Challenging operating conditions and complex tasks are key factors why the advances in automation are not transferable to construction. The emerging field of digital fabrication aims at introducing more efficient building processes, and enabling completely new methods in design and architecture by leveraging tools from digital design and computation, robotic fabrication and automation. This thesis deals with two main aspects of digital fabrication: Firstly, the automation of complex construction tasks through efficient distributed control of multi-robot systems, and secondly, a completely new building process for lightweight construction, enabled by the form control of a cable net based formwork.

Interconnected systems, such as cooperating multi-agent systems, have a great potential of performing highly complex tasks. In the first part of this thesis, contributions towards efficient scalable distributed control design for heterogeneous interconnected systems are presented. Based on a linear fractional representation of the system with a decentralized part and an interconnection part, the full block S-procedure is applied for controller synthesis. For scalability of the design, we introduce structural constraints on the Lyapunov and multiplier matrices, which allows us to decompose the matrix inequalities into smaller ones of the order of the individual subsystems. Furthermore, a distributed solution method of the resulting coupled synthesis equations based on the Alternating Direction Method of Multipliers is proposed. The design only requires nearest-neighbor communication and no central coordination. The proposed methods are applicable to general heterogeneous systems, and the communication topology of the controller is a design choice. By introducing a new system classification consisting of multiple groups of homogeneous subsystems and different interconnection types, a more compact controller synthesis is derived with improved computational scalability. In order to improve the control performance given a communication topology, the interconnected controller design methods are applied to an augmented state space representation of the system. The individual augmented subsystem models contain copies of states of neighboring subsystems, which provides them with model information about their couplings. This is particularly beneficial if the number of communication links is to be minimized. Moreover, we present efficient methods for the design of minimum communication topo-

logies to eliminate all so-called fixed modes, which would prevent the system from being stabilizable, or limit its performance, if not removed.

The second part of this thesis introduces a novel control application, where feedback-based optimal control is introduced into the construction process. Tensioned cable nets can be used as a component of lightweight flexible formwork for the construction of thin concrete architectural shells. However, meeting the structural and mechanical specifications of such shells requires precise positioning of the nodes of the cable net to precisely achieve the designed and optimized form. Therefore, the goal of the proposed control method is to minimize the deviations of the tensioned cable net from the target form in the presence of fabrication tolerances and model uncertainties. The form control is crucial for enabling the use of this efficient lightweight formwork. It is based on measurements of the nodal positions of the cable net and possible actuation of the boundary cable lengths. Because taking measurements and making cable lengths adjustments is time-consuming on the construction site, a two-step algorithm is proposed which exploits model knowledge and measurement data. In each control iteration, first, the measurements are used to identify model parameters by a distributed optimization method. Second, for the control input computation, a sequential quadratic programming variant is proposed. For a given identified model, it generates a sequence of feasible iterates for the form optimization problem. The efficient computations involve solving quadratic and second-order cone programs. The algorithm is proved to converge to a Karush-Kuhn-Tucker point of the form optimization problem. A sparsity-promoting optimization-based method is proposed to further reduce the number of cable adjustments. The developed control strategy is experimentally validated on a quarter-scale prototype of a flexible cable net formwork for a doubly-curved roof shell.

Zusammenfassung

Technologische Fortschritte und die Verfügbarkeit günstiger, mit Sensorik, Rechenleistung und Kommunikationsfähigkeit ausgestatteter Hardware haben in den letzten Jahren in vielen Industriezweigen einen Trend zur Digitalisierung und Automatisierung hervorgerufen. In den Bereichen der Architektur und der Bauindustrie ist dieser Trend allerdings kaum merkbar. Schwierige Arbeitsbedingungen und komplexe Bauprozesse sind Gründe dafür warum die Automatisierung anderer Industriezweige nicht auf das Bauwesen übertragbar sind. Die Ziele des neuen Forschungsfeldes der Digitalen Fabrikation sind zum Einen das Einführen effizienterer Bauprozesse, und zum Anderen das Ermöglichen komplett neuartiger Methoden sowie Design in der Architektur. Dies wird durch Techniken der computergestützten Berechnung und Entwurfs, sowie des robotergestützten Bauens und der Automatisierung, ermöglicht. Diese Dissertation beschäftigt sich mit zwei Aspekten der Digitalen Fabrikation: Zum Einen mit der Automatisierung komplexer Bauprozesse durch effiziente verteilte Regelung von Multi-Roboter-Systemen, und zum Anderen mit einem komplett neuartigen Bauprozess von Leichtbaustrukturen, der durch die Formregelung einer Seilnetz basierten Schalung ermöglicht wird.

Verteilte Systeme, wie zum Beispiel kooperative Multi-Roboter-Systeme, haben ein großes Potenzial komplexe Aufgabenstellungen zu bewältigen. Im ersten Teil der Dissertation werden Resultate für eine effiziente skalierbare Synthese verteilter Regelalgorithmen für heterogene verteilte Systeme präsentiert. Basierend auf einer *Linear Fractional Representation* des Systems in einen dezentralen Systemteil und einen Kopplungsteil, wird die *Full Block S-Procedure* für die Reglersynthese angewandt. Für die Skalierbarkeit der Synthese führen wir Bedingungen an die Struktur der Lyapunov und der *Multiplier* Matrizen ein, was es uns ermöglicht die Matrix Ungleichungen in kleinere in der Größenordnung der einzelnen Subsysteme zu zerlegen. Des Weiteren wird eine verteilte Lösungsmethode der gekoppelten Regleersynthesegleichungen eingeführt, welche auf der *Alternating Direction Method of Multipliers* basiert. Sie benötigt lediglich Kommunikation zwisichen gekoppelten Nachbarsystemen, jedoch keinerlei zentralisierte Koordination. Die Methoden sind auf heterogene Systeme anwendbar. Die Kommunikationstopologie des Reglers kann bei der Reglerauslegung frei vorgegeben werden. Durch die Einführung einer neuen Systemklasse, die aus mehreren Gruppen homogener Subsysteme mit verschiedenartigen Kopplungen bestehen, wird eine kompaktere Reglersynthese mit verbesserter Skalierbarkeit abgeleitet. Um unter einer gegebenen Reglerstruktur die Reglergüte zu verbessern, werden die Synthesemethoden des verteilten Reglers in ei-

nem erweiterten Zustandsraum angewandt. Die erweiterten Systemmodelle der einzelnen Subsysteme enthalten Kopien von benachbarten Subsystemen, und somit Informationen über deren Kopplungen. Das ist insbesondere dann von Bedeutung, wenn die Anzahl der Kommunikationsverbindungen minimiert werden soll. Wir stellen effiziente Methoden für das Auslegen minimaler Kommunikationstopologien vor, die alle sogenannten *Fixed Modes* eliminieren, welche die Stabilisierbarkeit des Systems verhindern oder die erreichbare Reglergüte beschränken würden.

Der zweite Teil dieser Dissertation präsentiert eine neuartige Regleranwendung, in der eine rückführungsbasierte optimale Regelung in den Bauprozess integriert wird. Vorgespannte Seilnetze können als Komponente einer flexiblen Leichtbauschalung für den Bau dünner architektonischer Betonschalen verwendet werden. Um allerdings die strukturellen und mechanischen Anforderungen an die Schalen zu gewährleisten, ist eine präzise Einhaltung der Seilnetzform unabdingbar um die entworfene und optimierte Form zu erreichen. Deshalb ist es Aufgabe der Regelung die Abweichungen der Netzseilkonstruktion von der Sollform unter Unsicherheiten und Toleranzen zu minimieren. Die vorgestellte Formregelung ist dadurch eine Schlüsselmethode, die die Verwendung solcher effizienter Leichtbauschalungen ermöglicht. Die Regelung basiert auf Positionsmessungen der Knotenpunkte des Seilnetzes und möglicher Aktuierung der Seillängen am Rand des Netzes. Da Messungen und Seillängenverstellungen auf der Baustelle zeitintensiv sind, wird ein zweischrittiger Algorithmus vorgestellt, der Modellwissen, sowie die Information der Messdaten ausnutzt. In jeder Iteration werden zuerst die Messdaten dazu genutzt die Modellparamter durch einen verteilten Optimierungsalgorithmus zu bestimmen. Dann wird für die Regeleingangsberechnung eine *Sequential Quadratic Programming* Variation vorgeschlagen. Für ein gegebenes Modell wird eine Folge an Punkten generiert, die die Nebenbedingungen des Formoptimierungsproblemes erfüllen. Die effizienten Berechnungen bestehen im Lösen von quadratischen und konischen Optimierungsproblemen. Der Algorithmus konvergiert zu einem *Karush-Kuhn-Tucker* Punkt des Formoptimierungsproblems. Um die Anzahl der Seillängenänderungen weiter zu reduzieren wird eine optimierungsbasierte Methode zur Berechnung dünnbesetzter Eingangsvektoren vorgestellt. Die entwickelte Regelstrategie wird an einem Seilnetzbasierten flexiblen Schalungsprototypensystem experimentell validiert.

Contents

Notation

Acronyms

ADMM	Alternating Direction Method of Multipliers
BMI	Bilinear Matrix Inequality
DFM	Decentralized Fixed Modes
DOF	Dynamic Output Feedback
DOFM	Decentralized Overlapping Fixed Mode
EMPA	Eidgenössische Materialprüfungs- und Forschungsanstalt
FBSP	Full Block S-Procedure
FM	Fixed Modes
GN	Gauss-Newton
HiLo	High Performance Low Energy
IQC	Integral Quadratic Constraint
KKT	Karush-Kuhn-Tucker
LFR	Linear Fractional Representation
LFT	Linear Fractional Transformation
LHS	Left-Hand Side
LMI	Linear Matrix Inequality
LPV	Linear Parameter Varying
LS	Line Search
LTI	Linear Time Invariant
MAS	Multi-Agent System
MPC	Model Predictive Control
NEST	Next Evolution in Sustainable Building Technologies
OCP	Optimal Control Problem
QP	Quadratic Program
RHS	Right-Hand Side
RMS	Root Mean Square
SOCP	Second Order Cone Program
SQP	Sequential Quadratic Programming
SSF	Static State Feedback
SVD	Singular Value Decomposition
UAV	Unmanned Aerial Vehicle

Symbols

Sets and Spaces

$\mathbb{R}$, $\mathbb{R}^n$, $\mathbb{R}^{n\times m}$	Set of real numbers, real valued n-dimensional vectors, real valued $n \times m$-dimensional matrices
$\lvert\mathcal{S}_1\rvert$	Cardinality of set $\mathcal{S}_1$
$\mathcal{S}_1 \cup \mathcal{S}_2$	Union of sets $\mathcal{S}_1$ and $\mathcal{S}_2$, i.e., $\mathcal{S}_1 \cup \mathcal{S}_2 = \{s \mid s \in \mathcal{S}_1 \text{ or } s \in \mathcal{S}_2\}$
$\mathcal{S}_1 \setminus \mathcal{S}_2$	Set difference $\mathcal{S}_1$ and $\mathcal{S}_2$, i.e., $\mathcal{S}_1 \setminus \mathcal{S}_2 = \{s \mid s \in \mathcal{S}_1 \text{ and } s \notin \mathcal{S}_2\}$
$\mathcal{S}_1 \cap \mathcal{S}_2$	Intersection of sets $\mathcal{S}_1$ and $\mathcal{S}_2$, i.e., $\mathcal{S}_1 \cap \mathcal{S}_2 = \{s \mid s \in \mathcal{S}_1 \text{ and } s \in \mathcal{S}_2\}$
$2^{\mathcal{S}}$	Power set of the set $\mathcal{S}$
$\mathcal{R}(V)$	Range space of V
$\mathcal{V}(a, b)$	Uniform distribution with support on the interval $[a, b]$

Functions and Operators

$\mathcal{I}_{(a)}(b)$	Indicator function for condition (a)
$\mathcal{L}$, $\mathcal{L}_\rho$	Lagrangian, augmented Lagrangian
$\nabla_x f$	Gradient of the function $f(x) : \mathbb{R}^n \mapsto \mathbb{R}$, i.e., $\nabla_x f = [\frac{\partial f}{\partial x_1} \ \cdots \ \frac{\partial f}{\partial x_n}]^\top$
$\nabla_{(r,u)} h$	Jacobian of the function $h(r, u) : \mathbb{R}^{n+p} \mapsto \mathbb{R}^m$, i.e., $\nabla_{(r,u)} h = \left[\nabla_r h \,\middle|\, \nabla_u h\right] = \left[\begin{array}{ccc\|ccc} \frac{\partial h_1}{\partial r_1} & \cdots & \frac{\partial h_1}{\partial r_n} & \frac{\partial h_1}{\partial u_1} & \cdots & \frac{\partial h_1}{\partial u_p} \\ \vdots & & \vdots & \vdots & & \vdots \\ \frac{\partial h_m}{\partial r_1} & \cdots & \frac{\partial h_m}{\partial r_n} & \frac{\partial h_m}{\partial u_1} & \cdots & \frac{\partial h_m}{\partial u_p} \end{array}\right]$
$\nabla_{(r,u)}$	Partial derivatives with respect to r and u
$\nabla_r h$, $\nabla_u h$	Partial Jacobians of $h(r, u)$ with respect to r, u
$\nabla_{(r,u)} h(r^\kappa, u^\kappa)$	Jacobian of $h(r, u)$ evaluated at the point (r^κ, u^κ)

Linear Algebra

$M^\top$	Transpose of a matrix M
M^{-1}, $M^\dagger$	Inverse and pseudoinverse of a matrix M
$M > 0$, $M \geq 0$	Positive (semi-)definite matrix M
$M < 0$, $M \leq 0$	Positive (semi-)negative matrix M
$M \otimes N$	Kronecker product of matrices M and N, i.e., $M \otimes N = \begin{bmatrix} M_{11}N & \dots & M_{1m}N \\ \vdots & \ddots & \vdots \\ M_{n1}N & \dots & M_{nm}N \end{bmatrix}$, for $M \in \mathbb{R}^{n\times m}$

I_n	Identity matrix in $\mathbb{R}^{n\times n}$
e_j	j-th Unit vector, i.e., vector of all zeros except that the j-th entry is one
$0_{n\times m}$	Matrix in $\mathbb{R}^{n\times m}$ with all zeros
$\hat{I}_{\{i\}}$	Square matrix of appropriate dimensions of all zeros except that the (i,i)-entry is one
$\lambda(M), \sigma(M)$	Eigenvalue, singular value of a matrix M
Λ	Diagonal matrix with eigenvalues $\lambda_1, ..., \lambda_N$ on the diagonal
$\text{spec}(M)$	Spectrum of matrix M, i.e., set of eigenvalues of matrix M
$\sigma_{\min}(\cdot)$, $\sigma_{\max}(\cdot)$	Minimum and maximum singular values
$\lambda_{\min}(\cdot)$, $\lambda_{\max}(\cdot)$	Minimum and maximum eigenvalues
$\text{cond}(M)$	Condition number of a matrix, i.e., $\text{cond}(M) = \frac{\sigma_{\min}(M)}{\sigma_{\max}(M)}$
$\text{rank}(M)$	Rank of a matrix
$\lvert m\rvert$	Vector 2-norm, absolute value
$\lVert m\rVert_2$	l_2-vector norm (Euclidean norm), i.e., $\lVert m\rVert_2 = \sqrt{m_1^2 + ... + m_n^2}$
$\lVert m\rVert_\infty$	l_∞-vector norm, i.e., $\lVert m\rVert_\infty = \max_{i\in 1,...,n}\{\lvert m_1\rvert, .., \lvert m_n\rvert\}$
$\lVert m\rVert_{l_0}$	l_0-vector "norm", i.e., the number of non-zero entries of vector m
$\lVert m\rVert_{l_1}$	l_1-vector norm, i.e., $\lVert m\rVert_{l_1} = m_1 + ... + m_n$
$\text{RMS}(m)$	Root Mean Square Error, i.e., $\text{RMS}(m) = \sqrt{\lVert m\rVert_2^2 / n}$ for $m \in \mathbb{R}^n$
$\text{diag}_{i=1}^n(M_i)$	Diagonal concatenation i.e., $\text{diag}_{i=1}^n(M_i) = \begin{bmatrix} M_1 & & \\ & \ddots & \\ & & M_n \end{bmatrix}$
$\text{concat}_{i=1}^n(M_i)$	Vertical concatenation, i.e., $\text{concat}_{i=1}^n(M_i) = \begin{bmatrix} M_1^\top \dots M_n^\top \end{bmatrix}^\top$
$\text{vect}(M)$	Vectorization of the matrix M, i.e., the elements of M are concatenated to a vector
$\lVert x\rVert_Q^2$	Weighted L_2-vector-norm with weighting matrix Q, i.e., $\lVert x\rVert_Q^2 = x^\top Q\, x$
$\lVert\cdot\rVert_{\mathcal{H}_2}$	System $\mathcal{H}_2$-norm
$\lVert\cdot\rVert_{\mathcal{H}_\infty}$	System $\mathcal{H}_\infty-$norm
$\mathcal{F}_{\{\text{l,u}\}}(M, P)$	Lower and upper Linear Fractional Transformation (LFT), i.e., $\mathcal{F}_\text{l}(M,P) = M_1 + M_2P(I - M_4P)^{-1}M_3$, $\mathcal{F}_\text{u}(M,P) = M_4 + M_3P(I - M_1P)^{-1}M_2$, of complex valued matrix $M = \begin{bmatrix} M_1 & M_2 \\ M_3 & M_4 \end{bmatrix}$, and matrix P
$\star$	Simplification for symmetric expressions, i.e., $\star^\top M_2 M_1 = M_1^\top M_2 M_1$

Symbols for Part II

Signals and Systems

G, $\mathcal{G}$	Open-loop, closed-loop LTI system
A, B, C, D	Open-loop system, input, output, feedthrough matrix
$\mathcal{A}$, $\mathcal{B}$, $\mathcal{C}$, $\mathcal{D}$	Closed-loop system, input, output, feedthrough matrix
$\left[\begin{array}{c\|c} \mathcal{A} & \mathcal{B} \\ \hline \mathcal{C} & \mathcal{D} \end{array}\right]$	Rosenbrock notation of closed-loop system
K	Controller
A^K, B^K, C^K, D^K	Open-loop controller, input, output, feedthrough matrix
$\mathbf{A}^{\mathbf{K}}$, $\mathbf{B}^{\mathbf{K}}$, $\mathbf{C}^{\mathbf{K}}$, $\mathbf{D}^{\mathbf{K}}$	Transformed controller matrices
A_ξ^K, B_ξ^K, C_ξ^K, D^K	Augmented controller gains
$\mathbf{A}^{\mathbf{K}d}_\xi$, $\mathbf{B}^{\mathbf{K}d}_\xi$, $\mathbf{C}^{\mathbf{K}d}_\xi$, $\mathbf{D}^{\mathbf{K}d}$	Set of all block-diagonal augmented controller gains
$A_\mathcal{E}^K$, $B_\mathcal{E}^K$, $C_\mathcal{E}^K$, $D_\mathcal{E}^K$	Augmented controller gains according to communication topology $\mathcal{E}$ in block-diagonal structure
x, ξ	State vector, augmented state vector
x^K, ξ^K	Controller state vector, augmented controller state vector
$x^c = \begin{bmatrix} x^\top & {x^K}^\top \end{bmatrix}^\top$	Closed-loop state of $\mathcal{G}$
$\bar{z}$, $\bar{w}$	Non-localized performance output, disturbance input of system $\bar{G}$
$\hat{v}$, $\hat{w}$	Process, measurement noise
z, w	Localized performance output and disturbance input of system G, i.e., $z = \operatorname{concat}_{i=1}^N \left(z_i^\top\right)^\top$ and $w = \operatorname{concat}_{i=1}^N \left(w_i^\top\right)^\top$
q, p	Interconnection input, output signal of the plant
q^K, p^K, q^c, p^c	Interconnection input, output signal of the controller, closed-loop
n_l	Dimension of signal l
B_p, D_{zp}, D_{yp}, C_q, D_{qw}, D_{qu}	System matrices related to the interconnection channel in LFR
$B_{p^K}, C_{p^K}, C_{q^K}, D_{q^K}$	Controller matrices related to the interconnection channel in LFR
V, U	Mapping from x to ξ, and back, with $UV = I$
M_A, M_{C_y}, $M_{C_{\bar{z}}}$, M_Q, M_R	Complementary matrices

Subscripts and Superscripts

$(\cdot)_i$	Related to individual subsystems or subcontrollers
$D_{zp,i}$	System matrices related to the interconnection channel p to z of subsystem i

$n_{q_i^K}$	Dimension of signal q_i^K belonging to subsystem i
$(\cdot)_\xi$	Related to augmented state/system
$(\cdot)^G$, $(\cdot)^K$, $(\cdot)^c$	Related to the system, controller, closed-loop
$(\cdot)^{GM}$, $(\cdot)^{KM}$	Related to the mirror graph of the plant/controller interconnection topology
$(\cdot)^d$	Related to decentralized/block-diagonal parts
$(\cdot)^i$	Related to interconnected/off-block-diagonal parts
$(\cdot)^\kappa$	Number of iterations

Graphs

N	Number of subsystems
$\mathcal{N}$	Index set of subsystems $\mathcal{N} = \{1, ..., N\}$
$\mathcal{E}^G$, $\mathcal{E}^K$, $\mathcal{E}$	Set of directed interconnection links of plant, controller, closed-loop
(i, k)	Directed interconnection link from subsystem k to i
$\mathcal{T}^G$, $\mathcal{T}^K$, $\mathcal{T}$	Underlying graph indicating the interconnection topology of the plant, controller, closed-loop, e.g., $\mathcal{T}^G = \{\mathcal{N}, \mathcal{E}^G\}$
$\mathcal{T}^{GM}$, $\mathcal{T}^{KM}$	Mirror graph of the plant, controller
$\mathcal{N}_s^G$, $\mathcal{N}_s^K$, $\mathcal{N}_s$	Index set of neighboring subsystems, subcontrollers, closed-loop subsystems of subsystem G_s, subcontroller K_s, closed-loop subsystem $\mathcal{G}_s$
P^G, P^K, P	Interconnection matrix on the level of the subsystems, subcontroller, closed-loop subsystems, $P \in \mathbb{R}^{N \times N}$
$\mathcal{P}^G$, $\mathcal{P}^K$, $\mathcal{P}$	Interconnection matrix on the level of the signals of plant, controller, closed-loop, $\mathcal{P} \in \mathbb{R}^{n_{p^c} \times n_{p^c}}$
α^G, α^K, α	Number of groups of homogeneous subsystems, subcontrollers, closed-loop subsystems
β^G, β^K, β	Number of different types of interconnections of the system, controller, closed-loop system
$\mathcal{E}_{\text{full}}$	Complete set of undirected interconnection links, i.e., $\mathcal{E}_{\text{full}} = \{(1, 2), ..., (N, N-1)\}$
$\mathcal{E}^y$, $\mathcal{E}^{\xi^K}$	Set of communication links of measurements, controller states
$\mathcal{E}^n$	Search set of controller communication links of node n
T^n	Set of added communication links for node n
T	Set of communication links to be minimized, representing $\mathcal{E}^y$ or $\mathcal{E}^{\xi^K}$
T^*	Minimal set of communication links
M_{λ,S_1,S_2}	Rank check matrix for fixed modes identification
B_{u,S_1}, C_{y,S_2}	Columns and rows of B_u, C_y belonging to index partitions S_1, S_2
$\mathbb{B}_{\{A,B,C,D\}}$, $\mathbb{C}_{\{A,B,C,D\}}$	Matrices capturing the communication structure of controller states and measurements
d_r	Rank-deficiency

$r = \{1, ..., R\}$	Enumeration of rank-deficient cases
$\bar{R}$	Number of links to remove all FMs
$n+$	Children of node n in search tree, i.e., nodes of the next level

Controller Synthesis

$\mathcal{X}$, $\mathcal{Y}$	Lyapunov matrix and its inverse, i.e., $\mathcal{Y} = \mathcal{X}^{-1}$
Q, R, S	Multiplier matrices in FBSP
Q_{ik}, $\hat{Q}_{ik}$, $\tilde{Q}_i$	Multiplier matrices per directed, undirected interconnection, per subsystem (analogously for R, S)
γ	Performance index, bound on $\mathcal{H}_\infty$-norm
ν	Linearizing variable substitution $\nu = \gamma^{-\frac{1}{2}}$
X_n, X_m, $(\bar{X}_n)$, $(\bar{X}_m)$	(Mean) Dimensions of nominal and multiplier conditions

Alternating Direction Method of Multipliers (ADMM)

l	Global variable vector
s_i, t_{ik}	Local variable vectors per subsystem i and edge (i, k)
λ, u, v	Dual multipliers
r, d	Primal, dual residuals
ρ	Penalty parameter
E_i, H_i	Selection matrices for global consensus
E_{ik}, T_{ik}	Selection matrices for local consensus
κ	Number of iterations
$\mathcal{L}_\rho$, $\mathcal{L}_{\rho,i}$	Augmented Lagrangian of system, subsystem i
$f(\cdot)$, $g(\cdot)$	Cost function, indicator function for constraints

Symbols for Part III

$\mathcal{E}$, $\bar{\mathcal{E}}$	Set of edges, tensioned edges
$\mathcal{N}$	Set of nodes
$\mathcal{G} = \{\mathcal{N}, \mathcal{E}\}$	Graph of the cable net topology
$\bar{\mathcal{G}} = \{\mathcal{N}, \bar{\mathcal{E}}\}$	Graph of the cable net topology of all tensioned edges
$\mathcal{N}_s$	Set of adjacent nodes to node s
n	Number of nodes
m	Number of edges
r	Nodal position coordinates, i.e., $r = [x^\top,\ y^\top,\ z^\top]^\top$

r_I, r_B, $\bar{r}_B$	Interior, boundary, fixed boundary nodes coordinates
r^{meas}, $r^{(k),\text{meas}}$	Measured, $k-$th measured, configuration
$r^{(\text{des})}$, $r^{(\text{ini})}$, $r^{(\text{con})}$	Desired, initial, controlled configuration
EA	Material parameters: Young's modulus $\times$ cross section area
$l_{0,(s,t)}$, $l_{(s,t)}$	Unstressed and actual length of edge (s,t), i.e., $l_{(s,t)} = \|r_s - r_t\|_2$
$u_{(s,t)}$	Control input, i.e., change in edge length $l_{0,(s,t)}$
$\bar{l}_{0,(s,t)}$	Unstressed length of edge (s,t) after applying input $u_{(s,t)}$, i.e., $\bar{l}_{0,(s,t)} = l_{0,(s,t)} - u_{(s,t)}$
α	Step length of line search
ρ	Step length reduction factor of backtracking line search
c_1, c_2	Constants in Wolfe conditions
c_c, c_w, $c_{c,1}$	Convergence bounds
$\Delta u_{\mathcal{P}_{\text{ocp,u}}}$	GN step on $\mathcal{P}_{\text{ocp,u}}$
Δp	GN step on $\mathcal{P}_{\text{ocp}}$, i.e., $\Delta p = [\Delta r^\top, \Delta u^\top]^\top$
$R(u)$	Mapping $u \mapsto r$, not explicitly known
H	Hessian approximation
Q_r	Weighting matrix
V	Energy function
$g \leq 0, h = 0$	Inequality, equality constraints

Subscripts and Superscripts

$(\cdot)_B$, $(\cdot)_I$	Related to boundary, interior (nodes, edges)
$(\cdot)^\kappa$	Iteration within control input computation (SQP), or within ADMM
$(\cdot)^\nu$	Iteration within sparse input computation
$(\cdot)^{(k)}$	k-th Configuration or input in complete control loop
$(\cdot)_{l_1}$	Related to sparse input vector

Optimization Problems

$\mathcal{P}_{\text{minE}}$	Energy minimization problem
$\mathcal{P}_{\text{ocp,u}}$, $f_{\text{ocp,u}}$	OCP and cost function in terms of u
$\mathcal{P}_{\text{ocp}}$, f_{ocp}	OCP and cost function in terms of r and u
$\mathcal{P}^\kappa_{\text{SQP}}$, $f^{\text{GN}}_{\text{ocp}}$	QP approximating $\mathcal{P}_{\text{ocp}}$ and GN-approximation of f_{ocp} in SQP-iteration
$f^{\text{GN}}_{\text{ocp,u}}$	GN-approximation of $f_{\text{ocp,u}}$ in GN-iteration

CHAPTER 1

Introduction

1.1 Digital Fabrication

The availability of inexpensive hardware, computational power, and sensors has given rise to a fast growing trend of digitization and automation in many domains. Digital technologies, robotics and smart infrastructures increasingly dominate many industries and applications: Service robots, the smart grid and self-driving cars are only a few of the numerous examples. While many branches of industry have significantly benefited from this transformation, others seem to have been far less affected. Obvious examples of the latter are the fields of architecture, building construction and civil engineering. In fact, many traditional processes in construction buildings have not changed much in the last decades.

However, when analyzing automated manufacturing processes, it can be noted that robots in automated production lines are limited to highly structured, static and controlled environments. Furthermore, the tasks are repetitive and predefined. Most of the tasks involve manipulating small objects which can easily be handled by one or two robots. All of this reduces uncertainties in the tasks and eliminates some of the major control challenges. In contrast, the conditions in building construction or civil engineering cause some unsolved challenges. Many of them arise due to highly unstructured, uncertain and dynamic environments and large fabrication tolerances. Building processes involve complex tasks and heavy objects of large dimensions. Safety of human workers who possibly share the workspace with robots also needs to be considered. The advances in automation of many other industries are not easily transferable to these demanding conditions. However, developing methods that can cope with the outlined challenges will have a tremendous impact on building construction and civil engineering. This is the goal of the new emerging field of digital fabrication.

Digital fabrication aims at revolutionizing the way buildings will be designed and built in the future. Besides allowing for more efficient and precise construction processes, completely new ways of designing and building will be enabled. Furthermore, digital fabrication can have an impact on the sustainability of building processes [1], [2]. This

field has recently seen a lot of innovation, such as robotic on-site fabrication [3]–[8], cooperative robotic fabrication [9], and new ways of designing reinforcement structures [10], [11]. However, commonly applied processes lack digitization and many challenges remain to be solved. The following section outlines how this thesis addresses some of the highlighted challenges.

1.2 Scope and Contribution

This thesis is structured into two main parts and provides contributions to two areas of digital fabrication. In particular, Part II is motivated by enabling automated construction processes through an efficient control of large-scale multi-robot systems, and Part III provides a control method that achieves precision in lightweight construction.

Many of the highly complex tasks in pre-fabrication or on-site fabrication seem to be too difficult for a single robot. Such tasks, for example, involve manipulating objects, holding in place and fixing elements, or stabilizing and assembling large structures. Cooperative multi-robot systems are well suited for these tasks. While the individual robots can be simple, an interconnected system of many, possibly different (heterogeneous), subsystems has the potential to perform very complex tasks. Efficient scalable control of heterogeneous large-scale systems however still poses open research questions. Limited infrastructure and disturbances are other challenges that are specifically related to the construction site and limit the available communication capabilities. The first part of this work thus focuses on scalable distributed control of heterogeneous interconnected systems with potentially reduced communication.

Apart from rendering building processes more efficient, another significant goal of digital fabrication is to enable completely new approaches in architecture by combining the potential of digital design, computation and automation. Motivated by lightweight construction and enabled by digital design tools, building structures are commonly optimized in their form with respect to minimal material use and maximal mechanical stability. However, such optimized structures are typically not very robust to uncertainties and deviations in their form. Due to large fabrication tolerances it is challenging to precisely achieve the designed form. High-precision construction processes which aim at minimizing deviations from the optimized form are therefore required. The second part of this work presents a novel construction method which introduces feedback-based optimal control to on-site construction in order to obtain a high-precision formwork that can be used for lightweight construction.

The thesis is structured as follows. Part I provides mathematical preliminaries. Part II focuses on scalable distributed control of interconnected systems. In Chapter 4, a detailed introduction, literature review and outline of the contributions related to Part II are given. The main results of Part II are given in Chapters 5 - 8. Part III addresses

the form control of a cable net based formwork. In Chapter 9, an introduction to the topic, and outlines of related work and of the contributions of Part III are provided. Chapters 10 - 13 present the main results of Part III. Part IV gives conclusions and an outlook.

1.3 Publications

The work presented in this thesis is the result of collaborations with many colleagues. The thesis is mainly based on the following publications.

1.3.1 Publications Related to Part II

- Yvonne R. Stürz, Annika Eichler and Roy S. Smith. "A framework for distributed control based on overlapping estimation for cooperative tasks". *IFAC World Congress,* pp. 14296–14301, July, 2017 [12].
- Yvonne R. Stürz, Annika Eichler and Roy S. Smith. "Fixed mode elimination by minimum communication within an estimator-based framework for distributed control". *IEEE Control Systems Letters,* vol. 1, no. 2, pp. 346–351, June, 2017 [13].
- Yvonne R. Stürz, Annika Eichler and Roy S. Smith. "Scalable controller synthesis for interconnected systems with heterogeneous subsystems and heterogeneous interconnections applicable to an overlapping control framework". *IEEE European Control Conference,* pp. 2561–2568, June, 2018 [14].
- Yvonne R. Stürz, Annika Eichler and Roy S. Smith. "Distributed control design for heterogeneous interconnected systems". *Transactions on Automatic Control,* [under review] [15].

1.3.2 Publications Related to Part III

- Yvonne R. Stürz, Manfred Morari and Roy S. Smith. "Sequential quadratic programming for the control of an architectural cable net geometry". *American Control Conference,* pp. 3503–3508, July, 2016 [16].
- Yvonne R. Stürz, Manfred Morari and Roy S. Smith. "Two methods for the identification of uncertain parameters of an architectural cable net geometry". *IEEE Conference on Control Applications,* pp. 3503–3508, September, 2016 [17].
- Andrew Liew, Yvonne R. Stürz, Sébastien Guillaume, Tom Van Mele, Roy S. Smith, and Philippe Block. "Active control of a rod-net formwork system prototype". *Automation in Construction,* vol. 96, pp. 128–140, December, 2018 [18].

- Yvonne R. Stürz, Manfred Morari and Roy S. Smith. "Control of an architectural cable net geometry". *IEEE Transactions on Control Systems Technology,* to appear, 2019 [19].

1.3.3 Other Publications

The following articles were published by the author during her PhD studies. However, they do not contribute to the content of this thesis.

- Yvonne R. Stürz, Lukas M. Affolter and Roy S. Smith. "Parameter identification of the KUKA LBR iiwa robot including constraints on physical feasibility". *IFAC World Congress,* pp. 6863–6868, July, 2017 [20].
- Angel Romero, Paul N. Beuchat, Yvonne R. Stürz, Roy S. Smith, John Lygeros. "Nonlinear control of quadcopters via approximate dynamic programming". *IEEE European Control Conference,* pp. 3752–3759, July, 2019 [21].
- Paul N. Beuchat, Yvonne R. Stürz, John Lygeros. "A teaching system for hands-on quadcopter control". *IFAC Conference on Advances in Control Education,* pp. 36–41, July, 2019 [22].

Part I

Preliminaries

CHAPTER 2

System Theory

In this chapter, some fundamental properties of continuous-time linear time-invariant (LTI) systems are introduced. The discussion is focused on results which will be used in Part II of this thesis.

2.1 LTI System Representation

We consider linear time-invariant (LTI) systems with continuous time dynamics given by

$$\begin{aligned} \dot{x}^c(t) &= \mathcal{A}x^c(t) + \mathcal{B}w(t), \\ z(t) &= \mathcal{C}x^c(t) + \mathcal{D}w(t), \end{aligned} \tag{2.1}$$

where $x^c \in \mathbb{R}^{n_{x^c}}$ is the state vector, $w \in \mathbb{R}^{n_w}$ is the input vector, and $z \in \mathbb{R}^{n_z}$ is the output vector. In the following, we will not explicitly indicate the dependency on the time variable t. The system in (2.1) can be represented by the following state-space description

$$\mathcal{G} : \begin{bmatrix} \dot{x}^c \\ z \end{bmatrix} = \begin{bmatrix} \mathcal{A} & \mathcal{B} \\ \mathcal{C} & \mathcal{D} \end{bmatrix} \begin{bmatrix} x^c \\ w \end{bmatrix}. \tag{2.2}$$

2.2 Lyapunov Stability

The system in (2.1) is stable if and only if there exists a symmetric, positive definite matrix $\mathcal{X}$ that satisfies [23]

$$\mathcal{A}^\top \mathcal{X} + \mathcal{X}\mathcal{A} < 0, \tag{2.3}$$

which can equivalently be formulated as

$$\begin{bmatrix} I & \mathcal{A}^\top \end{bmatrix} \begin{bmatrix} 0 & \mathcal{X} \\ \mathcal{X} & 0 \end{bmatrix} \begin{bmatrix} I \\ \mathcal{A} \end{bmatrix} < 0. \tag{2.4}$$

The matrix $\mathcal{X}$ is referred to as Lyapunov matrix.

Figure 2.1: System with performance channel from w to z.

2.3 System Performance Measures

We consider the system in Figure 2.1, with a stable transfer function matrix $\mathcal{G}(s)$. The performance is typically measured in terms of the input output behavior, i.e., by a measure of how large the output z can become for given allowed inputs w. In this work, we will mostly use the induced $\mathcal{L}_2$ system norm. In the case of LTI systems, this norm reduces to the $\mathcal{H}_\infty$ system norm, which is defined in the following.

2.3.1 $\mathcal{H}_\infty$ System Norm

Definition 2.1. *[23] Given a proper and stable LTI system $\mathcal{G}(s)$, the $\mathcal{H}_\infty$ norm is the induced $\mathcal{L}_2$ norm, defined in the frequency domain as*

$$\|\mathcal{G}\|_{\mathcal{H}_\infty} := \sup_{\omega\in\mathbb{R}} \sigma_{\max}\left(\mathcal{G}(i\omega)\right) = \sup_{\omega\in\mathbb{R}} \|\mathcal{G}(i\omega)\|_2. \tag{2.5}$$

Alternatively, in the time domain, the following characterization can be used,

$$\|\mathcal{G}\|_{\mathcal{H}_\infty} = \sup_{w\neq 0} \frac{\|z\|_2}{\|w\|_2} = \sup_{\|w\|_2=1} \|z\|_2. \tag{2.6}$$

In the course of this work, it will be of interest to provide an upper bound on the performance in terms of the performance index γ as follows

$$\|z\|_2 \leq \gamma \|w\|_2. \tag{2.7}$$

For an LTI system, this performance specification is equivalent to the system being strictly dissipative with respect to the supply rate $s(w,z) = \gamma^2\|w\|_2^2 - \|z\|_2^2$ [24]. In this case, it holds that

$$\int_0^\infty \begin{bmatrix} w^\top & z^\top \end{bmatrix} \begin{bmatrix} Q_p & S_p \\ S_p^\top & R_p \end{bmatrix} \begin{bmatrix} w \\ z \end{bmatrix} dt \leq 0, \tag{2.8}$$

with

$$\begin{bmatrix} Q_p & S_p \\ S_p^\top & R_p \end{bmatrix} = \begin{bmatrix} -\gamma^2 I & 0 \\ 0 & I \end{bmatrix}.$$

2.3.2 $\mathcal{H}_2$ System Norm

Instead of the $\mathcal{H}_\infty$ norm, the $\mathcal{H}_2$ norm can be used as performance measure, which is defined as follows.

Definition 2.2. *[23] Given a strictly proper and stable LTI system $\mathcal{G}(s)$ in state space realization, the $\mathcal{H}_2$ system norm is defined as*

$$\|\mathcal{G}(s)\|_{\mathcal{H}_2} := \sqrt{\frac{1}{2\pi}\int_{-\infty}^{\infty} \operatorname{tr}\left(\mathcal{G}(i\omega)^H \mathcal{G}(i\omega)\right) d\omega} \tag{2.9}$$

where ^{H} indicates the conjugate transpose and tr *indicates the trace, i.e., the sum of the diagonal elements.*

2.3.3 Bounded Real Lemma for LTI Systems

Using (2.4) and (2.8), the following necessary and sufficient conditions for stability and performance can be derived, similar to the Bounded Real Lemma:

Lemma 2.1. *[24] The LTI system $\mathcal{G}$ in* (2.1) *is stable and has an $\mathcal{L}_2$ gain less than γ, i.e., $\|\mathcal{G}\|_{\mathcal{H}_\infty} < \gamma$ if and only if there exists a symmetric matrix $\mathcal{X} > 0$ that satisfies*

$$\left[\begin{array}{cc:cc} I & \mathcal{A}^\top & 0 & \mathcal{C}^\top \\ 0 & \mathcal{B}^\top & I & \mathcal{D}^\top \end{array}\right] \left[\begin{array}{cc:cc} 0 & \mathcal{X} & 0 & 0 \\ \mathcal{X} & 0 & 0 & 0 \\ \hdashline 0 & 0 & -\gamma^2 I & 0 \\ 0 & 0 & 0 & I \end{array}\right] \left[\begin{array}{cc} I & 0 \\ \mathcal{A} & \mathcal{B} \\ \hdashline 0 & I \\ \mathcal{C} & \mathcal{D} \end{array}\right] < 0. \tag{2.10}$$

2.4 Interconnected LTI Systems

In Chapters 5 and 6, so-called interconnected systems that are assemblies of coupled subsystems will be considered, which will be defined in more detail in Chapter 4. We will use tools from robust control, which allows us to exploit the system structure to reduce the complexity of the controller synthesis. In the following, we briefly introduce the required tools.

2.4.1 LFR of an Interconnected System

We consider the interconnection of system $\mathcal{G}^d$ with $\mathcal{P}$ as illustrated in Figure 2.2. This interconnection has the same structure as usually encountered in robust control or linear-parameter-varying (LPV) control. In these cases, $\mathcal{P}$ is an uncertainty or a system part that depends on time-varying parameters, usually denoted as Δ. We will use this system structure to model interconnected systems, which are assemblies of coupled subsystems. In this case, $\mathcal{G}^d$ represents the decentralized system part, and $\mathcal{P}$ is introduced as an interconnection operator, which is assumed to be a static linear operator, i.e., a matrix, in the following. The interconnection of system $\mathcal{G}^d$ with $\mathcal{P}$ can be described by a linear

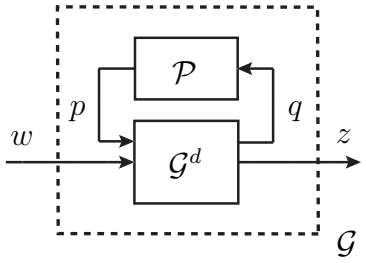

Figure 2.2: Interconnection of system $\mathcal{G}^d$ with $\mathcal{P}$.

fractional representation (LFR) given as

$$\mathcal{G}: \begin{cases} \mathcal{G}^d \left\{ \begin{bmatrix} \dot{x}^c \\ \hdashline z \\ \hdashline q^c \end{bmatrix} = \left[\begin{array}{c:cc} \mathcal{A} & \mathcal{B}_1 & \mathcal{B}_2 \\ \hdashline \mathcal{C}_1 & \mathcal{D}_{11} & \mathcal{D}_{12} \\ \hdashline \mathcal{C}_2 & \mathcal{D}_{21} & \mathcal{D}_{22} \end{array}\right] \begin{bmatrix} x^c \\ \hdashline w \\ \hdashline p^c \end{bmatrix}, \right. \\ p^c = \mathcal{P} q^c. \end{cases} \tag{2.11}$$

2.4.2 Full Block S-Procedure

In order to exploit the structure of the system in (2.11), the Full Block S-Procedure (FBSP) can be applied, which is a tool from robust control and LPV control. In these cases, interconnections of systems with uncertainties or with time-varying parameter dependencies are analyzed. In the case of system (2.11), the interconnection operator $\mathcal{P}$ plays the role of the uncertainty. The FBSP for the system in (2.11) is given as follows.

Theorem 2.1 ([25]: Bounded Real Lemma with Full Block S-Procedure)**.** *Given the stable continuous-time LTI system as in* (2.11)*, the system has an $\mathcal{L}_2$-gain from w to z smaller than γ if and only if there exist matrices $\mathcal{X} = \mathcal{X}^\top > 0$, $R = R^\top$, $Q = Q^\top$ and S of appropriate dimensions such that*

$$\left[\star\right]^\top \begin{bmatrix} Q & S \\ S^\top & R \end{bmatrix} \begin{bmatrix} \mathcal{P} \\ I \end{bmatrix} > 0, \tag{2.12}$$

$$\left[\star\right]^\top \left[\begin{array}{cc:cc:cc} 0 & \mathcal{X} & 0 & 0 & 0 & 0 \\ \mathcal{X} & 0 & 0 & 0 & 0 & 0 \\ \hdashline 0 & 0 & -\gamma^2 I & 0 & 0 & 0 \\ 0 & 0 & 0 & I & 0 & 0 \\ \hdashline 0 & 0 & 0 & 0 & Q & S \\ 0 & 0 & 0 & 0 & S^\top & R \end{array}\right] \left[\begin{array}{ccc} I & 0 & 0 \\ \mathcal{A} & \mathcal{B}_1 & \mathcal{B}_2 \\ \hdashline 0 & I & 0 \\ \mathcal{C}_1 & \mathcal{D}_{11} & \mathcal{D}_{12} \\ \hdashline 0 & 0 & I \\ \mathcal{C}_2 & \mathcal{D}_{21} & \mathcal{D}_{22} \end{array}\right] < 0. \tag{2.13}$$

Equations (2.12) and (2.13) in Theorem 2.1 are referred to as multiplier and nominal conditions, respectively.

The matrices Q, R, and S in the conditions in Theorem 2.1 are called the multiplier matrices. For full multipliers, i.e., with no assumptions on Q, R, and S, the conditions in Theorem 2.1 are equivalent to the ones in Lemma 2.1, i.e., they represent necessary and sufficient conditions for Lemma 2.1 to be satisfied.

In contrast to full block multipliers, structural conditions can be imposed, similar to the so-called D scalings and DG scalings in robust control. For D scalings, it is assumed that $R > 0$, $Q = -R$ and $S = 0$, and for DG scalings it is assumed that $R > 0$, $Q = -R$ and $S = -S^\top$. In the case of D scalings, it is easy to see that for $|\mathcal{P}| < 1$ and $R\,\mathcal{P} = \mathcal{P}\,R$, (2.12) holds. And for DG scalings, the same is true with the additional assumptions of $S\,\mathcal{P} = \mathcal{P}\,S$ and $\mathcal{P} = \mathcal{P}^\top$. The FBSP with full multipliers will be used in Chapters 5 and 6 in order to exploit the sparse structure of interconnected system matrices in the controller synthesis.

CHAPTER 3

Convex and Numerical Optimization

This chapter gives a brief overview about formulations and tools from convex and numerical optimization which will be relevant in the course of this thesis.

3.1 Function Definitions

Definition 3.1 (Convex Function)**.** *A function $f(\cdot) : \mathcal{D} \mapsto \mathbb{R}$ is convex if its domain $\mathcal{D} \subseteq \mathbb{R}^n$ is a convex set and if for any $x_1, x_2 \in \mathcal{D}$ and any $\lambda \in [0, 1]$, it holds that*

$$f(\lambda\, x_1 + (1 - \lambda)x_2) \leq \lambda f(x_1) + (1 - \lambda) f(x_2). \tag{3.1}$$

The function is called strictly convex if inequality (3.1) is strict for any $x_1, x_2 \in \mathcal{D}$ and any $\lambda \in [0, 1]$.

Definition 3.2 (Concave Function)**.** *A function $f(\cdot) : \mathcal{D} \mapsto \mathbb{R}$ is concave if the function $-f(x)$ is convex.*

Definition 3.3 (Lipschitz Continuous Function)**.** *A function $f(\cdot) : \mathcal{D} \mapsto \mathbb{R}$ with domain $\mathcal{D} \subseteq \mathbb{R}^m$ is Lipschitz continuous if there exists a constant $\gamma > 0$, such that for all $x_1, x_2 \in \mathcal{D}$, the following holds:*

$$\|f(x_1) - f(x_2)\|_2 \leq \gamma \, \|x_1 - x_2\|_2. \tag{3.2}$$

Definition 3.4 (Monotone Function [26])**.** *A set function $f : 2^E \to \mathbb{R}$ is monotone, if for every $T_1 \subseteq T_2 \subseteq E$, it holds that*

$$f(T_1) \leq f(T_2).$$

Definition 3.5 (Submodular Function [26])**.** *A set function $f : 2^E \to \mathbb{R}$ is submodular, if for every $T_1, T_2 \subseteq E$, it holds that*

$$f(T_1 \cap T_2) + f(T_1 \cup T_2) \leq f(T_1) + f(T_2).$$

Equivalently, a set function $f : 2^E \to \mathbb{R}$ is submodular, if for every $T_1 \subseteq T_2 \subseteq E$, and $e \in E \setminus T_2$, it holds that

$$f(T_1 \cup \{e\}) - f(T_1) \geq f(T_2 \cup \{e\}) - f(T_2).$$

This definition shows a diminishing returns property, i.e., increasing a set argument T_2 by an element e cannot give a larger increase than increasing a subset of the set argument $T_1 \subset T_2$ by e. The expression $f(T_1 \cup \{e\}) - f(T_1)$ is also referred to as the marginal gain of the function f at T_1 with respect to e.

3.2 Terminology in Optimization

A mathematical optimization problem consists of a cost function $f(\cdot) : \mathbb{R}^n \mapsto \mathbb{R}$, and a constraint set $\mathcal{S} \in \mathbb{R}^n$ in which the argument of the cost function is constrained to lie. The objective is to find a feasible decision $x \in \mathcal{S}$ which minimizes the cost $f(x)$. This is denoted as the program

$$\begin{aligned} \min_{x} \quad & f(x) \\ \text{s.t.} \quad & x \in \mathcal{S}. \end{aligned} \tag{3.3}$$

A feasible decision which has the minimum cost is denoted as a minimizer x^*. The problem is called feasible if the set $\mathcal{S}$ is non-empty, otherwise it is called infeasible. Similarly, the point x is called feasible if $x \in \mathcal{S}$, and otherwise it is infeasible. If $\mathcal{S} = \mathbb{R}^n$ the problem is unconstrained. It is called unbounded if for any $M > 0$ there exists a point $x \in \mathcal{S}$ such that $f(x) < -M$. A point x^* is a global minimizer if $f(x^*) \leq f(x)$ for all $x \in \mathcal{S}$. A point x^* is a (strict) local minimizer if there exists a neighborhood $\mathcal{N}(x^*)$ of x^* such that $f(x^*) \leq (<) f(x)$ for all $x \in \mathcal{N}(x^*) \cap \mathcal{S}$. For general cost functions and constraint sets, the optimization problem (3.3) can be hard to solve. Efficient solution methods exist for some common classes of convex optimization problems which will be of relevance in the course of this work. Therefore, they are introduced in the following.

3.3 Convex Optimization Problems

A significant advantage of convex optimization problems is that any local minimizer is also a global minimizer. Some common convex optimization problems which are relevant for this thesis are introduced in the following. For these classes of problems efficient solvers exist. For further details, the reader is referred to [27].

3.3.1 Quadratic Program

A quadratic Program (QP) has a quadratic cost function that is to be minimized subject to affine inequality constraints. A possible representation is the following,

$$\begin{aligned} \min_{x} \quad & x^\top H x + c^\top x \\ \text{s.t.} \quad & Ax = b, \\ & Cx \leq d, \end{aligned} \tag{3.4}$$

where $H \in \mathbb{R}^{n \times n}$ is required to be positive semi-definite in order for the program to be convex. If H is positive definite the program is strictly convex.

3.3.2 Linear Regression and Least-Squares

An example of a QP with a wide range of application is the so-called linear least-squares problem, or linear regression problem. The objective is to minimize the convex quadratic function

$$\min_{x} \ \|Ax - b\|_2^2.$$

If the problem is unconstrained, it can be solved analytically as $x^* = A^\dagger b$. However, if affine equality and inequality constraints are added, it no longer has an analytical solution. This problem will be of relevance in Chapter 11.

3.3.3 Second-Order Cone Program

A second-order cone program (SOCP) is characterized through a linear cost function that is to be minimized, subject to second-order cone constraints. The standard second-order cone of dimension n is defined as

$$\mathcal{K}_n = \left\{ \begin{bmatrix} v \\ t \end{bmatrix} \,\middle|\, v \in \mathbb{R}^{n-1}, t \in \mathbb{R}, \|v\|_2 \leq t \right\}. \tag{3.5}$$

An SOCP can be written as

$$\begin{aligned} \min_{x} \quad & c^\top x \\ \text{s.t.} \quad & Ax = b, \\ & \|P_i x + q_i\|_2 \leq r_i^\top x + s_i, \quad i = 1, ..., N, \end{aligned} \tag{3.6}$$

where $P_i \in \mathbb{R}^{(n_i-1) \times n}$, $q_i \in \mathbb{R}^{n_i-1}$, $r_i \in \mathbb{R}^n$ and $s_i \in \mathbb{R}$ form a second-order cone constraint of dimension n_i, which can equivalently be written as $\begin{bmatrix} P_i \\ r_i^\top \end{bmatrix} x + \begin{bmatrix} q_i \\ s_i \end{bmatrix} \in \mathcal{K}_{n_i}$. For more details on SOCPs the reader is referred to [28]. SOCPs will be of relevance in Chapters 10 and 12.

3.3.4 Semi-Definite Program

A semi-definite program (SDP) consists of a linear cost function that is to be minimized, subject to linear matrix inequality (LMI) constraints. It can be represented as

$$\begin{aligned} \min_{x} \quad & c^\top x \\ \text{s.t.} \quad & M_0 + \sum_{i=1}^{n} x_i M_i \geq 0, \end{aligned} \tag{3.7}$$

where $x_i \in \mathbb{R}$, $x = [x_1, ..., x_n]^\top \in \mathbb{R}^n$ and $M_i \in \mathbb{R}^{n \times n}, \forall i = 1, ..., n$. The constraint is an LMI and the left-hand side is thus constrained to be positive semi-definite. As the set of positive semi-definite matrices is a convex cone, SDPs are convex programs.

A variety of problems in control and system theory can be formulated as or relaxed to convex problems that involve LMIs. While for only some of these problems analytical solutions exist, they can be efficiently solved numerically, for example by interior-point methods [29]. The reader is referred to [24], [30] for an overview of LMIs and their applications in control and system theory. In this thesis, LMIs will be of importance in Chapters 5 and 6.

3.4 Lagrangian Duality

The general optimization problem in (3.3) can take the form

$$\begin{aligned} \min_{x} \quad & f(x) \\ \text{s.t.} \quad & h(x) = 0, \\ & g(x) \leq 0, \end{aligned} \tag{3.8}$$

where $f(x)$ is assumed to be bounded below, and the equality and inequality constraint functions, $h(x) : \mathbb{R}^n \mapsto \mathbb{R}^m$ and $g(x) : \mathbb{R}^n \mapsto \mathbb{R}^p$, respectively, are allowed to be non-convex. The so-called Lagrangian of (3.8) is defined as

$$\mathcal{L}(x, \nu, \lambda) = f(x) + \lambda^\top h(x) + \nu^\top g(x), \tag{3.9}$$

where ν and λ are referred to as Lagrange multipliers or dual multipliers.

The associated dual program of (3.8) is defined as

$$\max_{\nu \geq 0, \lambda} \quad d(\nu, \lambda), \tag{3.10}$$

with

$$d(\nu, \lambda) = \min_{x} \mathcal{L}(x, \nu, \lambda).$$

The dual function is a pointwise minimum over affine functions in the Lagrange multipliers ν and λ, and is thus a concave function. For primal feasible points $\bar{x}$, the

Lagrangian with $\nu \geq 0$ is a lower bound on the primal function value, i.e., $\mathcal{L}(\bar{x}, \lambda, \nu) \leq f(\bar{x}),\ \forall(\bar{x} \in \mathcal{S}, \nu \geq 0, \lambda)$. This implies that also the dual function is an under-estimator of the primal function value, i.e., $d(\nu, \lambda) = \min_x \mathcal{L}(x, \nu, \lambda) \leq f(x),\ \forall(x \in \mathcal{S}, \nu > 0, \lambda)$. In particular, the maximum of the dual problem in (3.10) always provides a lower bound on the minimum of the primal problem. If the maximum of the dual problem is equal to the minimum of the primal problem, so-called strong duality holds.

3.5 Distributed Optimization

If large-scale optimization problems are considered, first-order methods are particularly efficient. The computations in the iterations are typically inexpensive and can be executed in a distributed manner if the problem has some structure that can be exploited for its decomposition. Numerous methods for distributed optimization exist in the literature. For a comprehensive overview, the reader is referred to [31]. In this thesis, the Alternating Direction Method of Multipliers (ADMM) is chosen due to its fast convergence in practice.

3.5.1 Alternating Direction Method of Multipliers

The Alternating Direction Method of Multipliers (ADMM) is a Lagrangian based first-order method. It relies on a splitting of the optimization variables in order to decompose the problem into subproblems, which exhibit some (ideally sparse) coupling.

In this thesis, the consensus form ADMM is used in Chapters 5 and 11. It is assumed that a partitioning of the so-called global optimization variable vector $x = [x_1^\top, ..., x_N^\top]^\top \in \mathbb{R}^n$ into N global variable vectors $x_i \in \mathbb{R}^{n_i}$ associated with N subproblems is possible. The constraint set $\mathcal{S}$ is assumed to be decomposable into N constraint sets $\mathcal{S}_i$ which only depend on so-called local variables y_i. The objective function is decomposable into a sum of N objective functions that depend on only the local variables y_i, i.e., $f(x) = \sum_{i=1}^N f_i(y_i)$. In the consensus ADMM, the local variables y_i usually contain copies of entries of the global variable vector x. This introduces equality constraints, the so-called consensus constraints. The decomposed problem can be written in the form

$$\begin{aligned} \min_{x, y_1, ..., y_N} \quad & \sum_{i=1}^N f_i(y_i) \\ \text{s.t.} \quad & y_i \in \mathcal{S}_i, \quad \forall i = 1, ..., N, \\ & y_i = E_i x, \quad \forall i = 1, ..., N, \end{aligned} \tag{3.11}$$

where E_i are selector matrices, which for each local variable y_i select entries from the global variables of the vector x.

For ADMM the so-called augmented Lagrangian is of importance. It is denoted by $\mathcal{L}_\rho$ and is defined similarly to the Lagrangian in (3.9), with an additional quadratic term. The augmented Lagrangian for problem (3.11) is given as

$$\mathcal{L}_\rho(x, y, \lambda) = \sum_{i=1}^{N} \left(f_i(y_i) + \mathcal{I}_{\mathcal{S}_i}(y_i) + \lambda_i^\top (y_i - E_i x) + \frac{\rho}{2} \|y_i - E_i x\|_2^2 \right), \tag{3.12}$$

where $\mathcal{I}_{\mathcal{S}_i}(y_i)$ is the indicator function for the constraint $y_i \in \mathcal{S}_i$, and $\rho > 0$ is the so-called penalty parameter. This decomposition of the augmented Lagrangian into the sum $\mathcal{L}_\rho(x, y, \lambda) = \sum_{i=1}^{N} \mathcal{L}_{\rho,i}(x, y_i, \lambda)$ in (3.12) is possible due to the problem structure in (3.11). The individual terms $\mathcal{L}_{\rho,i}$ are referred to as the partial or local augmented Lagrangians.

ADMM is an iterative minimization scheme for computing a saddle point of the augmented Lagrangian. The distributed consensus ADMM steps are given in Algorithm 3.1. Often, the minimization step in x can be simplified by exploiting the (potentially sparse)

Algorithm 3.1 Distributed Consensus ADMM [32].

1: **Input:** Parameter $\rho > 0$,
2: **Initialization**: Set $\kappa = 0$, $\lambda^{(0)} = 0$, $x^{(0)} = 0$,
3: **while** *primal, dual residuals not converged* **do**
4: $\quad y_i^{(\kappa+1)} = \underset{y_i}{\operatorname{argmin}}\ \mathcal{L}_{\rho,i}(y_i, x^{(\kappa)}, \lambda^{(\kappa)}), \qquad \forall i = 1, ..., N,$
5: $\quad x^{(\kappa+1)} = \underset{x}{\operatorname{argmin}} \sum_{i=1}^{N} \mathcal{L}_{\rho,i}(y_i^{(\kappa+1)}, x, \lambda_i^{(\kappa)}),$
6: $\quad \lambda_i^{(\kappa+1)} = \lambda_i^{(\kappa)} + \rho(y_i^{(\kappa+1)} - E_i\, x^{(\kappa+1)}), \quad \forall i = 1, ..., N,$
7: $\quad \kappa = \kappa + 1,$
8: **end**

coupling structure of the subproblems. Furthermore, the λ-update step is only coupled through the $E_i x$ terms. Some communication between coupled subproblems is required for the steps in line 5 and 6 in Algorithm 3.1, however.

If the cost functions $f_i(y_i)$ are closed, proper and convex, and the unaugmented Lagrangian has a saddle point, i.e., there exists a point (x^*, y^*, λ^*), such that $\mathcal{L}_\rho(x^*, y^*, \lambda) \leq \mathcal{L}_\rho(x^*, y^*, \lambda^*) \leq \mathcal{L}_\rho(x, y, \lambda^*)$ [32], and if additionally local solutions to the x and y_i update steps in line 4 and 5 of Algorithm 3.1, respectively, exist [33], then strong duality holds for the problem. In this case, the cost function $\sum_{i=1}^{N} f_i(y_i)$ asymptotically converges to the primal optimum [32]. As convergence criteria, the so-called primal and dual residuals can be defined as $r_i^{(\kappa+1)} = E_i x^{(\kappa+1)} - y_i^{(\kappa+1)}$ and $s_i^{(\kappa+1)} = \rho E_i (x^{(\kappa+1)} - x^{(\kappa)})$, respectively, which asymptotically converge to zero. Note that the cost function does not need to be differentiable. In particular, the cost function can contain indicator functions of closed nonempty convex sets.

3.6 Optimality Conditions

The following results are used to characterize a solution of an optimization problem.

3.6.1 Linear Independence Constraint Qualifications

Given the optimization problem in (3.8), the active constraint set at a point $\bar{x}$ is defined as the union of the set of all equality constraints and the set of those inequality constraints that are active at $\bar{x}$, i.e., that hold with equality at the point $\bar{x}$.

Definition 3.6. *Let us consider the optimization problem* (3.8). *Given a point* $\bar{x}$ *and the active constraint set at that point* $\bar{x}$*, then the linear independence constraint qualification (LICQ) holds if the set of active constraint gradients* $\{\nabla h_i(x), i = 1, ..., m\} \cup \{\nabla g_j(x),\, j \mid g_j(x) = 0\}$ *is linearly independent.*

The LICQ implies that at a feasible point, the set of first-order feasible directions coincide with the tangent cone of the feasible constraint set.

3.6.2 Karush-Kuhn-Tucker Conditions

The first-order necessary optimality conditions for problem (3.8) with the Lagrangian defined in (3.9) are the following:

$$\begin{aligned} \nabla_x \mathcal{L}(x, \lambda, \nu) &= 0, \\ h(x) &= 0, \\ g(x) &\leq 0, \\ \nu_i g_i(x) &= 0, \quad \forall i = 1, ..., p, \\ \nu &\geq 0, \end{aligned} \tag{3.13}$$

where ν and λ are the Lagrange multipliers as introduced before. The conditions in (3.13) are known as the Karush-Kuhn-Tucker (KKT) conditions. They imply stationarity, primal and dual feasibility, and complementary slackness. If the constraint $\nu_i g_i(x) = 0$ is such that exactly one of the values, ν_i or $g_i(x)$ are zero, then strict complementarity holds. Together with the LICQ, these conditions guarantee that the optimal dual multipliers λ^*, ν^* are unique.

3.7 Numerical Optimization: Line Search Methods in Unconstrained Optimization

Except for special problems, finding an analytical solution of an optimization problem is in general not possible. Therefore, numerical methods are employed to find an approx-

imate solution in an iterative manner. Typically, a sequence of iterates is constructed that starts from an initial point and terminates at an approximate minimizer in a finite number of iterations. A necessary assumption is that the problem is feasible and tractable for the chosen optimization algorithm. In Chapter 12, line search methods will be used. For simplicity, let us consider an unconstrained problem as in (3.3) with $\mathcal{S} = \mathbb{R}^n$. Then, line search methods consist of iterations where first a descent direction is computed at the current iterate and then a step length is chosen. The iterations are given as

$$x^{\kappa+1} = x^{\kappa} + \alpha^{\kappa}\Delta x^{\kappa}, \tag{3.14}$$

with the chosen step length $\alpha^{\kappa} > 0$ and the descent direction Δx^{κ} of iteration κ. The descent direction is often chosen as

$$\Delta x^{\kappa} = -B(x^{\kappa})^{-1}\nabla f(x^{\kappa}), \tag{3.15}$$

with $B(x^{\kappa})$ being a symmetric and nonsingular matrix. For example, in the steepest descent method, $B(x^{\kappa})$ is the identity matrix, i.e., the descent direction is chosen to be the negative gradient of the cost function.

3.7.1 Newton's Method for Unconstrained Optimization

In Newton's method, the term $B(x^{\kappa})$ in (3.15) is motivated by a Taylor approximation and coincides with the Hessian, i.e., the descent direction Δx^{κ} is computed by solving

$$\nabla^2 f(x^{\kappa})\Delta x^{\kappa} = -\nabla f(x^{\kappa}). \tag{3.16}$$

However, the computation of the exact Hessian can be computationally expensive. Methods with inexact Hessian approximations, such as the Gauss-Newton method, can be used instead. Necessary assumptions for the application of the Newton method are that the problem is strongly convex, i.e., the Hessian is positive definite, and the cost function is Lipschitz continuous with a small Lipschitz constant, such that the Taylor approximation represents a good approximation of the problem. Then, a quadratic convergence rate can be reached by this method.

3.7.2 Gauss-Newton Method for Unconstrained Nonlinear Least-Squares

The cost function is considered to be the following nonlinear least squares problem

$$f(x) = \frac{1}{2}\sum_{i=1}^{N} r_i^2(x), \tag{3.17}$$

where $r_i(x)$ are the so-called residuals. The Gauss-Newton (GN) method differs from the Newton method by the approximation of the Hessian

$$\nabla^2 f(x^\kappa) \cong \nabla r(x^\kappa)^\top \nabla r(x^\kappa), \tag{3.18}$$

where $\nabla r(x^\kappa)$ is the Jacobian of $r(x) = [r_1(x), ..., r_N(x)]^\top$ with respect to x. A GN step is thus computed by solving

$$\nabla r(x^\kappa)^\top \nabla r(x^\kappa)\, \Delta x^\kappa = -\nabla f(x^\kappa). \tag{3.19}$$

The advantage of the GN method is that no exact Hessian information is required. In problems where the second order term in the Hessian is small, i.e., where the residuals $r_i(x^\kappa)$ are nearly affine or small, the approximation is close to the real Hessian and the convergence rate is similar to Newton's method. Furthermore, if the Jacobian $\nabla r(x^\kappa)$ has full rank and the gradient $\nabla f(x^\kappa)$ is non-zero, the GN direction is always a descent direction. This can be seen by first noting that $\nabla f(x^\kappa) = \nabla r(x^\kappa)^\top r(x^\kappa)$, which we then use, together with (3.19), to derive the following relation,

$$\begin{aligned} \Delta x^{\kappa\top} \nabla f(x^\kappa) &= \Delta x^{\kappa\top} \nabla r(x^\kappa)^\top x^\kappa \\ &= -\Delta x^{\kappa\top} \nabla r(x^\kappa)^\top \nabla r(x^\kappa) \Delta x^\kappa \\ &= -\|\nabla r(x^\kappa) \Delta x^\kappa\|_2^2 \leq 0. \end{aligned} \tag{3.20}$$

The last inequality is strict unless $\nabla r(x^\kappa)\Delta x^\kappa = 0$. In that case, with the assumption of $\nabla r(x^\kappa)$ being full rank, we have that $\nabla f(x^\kappa) = 0$, and x^κ thus is a stationary point.

Alternatively to solving (3.19), the GN direction can also be computed by solving the problem

$$\min_{\Delta x^\kappa} = \frac{1}{2}\|r(x^\kappa) + \nabla r(x^\kappa)\Delta x^\kappa\|. \tag{3.21}$$

The reader is referred to [34] for more details and related proofs. This method is exploited in Chapter 12.

3.7.3 Backtracking Line Search

In order to determine a step length α^κ, different methods can be used. If an unconstrained problem is considered, the line search needs to ensure that sufficient progress is made in terms of a sufficient decrease in the cost. If a constrained optimization problem is considered, the line search additionally needs to guarantee that the iterates do not become "too infeasible". In constrained optimization, the line search is therefore performed on a merit function $\Phi(x)$ which consists of a penalty term for the cost and a penalty term for the infeasibility of the point x. In general, computing an exact step length, i.e., computing the solution to the problem

$$\alpha^* = \min_\alpha \Phi(x^\kappa + \alpha \Delta x^\kappa) \tag{3.22}$$

is expensive. Inexact line search methods can be used instead. Such inexact methods aim at computing "good" step lengths α that satisfy conditions guaranteeing sufficient progress. A common inexact line search method is the so-called backtracking line search. Starting from the unit step length, i.e., $\alpha = 1$, the step length is iteratively reduced by a factor ρ with $0 < \rho < 1$, until some conditions for sufficient progress of the next iterate $x^\kappa + \alpha\Delta x^\kappa$ are satisfied. These conditions can for example be the so-called Wolfe conditions described in the following.

3.7.4 Wolfe Conditions

Wolfe conditions are commonly used conditions to determine the step lengths in inexact line search and are defined as follows

$$\begin{aligned} f(x^\kappa + \alpha^\kappa \Delta x^\kappa) &\leq f(x^\kappa) + c_1 \alpha^\kappa \nabla f(x^\kappa)^\top \Delta x^\kappa, \\ \nabla f(x^\kappa + \alpha^\kappa \Delta x^\kappa)^\top \Delta x^\kappa &\geq c_2 \nabla_x f(x^\kappa)^\top \Delta x^\kappa, \end{aligned} \tag{3.23}$$

with $0 < c_1 < c_2 < 1$. The first condition, the so-called Armijo's condition ensures a sufficient decrease in the cost, and the second condition ensures that the step length is large enough. While in (3.23), the Wolfe conditions are given in terms of the cost function $f(x)$, in constrained optimization, they usually need to be satisfied for a merit function $\Phi(x)$, as discussed before.

3.7.5 Convergence of the Gauss-Newton Iteration

The following assumptions are required for convergence of the GN-iteration from Section 3.7.2 to a stationary point of $f(x)$. The Jacobians $\nabla r(x^\kappa)$ are assumed to have their singular values uniformly bounded away from zero in the region of interest, i.e., $\exists\, \gamma > 0$ such that $\|\nabla r(x^\kappa)\Delta x^\kappa\|_2 \geq \gamma \|\Delta x^\kappa\|_2$ for all Δx^κ and for all x^κ in a neighborhood of the bounded level set $L = \{x^\kappa \mid f(x^\kappa) \leq f(x^0)\}$ with x^0 the starting point of the iteration. Furthermore, f is assumed to be bounded below and continuously differentiable in an open set containing the level set L. The residual functions $r_i(x^\kappa)$ are assumed to be Lipschitz continuously differentiable in a neighborhood of the bounded level set L, which implies that $\nabla f(x^\kappa)$ is Lipschitz continuous in some neighborhood of L. Then, the iterates x^κ generated by the GN-method with step lengths α^κ satisfiying the Wolfe conditions in (3.23), converge to a stationary point of $f(x^\kappa)$, i.e., it holds that $\lim_{k\to\infty} \nabla r(x^\kappa)^\top x^\kappa = 0$.

A sketch of the proof is the following. The GN direction Δx^κ is guaranteed to be a descent direction as noted in (3.20). Then, the proof consists of showing that the angle between the search direction Δx^κ and the negative gradient $-\nabla f(x^\kappa)$ is uniformly bounded away from $\frac{\pi}{2}$. Next, the so-called Zoutendijk condition implies that the gradient norms converge to zero since the search directions are not too close to orthogonality with

the gradient. For the detailed proof, the reader is referred to the proof of Theorem 10.1 in [34].

3.8 Sequential Quadratic Programming

Let us consider problem (3.8) again where $f(x)$, $g(x)$ and $h(x)$ are allowed to be non-convex. A possible solution method for the problem is Sequential Quadratic Programming (SQP). This algorithm generates a sequence of iterates by solving QPs. The QPs are approximations of the original optimization problem (3.8) at the current iterate. At iteration κ, the following QP is solved

$$\begin{aligned} \min_{\Delta x} \quad & \frac{1}{2}\Delta x^\top H^\kappa \Delta x + \nabla f(x^\kappa)^\top \Delta x \\ \text{s.t.} \quad & h(x^\kappa) + \nabla h(x^\kappa)^\top \Delta x = 0, \\ & g(x^\kappa) + \nabla g(x^\kappa)^\top \Delta x \leq 0, \end{aligned} \tag{3.24}$$

where H^κ is the Hessian of the Lagrangian or an approximation thereof. The sequence of iterates is then updated according to

$$x^{\kappa+1} = x + \alpha^\kappa \Delta x^\kappa, \tag{3.25}$$

where α^κ is a step size that, for example, satisfies the Wolfe conditions for a chosen merit function, and Δx^κ is the minimizer of (3.24). Some assumptions on regularity and boundedness of H^κ, f, g, h and their first and second derivatives need to be satisfied in order to guarantee convergence. The reader is referred to [35] for details. Chapter 12 will introduce an SQP variant with feasible iterates and convergence is shown in Section 12.2.

Part II

Distributed Control of Interconnected Systems

CHAPTER 4

Introduction to Interconnected Systems

This chapter gives an introduction to the topic of interconnected systems and a literature review about related work. Then, an overview about the contributions of Part II of this thesis is provided.

4.1 Interconnected Systems

Interconnected systems refer to systems that can be modeled as an ensemble of multiple subsystems which can be interconnected in different ways. In particular, the interconnections can be related to coupling in the dynamics, to a common task, i.e., a performance objective, or to sensing or communication.

Multi-agent systems (MAS) [36], [37] are a subclass of interconnected systems. The subsystems, or agents, are usually dynamically decoupled, as for example in groups of autonomous robots, formations of unmanned aerial vehicles (UAVs), satellites, underwater vehicles or vehicle platoons. In cooperative robotics, coupling forces may, however, arise through the manipulation of objects that can be interpreted as a coupling of the dynamics.

4.1.1 Cooperative Multi-Robot Systems in Digital Fabrication

Large-scale interconnected systems offer the potential of performing complex tasks while the system can be an assembly of simple subsystems. This gives multi-robot systems the potential to perform automated fabrication tasks in construction processes. In particular, complex tasks for constructing buildings, such as the manipulation of heavy or large objects, can be achieved by cooperative multi-robot systems [9].

Articulated robots, such as robotic arms with several rotary joints are often used for manipulation tasks. Even though they have highly nonlinear dynamics [38], [39], usually a hierarchical control architecture is used for manipulation tasks, where local lower-level controllers of the individual robots perform a feedback linearization. Lower-

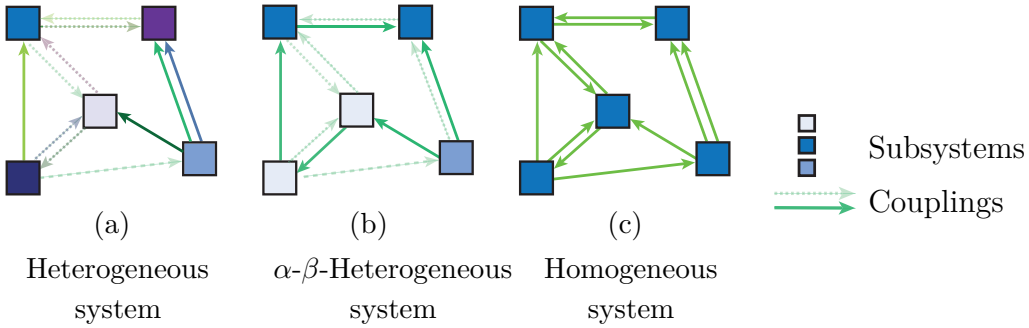

Figure 4.1: Classification of subsystems and interconnections with respect to homogeneity. Different box colors, and different arrow types symbolize different subsystems and different interconnections, respectively.

level impedance controllers, for instance, transform the closed-loop dynamics into virtual mass-spring damper systems [40]. This enables the control of the ratio between the force and the position of the end-effectors which is beneficial in two aspects: For the control task, it prevents from exerting high end-effector forces in the presence of uncertainties in the cooperation. For the higher-level control design, the robotic arm can be modeled as a linear time-invariant (LTI) system. This work therefore focuses on interconnected LTI subsystems which can be physically coupled as for example in cooperative manipulation tasks. More details about the subsystems and the interconnections are given in the following.

4.1.2 Classification of Subsystems and Interconnections

In this work, systems that consist of N interconnected finite-dimensional LTI subsystems are considered. While a homogeneous system consists of identical subsystems and identical interconnections, a heterogeneous system consists of subsystems and interconnections which may all be different. In Chapter 5, a new characterization of systems that parametrizes the structure of the interconnection is proposed, which is referred to as α-β-heterogeneous systems. They consist of α groups of homogeneous subsystems with β different types of interconnections. The different classes of systems are illustrated in Figure 4.1. We will refer to neighbors of a subsystem as those subsystems to which it is coupled.

4.1.3 Controller Architectures

Different approaches for the control of interconnected systems have been proposed. A centralized approach is able to find optimal control inputs by exploiting the full information about the system. However, the complexity, large scale and spatial distribution of

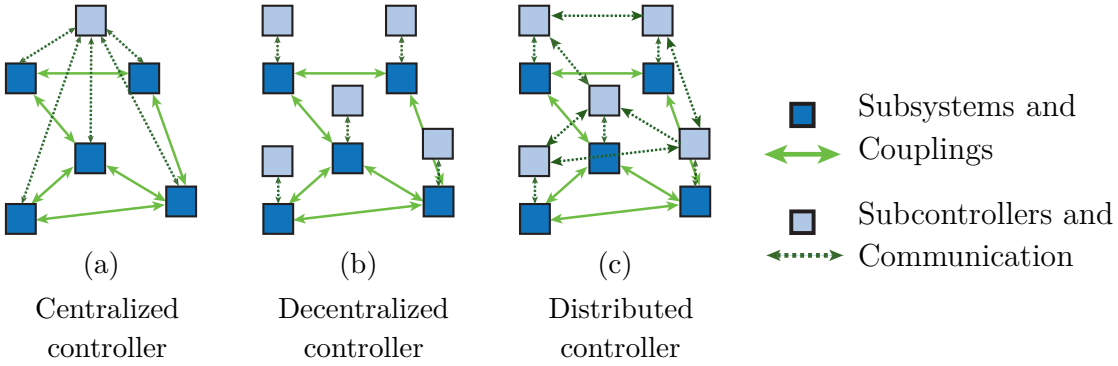

Figure 4.2: Classification of controller architectures for an examplary interconnected system. Centralized control unit (a) and subcontrollers without (b) and with (c) communication to neighboring subcontrollers.

such systems make the control by a central unit intractable. In contrast, a decentralized approach, where each subsystem has an individual subcontroller which computes its inputs based on local information, has less computational requirements [41], [42]. However, depending on the system and the task, the control performance may be unsatisfying. As a remedy to the downsides of both centralized and decentralized approaches, distributed architectures have been proposed [43], [44], where the subsystems have local sensing, control, and communication capacities. In contrast to decentralized control, communication between neighboring subcontrollers is introduced in distributed control to account for the coupling of the system and to increase the control performance. The different controller architectures are illustrated in Figure 4.2.

4.1.4 Challenges and Open Problems

In both the distributed controller synthesis and the implementation major open challenges exist. Distributed control design is a non-trivial task because of informational constraints [45]–[47], possible heterogeneity of the systems, and the coupling through dynamics, constraints or the objective. Furthermore, if large-scale systems are considered, centralized synthesis methods become computationally intractable. If the problem is solved in a distributed way, many design choices concerning the decomposition of the system or the communication topology need to be made. These choices imply a trade-off between the computational effort, the amount of communication and the achievable performance. In decentralized control schemes, so-called fixed modes can prevent the stabilizability of the system or limit the achievable performance [48], [49], which makes a minimum of communication necessary.

Some proposed algorithms rely on a distributed optimization that is performed online, or on information about future trajectories of neighboring subsystems, which requi-

res extensive communication [50], [51]. In many applications, however, communication between the subsystems however is unreliable, delayed, or restricted, which makes distributed control methods that rely on extensive communication schemes intractable. Examples of such applications are autonomous underwater vehicles, spacecraft formations, mining, or any applications with limited bandwidth and a large number of agents [52], [53]. Challenges related to the unreliability of communication potentially also arise on the construction site. They can be caused by missing infrastructure, by obstructions due to iron reinforced walls, or by disturbances from electromagnetic radiation, e.g., originating from welding processes.

4.2 Related Work

This section provides an overview of the state-of-the-art approaches for the topics related to the first part of this thesis. Specifically, related work on distributed control of complex interconnected systems, overlapping control, and decentralized fixed modes is presented. This overview is not exhaustive. The particular focus lies on approaches that will be relevant in the course of this work.

4.2.1 Modeling Approaches for Interconnected Systems

As large-scale distributed systems in general have high-dimensional state, input and output spaces, a centralized state-space representation is prohibitive and not useful for a scalable controller synthesis. In fact, the modeling of interconnected systems is closely linked to the distributed controller synthesis. Therefore, it is beneficial to model distributed systems as interconnected systems composed of a decentralized part and an interconnection part. The decentralized part is the ensemble of the individual subsystems, and the interconnection part can be modeled through an interconnection operator.

A general representation based on a linear fractional representation (LFR) of the system has been introduced by [54] and [55] for gain-scheduled and decentralized controller design, respectively, and later on has been used in [56] and [57] for distributed control design. In [43], [44], [58] similar models have been used to represent spatially interconnected systems by means of spatial shift operators. In these approaches, distributed controllers of heterogeneous systems over undirected graphs are synthesized, where the interconnection structure of the controller is assumed to be equal to the one of the plant.

In [59], [60] so-called decomposable systems are introduced, which can be modeled as an LFR resulting in a compact system model. The systems are required to be homogeneous and the interconnection topologies are restricted to be diagonalizable. Generalizations have been made that extend the approach to different groups of homogeneous subsystems [61], to time-varying subsystems [62], and to directed interconnection graphs

[63]. The system models in [61]–[63] are however restricted to equal interconnections within the groups of homogeneous subsystems.

4.2.2 Controller Synthesis for Interconnected Systems

Due to the described complexity of the problem, the controller synthesis for interconnected systems requires some form of decomposition. Based on the previously described modeling approaches which separate the system into a decentralized part and an interconnection part, tools from robust and gain-scheduled controller synthesis have successfully been applied [64], [65].

In [36], a consensus protocol for MAS is considered. A signal transformation in form of a Schur transformation is used to decouple the synthesis for homogeneous multi-agent LTI systems into synthesis conditions of the order of the subsystems that only differ by the Laplacian eigenvalues. This approach is limited to MAS. Furthermore, only stability guarantees are provided. In [66], the approach from [36] is extended to include performance objectives in form of the $\mathcal{H}_\infty$-norm. In [67] an approach for distributed stabilizing controller synthesis is presented, where a chordal decomposition is applied and a sequential design procedure is performed. However, if a performance criterion is to be optimized, this approach can in general lead to conservatism or infeasibility.

While the approaches in [36] and [66] are limited to dynamically decoupled MAS, a diagonalizing signal transformation to decomposable systems, which may be dynamically coupled, is applied in [60]. This allows for the system to be modeled as an LFR, to which the full block S-procedure (FBSP) can be applied [25], [68]. Under structural assumptions on the Lyapunov and multiplier matrices [60], this approach allows the decomposition of the synthesis matrix inequalities into equations of small dimensions for the individual subsystems. For the case of multiple groups of homogeneous subsystems interconnected over undirected graphs, applying a singular value decomposition (SVD) is proposed in [61] which results in a similar decomposition but potentially introduces more conservatism compared to applying the FBSP. Instead of the signal transformation in [59], a congruence transformation is proposed in [62] to cope with time-varying and heterogeneous subsystems. Groups of homogeneous subsystems are considered, which are required to be interconnected by undirected interactions within the groups and by directed ones between the groups. In [63], a transformation which can deal with directed graphs is introduced. The approaches in [61]–[63] however cannot handle different types of interconnections within the groups of homogeneous subsystems.

In addition to structural assumptions on the Lyapunov and multiplier matrices, structural constraints as in DG scalings are imposed in [56], which in general introduces further conservatism. Together with the assumption of undirected interconnections, synthesis equations for each subsystem are derived which are coupled to the equations of neighboring subsystems. The synthesis needs to be solved in a centralized way. In [69],

a distributed algorithm for controller synthesis is proposed which is based on a primal decomposition and subgradient method. Couplings in the synthesis equations given in [56] correspond to interconnections between subsystems. For each such connection, both involved subsystems compute subgradient information for the distributed synthesis algorithm, where the updates occur sequentially. The work in [57] makes use of a similar framework as in [56] for synthesizing a controller with an interconnection structure which does not need to replicate the structure of couplings in the plant. The FBSP is applied, however, no distributed synthesis method is proposed.

In [70]–[72] decentralized state feedback control design methods are introduced where not only the gains, but simultaneously the controller structure is optimized. The approaches iteratively solve convex relaxations of the design problem. In [73], these so-called sparsity-promoting control ideas are extended and applied to the control of power networks. In [74], gradient based methods are used in order to design the control gains and the control structure by means of placing virtual inertia in power grids.

Other distributed control approaches have been proposed in the framework of distributed model predictive control (MPC). Some cooperative distributed MPC schemes rely on extensive communication between the subcontrollers [75], [76]. Other directions have been explored where the subsystems are robust against the coupling in the system, such as in tube-based MPC [77], [78], where less communication is required. Plug and play schemes [79]–[81] hinge on the existence of weak interconnections in the system, which makes the system robust against certain changes in the interconnection topology.

In the so-called System Level Synthesis approach [82], the controller synthesis is transformed to an optimization problem over the closed-loop system responses. Based on the assumption of finite impulse responses, convex subspace constraints for the problem can be formulated, and the distributed structure of the system response can be included, as shown in [83].

4.2.3 Augmented Overlapping Control and Estimation

In numerous applications strong coupling between subsystems exists. Examples include physical coupling between robots, such as in cooperative manipulation tasks, or coupled control goals as in formation control. In these cases, completely decentralized controllers typically achieve a poor control performance. With the concepts that are introduced in [84], and extended in [42], [85], [86] and related literature, it has been shown to be beneficial to design decentralized controllers in an augmented overlapping state space, so that the augmented subsystems incorporate information about the strong coupling of the system.

The concept of overlapping decompositions is based on the Inclusion Principle [42], and has been intensively studied in the literature [42], [84], [85]. The goal in [42], [86] and related work is a tractable control design for large-scale systems. The computational

tractability is achieved through a decentralized controller synthesis in an augmented state space where the strong dynamic couplings are moved to the diagonal blocks of the overall augmented system matrices. Therefore, the subsystems are only coupled by weak interconnection terms on the off-diagonal blocks of the system matrices, which are neglected in the decentralized controller design. After the decentralized controller synthesis, the controller is contracted back to the original state space for implementation. The contracted controller has a distributed structure and thus potentially achieves a better performance than a decentralized controller in the original state space.

Distributed dynamic output feedback control can be viewed as a decentralized or distributed control scheme which is based on distributed estimation. Distributed estimation has been studied in the literature [87]–[89], with the goal of estimating the overall state of a plant with a consensus approach. In [90], [91], distributed moving horizon estimation schemes were proposed. In [52], distributed control is proposed based on parallel estimation where each subsystem estimates the whole system state. As the computational requirements of the individual subsystems scale linearly with the number of subsystems, this architecture becomes intractable for large-scale systems.

In [12], a distributed control scheme based on overlapping estimation is introduced. Instead of explicitly communicating states of interest to neighboring subsystems, the latter can implicitly gain information on states of interest by estimating them in addition to their own local states. As the computational requirement for each subsystem stays constant for a constant degree of overlap, the complexity scales linearly with the number of agents, which is beneficial for the control of larger systems. In [12], systems are considered which are small enough for centralized controller and estimator design but require decentralized implementation and communication. Implementing a distributed Kalman filter may require a lot of communication in general. Therefore, the structure of the estimator gains is a design choice, which corresponds to choosing the communication structure.

4.2.4 Fixed Modes and Minimum Communication Design

Decentralized fixed modes (DFMs) are defined in [48] as the modes of the system which are fixed under any decentralized controller. The concept of fixed modes (FMs) thus corresponds to the concept of decentralized controllability and observability. In [92], [93], different methods for the characterization of FMs are given. The method in [93] is based on rank tests. In [53], decentralized overlapping fixed modes (DOFMs) are introduced as FMs which cannot be moved by a controller of a given decentralized overlapping structure, corresponding to a distributed structure of the contracted controller. A method for their detection based on bipartite graphs is proposed. In [94] and subsequent work of the same authors, a measure of decentralized controllability is considered to give a metric for how far a system is away from having FMs. In [95], pole-placement for non-FMs is

addressed, which stabilizes the system if all FMs lie in the left half plane. In [96] an approximate DFM measure is used to improve the control performance.

If FMs exist that are not stabilizable or unacceptably limit the performance, they need to be removed. Methods to eliminate FMs have been considered in the literature, for example by changing the structure of the feedback matrix, [97] , or by approaches that are more general than LTI control for special cases of FMs [98]. Finding a minimum cost feedback pattern, i.e., an interaction structure of local LTI controllers with no structural FMs, is considered in [99]. The problem formulation is based on a graph-theoretic approach. In [100], finding an optimal information structure for overlapping systems is considered. Based on the characterization of DFMs in [53] the method can only handle unrepeated DFMs. In [101] a minimum cost constrained input-output and control configuration problem is stated that minimizes the required sets of inputs, outputs and feedback links that result in no FMs. Based on a graph-theoretic description, the problem is reduced to a maximum matching problem. In [102], FMs within a parallel estimation scheme of [52] are considered and a combinatorial search algorithm to find a minimal set of communication links is given.

4.2.5 ADMM for Distributed Control and Optimization

In the area of distributed control and optimization, ADMM, as introduced in Section 3.5, has become a widely used method [32]. It combines the advantages of dual decomposition, such as parallel and distributed computation, with the advantages of the method of multipliers, such as convexification. ADMM has been used in numerous applications, such as in electrical power systems [103]–[105], in distributed system and parameter identification for large-scale systems [17], [106], in optimal traffic flow problems [107], in sensor and actuator selection [108], or in distributed reinforcement learning [109]. In [110], ADMM is used in a distributed model predictive control scheme based on the system level synthesis.

4.3 Scope of Part II

In order to overcome some of the outlined limitations and challenges, Part II of this thesis focuses on the modeling of large-scale heterogeneous interconnected systems, on the scalability of the controller synthesis related to such systems, and on increasing the achievable controller performance while minimizing the number of required communication links.

4.3.1 Scalable Controller Synthesis for Heterogeneous Interconnected Systems

We make use of a modeling framework for heterogeneous interconnected systems that is similar to the one in [56], [57]. The N subsystems and the $|\mathcal{E}|$ directed interconnections can all be of different type. We propose a scalable controller design for large-scale heterogeneous interconnected systems. The proposed controller synthesis allows for the computation of a controller with a directed interconnection structure, which can differ from the plant coupling structure.

Through applying the FBSP and allowing for structured full block multipliers we potentially reduce conservatism compared to imposing a structure as in D or DG scalings as done in [56]. Based on a congruence transformation and on structural assumptions on the Lyapunov and multiplier matrices, we can decompose the synthesis equations. The resulting coupled matrix inequalities are of the order of the individual subsystems.

For general heterogeneous systems, the number of small decomposed synthesis equations grows linearly with the number of subsystems. To further improve the scalability of the controller synthesis, we propose a distributed method for solving these coupled synthesis conditions. The distributed synthesis is based on ADMM [32]. By choosing the variable splitting in a specific way, the ADMM algorithm can be simplified to two steps per iteration only involving communication with nearest neighbors.

4.3.2 Special Class of Heterogeneous Interconnected Systems

We introduce a novel classification of systems, referred to as α-β-heterogeneous systems. They consist of α groups of homogeneous subsystems with β different types of interconnections. Based on this classification, we show how the general heterogeneous system model of N subsystems and $|\mathcal{E}|$ interconnections can be transformed to a more compact model in the case where $1 < \alpha < N$ and $1 < \beta < |\mathcal{E}|$. As the controller synthesis is tightly linked to the modeling of the system, this more compact model is beneficial for the scalability of the controller synthesis.

This novel class of α-β-heterogeneous systems presents a significant extension with respect to the system class in [61], where different groups of homogeneous subsystems are required to have identical interconnections. While in [61], the interconnection topology of the controller needs to mirror the one of the plant, the controller interconnection topology can be chosen freely in the approach for α-β-heterogeneous systems that we propose. In particular, sparse interconnection topologies and therefore sparse communication topologies can be selected.

4.3.3 Increased Performance for Sparse Communication

Instead of improving the control performance of decentralized control schemes by adding explicit communication, the decentralized control performance can be improved by an increase in local model knowledge. This is achieved through overlapping subsystem dynamics in an augmented state space. Based on the idea in [12], where distributed control based on overlapping state estimation is designed in a centralized manner, we introduce a design of interconnected dynamic output feedback controllers in an augmented state space. The augmented system is modeled as an interconnected system. which allows us to employ the scalable controller synthesis methods based on the FBSP. The communication topology of the augmented controller is a design choice. In contrast to the existing similar approaches on overlapping control given in [42], [84], [85], and references therein, the local controllers that we synthesize in the augmented state space are not transformed back to the original state space, but they are implemented with the augmented state instead. Because of the increased overlap in the local models, more information of the overall system is incorporated in the local controllers. This controller design thus allows for a trade-off between the required communication, the computational effort, and the achievable control performance.

4.3.4 Minimum Communication Design

We consider so-called fixed modes (FMs), which prevent the interconnected system from being stabilizable or which restrict the achievable control performance under a decentralized controller. The input-output structure of the system is assumed to be given. We propose a method to identify FMs, based on rank tests from [93] and analyze the existence of a communication topology between the subcontrollers to remove all FMs. The communication of both measurements and controller states are considered.

The problem of finding the minimum communication topology to remove all FMs is formulated as a minimum cost coverage problem and the constraints are shown to be submodular. Therefore, a polynomial-time greedy algorithm is applicable and has a guaranteed suboptimality bound [111]. We propose an alternative algorithm which finds the communication set with the minimum amount of links based on a decision tree with efficient cuts.

4.4 Summary of the Contributions of Part II

The contributions of Part II of this thesis are summarized as follows.

1. A general modeling framework for interconnected systems which allows for heterogeneous subsystems and heterogeneous directed interconnections is considered in

Section 5.1. In Section 5.3, we show how general distributed systems with a centralized performance channel can be transformed into this interconnected system model such that the system norm is not changed under the transformation. This implies that the structure of the interconnected system model can be exploited in a scalable controller synthesis while guaranteeing the performance specification for the original system.

2. A controller synthesis for heterogeneous interconnected systems is proposed which is scalable in two aspects. First, a decomposition of the controller synthesis conditions based on the FBSP is introduced in Proposition 5.2. Second, a distributed solution method for the decomposed coupled synthesis conditions is proposed in Algorithm 5.1. It only requires communication between neighboring subsystems and no central coordination.

3. We introduce so-called α-β-heterogeneous systems which consist of α groups of homogeneous subsystems and β different interconnection types and can be classified to lie in between homogeneous and heterogeneous systems. α-β-Heterogeneous systems can be described by more compact system models than heterogeneous systems, which allow for a decomposed controller synthesis of reduced complexity, given in Proposition 6.4. The controller topology is a design choice, which is enabled by the consideration of different interconnection types.

4. In order to improve the control performance without increasing the explicit communication, we present an interconnected controller synthesis based on a system decomposition with overlapping augmented subsystems. We prove that the performance guarantees of the controller designed in the augmented space, given in Proposition 7.2, hold in interconnection with the original system.

5. To eliminate all FMs, we propose to introduce a minimum communication topology. In Lemma 8.2 we prove which conditions are required in order to guarantee the existence of a communication topology that eliminates all FMs. We show that the problem can be formulated as a minimum set coverage problem in (8.17), which is proved in Lemmas 8.3 and 8.4. Based on this result a suboptimal solution can be found by a polynomial greedy algorithm, or the optimum can be found by the tree search algorithm proposed in Algorithm 8.2.

4.5 Outline of Part II of the Thesis

Part II of the thesis is structured as follows. Chapters 5 and 6 present scalable controller synthesis methods for interconnected systems. While Chapter 5 focuses on heterogeneous systems, Chapter 6 considers special classes of systems, in particular homogeneous systems and α-β-heterogeneous systems, for which the controller synthesis can be reduced

in complexity. Chapters 7 and 8 propose methods for improving the control performance while decreasing the communication. Chapter 7 presents an augmented controller design which can improve the achievable control performance for a given sparse communication topology. Chapter 8 introduces an algorithm to identify FMs and to find the minimum communication topology required to remove them. Section 14.1 in Part IV provides conclusions and an outlook related to Part II.

CHAPTER 5

Heterogeneous Interconnected Systems

This chapter proposes a scalable controller synthesis for heterogeneous interconnected systems. As the modeling is closely linked to the controller synthesis, we will first present a framework which introduces the system as an ensemble of decentralized subsystems with an interconnection channel similarly as in [56], [57]. We apply multiplier-based methods from robust and gain-scheduled control, in particular the FBSP [25], [68], to this system model. We decompose the controller synthesis equations for a reduced complexity. In comparison to using DG scalings as in [56], full block multipliers are used, which potentially reduces conservatism. This chapter focuses on the most general case of heterogeneous systems where all subsystems and interconnections can be different. Because of the generality of the system model, the decomposed controller synthesis scales only linearly with both the number of subsystems and interconnections and polynomially with the number of neighboring subsystems. For a better scalability, we introduce a distributed method for solving the decomposed synthesis equations which requires only local communication. The interconnection topology of the synthesized controller can be freely chosen, in particular, a sparse communication structure can be selected. The contributions presented in this chapter have been submitted for publication in [15].

This chapter is organized as follows. Sections 5.1 and 5.2 introduce a framework for modeling the interconnected plant, controller and closed loop. Section 5.3 shows how a distributed system with centralized performance channel can be transformed into the presented model. In Section 5.4, the FBSP is employed. Based on some structural assumptions on the Lyapunov matrix and the multipliers, we decompose the synthesis matrix inequalities into small ones of the order of the individual subsystems. To solve the decomposed equations, we introduce a distributed ADMM algorithm without central coordination in Section 5.5. Numerical examples illustrate these results in Section 5.6 before Section 5.7 concludes this chapter.

5.1 Model of Heterogeneous Interconnected Systems

We consider a system of N different LTI subsystems which are coupled by different types of interconnections over an arbitrary directed graph. This section presents the interconnected system model.

5.1.1 Graph Structure

We consider a connected graph $\mathcal{T}^G = \{\mathcal{N}, \mathcal{E}^G\}$ where its vertices are N possibly different finite dimensional LTI subsystems, associated with the node set $\mathcal{N} = \{1, \ldots, N\}$, which is the index set of all subsystems $G_i, i \in \mathcal{N}$. We further define the set of directed edges $\mathcal{E}^G := \{(i,k)\}$ for all pairs (i,k) where subsystem i is influenced by subsystem k. The interconnection topology of the subsystems is captured by the interconnection matrix P^G, which is an $N \times N$ matrix, of all zeros except for non-zero entries in the places corresponding to interconnections between subsystems i and k, i.e., the entry ${P^G}_{ik}$ is non-zero if subsystem k influences subsystem i.

While the interconnection graph $\mathcal{T}^G$ capturing the interconnections between the subsystems may be directed, we will later on assume that subsystems interconnected by an edge in $\mathcal{E}^G$ can communicate in a bidirectional way during controller synthesis, which will be presented in Section 5.5. To this end, and for the interconnection representation which will be introduced in Section 5.1.3, we introduce the mirror graph $\mathcal{T}^{GM} := \{\mathcal{N}, \mathcal{E}^{GM}\}$ as the graph which completes $\mathcal{T}^G$ to an undirected one, i.e., for all directed edges $(i,k) \in \mathcal{E}^G$ for which there does not exist an edge $(k,i) \in \mathcal{E}^G$, there exists an edge (k,i) in $\mathcal{E}^{GM}$. The interconnection matrix P^{GM} is defined for $\mathcal{T}^{GM}$ analogously to P^G for $\mathcal{T}^G$.

5.1.2 Interconnected State Space Representations

The subsystems G_i admit continuous-time state space representations given by

$$G_i : \left\{ \begin{bmatrix} \dot{x}_i \\ \hdashline y_i \\ \hdashline z_i \\ \hdashline q_i \end{bmatrix} = \left[\begin{array}{c:c:c:c} A_i & B_{u,i} & B_{w,i} & B_{p,i} \\ \hdashline C_{y,i} & 0 & D_{yw,i} & D_{yp,i} \\ \hdashline C_{z,i} & D_{zu_i} & 0 & D_{zp,i} \\ \hdashline C_{q,i} & D_{qu,i} & D_{qw,i} & 0 \end{array}\right] \begin{bmatrix} x_i \\ \hdashline u_i \\ \hdashline w_i \\ \hdashline p_i \end{bmatrix}, \quad i = 1, ..., N, \tag{5.1}$$

with the state vector $x_i \in \mathbb{R}^{n_{x_i}}$, the local control input and measured output, $u_i \in \mathbb{R}^{n_{u_i}}$ and $y_i \in \mathbb{R}^{n_{y_i}}$, the local exogenous input and performance output, $w_i \in \mathbb{R}^{n_{w_i}}$ and $z_i \in \mathbb{R}^{n_{z_i}}$, and the interconnection signals $p_i \in \mathbb{R}^{n_{p_i}}$ and $q_i \in \mathbb{R}^{n_{q_i}}$, respectively.

Remark 5.1. The feedthrough matrices $D_{yu,i}$ and $D_{zw,i}$ have been set to zero, because for physical systems, $D_{yu,i}$ is usually zero, and $D_{zw,i}$ is often chosen to be zero by convention.

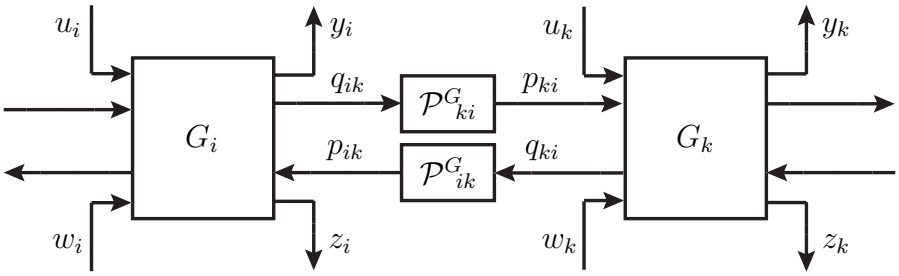

Figure 5.1: Interconnection with performance inputs and outputs.

The feedthrough matrix $D_{qp,i}$ is restricted to be zero, in order to avoid algebraic loops.

A transformation of a general distributed LTI system to the representation in (5.1) will be given in Section 5.3.

Note that the model in (5.1) can consider different process noise and measurement noise vectors. This is, for example, achieved by defining the stacked vector

$$w = \begin{bmatrix} \hat{v}^\top & \hat{w}^\top \end{bmatrix}^\top, \tag{5.2}$$

with $\hat{v}$ being the process noise and $\hat{w}$ the measurement noise. The stacked system matrices are accordingly defined by

$$\begin{aligned} B_w &= \begin{bmatrix} B_{\hat{v}}^\top & 0^\top \end{bmatrix}^\top, \\ D_{yw} &= \begin{bmatrix} 0^\top & D_{y\hat{w}}^\top \end{bmatrix}^\top. \end{aligned} \tag{5.3}$$

5.1.3 Interconnection Relations

We define the set of neighboring subsystems of subsystem i, denoted by $\mathcal{N}_i^G$, as the set of subsystems for which there exists an interconnection with subsystem i, i.e., an edge (i,k) in the union of edge sets $\mathcal{E}^G \cup \mathcal{E}^{GM}$,

$$\mathcal{N}_i^G := \{k \mid (i,k) \in \left(\mathcal{E}^G \cup \mathcal{E}^{GM}\right), \forall\, k \in \mathcal{N},\, k \neq i\}.$$

The interconnection signals p_i and q_i of the subsystems are further partitioned into

$$\begin{aligned} p_i &= \operatorname{concat}_{k \in \mathcal{N}_i^G}(p_{ik}), \\ q_i &= \operatorname{concat}_{k \in \mathcal{N}_i^G}(q_{ik}), \end{aligned} \tag{5.4}$$

where $p_{ik} \in \mathbb{R}^{n_{p_{ik}}}$, $q_{ik} \in \mathbb{R}^{n_{q_{ik}}}$ are the ingoing and outgoing interconnection signals of subsystem i from and to subsystem k, respectively. This is illustrated in Figure 5.1. The interconnection signals $p \in \mathbb{R}^{n_p}$ and $q \in \mathbb{R}^{n_q}$ of the system are then defined as

$$\begin{aligned} p &= \operatorname{concat}_{i \in \mathcal{N}}(p_i), \\ q &= \operatorname{concat}_{i \in \mathcal{N}}(q_i). \end{aligned} \tag{5.5}$$

Furthermore, we define the interconnection operator $\mathcal{P}^G$ through the relation

$$p = \mathcal{P}^G q. \tag{5.6}$$

The (i,k)-entries in $\mathcal{P}^G$ are the block elements $\mathcal{P}^G_{ik}$ of the individual interconnection relations $p_{ik} = \mathcal{P}^G_{ik}\, q_{ki}$, which are shown in Figure 5.1. In the following, we will consider ideal interconnections. In this case, the entries $\mathcal{P}^G_{ik}$ are constant matrices of appropriate dimensions.

Both P^G as well as $\mathcal{P}^G$ capture information about the interconnection topology of the system. While P^G directly encodes the interconnections between the subsystems, $\mathcal{P}^G$ describes the interconnections on the level of the edges, i.e., on the level of the ingoing and outgoing interconnection signals, p and q, respectively. The following numerical example illustrates the definition of the interconnection signals and the interconnection matrix.

Example 5.1 (Definition of interconnections q, p and interconnection matrix $\mathcal{P}^G$). We consider the following system composed of four subsystems with the interconnection matrix

$$P^G = \begin{bmatrix} 0 & P^G_{12} & 0 & 0 \\ P^G_{21} & 0 & P^G_{23} & P^G_{24} \\ 0 & P^G_{32} & 0 & 0 \\ 0 & P^G_{42} & 0 & 0 \end{bmatrix},$$

indicating the interconnection topology of the subsystems. The interconnection channel as defined in (5.5) is

$$\underbrace{\begin{bmatrix} p_{12} \\ p_{21} \\ p_{23} \\ p_{24} \\ p_{32} \\ p_{42} \end{bmatrix}}_{p} = \underbrace{\left[\begin{array}{c|c|c|c} 0 & \mathcal{P}^G_{12} & 0 & 0 \\ \hline \mathcal{P}^G_{21} & 0 & 0 & 0 \\ 0 & 0 & 0 & 0 \\ 0 & 0 & 0 & 0 \\ \hline 0 & 0 & \mathcal{P}^G_{32} & 0 \\ \hline 0 & 0 & 0 & \mathcal{P}^G_{42} \end{array}\right.}_{\mathcal{P}^G} \left.\begin{array}{c|c} 0 & 0 \\ \hline 0 & 0 \\ \mathcal{P}^G_{23} & 0 \\ 0 & \mathcal{P}^G_{24} \\ \hline 0 & 0 \\ \hline 0 & 0 \end{array}\right] \underbrace{\begin{bmatrix} q_{12} \\ q_{21} \\ q_{23} \\ q_{24} \\ q_{32} \\ q_{42} \end{bmatrix}}_{q}.$$

For example, subsystem 1 has an interconnection channel of dimensions from $n_{p_1} = n_{p_{12}}$ to $n_{q_1} = n_{q_{12}}$, and subsystem 2 has an interconnection channel of dimensions from $n_{p_2} = n_{p_{21}} + n_{p_{23}} + n_{p_{24}}$ to $n_{q_2} = n_{q_{21}} + n_{q_{23}} + n_{q_{24}}$.

In the following, we denote decentralized, i.e., block-diagonal parts by a superscript $(\cdot)^d$, and interconnection parts, i.e., off-block-diagonal parts by a superscript $(\cdot)^i$. The decentralized part of the plant, i.e., the ensemble of all G_i, $\forall i = 1, ..., N$, is therefore denoted as G^d. The overall interconnected system, G, is given by the LFR with decentralized part G^d and interconnection channel, as introduced in Section 2.4, as follows

$$G : \begin{cases} G^d = \mathrm{diag}_{i \in \mathcal{N}}(G_i)\,, \\ p = \mathcal{P}^G q\,. \end{cases} \tag{5.7}$$

Note that with the definition of p_i and q_i in (5.4) over the interconnections $(i,k) \in \mathcal{E}^G \cup \mathcal{E}^{GM}$ the interconnection matrix $\mathcal{P}^G$ is defined over the undirected graph $\mathcal{T}^G + \mathcal{T}^{GM}$, where $\mathcal{T}^{GM}$ introduces zero signals in the appropriate channels to complete the graph $\mathcal{T}^G$ to an undirected one. Therefore, in the following, w. l. o. g., we will consider undirected interconnection graphs, and $\mathcal{P}^G$ is thus symmetric.

The system G can also be written in terms of the stacked signal vectors of all subsystems, given as

$$\begin{aligned} x &= \operatorname{concat}_{i=1}^{N}(x_i)\,, \quad y = \operatorname{concat}_{i=1}^{N}(y_i)\,, \quad u = \operatorname{concat}_{i=1}^{N}(u_i)\,, \\ z &= \operatorname{concat}_{i=1}^{N}(z_i)\,, \quad w = \operatorname{concat}_{i=1}^{N}(w_i)\,, \\ p &= \operatorname{concat}_{i=1}^{N}(p_i)\,, \quad q = \operatorname{concat}_{i=1}^{N}(q_i)\,, \end{aligned} \tag{5.8}$$

and the block-diagonally stacked system matrices, given as

$$\begin{aligned} A^d &= \operatorname{diag}_{i=1}^{N}(A_i)\,, & {B_u}^d &= \operatorname{diag}_{i=1}^{N}(B_{u,i})\,, & {C_y}^d &= \operatorname{diag}_{i=1}^{N}(C_{y,i})\,, \\ {B_w}^d &= \operatorname{diag}_{i=1}^{N}(B_{w,i})\,, & {D_{yw}}^d &= \operatorname{diag}_{i=1}^{N}(D_{yw,i})\,, & D_{zw}^d &= \operatorname{diag}_{i=1}^{N}(D_{zw,i})\,, \\ C_z^d &= \operatorname{diag}_{i=1}^{N}(C_{z,i})\,, & {D_{zu}}^d &= \operatorname{diag}_{i=1}^{N}(D_{zu,i})\,, \end{aligned} \tag{5.9}$$

where the matrices on the diagonal are the subsystem matrices from (5.1). They are the decentralized system parts, e.g., $A_i = A_{ii} \in \mathbb{R}^{n_{x_i} \times n_{x_i}}$, $\forall i \in \{1, ..., N\}$. The system matrices of the decentralized system part G^d that are related to the interconnection channel are formed accordingly, as

$$\begin{aligned} B_p^d &= \operatorname{diag}_{i=1}^{N}(B_{p,i})\,, & D_{yp}^d &= \operatorname{diag}_{i=1}^{N}(D_{yp,i})\,, & {D_{zp}}^d &= \operatorname{diag}_{i=1}^{N}(D_{zp,i})\,, \\ {C_q}^d &= \operatorname{diag}_{i=1}^{N}(C_{q,i})\,, & {D_{qw}}^d &= \operatorname{diag}_{i=1}^{N}(D_{qw,i})\,. \end{aligned} \tag{5.10}$$

A possible realization of the subsystem matrices is the following

$$\begin{aligned} B_{p,i} &= \operatorname{concat}_{k \in \mathcal{N}_i^G}\left(\begin{bmatrix} A_{ik} & B_{u,ik} & B_{w,ik} \end{bmatrix}^\top\right)^\top, \\ D_{zp,i} &= \operatorname{concat}_{k \in \mathcal{N}_i^G}\left(\begin{bmatrix} C_{z,ik} & D_{zu,ik} & D_{zw,ik} \end{bmatrix}^\top\right)^\top, \\ D_{yp,i} &= \operatorname{concat}_{k \in \mathcal{N}_i^G}\left(\begin{bmatrix} C_{y,ik} & 0 & D_{yw,ik} \end{bmatrix}^\top\right)^\top, \\ C_{q,i} &= \operatorname{concat}_{k \in \mathcal{N}_i^G}\left(\begin{bmatrix} I_{n_{x_k}} & 0 & 0 \end{bmatrix}^\top\right), \\ D_{qw,i} &= \operatorname{concat}_{k \in \mathcal{N}_i^G}\left(\begin{bmatrix} 0 & 0 & I_{n_{w_k}} \end{bmatrix}^\top\right), \\ D_{qu,i} &= \operatorname{concat}_{k \in \mathcal{N}_i^G}\left(\begin{bmatrix} 0 & I_{n_{u_k}} & 0 \end{bmatrix}^\top\right). \end{aligned} \tag{5.11}$$

All the system matrices of G^d are thus block-diagonal.

Remark 5.2. If not all of the signals are interconnected, then the corresponding rows and columns can be deleted, reducing the dimensions of the interconnection channels.

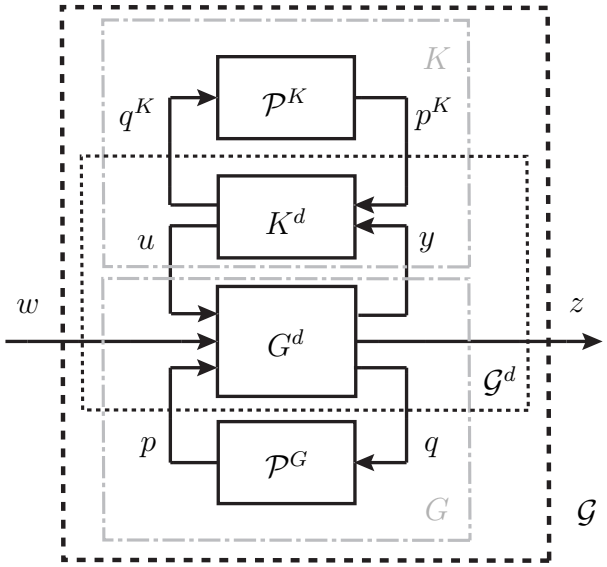

Figure 5.2: Structure of the open-loop plant $G = \mathcal{F}_\mathrm{l}(G^d, \mathcal{P}^G)$, the controller $K = \mathcal{F}_\mathrm{l}(K^d, \mathcal{P}^K)$ and the closed-loop system $\mathcal{G} = \mathcal{F}_\mathrm{l}(\mathcal{G}^d, \mathcal{P})$.

5.2 Controller Structure and Closed Loop System

This section provides details about the structure of the interconnected controller to be synthesized and the resulting closed-loop system.

5.2.1 Interconnected Controller Structure

The objective of the controller synthesis is to find another interconnected system, the controller K, such that the interconnection of the plant G with the controller K is stable and minimizes the induced $\mathcal{L}_2$-norm of the closed-loop system, which we denote by $\mathcal{G}$. The controller structure is chosen such that the closed-loop system can also be modeled as an LFR. This structure will be exploited in the controller synthesis. The structures of the open-loop plant $G = \mathcal{F}_\mathrm{l}(G^d, \mathcal{P}^G)$, the controller $K = \mathcal{F}_\mathrm{l}(K^d, \mathcal{P}^K)$ and the closed-loop system $\mathcal{G} = \mathcal{F}_\mathrm{l}(\mathcal{G}^d, \mathcal{P})$ are illustrated in Figure 5.2. The definitions of the individual parts will be given in the following.

The state-space realization of the subcontrollers K_i are given by

$$K_i : \left\{ \begin{bmatrix} \dot{x}_i^K \\ u_i \\ q_i^K \end{bmatrix} = \left[\begin{array}{cc:c} A^K{}_i & B^K{}_i & B_{p^K,i} \\ C^K{}_i & D^K{}_i & C_{p^K,i} \\ \hdashline C_{q^K,i} & D_{q^K,i} & 0 \end{array}\right] \begin{bmatrix} x_i^K \\ y_i \\ p_i^K \end{bmatrix}, \quad i = 1, ..., N. \tag{5.12}$$

A possible realization of the controller matrices is given as follows

$$\begin{aligned} B_{p^K,i} &= \mathrm{concat}_{k\in\mathcal{N}_i^K}\left(\begin{bmatrix} {A^K}_{ik} & {B^K}_{ik}\end{bmatrix}^\top\right)^\top, \\ C_{p^K,i} &= \mathrm{concat}_{k\in\mathcal{N}_i^K}\left(\begin{bmatrix} {C^K}_{ik} & {D^K}_{ik}\end{bmatrix}^\top\right)^\top, \\ C_{q^K,i} &= \mathrm{concat}_{k\in\mathcal{N}_i^K}\left(\begin{bmatrix} I & 0\end{bmatrix}^\top\right), \\ D_{q^K,i} &= \mathrm{concat}_{k\in\mathcal{N}_i^K}\left(\begin{bmatrix} 0 & I\end{bmatrix}^\top\right). \end{aligned} \tag{5.13}$$

In this case, the interconnection channel consists of the controller states and measured outputs of the neighboring plants. Other formulations are possible, where for example the controller states and the control inputs are communicated.

We define the neighboring subcontrollers of subcontroller i by

$$\mathcal{N}_i^K = \{k \mid (k,i) \in \left(\mathcal{E}^K \cup \mathcal{E}^{KM}\right)\}.$$

The interconnection signals of the subcontroller i, $p_i^K \in \mathbb{R}^{n_{p_i^K}}$ and $q_i^K \in \mathbb{R}^{n_{q_i^K}}$, are defined and partitioned analogously to the interconnection signals, p_i and q_i, of the subsystem i. Also the overall interconnection signals of the controller, $p^K \in \mathbb{R}^{n_{p^K}}$ and $q^K \in \mathbb{R}^{n_{q^K}}$, are defined analogously to the signals p and q of the plant. With the interconnection matrix $\mathcal{P}^K$, the relations of the interconnection signals of the controller are defined by

$$p^K = \mathcal{P}^K q^K.$$

As before for the plant, we define the interconnection graph $\mathcal{T}^K = \{\mathcal{N}, \mathcal{E}^K\}$ for the interconnected controller. Furthermore, we define the interconnection matrix P^K as the $N \times N$-matrix capturing the topology of the controller on the level of the subcontrollers. The mirror graph $\mathcal{T}^{KM}$, as well as the mirror interconnection matrix P^{KM} are defined analogously to $\mathcal{T}^{GM}$ and P^{GM} from before.

As before for the system, we denote the decentralized part of the controller, i.e., the ensemble of all K_i, $\forall i = 1, ..., N$, by K^d. The interconnected controller is then given by the decentralized part K^d and the interconnection channel as follows

$$K : \begin{cases} K^d = \mathrm{diag}_{i\in\mathcal{N}}(K_i)\,, \\ p^K = \mathcal{P}^K q^K\,. \end{cases} \tag{5.14}$$

Again, as for the plant, the interconnection signals, p^K and q^K, and the interconnection matrix $\mathcal{P}^K$ capture the topology described by the undirected graph $\mathcal{T}^K + \mathcal{T}^{KM}$.

The overall controller K can also be written in terms of the stacked signal vectors of all subcontrollers, as

$$x^K = \mathrm{concat}_{i=1}^N\left(x_i^K\right), \quad u = \mathrm{concat}_{i=1}^N(u_i)\,, \quad p^K = \mathrm{concat}_{i=1}^N\left(p_i^K\right), \tag{5.15}$$

and y and q^K, analogously. The controller matrices corresponding to the decentralized part K^d are given as

$$\begin{aligned} A^{K^d} &= \operatorname{diag}_{i=1}^{N}\left(A^K{}_i\right), \qquad B^{K^d} = \operatorname{diag}_{i=1}^{N}\left(B^K{}_i\right), \\ C^{K^d} &= \operatorname{diag}_{i=1}^{N}\left(C^K{}_i\right), \qquad D^{K^d} = \operatorname{diag}_{i=1}^{N}\left(D^K{}_i\right), \end{aligned} \tag{5.16}$$

where the subcontroller matrices $A^K{}_i$, $B^K{}_i$, $C^K{}_i$ and $D^K{}_i$ from (5.12) are the diagonal (decentralized) controller matrices, given as

$$A^{K^d}_i = A^K{}_{ii} \in \mathbb{R}^{n_{x_i^K} \times n_{x_i^K}}, \quad B^{K^d}_i = B^K{}_{ii} \in \mathbb{R}^{n_{x_i^K} \times n_{s_i}}, \tag{5.17}$$

and $C^{K^d}_i$ and $D^{K^d}_i$ analogously. The system matrices related to the interconnection channel are formed accordingly, as

$$B^d_{p^K} = \operatorname{diag}_{i=1}^{N}\left(B_{p^K,i}\right), \quad C^d_{p^K} = \operatorname{diag}_{i=1}^{N}\left(C_{p^K,i}\right), \tag{5.18}$$

and $C^d_{q^K}$ and $D^d_{q^K}$ analogously.

We also denote the off-block-diagonal parts of the system and controller matrices by a superscript $(\cdot)^i$. For example, in the case of the controller matrices, they are given as

$$\begin{aligned} A^{K^i} &= A^K - A^{K^d}, \qquad B^{K^i} = B^K - B^{K^d}, \\ C^{K^i} &= C^K - C^{K^d}, \qquad D^{K^i} = D^K - D^{K^d}. \end{aligned} \tag{5.19}$$

These matrices contain the blocks, e.g., $A^K_{ik}, \forall (i,k) \in \mathcal{E}^K$, which constitute the matrices related to the interconnection channel, e.g., $B_{p^K,i}$ as in (5.13).

5.2.2 Interconnected Closed-Loop System

We define the closed-loop of the system G interconnected with the controller K, as illustrated in Figure 5.2, as $\mathcal{G} = \mathcal{F}_u(G,K) = \mathcal{F}_u(\mathcal{F}_l(G^d,\mathcal{P}^G),\mathcal{F}_u(K^d,\mathcal{P}^K)) = \mathcal{F}_u(\mathcal{F}_l(\mathcal{G}^d,\mathcal{P}))$, with dynamics given by

$$\mathcal{G} : \begin{cases} \mathcal{G}^d = \operatorname{diag}_{i\in\mathcal{N}}(\mathcal{G}_i), \\ q^c = \mathcal{P} p^c, \end{cases} \tag{5.20}$$

with

$$\mathcal{G}_i = \begin{bmatrix} \dot{x}_i^c \\ z_i \\ q_i^c \end{bmatrix} = \left[\begin{array}{c|cc} \mathcal{A}_i & \mathcal{B}_{1,i} & \mathcal{B}_{2,i} \\ \hline \mathcal{C}_{1,i} & \mathcal{D}_{11,i} & \mathcal{D}_{12,i} \\ \mathcal{C}_{2,i} & \mathcal{D}_{21,i} & \mathcal{D}_{22,i} \end{array}\right] \begin{bmatrix} x_i^c \\ w_i \\ p_i^c \end{bmatrix}, \quad \forall i \in \mathcal{N}, \tag{5.21}$$

and where the state and interconnection signal vectors $x_i^c \in \mathbb{R}^{n_{x^c i}}$, $q_i^c \in \mathbb{R}^{n_{q^c i}}$ and $p_i^c \in \mathbb{R}^{n_{p^c i}}$ of the closed-loop system are defined as the stacked vectors of the system and the controller, given as

$$x_i^c = \begin{bmatrix} x_i \\ x_i^K \end{bmatrix}, \quad q_i^c = \begin{bmatrix} q_i \\ q_i^K \end{bmatrix}, \quad p_i^c = \begin{bmatrix} p_i \\ p_i^K \end{bmatrix}, \tag{5.22}$$

respectively. With the interconnected system and controller realizations in (5.11) and (5.13), the closed-loop matrices for subsystem i of a heterogeneous system are the following.

$$\begin{aligned}
\mathcal{A}_i &= \begin{bmatrix} A_i + B_{u,i} {D^K}_i C_{y,i} & B_{u,i} {C^K}_i \\ {B^K}_i C_{y,i} & {A^K}_i \end{bmatrix}, \\
\mathcal{B}_{1,i} &= \begin{bmatrix} B_{w,i} + B_{u,i} {D^K}_i D_{yw,i} \\ {B^K}_i D_{yw,i} \end{bmatrix}, \\
\mathcal{C}_{1,i} &= \begin{bmatrix} C_{z,i} + D_{zu,i} {D^K}_i C_{y,i} & D_{zu,i} {C^K}_i \end{bmatrix}, \\
\mathcal{D}_{11,i} &= \begin{bmatrix} D_{zw,i} + D_{zu,i} {D^K}_i D_{yw,i} \end{bmatrix}, \\
\mathcal{B}_{2,i} &= \begin{bmatrix} B_{p,i} & B_{u,i} C_{p^K,i} \\ 0 & B_{p^K,i} \end{bmatrix}, \\
\mathcal{C}_{2,i} &= \begin{bmatrix} C_{q,i} + D_{qu,i} {D^K}_i C_{y,i} & D_{qu,i} {C^K}_i \\ D_{q^K,i} C_{y,i} & C_{q^K,i} \end{bmatrix}, \\
\mathcal{D}_{21,i} &= \begin{bmatrix} D_{qw,i} + D_{qu,i} {D^K}_i D_{yw,i} \\ D_{q^K,i} D_{yw,i} \end{bmatrix}, \\
\mathcal{D}_{12,i} &= \begin{bmatrix} D_{zp,i} & D_{zu,i} C_{p^K,i} \end{bmatrix}, \\
\mathcal{D}_{22,i} &= \begin{bmatrix} 0 & D_{qu,i} C_{p^K,i} \\ 0 & 0 \end{bmatrix}.
\end{aligned} \tag{5.23}$$

Remark 5.3. From (5.23), we see that the closed-loop system can either have interconnected control inputs, i.e., off-block-diagonal terms $B_{u,ik} \neq 0$ which results in non-zero terms $D_{qu,i}$, or interconnected controller terms ${C^K}_{ik} \neq 0$ and ${D^K}_{ik} \neq 0$ which results in non-zero terms $C_{p^K,i}$. They are not allowed to be simultaneously non-zero. Otherwise, the term $\mathcal{D}_{22,i} \neq 0$ would create an infinite interconnection loop.

With

$$x^c = \operatorname{concat}_{i=1}^{N}(x_i^c), \qquad q^c = \operatorname{concat}_{i=1}^{N}(q_i^c), \qquad p^c = \operatorname{concat}_{i=1}^{N}(p_i^c), \tag{5.24}$$

the interconnection matrices P and $\mathcal{P}$ are then defined for the graph of the closed-loop system, $\mathcal{T}$, with $\mathcal{T} = \{\mathcal{N}, \mathcal{E}\}$, where the edge set $\mathcal{E}$ is given by

$$\mathcal{E} = \mathcal{E}^G \cup \mathcal{E}^{GM} \cup \mathcal{E}^K \cup \mathcal{E}^{KM}.$$

As before in (5.7), this interconnection structure can always be achieved by introducing zero signals in the appropriate channels. The set of neighboring subsystems of subsystem i in the closed-loop is defined analogously to the sets $\mathcal{N}_i^G$ and $\mathcal{N}_i^K$ for the closed loop and is thus the union of both sets, i.e., $\mathcal{N}_i = \mathcal{N}_i^G \cup \mathcal{N}_i^K$.

Note that the controller interconnection structure does not have to be the same as the plant interconnection structure, i.e., we allow for $\mathcal{P}^G \neq \mathcal{P}^K$. In particular, the controller interconnection topology can be chosen sparse if the communication is restricted.

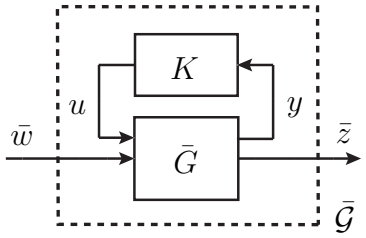

Figure 5.3: Closed-loop of system $\bar{G}$ with controller K.

5.3 Transformation to Interconnected State Space Representations

In general, the performance channel of a given distributed plant may not be localized as it is assumed in (5.1). For instance, for cooperative control tasks, system-wide performance goals can be formulated, and exogenous inputs can affect coupled parts of the system. In this case, the performance channel is not localized and the system cannot readily be modeled in the form given in (5.7), which, however, is required to achieve the structure of the closed-loop system in Figure 5.2.

5.3.1 Distributed Systems with Centralized Performance

Let us consider a distributed continuous-time LTI plant with the following dynamics

$$\bar{G}: \begin{cases} \dot{x} &= Ax + \sum_{i=1}^{N} B_{u,i}u_i + B_{\bar{w}}\bar{w}\,, \\ y_i &= C_{y,i}x + D_{y\bar{w},i}\bar{w}\,, \quad i = 1, ..., N\,, \\ \bar{z} &= C_{\bar{z}}x + D_{\bar{z}u}u, \end{cases} \tag{5.25}$$

with the stacked signal vectors x, u and y as in (5.8). The exogenous input and performance output, which in general are not local, are given by $\bar{w} \in \mathbb{R}^{n_{\bar{w}}}$ and $\bar{z} \in \mathbb{R}^{n_{\bar{z}}}$, respectively. We denote the closed-loop of system $\bar{G}$ with the controller K as $\bar{\mathcal{G}}$, which is illustrated in Figure 5.3.

In order to decompose the system into local interconnected subsystems G_i, we propose to augment the global performance input and output, $\bar{w}$ and $\bar{z}$, in (5.25), such that a local performance input and output can be assigned to each individual subsystem. This augmentation is given by

$$z = \bar{Q}^{\frac{1}{2}} S \bar{z} \quad \text{and} \quad w = \bar{R}^{-\frac{1}{2}} T \bar{w}, \tag{5.26}$$

with

$$z = \operatorname{concat}_{i=1}^{N}(z_i)\,, \qquad w = \operatorname{concat}_{i=1}^{N}(w_i)\,. \tag{5.27}$$

In (5.26), S and T are matrices of full rank, and the matrices $\bar{Q}$ and $\bar{R}$ are weightings which will be defined in Section 5.3.2. The augmentation of the related system matrices is defined as

$$\begin{aligned} C_z &= \bar{Q}^{\frac{1}{2}} S C_{\bar{z}} \qquad & D_{zu} &= \bar{Q}^{\frac{1}{2}} S D_{\bar{z}u}, \\ B_w &= B_{\bar{w}} T^{\dagger} \bar{R}^{\frac{1}{2}} \qquad & D_{yw} &= D_{y\bar{w}} T^{\dagger} \bar{R}^{\frac{1}{2}}, \end{aligned} \tag{5.28}$$

where the augmentation is chosen such that the resulting structure of the system matrices is localized, as

$$\begin{aligned} C_z &= \operatorname{concat}_{i=1}^{N}(C_{z,i}), \qquad & D_{zu} &= \operatorname{concat}_{i=1}^{N}(D_{zu,i}), \\ B_w &= \operatorname{concat}_{i=1}^{N}\left(B_{w,i}^{\top}\right)^{\top}, \qquad & D_{yw} &= \operatorname{concat}_{i=1}^{N}\left(D_{yw,i}^{\top}\right)^{\top}. \end{aligned} \tag{5.29}$$

Note that the performance channel does not need to be decentralized, i.e., the matrices are not required to be block-diagonal, e.g., C_z is not required to be of the form $\operatorname{diag}_{i=1}^{N}(C_{z,i})$, but each subsystem needs to be equipped with a (possibly interconnected) local performance channel w_i to z_i for the decomposed controller synthesis. This performance input-output-transformation in (5.26) and (5.28) with (5.31) leads to the system

$$G : \begin{cases} \dot{x} &= Ax + \sum_{i=1}^{N} B_{u,i} u_i + \sum_{i=1}^{N} B_{w,i} w_i, \\ y_i &= C_{y,i} x + D_{yw,i} w, \qquad i = 1, ..., N, \\ z_i &= C_{z,i} x + D_{zu,i} u, \qquad i = 1, ..., N, \end{cases} \tag{5.30}$$

which has local control and performance inputs and outputs, u_i, y_i, w_i, and z_i, respectively, and can thus readily be modeled as the interconnected system in (5.7).

5.3.2 System Norm-Invariant Transformation

As control objective, the $\mathcal{H}_\infty$-norm of the closed-loop transfer function from $\bar{w}$ to $\bar{z}$ of the system $\bar{G}$ under the controller K, i.e. $\|\bar{\mathcal{G}}\|_{\mathcal{H}_\infty}$, is to be minimized. For a scalable synthesis of K, the goal is to exploit the structure of G and thus to minimize $\|\mathcal{G}\|_{\mathcal{H}_\infty}$. We propose to chose the transformation of the performance channel such that under the same controller K, this norm is equal to the norm of $\mathcal{G}$, i.e., $\|\bar{\mathcal{G}}\|_{\mathcal{H}_\infty} = \|\mathcal{G}\|_{\mathcal{H}_\infty}$. Let us assume that the full rank matrices $\bar{Q}$ and $\bar{R}$ are chosen as

$$\bar{Q} = S^{\dagger\top} S^{\dagger} + M_Q, \qquad \bar{R} = T T^{\top} + M_R, \tag{5.31}$$

with

$$M_Q = M_Q^{\top}, \qquad M_R = M_R^{\top}, \qquad S^{\top} M_Q S = 0, \qquad T^{\dagger} M_R T^{\dagger\top} = 0.$$

The choice of the so-called complementary matrices M_Q and M_R is not unique. They can for example be chosen such that C_z and B_w are as decentralized as possible, i.e., have as few off-diagonal blocks as possible.

With the augmentation of the performance channel in (5.28) and the choice of weightings in (5.31), the equality of $\|\bar{\mathcal{G}}\|_{\mathcal{H}_\infty}$ and $\|\mathcal{G}\|_{\mathcal{H}_\infty}$ is stated in the following.

Theorem 5.1. *Given $\bar{\mathcal{G}}$ and $\mathcal{G}$, with the transformation in* (5.28) *and the weightings in* (5.31)*, it holds that*

$$\|\mathcal{G}\|_{\mathcal{H}_\infty} = \|\bar{\mathcal{G}}\|_{\mathcal{H}_\infty}.$$

Proof. Similarly as in Lemma 9 in [59], for a transformation of a system $\bar{\mathcal{G}}$ to $\mathcal{G}$ with $\mathcal{G} = T_l\,\bar{\mathcal{G}}\,T_r^\dagger$, the following performance bounds can be proved

$$\frac{\sigma_{\min}(T_r)}{\sigma_{\max}(T_l)}\|\mathcal{G}\|_{\mathcal{H}_\infty} \leq \|\bar{\mathcal{G}}\|_{\mathcal{H}_\infty} \leq \frac{\sigma_{\max}(T_r)}{\sigma_{\min}(T_l)}\|\mathcal{G}\|_{\mathcal{H}_\infty}. \tag{5.32}$$

With

$$T_l := \left(S^{\dagger\top}S^\dagger + M_Q\right)^{\frac{1}{2}}S, \qquad T_r := \left(TT^\top + M_R\right)^{-\frac{1}{2}}T,$$

we need to show that the transformation matrices T_l and T_r are semi-orthogonal, which is a generalization of orthogonality for rectangular matrices, i.e.,

$$T_r^\top T_r = I, \qquad T_l\,T_l^\top = I.$$

Semi-orthogonal $m \times n$ or $n \times m$-matrices have m singular values of 1, if $m \leq n$. Then, the bounds in (5.32) are tight since $\sigma_{max} = \sigma_{min} = 1$ and so the $\mathcal{H}_\infty$-norm is not changed under the system transformation. To show that T_r is semi-orthogonal, we see that

$$\begin{aligned} T_r^\top T_r &= \left((TT^\top + M_R)^{-\frac{1}{2}}T\right)^\top \left((TT^\top + M_R)^{-\frac{1}{2}}T\right) \\ &= T^\top \left((TT^\top + M_R)^{-\frac{1}{2}}\right)^\top (TT^\top + M_R)^{-\frac{1}{2}}T \\ &= T^\top (TT^\top + M_R)^{-1}T = I, \end{aligned}$$

which holds because of $M_R = M_R^\top$.

Showing that $T_l^\top T_l = I$ follows along the same lines. □

The following proposition suggests that the augmentation of the performance channel is also applicable for an $\mathcal{H}_2$-based controller synthesis.

Proposition 5.1. *Given $\bar{\mathcal{G}}$ and $\mathcal{G}$, it holds that*

$$\|\bar{\mathcal{G}}\|_{\mathcal{H}_2} = \|\mathcal{G}\|_{\mathcal{H}_2}.$$

Proof. As shown in [59], the $\mathcal{H}_2$-norm is also unitary-invariant, and therefore the same proof as in Theorem 5.1 can be applied to show that $\|\bar{\mathcal{G}}\|_{\mathcal{H}_2} = \|\mathcal{G}\|_{\mathcal{H}_2}$. □

5.4 Decomposed Synthesis

In the following, we will consider methods from robust and gain-scheduled controller synthesis, where the interconnection plays the role of the uncertainty, as it is introduced

in Section 2.4. The block-diagonal entries in the system matrices are dealt with in a decomposed way and the off-block-diagonal entries, modeled through the interconnection channel, need to be accounted for in multiplier conditions that are coupled over the subsystems. We present a decomposed synthesis for the interconnected controller K in (5.14) based on the system representation in (5.20).

We use the FBSP as introduced in Theorem 2.1 in Section 2.4 for the controller synthesis. This theorem can be directly applied to the system formulation in (5.20). We show in the following proposition how the conditions in Theorem 2.1 can then be decomposed into conditions of the dimensions of the subsystems by appropriate structural (block-diagonal) assumptions on the multipliers Q, R and S and on the Lyapunov matrix $\mathcal{X}$.

Proposition 5.2 (Decomposed FBSP for Heterogeneous Systems)**.** *Consider a heterogeneous system $G = \mathcal{F}_l(G^d, \mathcal{P}^G)$ given in (5.7). There exists an interconnected controller K with $\mathcal{P}^K$ as in (5.12) such that $\mathcal{G} = \mathcal{F}_u(\mathcal{G}^d, \mathcal{P})$ given in (5.20) is stable and has an $\mathcal{L}_2$-gain less than γ, if there exist matrices $\mathcal{X}_i = \mathcal{X}_i^\top > 0$, $\forall i \in \{1, ..., N\}$ and $R_{ik} = R_{ik}^\top$, $Q_{ik} = Q_{ik}^\top$ and S_{ik}, $\forall (i,k) \in \mathcal{E}$, such that*

$$\left[\star\right]^\top \begin{bmatrix} \hat{Q}_{ik} & \hat{S}_{ik} \\ \hat{S}_{ik}^\top & \hat{R}_{ik} \end{bmatrix} \begin{bmatrix} \hat{\mathcal{P}}_{ik} \\ I_{(n_{p^c{}_{ik}} + n_{p^c{}_{ki}})} \end{bmatrix} > 0, \qquad \forall (i,k) \in \mathcal{E}. \tag{5.33}$$

$$\left[\star\right]^\top \left[\begin{array}{cc:cc:cc} 0 & \mathcal{X}_i & 0 & 0 & 0 & 0 \\ \mathcal{X}_i & 0 & 0 & 0 & 0 & 0 \\ \hdashline 0 & 0 & -\gamma I & 0 & 0 & 0 \\ 0 & 0 & 0 & \frac{1}{\gamma} I & 0 & 0 \\ \hdashline 0 & 0 & 0 & 0 & \tilde{Q}_i & \tilde{S}_i \\ 0 & 0 & 0 & 0 & \tilde{S}_i^\top & \tilde{R}_i \end{array}\right] \left[\begin{array}{ccc} I & 0 & 0 \\ \mathcal{A}_i & \mathcal{B}_{1,i} & \mathcal{B}_{2,i} \\ \hdashline 0 & I & 0 \\ \mathcal{C}_{1,i} & \mathcal{D}_{11,i} & \mathcal{D}_{12,i} \\ \hdashline 0 & 0 & I \\ \mathcal{C}_{2,i} & \mathcal{D}_{21,i} & \mathcal{D}_{22,i} \end{array}\right] < 0, \qquad \forall i \in \{1, ..., N\}. \tag{5.34}$$

with

$$\tilde{Q}_i = \mathrm{diag}_{k \in \mathcal{N}_i}(Q_{ik}), \ \tilde{R}_i = \mathrm{diag}_{k \in \mathcal{N}_i}(R_{ik}), \ \tilde{S}_i = \mathrm{diag}_{k \in \mathcal{N}_i}(S_{ik}),$$
$$\hat{Q}_{ik} = \mathrm{diag}(Q_{ik}, Q_{ki}), \quad \hat{R}_{ik} = \mathrm{diag}(R_{ik}, R_{ki}), \quad \hat{S}_{ik} = \mathrm{diag}(S_{ik}, S_{ki}),$$

and with

$$\hat{\mathcal{P}}_{ik} = \begin{bmatrix} 0 & \mathcal{P}_{ik} \\ \mathcal{P}_{ki} & 0 \end{bmatrix}.$$

Proof. When applying Theorem 2.1 to the interconnected system in (5.20) with the structured Lyapunov matrix $\mathcal{X} = \mathrm{diag}_{i=1}^N(\mathcal{X}_i)$ and the structured multipliers

$$Q = \mathrm{diag}_{i \in \mathcal{N}}\left(\tilde{Q}_i\right), \quad R = \mathrm{diag}_{i \in \mathcal{N}}\left(\tilde{R}_i\right), \quad S = \mathrm{diag}_{i \in \mathcal{N}}\left(\tilde{S}_i\right),$$

the matrices in the nominal condition (2.13) are composed of only block-diagonal matrices and therefore completely decompose into one condition per subsystem as in (5.34).

With $\mathcal{T}$ being an undirected graph, and with the structured multipliers

$$\tilde{Q}_i = \mathrm{diag}_{k\in\mathcal{N}_i}(Q_{ik})\,, \quad \tilde{R}_i = \mathrm{diag}_{k\in\mathcal{N}_i}(R_{ik})\,, \quad \tilde{S}_i = \mathrm{diag}_{k\in\mathcal{N}_i}(S_{ik})\,,$$

the multiplier condition in (2.12) can be transformed into a block-diagonal matrix with the conditions of (5.33) on its diagonal blocks. To see this, let us consider the interconnection channel $p^c = \mathcal{P}q^c$ as defined in (5.20). Then, we can always find a permutation matrix T, that reorders the entries of the signals q^c and p^c in such a way that those corresponding to the same edge are consecutive, i.e.,

$$\bar{p^c} = Tp^c, \quad \bar{q^c} = Tq^c,$$

with

$$\bar{p^c} = [..., {p^c_{ik}}^\top,\ {p^c_{ki}}^\top, ...]^\top, \quad \bar{q^c} = [..., {q^c_{ik}}^\top,\ {q^c_{ki}}^\top, ...]^\top.$$

The similarity transformation of the multiplier condition with T leads to

$$\left[\star\right]^T \underbrace{\begin{bmatrix} T & 0 \\ 0 & T \end{bmatrix} \begin{bmatrix} Q & S \\ S^\top & R \end{bmatrix} \begin{bmatrix} T^{-1} & 0 \\ 0 & T^{-1} \end{bmatrix}}_{\begin{bmatrix} \bar{Q} & \bar{S} \\ \bar{S}^\top & \bar{R} \end{bmatrix}} \underbrace{\begin{bmatrix} T & 0 \\ 0 & T \end{bmatrix} \begin{bmatrix} \mathcal{P} \\ I_{n_{p^c}} \end{bmatrix} T^{-1}}_{\begin{bmatrix} \bar{\mathcal{P}} \\ I_{n_{p^c}} \end{bmatrix}} > 0, \tag{5.35}$$

involving the multiplier transformations

$$\bar{Q} = TQT^{-1}, \quad \bar{S} = TST^{-1}, \quad \bar{R} = TRT^{-1}.$$

As the multipliers Q, R and S are block-diagonal, this transformation results again in block-diagonal multipliers $\bar{Q}$, $\bar{R}$ and $\bar{S}$ with the same reordering of the blocks on the diagonal as for the interconnection signals. This completes the proof that K stabilizes $\mathcal{G} = \mathcal{F}_\mathrm{u}(G, K)$ and leads to an $\mathcal{H}_\infty$-norm less than γ. □

The following example illustrates the transformation in the proof of Proposition 5.2.

Example 5.2 (Transformation to block-diagonal $\mathcal{P}$). Let us consider a closed-loop system with the same interconnection structure as in Example 5.1. It is easy to see that the transformation

$$T = \begin{bmatrix} I & 0 & 0 & 0 & 0 & 0 \\ 0 & I & 0 & 0 & 0 & 0 \\ 0 & 0 & I & 0 & 0 & 0 \\ 0 & 0 & 0 & 0 & I & 0 \\ 0 & 0 & 0 & I & 0 & 0 \\ 0 & 0 & 0 & 0 & 0 & I \end{bmatrix},$$

applied to the system as in (5.35) gives

$$\underbrace{\begin{bmatrix} p_{12}^c \\ p_{21}^c \\ p_{23}^c \\ p_{32}^c \\ p_{24}^c \\ p_{42}^c \end{bmatrix}}_{\bar{p}^c} = \underbrace{\left[\begin{array}{cc:cc:cc} 0 & \mathcal{P}_{12} & 0 & 0 & 0 & 0 \\ \mathcal{P}_{21} & 0 & 0 & 0 & 0 & 0 \\ \hdashline 0 & 0 & 0 & \mathcal{P}_{23} & 0 & 0 \\ 0 & 0 & \mathcal{P}_{32} & 0 & 0 & 0 \\ \hdashline 0 & 0 & 0 & 0 & 0 & \mathcal{P}_{24} \\ 0 & 0 & 0 & 0 & \mathcal{P}_{42} & 0 \end{array}\right]}_{\bar{\mathcal{P}}} \underbrace{\begin{bmatrix} q_{12}^c \\ q_{21}^c \\ q_{23}^c \\ q_{32}^c \\ q_{24}^c \\ q_{42}^c \end{bmatrix}}_{\bar{q}^c}.$$

Corollary 5.1. *The controller K in Proposition 5.2 stabilizes $\bar{\mathcal{G}}$ and leads to a performance bound of less than γ for $\bar{\mathcal{G}}$.*

Proof. Note that from $\bar{G}$ to G, only the performance channel is transformed, and therefore stability of $\mathcal{G}$, which is guaranteed by Proposition 5.2, implies stability of $\bar{\mathcal{G}} = \mathcal{F}_{\mathrm{u}}(\bar{G}, K)$. Furthermore, it has been shown in Theorem 5.1 that the $\mathcal{H}_\infty$-norm is invariant under the transformation of the performance channel, and thus the performance bound γ for $\mathcal{G}$ also holds for $\bar{\mathcal{G}}$. □

Convexification of the Synthesis Conditions

The synthesis problem for the dynamic output feedback (DOF) controller in (5.34) is not convex. As proposed in [68], a variable transformation can be applied to transform (5.34) into bilinear matrix inequalities (BMI). Then, an iterative algorithm can be applied, iterating between fixing one set of variables and solving for the other one. Further details can be found in [68]. For convenience, the variable transformation and an outline of the iterative algorithm are given in (A.3) in Appendix A.1.

For the state feedback case, variable substitutions in the synthesis equations lead to a convex problem. The synthesis equations can thus be formulated into LMIs. The variable transformation is given in (A.8) in Appendix A.2. An overview about the different controller synthesis problems and their convexity will be given in Table 6.1 in Section 6.2.2.

5.5 Distributed Synthesis

The controller synthesis is based on the nominal conditions in (5.34) and on the multiplier conditions in (5.33). While the nominal conditions are completely decoupled into small conditions for each subsystem, the decomposed multiplier conditions in Proposition 5.2 introduce pairwise coupling between neighboring subsystems. Therefore, a decentralized controller synthesis is not possible, and we propose a distributed design method in the following. Our approach is based on a variant of the consensus ADMM [32], which has been introduced in Section 3.5. In the algorithm presented here, only bidirectional

communication to neighboring subsystems is required. This variant has been introduced in [112] where consensus ADMM for the distributed Lasso problem is considered. In [113] this consensus ADMM scheme has been further extended towards an inexact method for efficient computations in case of complex cost functions. In [114], the algorithm was generalized to deal with conic constraints in the consensus couplings.

5.5.1 Decomposed Control Design Problem

We define the global variable vector l containing the set of global structured controller gains A^K, B^K, C^K, D^K, as implicitly given in (5.19), the global block-diagonal Lyapunov matrix $\mathcal{X}$, the multipliers Q_{ik}, R_{ik}, S_{ik} from Proposition 5.2, and $\nu = \gamma^{-\frac{1}{2}}$, with γ being the performance bound in Theorem 2.1. The global synthesis problem of the distributed controller can then be formulated as

$$\min_{l} \;\; f(l) + g(l), \tag{5.36}$$

with $f(\cdot)$ and $g(\cdot)$ being defined as

$$\begin{aligned} f(l) &= -\nu, \\ g(l) &= \mathcal{I}_{(2.12)}(l) + \mathcal{I}_{(2.13)}(l). \end{aligned} \tag{5.37}$$

Herein, $\mathcal{I}_{(a)}(b)$ denotes the indicator function of b satisfying the conditions in (a), i.e.,

$$\mathcal{I}_{(a)}(b) := \begin{cases} 0 & \text{if } b \text{ satisfies } (a), \\ \infty & \text{otherwise.} \end{cases} \tag{5.38}$$

In order to decompose the global synthesis problem, we introduce the set of local variables s_i for all subsystems $i \in \mathcal{N}$, which contain copies of all variables of the global variable vector l that are relevant to the respective subsystem i. The local variable vector s_i thus contains the local controller gains of K_i in (5.12),

$$A_i^K, B_i^K, C_i^K, D_i^K, \;\; A_{ik}^K, B_{ik}^K, C_{ik}^K, D_{ik}^K, \;\; \forall k \in \mathcal{N}_i^K, \tag{5.39}$$

the local Lyapunov matrix $\mathcal{X}_i$, the local copies ν_i of ν, and the local copies of the multipliers involved in the local synthesis problem (5.33), (5.34) of subsystem i. In order to ensure consistency over local copies of variables by different interconnected subsystems i and k corresponding to the same parts of the global variable l, we further define the selection matrices E_{ik} and E_{ki} and formulate the following local consensus constraint

$$E_{ik}\, s_i = E_{ki}\, s_k, \quad \forall (i,k) \in \mathcal{E}.$$

We further define the dual multipliers of subsystem i, corresponding to the consensus constraints for s_i, as λ_i. The decomposed controller synthesis problem is now expressed

as

$$\begin{aligned} \min_{s_i} \quad & \sum_{i=1}^{N} \left(f_i(s_i) + g_i(s_i) \right), \\ \text{s.t.} \quad & E_{ik}\, s_i = E_{ki}\, s_k, \quad \forall (i,k) \in \mathcal{E}. \end{aligned} \tag{5.40}$$

with $f_i(\cdot)$ and $g_i(\cdot)$ being defined as

$$\begin{aligned} f_i(s_i) &= -\frac{1}{N}\nu_i, \\ g_i(s_i) &= \mathcal{I}_{(5.33)}(s_i) + \mathcal{I}_{(5.34)}(s_i). \end{aligned} \tag{5.41}$$

5.5.2 Distributed Control Design Without Global Coordination

We present the distributed consensus ADMM algorithm in Algorithm 5.1 with only nearest neighbor communication to solve the interconnected controller synthesis problem of Proposition 5.2. The communication during the synthesis is defined over the graph $\mathcal{T} = \{\mathcal{N}, \mathcal{E}\}$, where the edge set $\mathcal{E}$ is given by $\mathcal{E} = \mathcal{E}^G \cup \mathcal{E}^{GM} \cup \mathcal{E}^K \cup \mathcal{E}^{KM}$, as introduced in Section 5.2.2.

Algorithm 5.1 Consensus ADMM.

1: **Input:** Parameter $\rho > 0$, local subsystems G_i, interconnections $\mathcal{P}_{ik}^G \ \forall k \in \mathcal{N}_i^G$,
2: $\mathcal{P}_{ik}^K \ \forall k \in \mathcal{N}_i^K$, initial values $s_i^{(0)}$, $\forall i \in \mathcal{N}$,
3: **Initialization**: Set $\kappa = 0$, $\lambda_i^{(0)} = 0$,
4: **while** *not converged* **do**: $\forall i \in \mathcal{N}$ in parallel
5: Communicate $E_{ik}\, s_i^{(\kappa)}$ to neighboring nodes k in $\mathcal{N}_i$,
6: $\lambda_i^{(\kappa+1)} = \lambda_i^{(\kappa)} + \rho \sum_{k \in \mathcal{N}_i} \left(T_{ik}\, s_i^{(\kappa)} - T_{ki}\, s_k^{(\kappa)} \right)$,
7: $s_i^{(\kappa+1)} = \underset{s_i}{\operatorname{argmin}} \{ f_i(s_i) + g_i(s_i) + s_i^\top \lambda_i^{(\kappa+1)}$,
8: $\qquad + \rho \sum_{k \in \mathcal{N}_i} \| T_{ik}\, s_i - \frac{T_{ik}\, s_i^{(\kappa)} + T_{ki}\, s_k^{(\kappa)}}{2} \|_2^2 \}$,
9: $\kappa = \kappa + 1$,
10: **end**
11: **Output:** Local controller gains in (5.39), bounds $\gamma_i = \gamma$.

In step 6 of Algorithm 5.1, the matrices T_{ik} and T_{ki} select the elements over which a consensus should be reached and place them in the right positions for the consensus constraint with respect to λ_i. For convenience, a derivation of the steps of Algorithm 5.1 is given in Appendix A.3. A similar derivation of the steps can be found in [112], [114].

Primal and Dual Residuals

As convergence criteria, the primal and dual residuals can be considered, which are given as

$$\begin{aligned} r^{(\kappa+1)} &= \operatorname{concat}_{i=1}^{N}\Big(\operatorname{concat}_{k\in\mathcal{N}_i}\Big(r_{ik}^{(\kappa+1)}\Big)\Big), \\ d^{(\kappa+1)} &= \operatorname{concat}_{i=1}^{N}\Big(\operatorname{concat}_{k\in\mathcal{N}_i}\Big(d_{ik}^{(\kappa+1)}\Big)\Big), \end{aligned} \tag{5.42}$$

respectively, with

$$\begin{aligned} r_{ik}^{(\kappa+1)} &= \frac{1}{2}\left(E_{ik}s_i^{(\kappa+1)} - E_{ki}s_k^{(\kappa+1)}\right), \\ d_{ik}^{(\kappa+1)} &= \frac{1}{2}\left(E_{ik}(s_i^{(\kappa+1)} - s_i^{(\kappa)}) + E_{ki}(s_k^{(\kappa+1)} - s_k^{(\kappa)})\right). \end{aligned} \tag{5.43}$$

For their derivation, we refer to (A.22) in Appendix A.4.

Note that for determining convergence, the primal and dual residuals, r_i and d_i, can be computed locally. Some higher-level communication protocol of only low communication frequency is required to detect when convergence among all subsystems is reached.

As seen in Section 5.4, and as will be summarized in Table 6.1 in Section 6.2.2, the controller synthesis equations (5.34) are convex in the state feedback case, and the ADMM convergence results in [32] hold for the distributed synthesis in Algorithm 5.1. If a dynamic output feedback controller is to be synthesized, the decomposed synthesis equations are non-convex (bilinear) and need to be solved iteratively in step 7 in Algorithm 5.1, and therefore no convergence guarantee for the ADMM iterations can be given in this case. In the case of distributed output feedback control design, further numerical techniques could be investigated in order to reduce the number of iterations to convergence of the proposed ADMM scheme, such as warm-starting with solutions of the previous ADMM iteration or early termination, such as proposed in [115] for real-time ADMM.

Remark 5.4. Note that in addition to imposing the block-diagonal structure on the multipliers, one could consider further restricting them to DG scalings or diagonal multipliers, which would reduce the dimension of the consensus variables, and therefore both the dimension of the communicated signals as well as the computation and convergence time could possibly be reduced. Since this would introduce more conservatism, we chose to allow for (block-diagonally structured) full blocks.

5.6 Numerical Example

In the following, we consider randomly generated example systems based on coupled mass-spring-damper subsystems. Each subsystem has a mass $m_i \in \mathcal{V}(5, 10)$, spring and damping coefficients, $k_i \in \mathcal{V}(0.8, 1.2)$ and $d_i \in \mathcal{V}(0.8, 1.2)$, respectively, where $\mathcal{V}(a, b)$

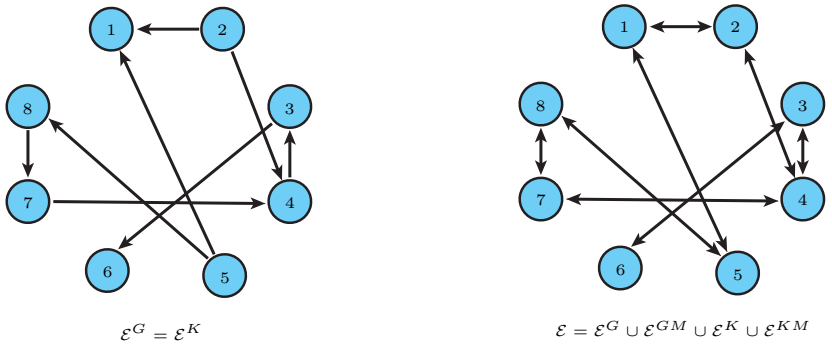

Figure 5.4: Interaction graph of the example system of $N = 8$ subsystems and subcontrollers $\mathcal{E}^G = \mathcal{E}^K$ and the communication graph for distributed control design $\mathcal{E} = \mathcal{E}^G \cup \mathcal{E}^{GM} \cup \mathcal{E}^K \cup \mathcal{E}^{KM}$.

denotes the uniform distribution with support on the interval $[a, b]$. The interconnections between the subsystems are described by the spring and damping coupling coefficients, $k_{ik} \in \mathcal{V}(0.2, 0.4)$ and $d_{ik} \in \mathcal{V}(0.2, 0.4)$. The system matrices are given by

$$\begin{aligned} A_{ii} &= \begin{bmatrix} 0 & 1 \\ -\frac{\sum_{k\in\mathcal{N}_i} k_{ik}}{m_i} & -\frac{\sum_{k\in\mathcal{N}_i} d_{ik}}{m_i} \end{bmatrix}, \quad A_{ik} = \begin{bmatrix} 0 & 0 \\ \frac{k_{ik}}{m_k} & \frac{d_{ik}}{m_k} \end{bmatrix}, \\ B_{u,i} &= \begin{bmatrix} 0 \\ b_{u,i} \end{bmatrix}, \quad D_{zu,i} = \begin{bmatrix} 0_{n_{x_i}\times n_{u_i}} \\ d_{zu,i} \end{bmatrix}, \quad \text{with } b_{u,i},\ d_{zu,i} \in \mathcal{V}(1, 1.3), \\ C_{y,i} &= I, \quad C_{z_i} = \begin{bmatrix} I \\ 0_{n_{w_i}-n_{x_i},n_{x_i}} \end{bmatrix}, \\ B_{w,i} &= \begin{bmatrix} 0 \\ b_{w,i} \end{bmatrix}, \quad \text{with } b_{w,i}, \in \mathcal{V}(1, 1.2), \end{aligned} \tag{5.44}$$

and the remaining system matrices are zero.

We present the convergence of the ADMM scheme in Algorithm 5.1 for two example systems. The first one contains $N = 8$ interconnected subsystems with matrices randomly chosen, as given in (5.44), and the interconnection topology is chosen to be $\mathcal{E}^G = \{$ $(1, 5)$, $(2, 1)$, $(3, 4)$, $(4, 2)$, $(4, 7)$, $(5, 6)$, $(6, 3)$, $(7, 8)$, $(8, 5)$ $\}$, as shown in Figure 5.4. The second example system is composed of $N = 3$ subsystems, which are interconnected in a ring, as shown in Figure 5.6. We consider the synthesis of interconnected static state feedback controllers, which are chosen to have the same interconnection structures as the systems, i.e., $\mathcal{E}^K = \mathcal{E}^G$. The communication topologies that are used for the distributed controller synthesis, given by $\mathcal{E} = \mathcal{E}^G \cup \mathcal{E}^{GM} \cup \mathcal{E}^K \cup \mathcal{E}^{KM}$, are also shown in Figures 5.4 and 5.6. Figures 5.5 and 5.7 show the convergence of the bounds γ_i on the $\mathcal{H}_\infty$-norm of the two example systems, and the convergence of the primal and dual residuals, as given in (5.42). This convergence behavior is representative for the simulated example systems. The convergence time and the oscillatory behavior, however, depend on the number of subsystems and on the interconnection topology.

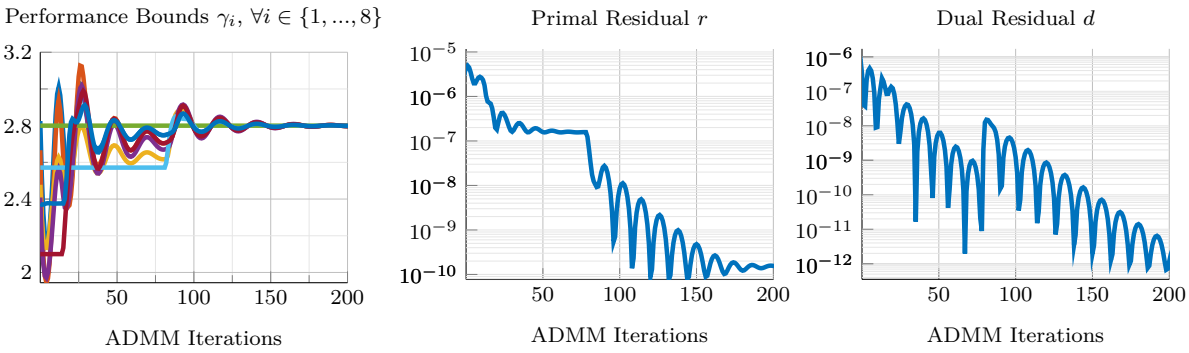

Figure 5.5: Convergence results for the ADMM scheme in Algorithm 5.1 for an example system of $N = 8$ interconnected subsystems.

Figure 5.6: Interaction graph of the example system of $N = 3$ subsystems and subcontrollers $\mathcal{E}^G = \mathcal{E}^K$ and the communication graph for distributed control design $\mathcal{E} = \mathcal{E}^G \cup \mathcal{E}^{GM} \cup \mathcal{E}^K \cup \mathcal{E}^{KM}$.

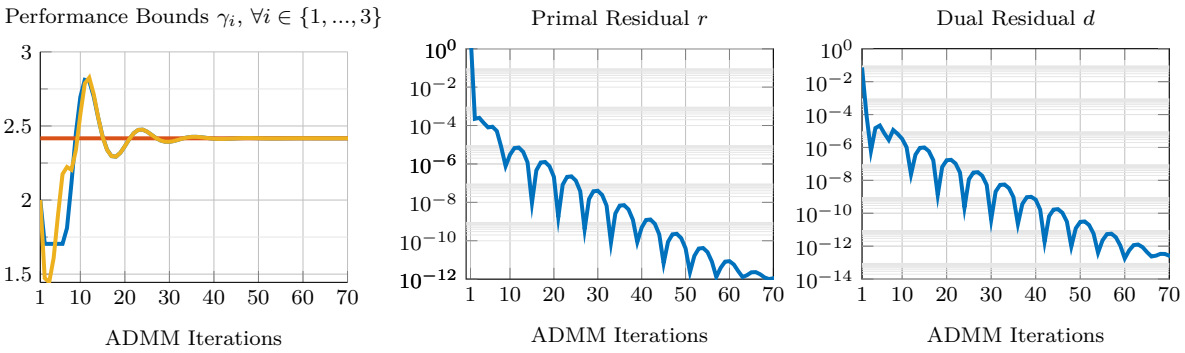

Figure 5.7: Convergence results for the ADMM scheme in Algorithm 5.1 for an example system of $N = 3$ interconnected subsystems.

The scalability of this distributed synthesis method will be illustrated in a numerical example in Section 6.3, where it will be compared to the centralized synthesis and to a more compact synthesis for special classes of interconnected systems which will be presented in Chapter 6.

5.7 Conclusions

A modeling framework has been presented for heterogeneous systems interconnected over arbitrary graphs, to which the FBSP can be applied. Under some structural assumptions on the Lyapunov matrix and multipliers, the controller synthesis equations have been decomposed into small matrix inequalities of the size of the individual subsystems. These decomposed equations are pairwise coupled according to the edges of the interconnection graph. A distributed solution method based on an ADMM scheme without central coordination has been presented. The computational effort of each individual subsystem per ADMM iteration scales linearly with the number of neighboring subsystems. The communication topology of the synthesized interconnected controller is a design choice and may differ from the plant coupling structure. In particular, a sparse controller interconnection topology can be chosen in order to avoid excessive communication. Numerical examples have demonstrated the convergence of the distributed synthesis. The scalability of the decomposed and distributed synthesis algorithm will be illustrated in Section 6.3 of Chapter 6, where they will be compared to methods tailored to special classes of systems.

CHAPTER 6

Special Classes of Interconnected Systems

Depending on the degree of homogeneity of the subsystems, special classes of interconnected systems can be defined. First, we review the case of homogeneous systems where all subsystems are identical [59] and show how the model of heterogeneous systems and the model for homogeneous systems are related by a transformation. Then we introduce a new class of systems, referred to as α-β-heterogeneous systems. They consist of multiple groups of homogeneous subsystems with different interconnections. We show how the general model for heterogeneous systems from Chapter 5 can be transformed into a more compact model for this special class of systems. This allows for a more scalable controller synthesis. α-β-Heterogeneous systems are a significant extension with respect to [61] where multiple groups of homogeneous subsystems are considered, but all interconnections are required to be identical. In particular, the system model of α-β-heterogeneous systems allows for a controller synthesis where the interconnection topology of the controller is a design choice. This chapter is based on work that has been published in [14].

The chapter is structured as follows. Section 6.1 addresses the special case of homogeneous systems. In Section 6.2 we introduce the new class of α-β-heterogeneous systems. In Section 6.3, we present numerical results that demonstrate the scalability of the decomposed methods from this chapter and we compare them with the methods for heterogeneous systems presented in Chapter 5.

6.1 Homogeneous Systems

First, we present the most special class of interconnected systems, where all subsystems and all interconnections are identical. This has been presented in [59] as decomposable systems. We will show how the compact model of homogeneous systems [59] can be derived by a transformation from the general model of heterogeneous systems presented in Chapter 5. As the modeling framework and the synthesis methods are closely linked, also the controller synthesis is simplified with respect to the formulation for heterogeneous systems.

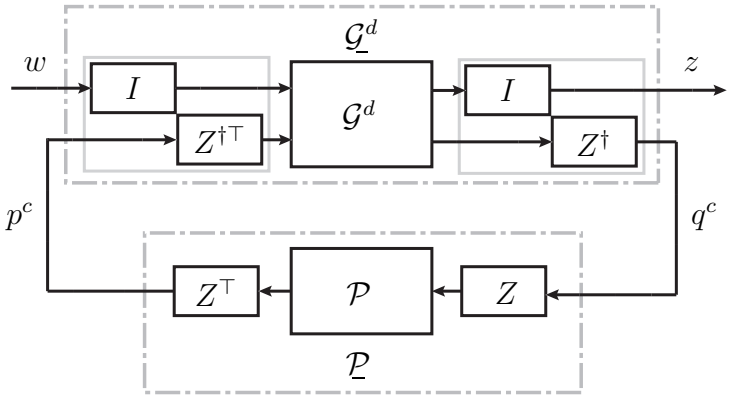

Figure 6.1: Transformation of the interconnection channel.

6.1.1 Model of Homogeneous Systems

Definition 6.1 (Homogeneous System)**.** *Let M represent all system matrices A, B_u, C_y, D_{yw}, C_z, D_{zu}, D_{zw}, in* (5.9)*. We define a homogeneous system if its system matrices can be written as*

$$M = \underbrace{I_N \otimes M_{ii}}_{M^d} + \underbrace{P^G \otimes M_{ik}}_{M^i}, \tag{6.1}$$

with P^G as defined in Section 5.1.1. This means that for a homogeneous system all local subsystem matrices M_{ii}, $\forall i \in \mathcal{N}$ (on the diagonal) are identical and all interconnection subsystem matrices M_{ik}, $\forall (i,k) \in \mathcal{E}^G$ (the off-diagonal block matrices) are identical.

Proposition 6.1. *If the controller K is also chosen as a homogeneous controller, i.e., such that* (6.1) *holds with M representing the controller matrices A^K, B^K, C^K and D^K, and if $P^G = P^K$, then, the interconnected closed loop system in* (5.20) *can be transformed to a representation where the interconnection operator takes the form*

$$\underline{\mathcal{P}} = P \otimes I_{n_{p^c}}, \tag{6.2}$$

with $P = P^G = P^K$, and the system matrices of (5.1) *are transformed accordingly, such that the closed loop system is not changed under the transformation.*

Proof. We define the transformations of the interconnection channel, $\mathcal{P}$, and of the decentralized system part, $\mathcal{G}^d$, as

$$\begin{aligned} \underline{\mathcal{P}} &= Z^\top \mathcal{P} Z, \\ \underline{\mathcal{G}}^d &= \operatorname{diag}\left(I, Z^\dagger\right) \mathcal{G}^d \operatorname{diag}\left(I, Z^{\dagger\top}\right). \end{aligned} \tag{6.3}$$

The transformation matrix Z is defined as the $|\mathcal{E}| \times N$ matrix of all zeros except for ones in the entries corresponding to an interconnection of an edge to a subsystem. The interconnection topology is captured in $\underline{\mathcal{P}} = P \otimes I_{n_p^c}$ and the interconnections are summarized into one channel per subsystem. □

The transformation in (6.3) in the proof of Proposition 6.1 is shown in Figure 6.1.

The following numerical example illustrates the transformation in (6.3).

Example 6.1 (Transformation to more compact representation for homogeneous systems). Let us consider the system in Example 5.1 in Section 5.1.3 again, which we assume to be a homogeneous system. In interconnection with a homogeneous controller of the same interconnection topology, the resulting closed-loop system can be described by the interconnection matrix

$$P = \begin{bmatrix} 0 & P_{12} & 0 & 0 \\ P_{21} & 0 & P_{23} & P_{24} \\ 0 & P_{32} & 0 & 0 \\ 0 & P_{42} & 0 & 0 \end{bmatrix}.$$

The interconnection channel, as defined in (5.5), for the closed-loop system is given as

$$\underbrace{\begin{bmatrix} \underline{p}_{12}^c \\ p_{21}^c \\ p_{23}^c \\ \underline{p}_{24}^c \\ \underline{p}_{32}^c \\ p_{42} \end{bmatrix}}_{p^c} = \underbrace{\left[\begin{array}{c|c|c|c} 0 & \mathcal{P}_{12} & 0 & 0 \\ \hline \mathcal{P}_{21} & 0 & 0 & 0 \\ 0 & 0 & 0 & 0 \\ 0 & 0 & 0 & 0 \\ \hline 0 & 0 & \mathcal{P}_{32} & 0 \\ \hline 0 & 0 & 0 & \mathcal{P}_{42} \end{array}\right.}_{\mathcal{P}} \left.\begin{array}{c|c} 0 & 0 \\ \hline 0 & 0 \\ \mathcal{P}_{23} & 0 \\ 0 & \mathcal{P}_{24} \\ \hline 0 & 0 \\ \hline 0 & 0 \end{array}\right] \underbrace{\begin{bmatrix} \underline{q}_{12}^c \\ q_{21}^c \\ q_{23}^c \\ \underline{q}_{24}^c \\ \underline{q}_{32}^c \\ q_{42} \end{bmatrix}}_{q^c}.$$

As the system is assumed to be a homogeneous system, all the interconnection channels over the different edges of a subsystem are identical, because all off-block-diagonal matrices M_{ik} are identical. Therefore, we can apply the transformation

$$Z = \begin{bmatrix} I & 0 & 0 & 0 \\ 0 & I & 0 & 0 \\ 0 & I & 0 & 0 \\ 0 & I & 0 & 0 \\ 0 & 0 & I & 0 \\ 0 & 0 & 0 & I \end{bmatrix},$$

which leads to the interconnection matrix

$$\begin{aligned} \underline{\mathcal{P}} = Z^\top \mathcal{P} Z &= \begin{bmatrix} 0 & \mathcal{P}_{12} & 0 & 0 \\ \mathcal{P}_{21} & 0 & \mathcal{P}_{23} & \mathcal{P}_{24} \\ 0 & \mathcal{P}_{32} & 0 & 0 \\ 0 & \mathcal{P}_{42} & 0 & 0 \end{bmatrix} \\ &= P \otimes I_{n_p^c}. \end{aligned} \tag{6.4}$$

The transformed interconnection matrix $\underline{\mathcal{P}}$ captures the information about the interconnection topology on the level of the subsystems and summarizes all interconnection signals from different subsystems to the same subsystem in one channel. The last equality in (6.4) assumes that the individual interconnection matrices $\mathcal{P}_{ik}$ can be captured

in the form involving the interconnection matrix $P_{ik} \otimes I_{n_{p^c}}$. The decentralized part of the system, $\mathcal{G}^d$ is transformed according to (6.3) such that the closed loop system is not changed.

The system matrices in (5.1) are thus transformed to the system matrices of $\underline{\mathcal{G}}^d$ as follows

$$\begin{aligned} B_{p,i} &= \begin{bmatrix} A_{ik} & B_{u,ik} & B_{w,ik} \end{bmatrix}, \\ D_{zp,i} &= \begin{bmatrix} C_{z,ik} & D_{zu,ik} & D_{zw,ik} \end{bmatrix}, \\ D_{yp,i} &= \begin{bmatrix} C_{y,ik} & 0 & D_{yw,ik} \end{bmatrix}, \\ C_{q,i} &= \begin{bmatrix} I_{n_{x_k}} & 0 & 0 \end{bmatrix}^\top, \\ D_{qw,i} &= \begin{bmatrix} 0 & 0 & I_{n_{w_k}} \end{bmatrix}^\top, \\ D^d_{qu,i} &= \begin{bmatrix} 0 & I_{n_{u_k}} & 0 \end{bmatrix}^\top. \end{aligned} \tag{6.5}$$

The controller matrices corresponding to the interconnection channel of subcontroller i for a homogeneous controller can be defined as

$$\begin{aligned} B_{p^K,i} &= \begin{bmatrix} {A^K}_{ik} & {B^K}_{ik} \end{bmatrix}, \\ C_{p^K,i} &= \begin{bmatrix} {C^K}_{ik} & {D^K}_{ik} \end{bmatrix}, \\ C_{q^K,i} &= \begin{bmatrix} I & 0 \end{bmatrix}^\top, \\ D_{q^K,i} &= \begin{bmatrix} 0 & I \end{bmatrix}^\top. \end{aligned} \tag{6.6}$$

Note that the representations in (6.5) and (6.6) are not unique. A similar model of interconnected systems has been used in [59]. In this representation, the controller synthesis equations can be simplified as described in the following.

6.1.2 Decomposed Synthesis for Homogeneous Systems

We state the following result without a proof. In the following, we will extend these results to a broader class of systems and will give the derivations and proofs.

Proposition 6.2 (Decomposed Full-Block S-Procedure for Homogeneous Systems, [59])**.** *Let us consider a homogeneous system $G = \mathcal{F}_l(G^d, \mathcal{P}^G)$, which is given in* (5.7) *with $\mathcal{P}^G = P^G \otimes I_{n_p}$ structured as in* (6.2)*, assumed to be normal, and the system matrices are structured as in* (6.1)*. Then, there exists a controller K as in* (5.12) *with $P^K = P^G = P$, and with controller matrices satisfying* (6.1)*, such that $\mathcal{G} = \mathcal{F}_u(G, K)$ is stable and has an $\mathcal{L}_2$-gain less than γ, if there exist matrices $\mathcal{X}_i = \mathcal{X}_i^\top > 0$, and $\tilde{Q}_i = \tilde{Q}_i^\top$, $\tilde{R}_i = \tilde{R}_i^\top$ and $\tilde{S}_i$, such that* (5.34) *and*

$$\begin{bmatrix} \star \end{bmatrix}^T \begin{bmatrix} \tilde{Q}_i & \tilde{S}_i \\ \tilde{S}_i^\top & \tilde{R}_i \end{bmatrix} \begin{bmatrix} \lambda I_{n_{p^c}} \\ I_{n_{p^c}} \end{bmatrix} > 0, \ \forall \lambda \in \operatorname{spec}(P), \tag{6.7}$$

where $\operatorname{spec}(\cdot)$ *means the spectrum, i.e., the set of eigenvalues.*

The implementation of the synthesis problem for homogeneous subsystems can be done in a centralized way, or each subsystem can solve it in a decentralized way, assuming knowledge of the eigenvalues of the interconnection matrices.

Note that the decomposed synthesis equations of Proposition 5.2 can also be used in the case of homogeneous systems. Choosing identical multipliers Q_{ik}, R_{ik} and S_{ik}, respectively, for all edges (i,k), allows us to decompose the nominal and multiplier conditions to identical small ones of the size of the individual subsystems. However, as less structural knowledge about the interconnected system is exploited, in general more conservatism can be introduced by the controller design in Proposition 5.2 than by the one in Proposition 6.2. In particular, no information about the interconnection topology of the subsystems is captured in the system representation. It can be observed that the bound γ of the resulting closed-loop system under the synthesized controller from Proposition 5.2 is equal to the one from Proposition 6.2 (and therefore no additional conservatism is introduced), only if the graph is regular, and if the spectrum of the interconnection matrix is symmetric, i.e., if the smallest and largest eigenvalues satisfy $\lambda_{\min}(P) = -\lambda_{\max}(P)$. If these conditions are not met, it can be observed that Proposition 6.2 is less conservative than the synthesis based on Proposition 5.2 with identical multipliers for all edges.

6.2 α-β-Heterogeneous Systems

In the following, we consider a more general model, where the system consists of different groups of homogeneous subsystems with different interconnections. This modeling approach extends the special case in [61], which allows for different groups of homogeneous subsystems, but where the interconnections are restricted to be all identical. While the synthesized controller in [61] needs to have the same interconnection topology as the plant, the interconnection topology of the controller synthesized for the α-β-heterogeneous systems is a design choice. Furthermore, instead of the singular-value decomposition of the interconnection operator in [61], we propose a congruence transformation which potentially reduces conservatism.

6.2.1 Model of α-β-Heterogeneous Systems

Definition 6.2 (α-β-Heterogeneous Systems)**.** *We define a system of α groups of homogeneous subsystems with β different interconnection types, referred to as α-β-heterogeneous systems, if the system matrices can be written as*

$$M = \underbrace{\sum_{i=1}^{\alpha} I_{(\Theta_{i-1}+1):\Theta_i} \otimes M_{ii}}_{M^d} + \underbrace{\sum_{i=1}^{\alpha} \sum_{j=1}^{\beta^G} \left(I_{(\Theta_{i-1}+1):\Theta_i} P^G_j \otimes M_{ij} \right)}_{M^i}, \tag{6.8}$$

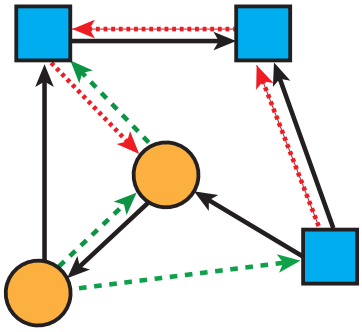

Figure 6.2: Two groups of homogeneous subsystems interconnected by three different interconnections ($\beta^G = 3$) symbolized by the different arrow types.

where P^G_j are different interconnection matrices, and $I_{(\Theta_{i-1}+1):\Theta_i}$ is an $N \times N$ matrix of all zeros except that the diagonal entries corresponding to the indices from $\Theta_{i-1}+1$ to Θ_i are ones. The index set variable Θ_i is defined as $\Theta_i = \sum_{l=1}^{i} N_l$ with $\Theta_0 = 0$, where N_l is the number of subsystems in the group $l \in \{1, ..., \alpha\}$.

This means that within each of the α groups, all subsystems have equal matrices M_{ii} and can have β^G different matrices M_{ij} interconnected through the interconnection matrices ${P^G}_j$, respectively.

Figure 6.2 shows an example with two groups of homogeneous subsystems and $\beta^G = 3$ different interconnections. The matrices M_{ij} correspond to those off-diagonal blocks of M which represent the influence from all subsystems specified by the structure of P^G_j on the subsystems i.

Proposition 6.3. *If the controller K is also chosen to be composed of groups of homogeneous subcontrollers with different interconnection types, i.e., such that (6.8) holds with M representing the controller matrices A^K, B^K, C^K and D^K, and with P^K_j and β^K instead of P^G_j and β^G, then the interconnected closed loop system in (5.20) can be transformed to a representation where the interconnection matrix takes the form*

$$\underline{\mathcal{P}} = \operatorname{diag}_{j=1}^{\beta}\Big(P_j \otimes I_{n_{p_j^c}}\Big), \tag{6.9}$$

with $\bigcup_{j=1...\beta} P_j$ being the union of the different interconnection matrices of the system and the controller, i.e., β is the number of different interconnection matrices ${P^G}_j$ and ${P^K}_j$ in the closed-loop system.

Proof. We define the transformations of the interconnection channel and of the decentralized system part similarly as in (6.3) as $\underline{\mathcal{P}} = Z^\top \mathcal{P} Z$ and $\underline{\mathcal{G}}^d = Z^{-1}\mathcal{G}^d Z^{-\top}$, respectively. For the α-β-heterogeneous system, the transformation matrix Z is defined as the $|\mathcal{E}| \times (\beta\, N)$ concatenated matrix $Z = \operatorname{concat}_{j=1}^{\beta}(Z_j)$, where Z_j are the $|\mathcal{E}| \times N$ matrices of all zeros except for ones in the entries corresponding to an interconnection defined

in P_j between an edge and a system. With this transformation, the β interconnection topologies are captured in $\underline{\mathcal{P}} = \operatorname{diag}_{j=1}^{\beta}\Big(P_j \otimes I_{n_{p^c}}\Big)$. □

The transformation in (6.3) is shown in Figure 6.1. The following numerical example illustrates this transformation for an α-β-heterogeneous system.

Example 6.2 (Transformation to more compact system representation for α-β-heterogeneous systems). Let us consider the system from Example 6.1 again. Now, we assume that the closed-loop subsystems 1 and 2 have equal diagonal matrices, i.e., $M_{11} = M_{22} =: M_1$ and therefore form a homogeneous group and subsystems 3 and 4 form another one, i.e., $M_{33} = M_{44} =: M_2$, and thus $\alpha = 2$. Furthermore, we assume that M_{12} and M_{21} are equal and form one group of homogeneous interconnections, and M_{23}, M_{32}, M_{24} and M_{42} are equal and form another one, and thus $\beta = 2$. The different interconnection types are important for the modeling of the interconnection matrices P_j, which, for this example, can be represented as

$$P_1 = \begin{bmatrix} 0 & P_{12} & 0 & 0 \\ P_{21} & 0 & 0 & 0 \\ 0 & 0 & 0 & 0 \\ 0 & 0 & 0 & 0 \end{bmatrix}, \quad P_2 = \begin{bmatrix} 0 & 0 & 0 & 0 \\ 0 & 0 & P_{23} & P_{24} \\ 0 & P_{32} & 0 & 0 \\ 0 & P_{42} & 0 & 0 \end{bmatrix}.$$

We can apply the following transformation

$$Z = \left[\begin{array}{ccc:c} I & & & 0 \\ & I & & \\ & 0 & & \\ & & 0 & \\ \hdashline & & & \end{array}\right.\begin{array}{c:ccc} & & & \\ 0 & & & \\ I & & & \\ I & & & \\ & I & & \\ & & I & \end{array}\left.\right],$$

which leads to the interconnection matrix

$$\begin{aligned} \underline{\mathcal{P}} = Z^\top \mathcal{P} Z &= \left[\begin{array}{cccc:cccc} 0 & \mathcal{P}_{12} & 0 & 0 & 0 & 0 & 0 & 0 \\ \mathcal{P}_{21} & 0 & 0 & 0 & 0 & 0 & 0 & 0 \\ 0 & 0 & 0 & 0 & 0 & 0 & 0 & 0 \\ 0 & 0 & 0 & 0 & 0 & 0 & 0 & 0 \\ \hdashline 0 & 0 & 0 & 0 & 0 & 0 & 0 & 0 \\ 0 & 0 & 0 & 0 & 0 & 0 & \mathcal{P}_{23} & \mathcal{P}_{24} \\ 0 & 0 & 0 & 0 & 0 & \mathcal{P}_{32} & 0 & 0 \\ 0 & 0 & 0 & 0 & 0 & \mathcal{P}_{42} & 0 & 0 \end{array}\right] \\ &= \operatorname{diag}(P_1 \otimes I_{n_{p_1^c}}, P_2 \otimes I_{n_{p_2^c}}) = \operatorname{diag}_{j=1}^{\beta}\left(P_j \otimes I_{n_{p_j^c}}\right). \end{aligned}$$

The last equality uses the assumption that the individual interconnection matrices $\mathcal{P}_{ik}$ can be expressed in the form $P_{ik} \otimes I_{n_{p^c}}$. The decentralized part of the system, $\mathcal{G}^d$ is transformed according to the transformation in (6.3) such that the closed-loop system is not changed. Note that this modeling is not unique.

A possible realization of the transformed system matrices of $\underline{\mathcal{G}}^d$ is given as follows.

$$\begin{aligned}
B_{p,i} &= \sum_{j=1}^{\beta^G} \left(e_j^\top \otimes \begin{bmatrix} A_{ij} & B_{u,ij} & B_{w,ij} \end{bmatrix} \right), \\
D_{zp,i} &= \sum_{j=1}^{\beta^G} \left(e_j^\top \otimes \begin{bmatrix} C_{z,ij} & D_{zu,ij} & D_{zw,ij} \end{bmatrix} \right), \\
D_{yp,i} &= \sum_{j=1}^{\beta^G} \left(e_j^\top \otimes \begin{bmatrix} C_{y,ij} & 0 & D_{yw,ij} \end{bmatrix} \right), \\
C_{q,i} &= \sum_{j=1}^{\beta^G} \left(e_j \otimes \begin{bmatrix} I_{n_{x_j}} & 0 & 0 \end{bmatrix}^\top \right), \\
D_{qw,i} &= \sum_{j=1}^{\beta^G} \left(e_j \otimes \begin{bmatrix} 0 & 0 & I_{n_{w_j}} \end{bmatrix}^\top \right), \\
D^d_{qu,i} &= \sum_{j=1}^{\beta^G} \left(e_j \otimes \begin{bmatrix} 0 & I_{n_{u_j}} & 0 \end{bmatrix}^\top \right).
\end{aligned} \tag{6.10}$$

The controller matrices corresponding to the interconnection channel of subcontroller i for an α-β-heterogeneous controller can be realized as

$$\begin{aligned}
B_{p^K,i} &= \sum_{j=1}^{\beta^K} \left(e_j^\top \otimes \begin{bmatrix} {A^K}_{ij} & {B^K}_{ij} \end{bmatrix} \right), \\
C_{p^K,i} &= \sum_{j=1}^{\beta^K} \left(e_j^\top \otimes \begin{bmatrix} {C^K}_{ij} & {D^K}_{ij} \end{bmatrix} \right), \\
C_{q^K,i} &= \sum_{j=1}^{\beta^K} \left(e_j^\top \otimes \begin{bmatrix} I & 0 \end{bmatrix} \right), \\
D_{q^K,i} &= \sum_{j=1}^{\beta^K} \left(e_j^\top \otimes \begin{bmatrix} 0 & I \end{bmatrix} \right).
\end{aligned} \tag{6.11}$$

As in the homogeneous case, instead of stacking multiple identical interconnection channels for neighboring subsystems, they are summarized in one interconnection channel per subsystem. In order to transform the representation to this form, the interconnection channel of each subsystem is augmented (by zero signals) such that each subsystem has interconnection signals belonging to all different interconnection matrices P_j. Therefore, this formulation in general involves a larger dimension of the interconnection channel. It depends on the degree of homogeneity of the system, i.e., on the values of α and β, whether this formulation is beneficial for a reduction in complexity compared to Proposition 5.2.

Remark 6.1. In comparison to the model in [61], the subsystems can have different interconnections. For example, the states can be interconnected through a different interconnection matrix than the performance inputs or outputs, or the control inputs. An example will be given in Section 7.3.2 where the interconnected α-β-heterogeneous system results from an augmented overlapping system representation.

In the following, we will show how the controller synthesis can be decoupled and made more compact based on the system representation in (6.8).

6.2.2 Decomposed Synthesis for α-β-Heterogeneous Systems

Proposition 6.4 (Decomposed Full-Block S-Procedure for α-β-Heterogeneous Systems)**.** *Let us consider the system $G = \mathcal{F}_l(G^d, \mathcal{P}^G)$, as given in (5.7), with system matrices as defined in (6.8), Then there exists a controller K as in (5.14) with controller matrices satisfying (6.8), such that the interconnection matrix of the closed-loop system is given in (6.9), and such that $\mathcal{G} = \mathcal{F}_u(G, K)$ is stable and has an $\mathcal{L}_2$-gain less than γ, if there exist $\mathcal{X}_i = \mathcal{X}_i^\top > 0$, and $\tilde{Q} = \operatorname{diag}_{j=1}^{\beta}\left(\tilde{Q}_j\right)$, $\tilde{R} = \operatorname{diag}_{j=1}^{\beta}\left(\tilde{R}_j\right)$ and $\tilde{S} = \operatorname{diag}_{j=1}^{\beta}\left(\tilde{S}_j\right)$, with $\tilde{Q}_j = \tilde{Q}_j^\top$, $\tilde{R}_j = \tilde{R}_j^\top$ and $\tilde{S}_j$, $\forall j = \{1, ..., \beta\}$, such that*

$$\left[\star\right]^T \begin{bmatrix} I_N \otimes \tilde{Q}_j & I_N \otimes \tilde{S}_j \\ I_N \otimes \tilde{S}_j^\top & I_N \otimes \tilde{R}_j \end{bmatrix} \begin{bmatrix} P_j \otimes I_{n_{p_j^c}} \\ I_{N n_{p_j^c}} \end{bmatrix} > 0, \quad \forall j \in \{1, ..., \beta\}, \tag{6.12}$$

$$\left[\star\right]^\top \left[\begin{array}{cc:cc:cc} 0 & \mathcal{X}_i & 0 & 0 & 0 & 0 \\ \mathcal{X}_i & 0 & 0 & 0 & 0 & 0 \\ \hdashline 0 & 0 & -\gamma I & 0 & 0 & 0 \\ 0 & 0 & 0 & \frac{1}{\gamma} I & 0 & 0 \\ \hdashline 0 & 0 & 0 & 0 & \tilde{Q} & \tilde{S} \\ 0 & 0 & 0 & 0 & \tilde{S}^\top & \tilde{R} \end{array}\right] \left[\begin{array}{ccc} I & 0 & 0 \\ \mathcal{A}_i & \mathcal{B}_{1,i} & \mathcal{B}_{2,i} \\ \hdashline 0 & I & 0 \\ \mathcal{C}_{1,i} & \mathcal{D}_{11,i} & \mathcal{D}_{12,i} \\ \hdashline 0 & 0 & I \\ \mathcal{C}_{2,i} & \mathcal{D}_{21,i} & \mathcal{D}_{22,i} \end{array}\right] < 0, \quad \forall i \in \{1, ..., \alpha\}. \tag{6.13}$$

Proof. The proof follows along the same lines as the one of Proposition 5.2 with the structured Lyapunov matrix $\mathcal{X} = \operatorname{diag}_{i=1}^{\alpha}(I_{N_i} \otimes \mathcal{X}_i)$ and the structured multipliers $Q = \operatorname{diag}_{j=1}^{\beta}\left(I_N \otimes \tilde{Q}_j\right)$, $R = \operatorname{diag}_{j=1}^{\beta}\left(I_N \otimes \tilde{R}_j\right)$ and $S = \operatorname{diag}_{j=1}^{\beta}\left(I_N \otimes \tilde{S}_j\right)$. Herein, N_i is the number of subsystems within the group i. □

Note that if the system G is the transformed system from $\bar{G}$ in (5.25), Corollary 5.1 applies such that Proposition 6.4 also holds for $\bar{\mathcal{G}}$. Furthermore, Lemma 6.1 from [63] can be applied in order to decompose the multiplier condition into small conditions.

Lemma 6.1 (adapted from [63])**.** *Given the normal, real-valued interconnection matrices $\mathcal{P}_j = P_j \otimes I_{n_{p_j}}$ with eigenvalues λ, then the following statements are equivalent*

$$\text{(i)} \left[\star\right]^\top \begin{bmatrix} \tilde{Q}_j & \tilde{S}_j \\ \tilde{S}_j^\top & \tilde{R}_j \end{bmatrix} \begin{bmatrix} \lambda I_{n_{p_j^c}} \\ I_{n_{p_j^c}} \end{bmatrix} > 0, \ \forall \lambda \in \operatorname{spec}(P_j), \quad \forall j \in \{1, ..., \beta\},$$

$$\text{(ii)} \left[\star\right]^T \begin{bmatrix} I_N \otimes \tilde{Q}_j & I_N \otimes \tilde{S}_j \\ I_N \otimes \tilde{S}_j^\top & I_N \otimes \tilde{R}_j \end{bmatrix} \begin{bmatrix} P_j \otimes I_{n_{p_j^c}} \\ I_{N n_{p_j^c}} \end{bmatrix} > 0, \ \forall j \in \{1, ..., \beta\}.$$

Proof. We consider a diagonalizing transformation $F^\top P_j F = \Lambda_j$, which is guaranteed to exist because P_j is assumed to be normal. Then, the following regular transformation

with $Z = F \otimes I$ and $Z^\top Z = I$ can be applied. Using the properties of the Kronecker product, this transformation yields the following equivalent statements,

$$\begin{aligned} Z^\top [\star]^\top \begin{bmatrix} Z & 0 \\ 0 & Z \end{bmatrix} \begin{bmatrix} Z & 0 \\ 0 & Z \end{bmatrix}^\top \begin{bmatrix} I_N \otimes \tilde{Q}_j & I_N \otimes \tilde{S}_j \\ I_N \otimes \tilde{S}_j^\top & I_N \otimes \tilde{R}_j \end{bmatrix} \begin{bmatrix} Z & 0 \\ 0 & Z \end{bmatrix} \begin{bmatrix} Z & 0 \\ 0 & Z \end{bmatrix}^\top \begin{bmatrix} P_j \otimes I \\ I_{n_{p_j^c}} \end{bmatrix} Z > 0, \\ \forall j = 1, ..., \beta, \\ \iff [\star]^\top \begin{bmatrix} I_N \otimes \tilde{Q}_j & I_N \otimes \tilde{S}_j \\ I_N \otimes \tilde{S}_j^\top & I_N \otimes \tilde{R}_j \end{bmatrix} \begin{bmatrix} \Lambda_j \otimes I \\ I_{n_{p_j^c}} \end{bmatrix} > 0, \\ \forall j = 1, ..., \beta, \end{aligned} \tag{6.14}$$

The last inequality is equivalent to

$$\begin{aligned} &[\star]^\top \begin{bmatrix} \tilde{Q}_j & \tilde{S}_j \\ \tilde{S}_j^\top & \tilde{R}_j \end{bmatrix} \begin{bmatrix} \lambda I \\ I_{n_{p_j^c}} \end{bmatrix} > 0, \quad \forall \lambda \in \operatorname{spec}(P_j), \\ &\forall j \in \{1, ..., \beta\}, \end{aligned} \tag{6.15}$$

since $\Lambda_j = \operatorname{diag}_{\lambda \in \operatorname{spec}(P_j)}(\lambda)$. □

Introducing the additional constraint of $\tilde{Q}_j$ being negative definite imposes concavity of the decomposed multiplier conditions in λ, which reduces the set of multiplier conditions to the following

Corollary 6.1. *If the interconnection matrices $\mathcal{P}_j$ are normal, they can always be transformed into diagonal matrices with their eigenvalues on the diagonal. Introducing the additional constraint $\tilde{Q}_j < 0$ guarantees concavity of the multiplier condition in λ. This leads to the multiplier conditions*

$$\begin{aligned} \left[\star\right]^T \begin{bmatrix} \tilde{Q}_j & \tilde{S}_j \\ \tilde{S}_j^\top & \tilde{R}_j \end{bmatrix} \begin{bmatrix} \lambda I_{n_{p_j^c}} \\ I_{n_{p_j^c}} \end{bmatrix} > 0, \ \forall \lambda \in \{\lambda_{\min}(P_j), \lambda_{\max}(P_j)\} \\ \forall j \in \{1, ..., \beta\}. \end{aligned} \tag{6.16}$$

Remark 6.2. Corollary 6.1 can be applied w. l. o. g. if any P_j is not normal, as any given interconnection matrix can be transformed and augmented into a normal one. For simplicity the normal case is considered here. Possible transformations to obtain normal interconnection matrices are given in [63].

Thus, in the case of α groups of homogeneous subsystems, there are α small nominal conditions to be solved. Furthermore, for each of the β interconnection types, two multiplier conditions (for the smallest and largest eigenvalues of the P_j), need to be solved.

Remark 6.3. If some P_j are simultaneously diagonalizable, i.e., if they commute in the multiplication and are diagonalizable [59], [116], then β can be further reduced at the cost of increased conservatism.

Synthesis	Problems	DOF	SSF
Centralized	(5.36), i.e., (2.12) / (2.13)	convex (LMIs) / nonconvex (BMIs)	convex (LMIs) / convex (LMIs)
Decomposed heterogeneous	(5.33) / (5.34)	convex (LMIs) / nonconvex (BMIs)	convex (LMIs) / convex (LMIs)
Distributed heterogeneous	(5.40), i.e., (5.33) / (5.34)	convex (LMIs) / nonconvex (BMIs)	convex (LMIs) / convex (LMIs)
Decomposed homogeneous	(6.7) / (5.34)	convex (LMIs) / nonconvex (BMIs)	convex (LMIs) / convex (LMIs)
Decomposed α-β-heterogeneous	(6.12) / (6.13)	convex (LMIs) / nonconvex (BMIs)	convex (LMIs) / convex (LMIs)

Table 6.1: Overview of the different interconnected controller synthesis problems introduced in Chapters 5 and 6. The resulting convexity of the optimization problems after the variable transformations given in Appendices A.1 and A.2, for dynamic output feedback (DOF) and static state feedback (SSF), respectively, are indicated.

Controller Synthesis

As discussed before, the synthesis conditions in Propositions 6.2 and 6.4 can be transformed into convex ones in the case of state feedback. In the case of dynamic output feedback, a variable transformation leads to bilinear matrix inequalities which need to be solved iteratively. The transformations from (A.3) and (A.8) can be applied with the simplifications due to the special cases of homogeneous or α-β-heterogeneous interconnected systems. An overview of the different synthesis problems presented in Chapters 5 and 6, and their convexity after the variable transformations, is given in Table 6.1.

If the values of α and β are small, the decomposed synthesis equations can be solved efficiently in a centralized way, i.e., simultaneously in one computer, or they can be solved in a decentralized way by each individual subsystem, if all the required information is available. For better scalability, the distributed design method in Algorithm 5.1 can be used to compute a consensus over the multiplier matrices which introduces coupling between the synthesis equations.

6.3 Numerical Example

In the following, we compare the computational scalability of the centralized synthesis with full block multipliers for heterogeneous systems in Theorem 2.1 with the decom-

Synthesis	Nominal condition		Multiplier condition	
	Number	Size	Number	Size
Centralized	1	$N\bar{X}_{\mathrm{n}} \times N\bar{X}_{\mathrm{n}}$	1	$\lvert\mathcal{E}\rvert X_{\mathrm{m}} \times \lvert\mathcal{E}\rvert X_{\mathrm{m}}$
Decomposed homogeneous	1	$X_{\mathrm{n}} \times X_{\mathrm{n}}$	2	$X_{\mathrm{m}} \times X_{\mathrm{m}}$
Decomposed α-β-heterogeneous	α	$X_{\mathrm{n}} \times X_{\mathrm{n}}$	$2\,\beta$	$X_{\mathrm{m}} \times X_{\mathrm{m}}$
Decomposed heterogeneous	N	$\bar{X}_{\mathrm{n}} \times \bar{X}_{\mathrm{n}}$	$\lvert\mathcal{E}\rvert$	$X_{\mathrm{m}} \times X_{\mathrm{m}}$
Distributed heterogeneous*	1	$\bar{X}_{\mathrm{n}} \times \bar{X}_{\mathrm{n}}$	$\lvert\mathcal{N}_i\rvert$	$X_{\mathrm{m}} \times X_{\mathrm{m}}$

Table 6.2: Numbers and dimensions of synthesis conditions for the centralized (Theorem 2.1) and decomposed synthesis for homogeneous subsystems (Proposition 6.2), α-β-heterogeneous systems (Proposition 6.4), and heterogeneous subsystems (Proposition 5.2), with the (mean) dimensions of the nominal, X_{n} ($\bar{X}_{\mathrm{n}}$), and the multiplier conditions, X_{m} ($\bar{X}_{\mathrm{m}}$), for the single subsystems. * Numbers and sizes of matrix inequalities are given per subsystem i and per iteration of Algorithm 5.1.

posed synthesis for heterogeneous systems in Proposition 5.2, and for the special cases of homogeneous systems and α-β-heterogeneous systems in Propositions 6.2 and 6.4, respectively, for a growing number of subsystems, N, and groups α, respectively. For comparability, these problems are solved in a centralized way, i.e., in one computer. Their scalability for a growing number of subsystems, N, or groups of homogeneous subsystems, α, and for a growing number of interconnections $|\mathcal{E}|$, is investigated in terms of matrix inequality size, optimization variables, and solver times. A direct comparison of the computational scalability of the centralized decomposed synthesis methods with the distributed synthesis method in Algorithm 5.1 in terms of solver time is not possible, because the convergence time of the distributed synthesis heavily depends on the interconnection topology of the system. Therefore, we compare the scalability of the centralized decomposed synthesis methods with the computational effort for one subsystem in one iteration of the distributed synthesis.

The system matrices are chosen as in (5.44). We consider the worst case interconnection topology with respect to computational scalability, i.e., the case where all subsystems are interconnected with all other subsystems. Table 6.2 shows the number and dimensions of matrix inequalities to be solved for the centralized and the decomposed controller syntheses, and for the distributed synthesis per subsystem and ADMM iteration. For simplicity, we assume that the dimensions of the single subsystems are equal although they can be heterogeneous. We denote the dimensions of the decomposed

nominal conditions by X_{n}, and the dimension of the decomposed multiplier conditions by X_{m}. Note that this is a simplification, as in general, the dimensions of the nominal and the multiplier conditions for the different formulations in Propositions 5.2, 6.2, and 6.4, are not equal, but also depend on the number of neighboring subsystems (in Propositions 5.2 and 6.4). This is indicated by $\bar{X}_{\mathrm{n}}$, which represents the mean value of the size of the synthesis conditions.

While the centralized synthesis scales polynomially with both the number of subsystems, N, and the number of edges, $|\mathcal{E}|$, the decomposed approach for heterogeneous systems scales linearly in both the number of subsystems, N, and the number of edges, $|\mathcal{E}|$, and polynomially in the number of neighboring subsystems, $|\mathcal{N}_i|$. In the case of α-β-heterogeneous systems this scaling is linear in α and β, respectively. The factor 2 in Table 6.2 applies to the normal case accounting for the smallest and largest eigenvalues of P, or each P_j, as in Corollary 6.1. For homogeneous systems, the computational effort for the synthesis is constant, i.e., it does not depend on N and $|\mathcal{E}|$. For each subsystem in each iteration of the ADMM scheme in Algorithm 5.1, the number of matrix inequalities and their size, the number of optimization variables, and the amount of communication, all scale linearly with the number of neighboring subsystems to which the respective subsystem is interconnected. All of these variables are independent of the total number of subsystems N. This result can also be seen in Table 6.2.

The number of optimization variables and the solver times, averaged over 10 computations, are shown in Figure 6.3 on a logarithmic scale. Note that for the α-β-heterogeneous system, we assume that $\beta = 1$ and the scaling is shown over the number of groups, α. Therefore, the heterogeneous system involves more optimization variables, since it does not only scale with the number of subsystems, but also with the number of neighboring subsystems. However, this is compensated by less coupling because of the more structured multipliers, which is why the solver times for both systems (in terms of one ADMM iteration per subsystem for the latter) are very similar. Also note that for the centralized synthesis of Theorem 2.1, we chose the multipliers to be block-diagonal for the subsystems. Even with this simplification, the solver times rapidly become prohibitive.

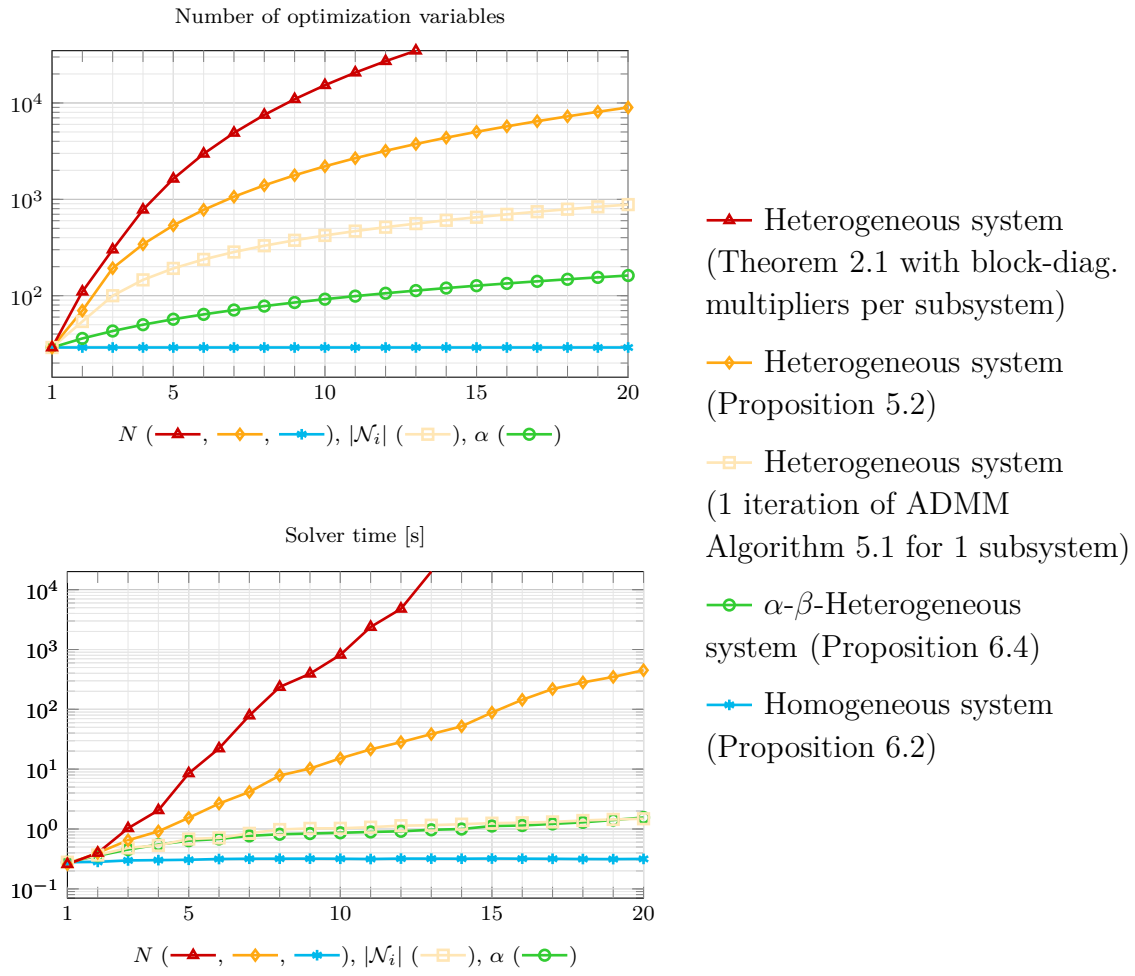

Figure 6.3: Number of optimization variables and solver times over the number of subsystems N, the number of neighboring subsystems $|\mathcal{N}_i|$, and the number of groups α.

6.4 Conclusions

Special classes of systems have been considered in this chapter. In particular, we have reviewed the properties of homogeneous systems where all subsystems are identical. We have shown how the general description for heterogeneous systems in Chapter 5 can be transformed to a more compact model in the case of homogeneous systems. As the controller synthesis is closely linked to the modeling framework, the control design for homogeneous systems also simplifies. We have introduced α-β-heterogeneous systems as a new class of systems in between homogeneous and heterogeneous systems. This extends the class in [61] and includes not only the case of multiple groups of homogeneous subsystems, but also allows for different interconnection types. In particular, a choice of interconnection topology of the controller is enabled. A further advantage is the potentially improved scalability of the controller design with respect to heterogeneous systems, because the number of decomposed synthesis conditions scales linearly with the values of α and β, instead of linearly with N and $|\mathcal{E}|$ and polynomially with $|\mathcal{N}_i|$. Numerical examples have been presented to show and to compare the scalability properties of the introduced synthesis methods for the different classes of systems from Chapters 5 and 6.

CHAPTER 7

Augmented Distributed Control

Choosing between a decentralized, centralized or distributed control architecture implies trading off between the required communication and computational effort and the achievable control performance. While decentralized control schemes do not require any communication, their control performance can be unsatisfactory, in particular for dynamically coupled systems. This chapter aims at introducing methods to improve the control performance for control schemes that are decentralized or that have a sparse communication topology. In particular, the synthesis of a controller based on a model with an augmented overlapping state space is presented. In the augmented representation the individual subsystems contain copies of states of neighboring subsystems and thus capture more model information about the overall system dynamics than in the original state space, where only information about their own local states is captured. This potentially improves the control performance with respect to a controller with the same interconnection topology but without model overlap. By designing the overlapping state space, where the degree of overlap is a design choice, and by designing the structure of the explicit communication, the trade off between the required computational effort, the communication and the achievable performance can be made. With the augmented state space representation, the plant can be modeled and classified according to the frameworks presented in Chapters 5 or 6, depending on its heterogeneity, and the scalable control design methods can be applied. This chapter is based on the publications [12] and [14].

The chapter is structured as follows. In Section 7.1, we present the mapping of a distributed system to an augmented overlapping state space. Section 7.2 introduces a model transformation that leads to an interconnected representation of the system in the augmented state space. We prove that the performance guarantees for the controller synthesis in the augmented state space also hold for the original system. In Section 7.3 we present numerical examples to illustrate the introduced concepts and to demonstrate how increasing the overlap of the subsystem models causes an improvement in the control performance for decentralized control, i.e., without communication between the subcontrollers.

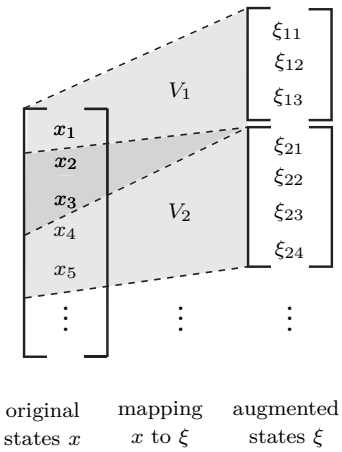

Figure 7.1: Augmentation of the original system to the augmented state space.

7.1 Augmented State Space

For distributed systems with strong coupling in the dynamics or in the performance, it is beneficial for the subsystems to have overlapping information. Therefore, we are interested in designing a distributed controller based on an augmented system description, where the control actions of the subsystems depend on overlapping parts of the state vector. A reasonable choice of this overlap in the states of the subsystems depends on the coupling to neighboring subsystems. For the controller design, the system is transformed to an augmented state space, where the structural constraints on the controller become block-diagonal. The augmented state space is obtained by expanding the original one through creating copies of the overlapping state variables. This augmentation of the state space is illustrated in Figure 7.1. More formally, we define the mapping from the state vector x to the augmented state vector ξ_i by the matrix $V_i \in \mathbb{R}^{n_{\xi i} \times n_x}$. The overall augmented state vector ξ is the collection of all $\xi_i \in \mathbb{R}^{n_{\xi i}},\ i = 1, ..., N$, i.e.,

$$\xi = \text{concat}_{i=1}^{N}(\xi_i) \in \mathbb{R}^{n_\xi}. \tag{7.1}$$

The augmented state vector ξ is obtained from x through the mapping V as

$$\xi = Vx, \tag{7.2}$$

where V is given by the collection of the matrices V_i as

$$V = \text{concat}_{i=1}^{N}(V_i) \in \mathbb{R}^{n_\xi \times n_x}. \tag{7.3}$$

The matrix V is assumed to have full column rank, i.e., the original state space of x is completely spanned by the augmented state space of ξ.

7.1.1 Augmented System

In the following, we will use a subscript ξ to denote variables related to the augmented state space. In order to describe the system in the augmented state space, let U be a matrix of full row rank that satisfies

$$UV = I.$$

Then, the dynamics of the overall system (5.25) in the augmented state space are given by

$$\bar{G}_\xi : \begin{cases} \dot{\xi} &= A_\xi \xi + B_{\xi\bar{w}} \bar{w} + B_{\xi u} u, \\ y &= C_{\xi y} \xi + D_{y\bar{w}} \bar{w}, \\ \bar{z} &= C_{\xi\bar{z}} \xi + D_{\bar{z}u} u, \end{cases} \tag{7.4}$$

with the augmented system matrices

$$\begin{aligned} A_\xi &= VAU + M_A, & B_{\xi u} &= VB_u, & B_{\xi\bar{w}} &= VB_{\bar{w}}, \\ C_{\xi y} &= C_y U + M_{C_y}, & C_{\xi\bar{z}} &= C_{\bar{z}} U + M_{C_{\bar{z}}}. \end{aligned} \tag{7.5}$$

The complementary matrices $M_A, M_{C_y}, M_{C_{\bar{z}}}$, as in [85], are degrees of freedom, which will be discussed in more detail in the following. In the trivial case of $V = I$, it is obvious that the augmented system is equal to the original system.

Inclusion Principle

The following results are based on the so-called Inclusion Principle [117]. As it is formulated for a nominal system, let us consider the modified systems $\bar{G}^{\text{nom}}$ and $\bar{G}_\xi^{\text{nom}}$, given by the systems $\bar{G}$ in (5.25) and $\bar{G}_\xi$ in (7.4), with $B_{\bar{w}}$, $D_{y\bar{w}}$, $C_{\bar{z}}$, $D_{\bar{z}u}$, and the corresponding matrices for $\bar{G}_\xi$, all being equal to zero. Then the following holds.

Definition 7.1 (Inclusion Principle [117])**.** *The system $\bar{G}_\xi^{\text{nom}}$ is said to include the system $\bar{G}^{\text{nom}}$, if there exists U and V, with $UV = I$, such that for any initial state $x(0)$ of $\bar{G}^{\text{nom}}$ and any fixed input $u(t)$, it holds that*

$$x(t, x(0), u(t)) = U\xi(t, Vx(0), u(t)), \quad y(x(t)) = y(\xi(t)), \quad \forall t \geq 0.$$

Definition 7.2 (Restriction [117])**.** *We consider the special case of a monic V, i.e., of full column rank. If it holds that*

$$\xi(t, Vx(0), u(t)) = Vx(t, x(0), u(t)), \quad y(\xi(t)) = y(x(t)), \quad \forall t \geq 0, \tag{7.6}$$

then $\bar{G}^{\text{nom}}$ is called a restriction of $\bar{G}_\xi^{\text{nom}}$ to $\mathcal{R}(V)$, where $\mathcal{R}(V)$ is the range space of V. This subspace $\mathcal{R}(V)$ is invariant in the sense that the solutions $\xi(t)$ of $\bar{G}_\xi^{\text{nom}}$ starting from an initial state $\xi(t) \in \mathcal{R}(V)$ stay in $\mathcal{R}(V)$ for any input $u(t)$ and such solutions $\xi(t)$ are represented by the solutions $x(t)$ of $\bar{G}^{\text{nom}}$. Since V is monic, there exists an epic U such that $UV = I$ and inclusion of $\bar{G}^{\text{nom}}$ by $\bar{G}_\xi^{\text{nom}}$ is therefore implied.

Theorem 7.1 (Restriction [117]). *Given the nominal systems $\bar{G}^{\text{nom}}$ and $\bar{G}_{\xi}^{\text{nom}}$, as defined before, and with V monic, then $\bar{G}^{\text{nom}}$ is included in $\bar{G}_{\xi}^{\text{nom}}$, if and only if the following holds*

$$M_A V = 0, \quad M_{C_y} V = 0. \tag{7.7}$$

Proof. The proof can be given by rewriting the equality of $\xi(t, Vx(0), u) = Vx(t, x(0), u)$ in Definition 7.2 as

$$Ve^{At}x(0) + V\int_0^t e^{A(t-\tau)}Bu(\tau)d\tau \tag{7.8}$$

$$= e^{(VAU+M_A)t}Vx(0) + \int_0^t e^{(VAU+M_A)(t-\tau)}Bu(\tau)d\tau, \forall x(0), u(t), \tag{7.9}$$

which can easily be proved to be true if and only if the condition $M_A V = 0$ in (7.7) holds. Furthermore, the requirement $y(\xi(t)) = y(x(t))$, i.e., $C_y x = (C_y U + M_{C_y})\xi$ holds if and only if $M_{C_y}\xi = M_{C_y}V\xi = 0$, and therefore $M_{C_y}V = 0$. □

As the mappings between $\bar{G}^{\text{nom}}$ and $\bar{G}_{\xi}^{\text{nom}}$ involves singular transformations, it is clear that $\bar{G}^{\text{nom}}$ and $\bar{G}_{\xi}^{\text{nom}}$ are not algebraically equivalent. For example, for a fixed $u(t)$ and a fixed initial state $x(0)$ of $\bar{G}^{\text{nom}}$, there always exists an initial state $\xi(0)$ of $\bar{G}_{\xi}^{\text{nom}}$ such that $y(x(t)) = y(\xi(t))$. However, the opposite is not true in general. For compatible initial states $\xi(0) = Vx(0)$ however, the input-output behavior of the systems $\bar{G}^{\text{nom}}$ and $\bar{G}_{\xi}^{\text{nom}}$ are equal.

Generalizations to Performance Channel

Considering the systems $\bar{G}$ and $\bar{G}_{\xi}$ in (5.25) and (7.4), we assume in the following that the complementary matrices satisfy the following conditions.

$$M_A V = 0\,, \quad M_{C_y} V = 0\,, \quad M_{C_{\tilde{z}}} V = 0\,. \tag{7.10}$$

With this choice of augmentation in (7.5) and complementary matrices in (7.10), we propose the following results, which are a generalization of the restriction in Theorem 7.1.

Proposition 7.1. *Given the augmented system $\bar{G}_{\xi}$ in (7.4) with the augmented system matrices in (7.5) and the complementary matrices satisfying (7.10), and given the original system $\bar{G}$ in (5.25), then for the choice $\xi(0) = Vx(0)$, the following holds for the trajectory of the state $x(t)$ and the augmented state $\xi(t)$,*

$$\xi(t, Vx(0), u(t), \bar{w}(t)) = Vx(t, x(0), u(t), \bar{w}(t)). \tag{7.11}$$

Furthermore, it holds that

$$\begin{aligned} \bar{z}(t, \xi(t, Vx(0), u(t), \bar{w}(t))) &= \bar{z}(t, x(t, x(0), u(t), \bar{w}(t))), \\ y(t, \xi(t, Vx(0), u(t), \bar{w}(t))) &= y(t, x(t, x(0), u(t), \bar{w}(t))). \end{aligned} \tag{7.12}$$

Proof. Redefining the input of system $\bar{G}^{\text{nom}}$ in Theorem 7.1 as $[u(t)^\top, \bar{w}(t)^\top]^\top$ and equivalently the system matrix as $[B_u \; B_{\bar{w}}]$, the results from Theorem 7.1 can directly be applied to show that (7.11) holds. Furthermore, it holds that

$$C_{\xi\bar{z}}\,\xi(t, Vx(0), u(t), \bar{w}(t)) = \underbrace{(C_{\bar{z}}U + M_{C_{\bar{z}}})V}_{C_{\bar{z}}}\, x(t, x(0), u(t), \bar{w}(t)).$$

The same can be shown for $y(t)$, and thus the results in (7.12) follow. □

Due to Proposition 7.1, also the input-output behavior from $\bar{w}$ to $\bar{z}$ of the original system $\bar{G}$ and of the augmented system $\bar{G}_\xi$ under the same input $u(t)$ are equivalent.

Modes of the Augmented System

In the case of a restriction of the system $\bar{G}_\xi^{\text{nom}}$ onto $\bar{G}^{\text{nom}}$, the complementary matrix M_A can be chosen as [117], [118]

$$M_A = Y(I - VU) = Y\hat{V}\hat{U}, \tag{7.13}$$

where Y is an arbitrary $n_\xi \times n_\xi$ matrix, $\hat{V}$ is a basis matrix for the null space of U, and $\hat{U}$ is the unique left inverse of $\hat{V}$, such that the null space of $\hat{V}$ is equal to the range space of V. The choice of M_A as in (7.13) implies $M_A V = 0$. In the case of a restriction of the system $\bar{G}_\xi$ to $\bar{G}$, the spectrum of the augmented system matrix A_ξ is the union of the spectra of A and of $\hat{U}M_A\hat{V}$. This means that the complementary matrix M_A introduces $n_\xi - n$ additional modes into the augmented system dynamics, which are given by the eigenvalues of $\hat{U}M_A\hat{V}$. We will later see that these modes are not controllable. In order to show the introduction of these additional modes, we consider the closed-loop dynamics of the system and a static state feedback control $C_x^K i$, which corresponds to $C_\xi^K V = C^K$ in the original state-space. Then, we define the matrices $W = [V \; \hat{V}]$ and $W^{-1} = [U^\top \; \hat{U}^\top]^\top$ and perform the following transformation

$$W^{-1}\left(A_\xi + B_{\xi u}C_\xi^K\right)W = \begin{bmatrix} A + B_u C^K & UM_A\hat{V} \\ 0 & \hat{U}M_A\hat{V} \end{bmatrix}, \tag{7.14}$$

which follows from the assumptions of the restriction and with $\hat{U}V = 0$ and $U\hat{V} = 0$ by definition. The additional modes $\text{spec}(\hat{U}M_A\hat{V})$ can be observable depending on the complementary matrix M_{C_y}. However, they are not controllable by the original control inputs u. These modes are therefore so-called fixed modes (FMs), which will be further analyzed in Chapter 8. As these modes only appear in the augmented dynamics, they do not influence the original system $\bar{G}$. For the controller synthesis in the following, the complementary matrices however need to be chosen such that the pairs $(A_\xi, B_{\xi u})$ and $(A_\xi, C_{\xi y})$ are stabilizable and reachable, and such that the introduced FMs do not limit the achievable control performance. The complementary matrices can for example be designed such that they minimize the condition number of the observability matrix, and such that the additional modes introduce fast dynamics.

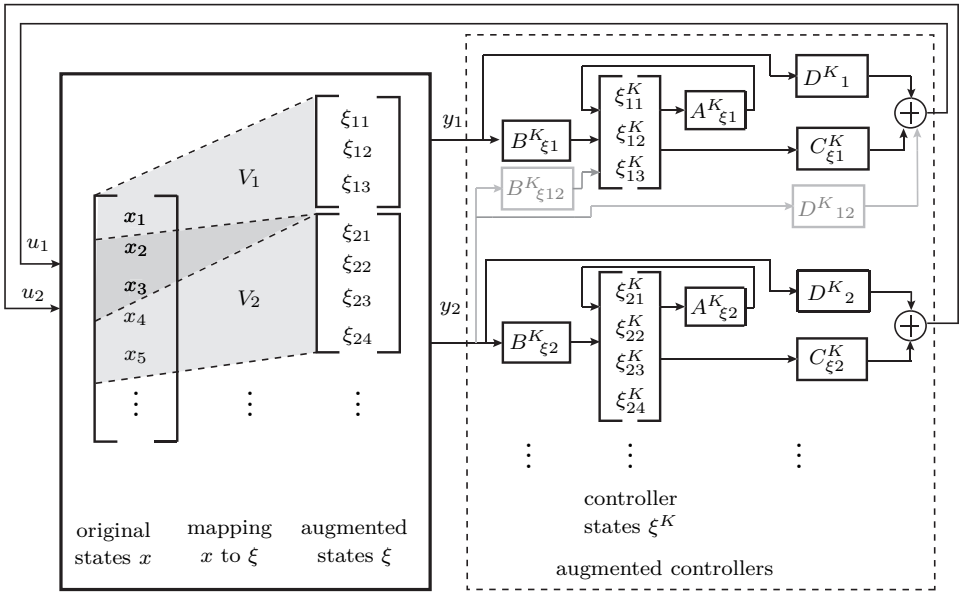

Figure 7.2: Block-diagram of the original system and the dynamic output feedback controllers in the augmented state space. The gray parts indicate the interconnections of the subcontrollers enabled by communication (of measurements y_2 to subsystem 1 in this example).

7.1.2 Interconnected Augmented System, Controller and Closed-Loop

The goal is to design an augmented interconnected dynamic output feedback controller, K_ξ, which has the same structure as K in (5.14), given as

$$K_\xi : \begin{cases} K_\xi^d = \operatorname{diag}_{i\in\mathcal{N}}(K_{\xi i})\,, \\ p^K = \mathcal{P}^K q^K\,. \end{cases} \tag{7.15}$$

with

$$K_{\xi i} : \left\{ \begin{bmatrix} \dot{\xi}_i^K \\ u_i \\ q_i^K \end{bmatrix} = \left[\begin{array}{cc:c} A^K{}_{\xi i} & B^K{}_{\xi i} & B_{p^K,i} \\ C^K{}_{\xi i} & D^K{}_i & C_{p^K,i} \\ \hdashline C_{q^K,i} & D_{q^K,i} & 0 \end{array}\right] \begin{bmatrix} \xi_i^K \\ y_i \\ p_i^K \end{bmatrix} . \right. \tag{7.16}$$

The augmented controller states of the subcontrollers have the same dimensions as the states of the corresponding subsystems, i.e., ${\xi_i}^K \in \mathbb{R}^{n_{\xi_i}}$. As before, we denote the block-diagonal and off-block-diagonal parts of the augmented controller gains with superscripts $(\cdot)^d$ and $(\cdot)^i$, respectively, e.g., $A^K{}_\xi = A^{K^d}_\xi + A^{K^i}_\xi$. The structure of this augmented interconnected controller is illustrated in Figure 7.2.

The objective is to apply the scalable controller synthesis methods from Chapters 5 and 6 to design the augmented interconnected controller K_ξ. In order for the methods

to be applicable, the system $\bar{G}_\xi$ in (7.4) is transformed into the following form.

$$G_\xi : \begin{cases} G_\xi^d = \mathrm{diag}_{i\in\mathcal{N}}(G_{\xi i})\,, \\ p = \mathcal{P}^G q, \end{cases} \tag{7.17}$$

where $G_{\xi i}$ has the same structure as G_i in (5.1), but in the augmented state space. A possible transformation from $\bar{G}_\xi$ to G_ξ that has desirable properties for the controller synthesis will be given in Section 7.2.

Then, we can define the closed-loop system of $\mathcal{G}_\xi$ in (7.17) and K_ξ in (7.16) as

$$\mathcal{G}_\xi : \begin{cases} \mathcal{G}_\xi^d = \mathrm{diag}_{i\in\mathcal{N}}(\mathcal{G}_{\xi i}) \\ q^c = \mathcal{P} p^c, \end{cases} \tag{7.18}$$

with

$$\mathcal{G}_{\xi i} : \left\{ \begin{bmatrix} \dot{\xi}_i^c \\ z_i \\ q_i^c \end{bmatrix} = \left[\begin{array}{c|cc} \mathcal{A}_{\xi,i} & \mathcal{B}_{\xi 1,i} & \mathcal{B}_{\xi 2,i} \\ \hline \mathcal{C}_{\xi 1,i} & \mathcal{D}_{\xi 11,i} & \mathcal{D}_{\xi 12,i} \\ \mathcal{C}_{\xi 2,i} & \mathcal{D}_{\xi 21,i} & \mathcal{D}_{\xi 22,i} \end{array}\right] \begin{bmatrix} \xi_i^c \\ w_i \\ p_i^c \end{bmatrix}, \quad \forall i \in \mathcal{N}, \right. \tag{7.19}$$

and with

$$\xi_i^c = \begin{bmatrix} \xi_i{}^\top & \xi_i^K{}^\top \end{bmatrix}^\top, \quad \xi^c = \mathrm{concat}_{i=1}^N(\xi_i^c)\,, \tag{7.20}$$

and with the other signal vectors being defined analogously as before. The system matrices for the closed-loop of the augmented system and the augmented controller, $\mathcal{A}_{\xi,i}$, $\mathcal{B}_{\xi 1,i}$, $\mathcal{C}_{\xi 1,i}$, $\mathcal{D}_{\xi 11,i}$ and $\mathcal{D}_{\xi 12,i}$, are formed in the same way as the closed-loop matrices in (5.23).

7.2 Transformation to an Interconnected Augmented System

In order to model the augmented system $\bar{G}_\xi$ as an interconnection of local subsystems $G_{\xi i}$, as given in (7.17), we can transform the performance channel of the augmented system such that each subsystem is equipped with a local performance channel w_i to z_i. This is done similarly to the input-output transformation of the non-augmented system $\bar{G}$ to the system G in Chapter 5.

Norm-Invariant Augmentation of the Performance Channel

The objective is to transform the global performance input and output, $\bar{w}$ and $\bar{z}$, of system $\bar{G}_\xi$ into a performance channel from $w = [w_1^\top, ..., w_N^\top]^\top$ to $z = [z_1^\top, ..., z_N^\top]^\top$ that

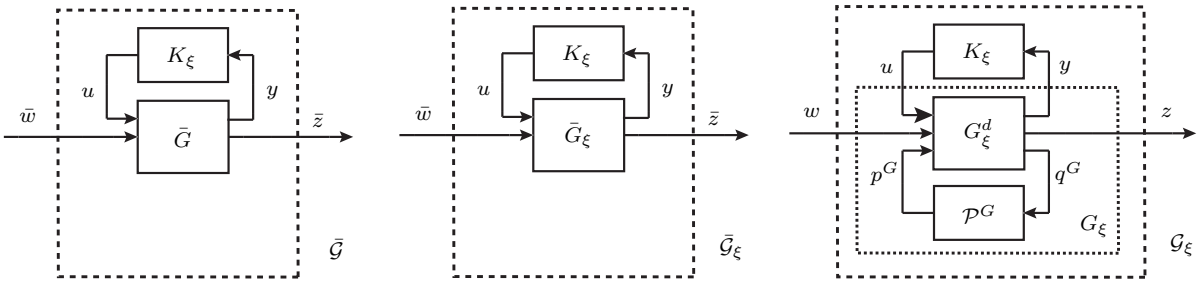

Figure 7.3: Closed-loops of original system $\bar{G}$ and augmented systems $\bar{G}_\xi$ and G_ξ with the controller K_ξ. The block-diagonal parts of G_ξ are in G_ξ^d and the off-block-diagonal parts in the interconnection $\mathcal{P}^G$.

can be decomposed into local ones for the individual subsystems. The augmentation of the performance channel is defined analogously to the one in (5.26), and is given as

$$\begin{aligned} C_{\xi z} &= \bar{Q}^{\frac{1}{2}} S C_{\xi \bar{z}} + M_{C_{\xi \bar{z}}}, & D_{zu} &= \bar{Q}^{\frac{1}{2}} S D_{\bar{z}u}, \\ B_{\xi w} &= B_{\xi \bar{w}} T^\dagger \bar{R}^{\frac{1}{2}} & D_{yw} &= D_{y\bar{w}} T^\dagger \bar{R}^{\frac{1}{2}}, \end{aligned} \tag{7.21}$$

where the matrices $\bar{Q}$ and $\bar{R}$ again are assumed to have full rank and they have to satisfy (5.31). The additional complementary matrix $M_{C_{\xi z}}$ has to satisfy the constraint $M_{C_{\xi \bar{z}}} V = 0$. Apart from this constraint, $M_{C_{\xi \bar{z}}}$ is a degree of freedom, in addition to the choice of the complementary matrices M_Q and M_R as in (5.31). They can for example be chosen to introduce sparsity into the matrices $C_{\xi z}$ and $B_{\xi w}$.

Control Design Concept

The goal is to design an augmented controller K_ξ, as given in (7.15), such that the $\mathcal{H}_\infty$-norm of the closed-loop transfer function from $\bar{w}$ to $\bar{z}$ of the closed-loop, i.e., $\|\bar{\mathcal{G}}\|_{\mathcal{H}_\infty}$, with $\bar{\mathcal{G}} = \mathcal{F}_\mathrm{u}(\bar{G}, K_\xi)$, is minimized. For a scalable synthesis of K_ξ, the methods introduced in Chapters 5 and 6 can be applied. This is possible by exploiting the structure of the interconnected augmented system model G_ξ. In the controller synthesis, we thus minimize $\|\mathcal{G}_\xi\|_{\mathcal{H}_\infty}$, with $\mathcal{G}_\xi = \mathcal{F}_\mathrm{u}(G_\xi, K_\xi)$. The controller K_ξ will be implemented in the original system $\bar{G}$ resulting in the closed-loop system $\bar{\mathcal{G}}$. The system $\bar{\mathcal{G}}_\xi$ is used as an intermediate system for proving stability and performance of the closed-loop $\bar{\mathcal{G}}$. Figure 7.3 shows all three closed-loop structures of the original system $\bar{G}$, and the augmented systems $\bar{G}_\xi$ and G_ξ, under the controller K_ξ, given by $\bar{\mathcal{G}} = \mathcal{F}_\mathrm{u}(\bar{G}, K_\xi)$, $\bar{\mathcal{G}}_\xi = \mathcal{F}_\mathrm{u}(\bar{G}_\xi, K_\xi)$, and $\mathcal{G}_\xi = \mathcal{F}_\mathrm{u}(G_\xi, K_\xi)$, respectively.

In the following, we show that the stability and performance guarantees from designing the controller K_ξ for the system G_ξ are preserved when implementing the controller K_ξ at the physical system $\bar{G}$. First, we state an intermediate result showing that the choice of weightings $\bar{Q}$ and $\bar{R}$ in (5.31) leads to an input-output transformation of the system which leaves the system norm invariant. Equality of $\|\bar{\mathcal{G}}_\xi\|_{\mathcal{H}_\infty}$ and $\|\mathcal{G}_\xi\|_{\mathcal{H}_\infty}$ is stated

in the following result.

Corollary 7.1. *The closed-loop transfer functions $\mathcal{G}_\xi = \mathcal{F}_u(G_\xi, K_\xi)$ and $\bar{\mathcal{G}}_\xi = \mathcal{F}_u(\bar{G}_\xi, K_\xi)$, from w to z with G_ξ in (7.17), and from $\bar{w}$ to $\bar{z}$ with $\bar{G}_\xi$ in (7.4), respectively, are given. With the transformation in (7.21) and the weightings $\bar{Q} = S^{\dagger\top} S^\dagger + M_Q$ and $\bar{R} = TT^\top + M_R$, with $M_Q = M_Q^\top$, $M_R = M_R^\top$, $S^\top M_Q S = 0$, $T^\dagger M_R T^{\dagger\top} = 0$, as in (5.31), and with $M_{C_{\xi\bar{z}}} V = 0$, it holds that*

$$\|\bar{\mathcal{G}}_\xi\|_{\mathcal{H}_\infty} = \|\mathcal{G}_\xi\|_{\mathcal{H}_\infty}.$$

Proof. First, we note that because of the restriction of G_ξ onto $\mathcal{R}(V)$, and with $M_{C_{\xi\bar{z}}} V = 0$, it holds that $z(t) = \left(\bar{Q}^{\frac{1}{2}} S C_{\xi\bar{z}} + M_{C_{\xi\bar{z}}}\right) V x(t) = \bar{Q}^{\frac{1}{2}} S C_{\xi\bar{z}} V x(t)$. Then, the proof is analogous to the one of Theorem 5.1, to prove the performance bounds

$$\frac{\sigma_{\min}(T_r)}{\sigma_{\max}(T_l)} \|\mathcal{G}_\xi\|_{\mathcal{H}_\infty} \leq \|\bar{\mathcal{G}}_\xi\|_{\mathcal{H}_\infty} \leq \frac{\sigma_{\max}(T_r)}{\sigma_{\min}(T_l)} \|\mathcal{G}_\xi\|_{\mathcal{H}_\infty}. \tag{7.22}$$

with the transformations $T_l := \left(S^{\dagger T} S^\dagger + M_Q\right)^{\frac{1}{2}} S$ and $T_r := \left(TT^T + M_R\right)^{-\frac{1}{2}} T$. □

This result is used in the following to show that the norms of the original system $\bar{G}$ and the augmented system G_ξ, both in interconnection with the controller K_ξ are equal.

Proposition 7.2. *Given the original system $\bar{G}$ in (5.30) and the augmented system G_ξ in (7.17), the following holds for the closed-loops under the augmented controller K_ξ:*

$$\|\mathcal{G}_\xi\|_{\mathcal{H}_\infty} = \|\bar{\mathcal{G}}\|_{\mathcal{H}_\infty}.$$

Proof. We show that the following equalities hold:

$$\|\mathcal{G}_\xi\|_{\mathcal{H}_\infty} = \|\bar{\mathcal{G}}_\xi\|_{\mathcal{H}_\infty} = \|\bar{\mathcal{G}}\|_{\mathcal{H}_\infty},$$

where the first one has already been proved in Corollary 7.1. For the second equality, recall that $\bar{G}$ and $\bar{G}_\xi$ under the same input u have the same input-output behavior from $\bar{w}$ to $\bar{z}$, and the same output $y(t)$, as shown in Proposition 7.1. This means that the closed-loops of $\bar{G}$ and $\bar{G}_\xi$ interconnected with the same output feedback controller K_ξ, i.e., $\bar{\mathcal{G}} = \mathcal{F}_{\mathrm{u}}(\bar{G}, K_\xi)$ and $\bar{\mathcal{G}}_\xi = \mathcal{F}_{\mathrm{u}}(\bar{G}_\xi, K_\xi)$, have the same input-output behavior from $\bar{w}$ to $\bar{z}$ and thus the norms of the transfer functions $\bar{\mathcal{G}}$ and $\bar{\mathcal{G}}_\xi$ are equal. □

The following corollary suggests that the augmentation of the performance channel is also applicable for an $\mathcal{H}_2$-based controller synthesis.

Corollary 7.2. *Given the closed-loop systems $\bar{\mathcal{G}}$ and $\mathcal{G}_\xi$, of the original system $\bar{G}$ in (5.30) and the augmented system G_ξ in (7.17), respectively, then it holds that*

$$\|\bar{\mathcal{G}}\|_{\mathcal{H}_2} = \|\mathcal{G}_\xi\|_{\mathcal{H}_2}.$$

Proof. The proof is analogous to the one of Proposition 7.2 making use of the unitary-invariance property of the $\mathcal{H}_2$-norm. □

Corollary 7.3. *Given a controller K_ξ that stabilizes $\mathcal{G}_\xi$ and leads to a $\mathcal{H}_\infty$-bound of less than γ for $\mathcal{G}_\xi$, then it also stabilizes $\bar{\mathcal{G}}$ and leads to the same performance bound for $\bar{\mathcal{G}}$.*

Proof. The invariance of the performance bound has been shown in Proposition 7.2. From $\bar{G}_\xi$ to G_ξ, only the performance channel is transformed, and therefore stability of $\mathcal{G}_\xi$ implies stability of $\bar{\mathcal{G}}_\xi$. Furthermore, the eigenvalues of $\bar{\mathcal{G}}$ are a subset of the ones of $\bar{\mathcal{G}}_\xi$ (without the additional FMs introduced by the complementary matrix M_A). Therefore, stability of $\bar{\mathcal{G}}_\xi$ implies stability of $\bar{\mathcal{G}}$. □

Depending on whether the augmented system is a homogeneous, α-β-heterogeneous, or heterogeneous system, the decomposed and distributed synthesis methods from Chapters 5 and 6 can be used for the controller design. The sparsity of the augmented system matrices in (7.17) depends on the mapping V, the original system matrices and the complementary matrices M_A, M_{C_y}, M_{C_z} in (7.5) and $M_{C_{\bar{z}\xi}}$ in (7.21). As a sparser structure of the augmented system matrices introduces less coupling in the synthesis equations from Chapters 5 and 6, the complementary matrices can be chosen such that the interconnection topology of the augmented system is as sparse as possible. This augmentation is illustrated in a numerical example in Section 7.3.

7.3 Numerical Example

In a first example, we illustrate the benefit of the augmented system representation in terms of increased model information. Then, a numerical example is given, which shows the modeling of a system as an interconnected system in the augmented state space and the synthesis of the augmented interconnected controller. It is demonstrated how the performance of decentralized control improves with an increased overlap in the models of the subsystems.

7.3.1 Structural Degrees of Freedom

We consider an example system composed of three subsystems, which are dynamically coupled, as shown on the left hand-side of Figure 7.4 (a). For illustration purposes, the following distributed static state feedback (SSF) control in the original state space is considered,

$$\begin{bmatrix} u_1 \\ u_2 \\ u_3 \end{bmatrix} = \begin{bmatrix} C^K_{\xi_{11}} & C^K_{\xi_{12}} & 0 \\ 0 & C^K_{\xi_{22}} & C^K_{\xi_{23}} \\ C^K_{\xi_{31}} & 0 & C^K_{\xi_{33}} \end{bmatrix} \begin{bmatrix} x_1 \\ x_2 \\ x_3 \end{bmatrix}. \tag{7.23}$$

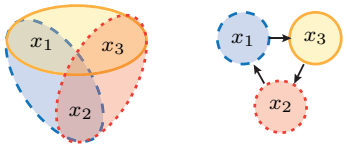

(a) Left: Original state-space with dynamic coupling indicated by ellipses. Right: Communication structure between subsystems.

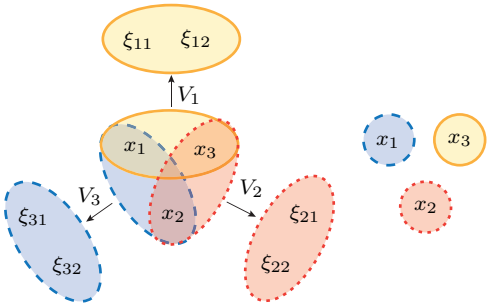

(b) Overlapping state-space indicated by ellipses, disjoint partitions in augmented state-space. Right: Decentralized structure without communication.

Figure 7.4: Model and communication structure of 3 interconnected subsystems.

We assume local inputs and measurements, such that subsystem 1 has the input u_1 and measured output (state) x_1, and for the other subsystems accordingly. In order to implement the distributed control law in (7.23), a communication structure is required, which is shown in Figure 7.4 (a). In contrast, if the system is mapped to an augmented state-space, where the dynamic couplings are included in the individual augmented subsystems, then these subsystems become disjoint, as illustrated on the left hand-side of Figure 7.4 (b). A block-diagonal SSF controller can be designed in the augmented state-space, which is given as

$$\begin{bmatrix} u_1 \\ u_2 \\ u_3 \end{bmatrix} = \begin{bmatrix} C^K_{\xi_{11}} & C^K_{\xi_{12}} & 0 & 0 & 0 & 0 \\ 0 & 0 & C^K_{\xi_{22}} & C^K_{\xi_{23}} & 0 & 0 \\ 0 & 0 & 0 & 0 & C^K_{\xi_{31}} & C^K_{\xi_{33}} \end{bmatrix} \begin{bmatrix} \xi_{11} \\ \xi_{12} \\ \xi_{21} \\ \xi_{22} \\ \xi_{31} \\ \xi_{32} \end{bmatrix}.$$

If it was contracted back to the original state-space, it would have the same structure, and thus the same degrees of freedom, as the controller in (7.23). However, no communication is required for the implementation of this augmented controller.

7.3.2 Robotic Example System

A simplified robotic system is considered, which is composed of $N = 3$ robotic subsystems that cooperatively transport an object, to which they are physically coupled. In order to avoid high interaction forces and possible damage to the object, the robots are controlled by lower-level decentralized impedance controllers [119], which allow us to model their closed-loop dynamics as second-order LTI systems [38], [40], given as

$$m_i \ddot{x}_i + d_i(\dot{x}_i - \dot{x}_{id}) + k_i(x_i - x_{id}) = f_i - f_{id}\,, \quad i = 1, ..., 3.$$

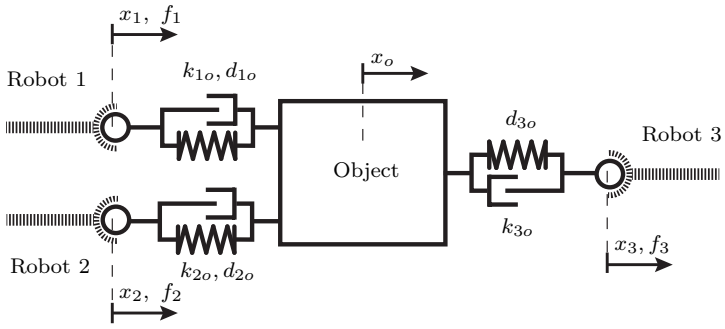

Figure 7.5: Model of robots coupled through an object.

In a reduced form, they are given as

$$m_i\ddot{x}_i + d_i\dot{x}_i + k_i x_i = f_i + b_i u_i,$$

with $x_i,\ \dot{x}_i,\ \ddot{x}_i,\ f_i$ being the position, velocity, acceleration, and force of the end-effector of the i-th robot. The parameters $m_i,\ d_i,\ k_i$ represent the virtual mass, damping, and stiffness of the i-th robot. The contact between the i-th robot and the object is also modeled as second-order dynamics with k_{io} and d_{io} the stiffness and damping parameters, respectively. The system is depicted in Figure 7.5.

The states of subsystem $i,\ i = 1, ..., 3$, are the position and velocity of robot i, denoted by $\underline{x}_i := [x_i,\ \dot{x}_i]^\top$. The states of the object are $\underline{x}_o := [x_o,\ \dot{x}_o]^\top$. The overall dynamics are

$$\underbrace{\begin{bmatrix}\dot{\underline{x}}_1\\ \dot{\underline{x}}_2\\ \dot{\underline{x}}_3\\ \dot{\underline{x}}_o\end{bmatrix}}_{\dot{x}} = \underbrace{\begin{bmatrix}a_{11} & 0 & 0 & a_{1o}\\ 0 & a_{22} & 0 & a_{2o}\\ 0 & 0 & a_{33} & a_{3o}\\ a_{o1} & a_{o2} & a_{o3} & a_{oo}\end{bmatrix}}_{A}\underbrace{\begin{bmatrix}\underline{x}_1\\ \underline{x}_2\\ \underline{x}_3\\ \underline{x}_o\end{bmatrix}}_{x} + \underbrace{\begin{bmatrix}B_{u,11} & 0 & 0\\ 0 & B_{u,22} & 0\\ 0 & 0 & B_{u,33}\\ 0 & 0 & 0\end{bmatrix}}_{[B_{u,1}\ \ B_{u,2}\ \ B_{u,3}]}\underbrace{\begin{bmatrix}u_1\\ u_2\\ u_3\end{bmatrix}}_{u} + \underbrace{\begin{bmatrix}B_{\bar{w},11} & 0 & 0 & 0\\ 0 & B_{\bar{w},22} & 0 & 0\\ 0 & 0 & B_{\bar{w},33} & 0\\ 0 & 0 & 0 & B_{\bar{w},oo}\end{bmatrix}}_{B_{\bar{w}}}\underbrace{\begin{bmatrix}\bar{w}_1\\ \bar{w}_2\\ \bar{w}_3\\ \bar{w}_o\end{bmatrix}}_{\bar{w}},$$

$$\underbrace{\begin{bmatrix}y_1\\ y_2\\ y_3\end{bmatrix}}_{y} = \begin{bmatrix}x_1\\ x_2\\ x_3\end{bmatrix} = \underbrace{\begin{bmatrix}1&0&0&0&0&0&1&0\\ 0&0&1&0&0&0&1&0\\ 0&0&0&0&1&0&1&0\end{bmatrix}}_{C_y=[C_{y,1}^\top,\ C_{y,2}^\top,\ C_{y,3}^\top]^\top}\underbrace{\begin{bmatrix}\underline{x}_1\\ \underline{x}_2\\ \underline{x}_3\\ \underline{x}_o\end{bmatrix}}_{x},$$

$$\underbrace{\begin{bmatrix}\bar{z}_x\\ \bar{z}_u\end{bmatrix}}_{\bar{z}} = \underbrace{\begin{bmatrix}C_{\bar{z}x}\\ 0_{n_u\times n_x}\end{bmatrix}}_{C_{\bar{z}}}x, + \underbrace{\begin{bmatrix}0_{n_x\times n_u}\\ D_{\bar{z}uu}\end{bmatrix}}_{D_{\bar{z}u}}u, \tag{7.24}$$

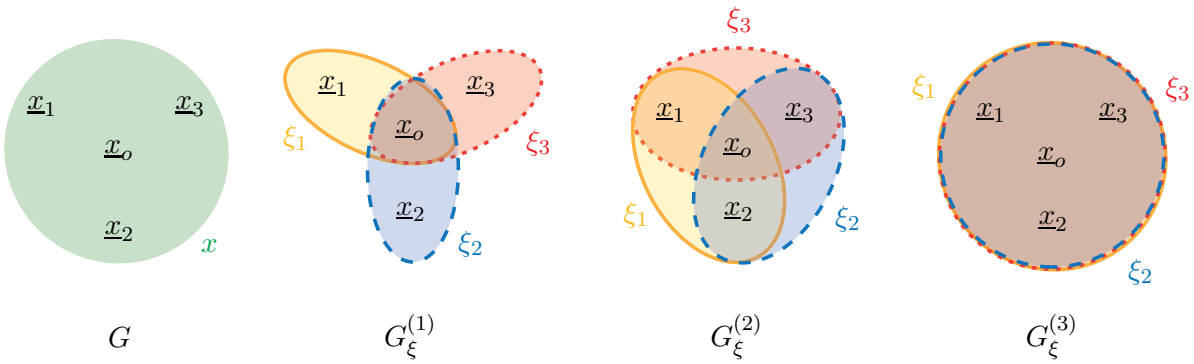

Figure 7.6: Illustration of the original state space (with state vector x) and of the different overlaps within the augmented state spaces (with ξ_1, ξ_2, and ξ_3 of the subsystems 1, 2, 3).

with

$$a_{ii} = \begin{bmatrix} 0 & 1 \\ -\frac{1}{m_i}(k_i + k_{io}) & -\frac{1}{m_i}(d_i + d_{io}) \end{bmatrix}, \quad a_{io} = a_{oi} = \begin{bmatrix} 0 & 0 \\ \frac{k_{io}}{m_o} & \frac{d_{io}}{m_o} \end{bmatrix},$$
$$a_{oo} = \begin{bmatrix} 0 & 1 \\ -\frac{1}{m_o}(k_{1o} + k_{2o} + k_{3o}) & -\frac{1}{m_o}(d_{1o} + d_{2o} + d_{3o}) \end{bmatrix},$$
$$B_{u,ii} = \begin{bmatrix} 0 & \frac{10}{m_i} \end{bmatrix}^\top, \quad B_{\bar{w},ii} = \begin{bmatrix} 0 & \frac{10}{m_o} \end{bmatrix}^\top, \quad C_{\bar{z}x} = I_{n_x}, \quad D_{\bar{z}uu} = 100 I_{n_u}.$$

In the following, the parameters are given as $k_i = 0.4,\ d_i = 0.6,\ m_i = 5,\ k_{io} = 0.3,\ d_{io} = 0.8,\ m_o = 4,\ \forall i = 1, ..., 3$, and therefore define homogeneous subsystems.

Augmentation to Different Overlapping State Spaces

The model of the augmented system is considered for three different overlaps of the augmented states of the subsystems, which are illustrated in Figure 7.6. They are chosen to be symmetric for the subsystems. Therefore, for the homogeneous subsystems in the original state space, the augmented subsystems also form one group of homogeneous subsystems, i.e., $\alpha^G = 1$, with different interconnection types for some of the overlaps, i.e., $\beta^G \geq 1$.

Augmented System $G_\xi^{(1)}$ with Overlap 1

The states of the object overlap for each augmented state vector of the subsystems. The overall augmented state vector is given by $\xi = \begin{bmatrix} \xi_1^\top & \xi_2^\top & \xi_3^\top \end{bmatrix}^\top$ with $\xi_i = \begin{bmatrix} \underline{x}_i^\top & \underline{x}_o^\top \end{bmatrix}^\top$. The disturbance input and performance output are augmented to $w = \begin{bmatrix} w_1^\top & w_2^\top & w_3^\top \end{bmatrix}^\top$, with $w_i = \begin{bmatrix} \bar{w}_i & \bar{w}_o \end{bmatrix}^\top$, and $z = \begin{bmatrix} z_1^\top & z_2^\top & z_3^\top \end{bmatrix}^\top$, with $z_i = \begin{bmatrix} \underline{x}_i & \underline{x}_o \end{bmatrix}^\top$. The augmented system

matrices are given as

$$
\begin{aligned}
A_\xi &= VAU + M_A \\
&= \begin{bmatrix}
a_{11} & \frac{a_{1o}}{3} & 0 & \frac{a_{1o}}{3} & 0 & \frac{a_{1o}}{3} \\
a_{1o} & \frac{a_{oo}}{3} & a_{2o} & \frac{a_{\xi oo}}{3} & a_{3o} & \frac{a_{oo}}{3} \\
0 & \frac{a_{2o}}{3} & a_{22} & \frac{a_{2o}}{3} & 0 & \frac{a_{2o}}{3} \\
a_{1o} & \frac{a_{oo}}{3} & a_{2o} & \frac{a_{oo}}{3} & a_{3o} & \frac{a_{oo}}{3} \\
0 & \frac{a_{3o}}{3} & 0 & \frac{a_{3o}}{3} & a_{33} & \frac{a_{3o}}{3} \\
a_{1o} & \frac{a_{oo}}{3} & a_{2o} & \frac{a_{oo}}{3} & a_{3o} & \frac{a_{oo}}{3}
\end{bmatrix} + \begin{bmatrix}
0 & \frac{2}{3}a_{1o} & 0 & -\frac{1}{3}a_{1o} & 0 & -\frac{1}{3}a_{1o} \\
0 & \frac{2}{3}a_{oo} & 0 & -\frac{1}{3}a_{oo} & 0 & -\frac{1}{3}a_{oo} \\
0 & -\frac{1}{3}a_{2o} & 0 & \frac{2}{3}a_{2o} & 0 & -\frac{1}{3}a_{2o} \\
0 & -\frac{1}{3}a_{oo} & 0 & \frac{2}{3}a_{oo} & 0 & -\frac{1}{3}a_{oo} \\
0 & -\frac{1}{3}a_{3o} & 0 & -\frac{1}{3}a_{3o} & 0 & \frac{2}{3}a_{3o} \\
0 & -\frac{1}{3}a_{oo} & 0 & -\frac{1}{3}a_{oo} & 0 & \frac{2}{3}a_{oo}
\end{bmatrix} \\
&= \left[\begin{array}{cc:cc:cc}
a_{11} & a_{1o} & 0 & 0 & 0 & 0 \\
a_{1o} & a_{oo} & a_{2o} & 0 & a_{3o} & 0 \\
\hdashline
0 & 0 & a_{22} & a_{20} & 0 & 0 \\
a_{1o} & 0 & a_{2o} & a_{oo} & a_{3o} & 0 \\
\hdashline
0 & 0 & 0 & 0 & a_{33} & a_{3o} \\
a_{1o} & 0 & a_{2o} & 0 & a_{3o} & a_{oo}
\end{array}\right] = \begin{bmatrix}
A_{\xi 11} & A_{\xi 2o} & A_{\xi 3o} \\
A_{\xi 1o} & A_{\xi 22} & A_{\xi 3o} \\
A_{\xi 1o} & A_{\xi 2o} & A_{\xi 33}
\end{bmatrix}.
\end{aligned}
$$

For the homogeneous original system, it holds that $A_{\xi 11} = A_{\xi 22} = A_{\xi 33} = A_{\xi ii} =: A_{\xi i}$ and $A_{\xi 1o} = A_{\xi 2o} = A_{\xi 3o} = A_{\xi io} =: A_{\xi i,1}$. The augmentation of the other system matrices is similar. Thus, the augmented system is rewritten as in (6.1),

$$
\begin{aligned}
A_\xi &= I_N \otimes A_{\xi i} + P_1^G \otimes A_{\xi i,1}, \\
B_{\xi u} &= I_N \otimes B_{\xi u,i}, \\
C_{\xi y} &= I_N \otimes C_{\xi y,i}, \\
B_{\xi w} &= I_N \otimes B_{\xi w,i} + P_1^G \otimes B_{\xi w,i,1}, \\
C_{\xi z} &= I_N \otimes C_{\xi z,i},
\end{aligned}
$$

with the interconnection matrix

$$
P_1^G = \begin{bmatrix}
0 & 1 & 1 \\
1 & 0 & 1 \\
1 & 1 & 0
\end{bmatrix}.
$$

The augmented measurement output and control input matrices are local, and the augmented performance output, computed as in (5.28), is also local with

$$
C_{\xi z,i} = \begin{bmatrix}
I_{n_{x_i}} & 0 \\
0 & \frac{\sqrt{3}}{3} I_{n_{x_i}}
\end{bmatrix}.
$$

The augmented disturbance input matrix is computed as $B_{\xi w} = V B_{\bar{w}} T^\dagger \bar{R}^{-\frac{1}{2}}$, resulting in

$$
B_{\xi w,i} = \begin{bmatrix}
B_{\bar{w},ii} & 0 \\
0 & \frac{\sqrt{3}}{3} B_{\bar{w},oo}
\end{bmatrix}, \qquad B_{\xi w,i,1} = \begin{bmatrix}
0 & 0 \\
0 & \frac{\sqrt{3}}{3} B_{\bar{w},oo}
\end{bmatrix}.
$$

Augmented System $G_\xi^{(2)}$ with Overlap 2

For each robot, the augmented state contains its own state, the state of the object, and the state of one neighbor, i.e., $\xi = \begin{bmatrix}\xi_1^\top & \xi_2^\top & \xi_3^\top\end{bmatrix}^\top$ with $\xi_1 = \begin{bmatrix}\underline{x}_1^\top & \underline{x}_2^\top & \underline{x}_o^\top\end{bmatrix}^\top$, $\xi_2 = \begin{bmatrix}\underline{x}_2^\top & \underline{x}_3^\top & \underline{x}_o^\top\end{bmatrix}^\top$ and $\xi_3 = \begin{bmatrix}\underline{x}_3^\top & \underline{x}_1^\top & \underline{x}_o^\top\end{bmatrix}^\top$. The disturbance input and performance output are augmented to $w = \begin{bmatrix}w_1^\top & w_2^\top & w_3^\top\end{bmatrix}^\top$ and $z = \begin{bmatrix}z_1^\top & z_2^\top & z_3^\top\end{bmatrix}^\top$, with $w_1 = \begin{bmatrix}\bar{w}_1 & \bar{w}_2 & \bar{w}_o\end{bmatrix}^\top$, $z_1 = \begin{bmatrix}\underline{x}_1 & \underline{x}_2 & \underline{x}_o\end{bmatrix}^\top$, and w_2, z_2, w_3, and z_3 similar, according to the structure of ξ_2 and ξ_3. The augmented system matrices are given as

$$\begin{aligned}
A_\xi &= I_N \otimes A_{\xi i} + P_1^G \otimes A_{\xi i,1},\\
B_{\xi u} &= I_N \otimes B_{\xi u,i} + P_2^G \otimes B_{\xi u,i,2},\\
C_{\xi y} &= I_N \otimes C_{\xi y,i},\\
B_{\xi w} &= I_N \otimes B_{\xi w,i} + P_1^G \otimes B_{\xi w,i,1} + P_2^G \otimes B_{\xi w,i,2},\\
C_{\xi z} &= I_N \otimes C_{\xi z,i},
\end{aligned}$$

with $\beta^G = 2$, and with

$$P_1^G = \begin{bmatrix}0 & 0 & 1\\ 1 & 0 & 0\\ 0 & 1 & 0\end{bmatrix}, \qquad P_2^G = \begin{bmatrix}0 & 1 & 0\\ 0 & 0 & 1\\ 1 & 0 & 0\end{bmatrix}.$$

Again, $C_{\xi z}$ and $B_{\xi w}$ are computed as in (5.28) resulting, e.g., in

$$C_{\xi z,i} = \operatorname{diag}\left(\frac{\sqrt{2}}{2} I_{n_{x_i}}, \frac{\sqrt{2}}{2} I_{n_{x_i}}, \frac{\sqrt{3}}{3} I_{n_{x_o}}\right).$$

Augmented System $G_\xi^{(3)}$ with Overlap 3

In [52], the so-called parallel estimation case with a complete overlap of the augmented state estimates was considered. For this case of complete overlap, we define the augmented state vectors as $\xi = \begin{bmatrix}\xi_1^\top & \xi_2^\top & \xi_3^\top\end{bmatrix}^\top$ with $\xi_1 = \begin{bmatrix}\underline{x}_1^\top & \underline{x}_2^\top & \underline{x}_3^\top & \underline{x}_o^\top\end{bmatrix}^\top$, $\xi_2 = \begin{bmatrix}\underline{x}_2^\top & \underline{x}_3^\top & \underline{x}_1^\top & \underline{x}_o^\top\end{bmatrix}^\top$ and $\xi_3 = \begin{bmatrix}\underline{x}_3^\top & \underline{x}_1^\top & \underline{x}_2^\top & \underline{x}_o^\top\end{bmatrix}^\top$. In this case, the augmented system matrices are given as

$$\begin{aligned}
A_\xi &= I_N \otimes A_{\xi i},\\
B_{\xi u} &= I_N \otimes B_{\xi u,i} + P_1^G \otimes B_{\xi u,i,1} + P_2^G \otimes B_{\xi u,i,2},\\
C_{\xi y} &= I_N \otimes C_{\xi y,i},\\
B_{\xi w} &= I_N \otimes B_{\xi w,i} + P_1^G \otimes B_{\xi w,i,1} + P_2^G \otimes B_{\xi w,i,2},\\
C_{\xi z} &= I_N \otimes C_{\xi z,i},
\end{aligned}$$

with $\beta^G = 2$, and P_1^G and P_2^G as in $G_\xi^{(2)}$. Again, $C_{\xi z}$ and $B_{\xi w}$ are computed as in (5.28) resulting, e.g., in $C_{\xi z} = I_N \otimes \frac{1}{\sqrt{3}} I_{3n_{x_i}}$.

	$\bar{\mathcal{G}}^{(1)}$	$\bar{\mathcal{G}}^{(2)}$	$\bar{\mathcal{G}}^{(3)}$	$\bar{\mathcal{G}}^{(c)}$
γ	80.70	68.65	44.28	41.63
$\|\cdot\|_{\mathcal{H}_\infty}$	49.77	41.62	41.69	41.58

Table 7.1: Dynamic output feedback closed-loop performance for $\bar{\mathcal{G}}^{(i)} = \mathcal{F}_{\mathrm{u}}(\bar{G}, K_\xi^{(i)})$, with controllers $K_\xi^{(i)}$ of overlaps $i = 1, 2, 3$, and $\bar{\mathcal{G}}^{(c)} = \mathcal{F}_{\mathrm{u}}(\bar{G}, K^{(c)})$ with central controller $K^{(c)}$ in original state space.

The choices of different overlaps imply different structures of the augmented state spaces and system representations. However, the local inputs and outputs are not changed. In particular, the sensing and actuation of the original system stays unchanged. Based on these different augmented system representations, augmented controllers are designed, where the interconnection topology is a design choice. In the following, we chose to synthesize decentralized augmented DOF controllers.

Decentralized Augmented Dynamic Output Feedback Control

As the three augmented systems all belong to the class of α-β-heterogeneous systems, we use the decomposed synthesis, as given in Proposition 6.4, to design augmented dynamic output feedback controllers. In order to compare the performance of the controllers in the different augmented state spaces, we chose to design completely decentralized controllers, i.e., no explicit communication between the subcontrollers exists. For the controller synthesis, the iterative procedure described in Section A.1 is applied. The synthesized controllers in the different augmented state spaces are denoted by $K_\xi^{(i)}$ for the overlaps $i = 1, 2, 3$. The control performance bounds γ and $\mathcal{H}_\infty$-norms of the closed-loop transfer functions $\bar{\mathcal{G}}^{(i)} = \mathcal{F}_{\mathrm{u}}(\bar{G}, K_\xi^{(i)})$ are given in Table 7.1. Note that the system norms of the augmented systems $G_\xi^{(i)}$ and $\bar{G}_\xi^{(i)}$, and of the original system $\bar{G}$, under the controller $K_\xi^{(i)}$ are equal, i.e., $\|\bar{\mathcal{G}}^{(i)}\|_{\mathcal{H}_\infty} = \|\bar{\mathcal{G}}_\xi^{(i)}\|_{\mathcal{H}_\infty} = \|\mathcal{G}_\xi^{(i)}\|_{\mathcal{H}_\infty}$ with $\mathcal{G}_\xi^{(i)} = \mathcal{F}_{\mathrm{u}}(G_\xi^{(i)}, K_\xi^{(i)})$ and $\bar{\mathcal{G}}_\xi^{(i)} = \mathcal{F}_{\mathrm{u}}(\bar{G}_\xi^{(i)}, K_\xi^{(i)})$. For comparison, the case of a centralized controller in the original state space is also given, denoted by $K^{(c)}$ with $\bar{\mathcal{G}}^{(c)} = \mathcal{F}_{\mathrm{u}}(\bar{G}, K^{(c)})$. The results show an obvious trend. The larger the overlap of the augmented controllers, the better the control performance.

7.4 Conclusions

In order to improve the control performance without increasing the communication, we propose the design of an overlapping augmented controller. The degree of overlap and the amount of added communication are design choices, which allow for a trade-off between the required computational effort, the communication and the achievable performance. The performance is improved by increasing the amount of model information available

to the individual subsystems. The concept can be interpreted as the controller having more degrees of freedom if it was contracted back from the augmented to the original state space. The augmented controller can alternatively be interpreted as a higher order decentralized controller. In the augmented state space, the system can be modeled as an interconnected system that fits the frameworks introduced in Chapters 5 or 6 and the scalable control design methods can be applied. A numerical example of decentralized control was presented to demonstrate that an increase in the overlap of the augmented subsystems leads to an improvement of the control performance. While the subsystem models have the same local control inputs and measured outputs, the increase in the overlap leads to an increased amount of local information.

CHAPTER 8

Minimum Communication Topology Design

For the methods presented in Chapters 5 and 6, the interconnection topology and thus the communication within the controller is a design choice. Chapter 7 aims at increasing the control performance for a sparse communication topology or for decentralized control. Implementing a decentralized control scheme is however not always possible. This chapter addresses the topic of decentralized fixed modes (DFMs) [48] which are modes of the closed-loop system that cannot be moved by any decentralized controller. Fixed modes (FMs) that are not stabilizable or critically limit the performance need to be removed, which can be achieved by adding sensors, actuators or communication. In this work, we assume that the input-output structure of the system is given and that the communication topology is the only remaining design choice. The goal is to find the sparsest possible communication structure that eliminates all FMs. We formulate the problem of finding a minimum communication topology in order to eliminate all FMs as a minimum cost coverage problem with submodular constraints. Two methods are proposed for the elimination of FMs: The greedy algorithm of polynomial complexity which has a guaranteed suboptimality bound, and a tree-search algorithm of exponential complexity which finds the optimal solution. Although this chapter considers the augmented state space representation introduced in Chapter 7, all results are directly transferable to the special case of a non-augmented system representation. The work presented in this chapter has been published in [13].

This chapter is structured as follows. In Section 8.1, a characterization of FMs in the augmented state space representation is given. Furthermore, a method for identifying FMs is provided. Section 8.2 states structural conditions, under which FMs can be eliminated by communication. In Section 8.3, we propose methods to eliminate the identified FMs by introducing a minimum set of communication links. Section 8.4 presents a numerical example to illustrate the results before we conclude the chapter in Section 8.5.

8.1 Characterization of Fixed Modes

We will first give a characterization of FMs, and a deterministic method of identifying them.

System and Controller Dynamics

In this chapter, we consider the centralized representation of the augmented system dynamics as defined in (7.4). For the purpose of considering FMs of the system, we neglect the exogenous input and the performance output and focus on the nominal system, i.e., (7.4) where $B_{\xi\bar{w}} = 0$, $D_{y\bar{w}} = 0$, $C_{\xi\bar{z}} = 0$ and $D_{\bar{z}u} = 0$. In particular, we consider the framework of augmented dynamic output feedback control as given by

$$K_\xi : \left\{ \begin{bmatrix} \dot{\xi}^K \\ u \end{bmatrix} = \begin{bmatrix} {A^K}_\xi & {B^K}_\xi \\ {C^K}_\xi & D^K \end{bmatrix} \begin{bmatrix} \xi^K \\ y \end{bmatrix} . \right. \tag{8.1}$$

As before, the block-diagonal and off-block-diagonal parts of the augmented controller gains are denoted with superscripts $(\cdot)^d$ and $(\cdot)^i$, respectively. The controller gains are thus given by, e.g., ${A^K}_\xi = {A^{Kd}}_\xi + {A^{Ki}}_\xi$. The closed-loop matrix $\mathcal{A}_\xi$ of the system $\bar{G}_\xi$ with the controller K_ξ will be of importance for the results in this chapter. It is given by

$$\mathcal{A}_\xi = \begin{bmatrix} A_\xi + B_{\xi u} D^K C_{\xi y} & B_{\xi u} {C^K}_\xi \\ {B^K}_\xi C_{\xi y} & {A^K}_\xi \end{bmatrix} . \tag{8.2}$$

Although this chapter is based on the augmented system and controller representations, all the results presented in the following also hold for non-overlapping systems, which represent the special case of $V = I$ and $\xi^c = x^c$.

Definition of Fixed Modes

Decentralized fixed modes (DFMs) have been introduced in [93] as modes of the closed-loop system that cannot be moved by decentralized output feedback. For the system $\bar{G}_\xi$, as given in (7.4), with the controller K_ξ, as given in (8.1), DFMs are eigenvalues of the closed-loop matrix $\mathcal{A}_\xi$ in (8.2), which, for a given overlapping structure, cannot be moved by any decentralized controller. We denote the sets of all decentralized augmented controller gains by $\boldsymbol{A}^{\boldsymbol{Kd}}_{\boldsymbol{\xi}}$, $\boldsymbol{B}^{\boldsymbol{Kd}}_{\boldsymbol{\xi}}$, $\boldsymbol{C}^{\boldsymbol{Kd}}_{\boldsymbol{\xi}}$, and $\boldsymbol{D}^{\boldsymbol{Kd}}$, with

$$\boldsymbol{A}^{\boldsymbol{Kd}}_{\boldsymbol{\xi}} = \left\{ {A^{Kd}}_\xi \in \mathbb{R}^{n_\xi \times n_\xi} \middle| {A^{Kd}}_\xi = \operatorname{diag}_{i=1}^{N}\left({A^{Kd}}_{\xi i} \right),\ {A^{Kd}}_{\xi i} \in \mathbb{R}^{n_{\xi_i} \times n_{\xi_i}} \right\},$$

and $\boldsymbol{B}^{\boldsymbol{Kd}}_{\boldsymbol{\xi}}$, $\boldsymbol{C}^{\boldsymbol{Kd}}_{\boldsymbol{\xi}}$ and $\boldsymbol{D}^{\boldsymbol{Kd}}$ are defined accordingly. For the DFM λ, it thus holds

$$\lambda \in \bigcap_{\substack{{A^K}^d_\xi \in \boldsymbol{A}^{\boldsymbol{Kd}}_{\boldsymbol{\xi}},\, {B^K}^d_\xi \in \boldsymbol{B}^{\boldsymbol{Kd}}_{\boldsymbol{\xi}}, \\ {C^K}^d_\xi \in \boldsymbol{C}^{\boldsymbol{Kd}}_{\boldsymbol{\xi}},\, {D^K}^d \in \boldsymbol{D}^{\boldsymbol{Kd}}}} \operatorname{eig}(\mathcal{A}_\xi) . \tag{8.3}$$

Identification of Fixed Modes

As unstable FMs are not stabilizable under the given structural constraints and stable FMs can limit the performance, they need to be identified and if possible removed via communication or additional measurements or control inputs. However, as $\boldsymbol{A}_{\boldsymbol{\xi}}^{\boldsymbol{K^d}}$, $\boldsymbol{B}_{\boldsymbol{\xi}}^{\boldsymbol{K^d}}$, $\boldsymbol{C}_{\boldsymbol{\xi}}^{\boldsymbol{K^d}}$ and $\boldsymbol{D}^{\boldsymbol{K^d}}$ are infinite sets, checking (8.3) is not practical for a deterministic test. In the following, the characterization of FMs is based on the rank conditions in [93]. Then, the following characterization of FMs holds.

Proposition 8.1. *The closed-loop eigenvalue $\lambda \in \operatorname{eig}(\mathcal{A}_\xi)$ is a FM if and only if there exists a partition of the index set $S = \{1, \dots, N\}$ of all input and output channels into two disjoint subsets $S_1 = \{i_1, \dots, i_k\}$ and $S_2 = \{i_{k+1}, \dots, i_N\}$ with $S_1 \cup S_2 = S$ and $S_1 \cap S_2 = \varnothing$, such that*

$$\operatorname{rank}\left(M_{\lambda,S_1,S_2}\right) < 2n_\xi,$$

where

$$M_{\lambda,S_1,S_2} = \left[\begin{array}{c|c} \lambda I_{2n_\xi} - \hat{A} & \hat{B}_{S_1} \\ \hline \hat{C}_{S_2} & 0 \end{array}\right], \tag{8.4}$$

with

$$\hat{A} = \left[\begin{array}{ccc} A & \tilde{M}_A & 0 \\ 0 & \hat{M}_A & 0 \\ 0 & 0 & 0 \end{array}\right], \qquad \hat{B}_{S_1} = \left[\begin{array}{cccc} B_{u,S_1} & B_{u,S_1} & 0 & 0 \\ 0 & 0 & 0 & 0 \\ 0 & 0 & \hat{I}_{S_1} & \hat{I}_{S_1} \end{array}\right], \qquad \hat{C}_{S_2} = \left[\begin{array}{ccc} C_{y,S_2} & 0 & 0 \\ 0 & 0 & \hat{I}_{S_2} \\ C_{y,S_2} & 0 & 0 \\ 0 & 0 & \hat{I}_{S_2} \end{array}\right]. \tag{8.5}$$

The matrices B_{u,S_1} and $\hat{I}_{S_1}$ are given as

$$B_{u,S_1} = \operatorname{concat}_{l=1}^{k}\left(B_{u,i_l}^\top\right)^\top, \qquad \hat{I}_{S_1} = \operatorname{concat}_{l=1}^{k}\left(\hat{I}_{i_l}^\top\right)^\top, \tag{8.6}$$

with

$$\hat{I}_{i_l} = \begin{bmatrix} 0_{n_{\xi i_l} \times n_{\xi i_1}} & \cdots & 0_{n_{\xi i_l} \times n_{\xi i_{l-1}}} & I_{n_{\xi i_l}} & 0_{n_{\xi i_l} \times n_{\xi i_{l+1}}} & \cdots & 0_{n_{\xi i_l} \times n_{\xi i_N}} \end{bmatrix}^\top.$$

The matrices $C_{y_{S_2}}$ and $\hat{I}_{S_2}$ are defined accordingly. From (7.14)*, $\hat{M}_A$ is given by $\hat{M}_A = \hat{U} M_A \hat{V}$, and $\tilde{M}_A$ is defined as $\tilde{M}_A = U M_A \hat{V}$, where $\hat{V}$, U and $\hat{U}$ are as defined in* (7.13)*.*

Proof: We rewrite the matrix $\mathcal{A}_\xi$ in (8.2) as

$$\mathcal{A}_\xi = \tilde{A} + \tilde{B}^d \tilde{K}^d \tilde{C}^d = \left[\begin{array}{cc} A_\xi & 0 \\ 0 & 0 \end{array}\right] + \left[\begin{array}{cccc} B_{\xi u} & B_{\xi u} & 0 & 0 \\ 0 & 0 & I_{n_\xi} & I_{n_\xi} \end{array}\right] \begin{bmatrix} D^{K^d} & 0 & 0 & 0 \\ 0 & C^{K^d}{}_\xi & 0 & 0 \\ 0 & 0 & B^{K^d}{}_\xi & 0 \\ 0 & 0 & 0 & A^{K^d}{}_\xi \end{bmatrix} \left[\begin{array}{cc} C_{\xi y} & 0 \\ 0 & I_{n_\xi} \\ C_{\xi y} & 0 \\ 0 & I_{n_\xi} \end{array}\right].$$

Then, we perform the following transformation of $\mathcal{A}_\xi$ to

$$\hat{A} = \tilde{W}^{-1}\tilde{A}\tilde{W}, \qquad \hat{B}^d = \tilde{W}^{-1}\tilde{B}^d, \qquad \hat{C}^d = \tilde{C}^d\tilde{W},$$

with

$$\tilde{W} = \begin{bmatrix} V & \hat{V} & 0 \\ 0 & 0 & I \end{bmatrix}, \qquad \tilde{W}^{-1} = \begin{bmatrix} U & 0 \\ \hat{U} & 0 \\ 0 & I \end{bmatrix}.$$

The matrices $\hat{V}$, U and $\hat{U}$ are as defined in (7.13). This transformation leads to

$$\hat{\mathcal{A}} = \hat{A} + \hat{B}^d\tilde{K}^d\hat{C}^d = \left[\begin{array}{cc:c} A & \tilde{M}_A & 0 \\ 0 & \hat{M}_A & 0 \\ \hdashline 0 & 0 & 0 \end{array}\right] + \left[\begin{array}{cc:cc} B_u & B_u & 0 & 0 \\ 0 & 0 & 0 & 0 \\ \hdashline 0 & 0 & I_{n_\xi} & I_{n_\xi} \end{array}\right] \begin{bmatrix} D^{K^d} & 0 & 0 & 0 \\ 0 & C^{K^d}_{\xi} & 0 & 0 \\ 0 & 0 & B^{K^d}_{\xi} & 0 \\ 0 & 0 & 0 & A^{K^d}{}_{\xi} \end{bmatrix} \left[\begin{array}{cc:c} C_y & 0 & 0 \\ 0 & 0 & I_{n_\xi} \\ C_y & 0 & 0 \\ 0 & 0 & I_{n_\xi} \end{array}\right], \tag{8.7}$$

for which the characterization of FMs in [93] is applicable, as the controller gain $\tilde{K}^d = \mathrm{diag}(D^{K^d}, C^{K^d}_{\xi}, B^{K^d}_{\xi}, A^{K^d}_{\xi},)$ is block-diagonal. □

Note that in Proposition 8.1, all disjoint partitions of S need to be checked, including $S_1 = \varnothing$, $S_2 = S$ and vice versa. Proposition 8.1 will be used in Section 8.2 when we add communication links to the system. For the detection of FMs of system (7.18) without communication, we state the following result that simplifies the necessary rank checks.

Lemma 8.1. *The rank deficiency* $d_r := 2n_\xi - \mathrm{rank}\,(M_{\lambda,S_1,S_2})$*, with* M_{λ,S_1,S_2} *in* (8.4)*, is equal to the rank deficiency* $\tilde{d}_r := \underbrace{n_x - \mathrm{rank}\left(\tilde{M}_{\lambda,S_1,S_2}\right)}_{\lambda\in\mathrm{spec}(A)} + \underbrace{\left(n_\xi - n_x - \mathrm{rank}(\lambda I - \hat{M}_A)\right)}_{\lambda\in\mathrm{spec}(\hat{M}_A)}$*,*

with

$$\tilde{M}_{\lambda,S_1,S_2} = \begin{bmatrix} \lambda I_{n_x} - A & B_{u,S_1} \\ C_{y,S_2} & 0 \end{bmatrix}. \tag{8.8}$$

Proof: To show this, we transform the matrix M_{λ,S_1,S_2} into

$$M_{\lambda,S_1,S_2} = \mathrm{diag}\left(\left[\begin{array}{ccc:c} \lambda I_{n_x} - A & B_{u,S_1} & B_{u,S_1} & -\tilde{M}_A \\ C_{y,S_2} & 0 & 0 & 0 \\ C_{y,S_2} & 0 & 0 & 0 \\ \hdashline 0 & 0 & 0 & \lambda I_{n_\xi - n_x} - \hat{M}_A \end{array}\right], \begin{bmatrix} \lambda I_{n_\xi} & \hat{I}_{S_1} & \hat{I}_{S_1} \\ \hat{I}_{S_2} & 0 & 0 \\ \hat{I}_{S_2} & 0 & 0 \end{bmatrix}\right). \tag{8.9}$$

The rank of the second block is n_ξ, as S_1 and S_2 are disjoint. The first block is rank deficient if $\lambda \in \mathrm{spec}(\hat{M}_A)$ and if $\begin{bmatrix} \lambda I_{n_x} - A & B_{u,S_1} \\ C_{y,S_2} & 0 \end{bmatrix}$ is rank deficient. Therefore, the rank deficiency d_r is caused by FMs $\lambda \in \mathrm{spec}(\hat{M}_A)$ or by the rank deficiency of $\tilde{M}_{\lambda,S_1,S_2}$. □

Indeed, the possible FM candidates are the eigenvalues of A and of $\hat{M}_A$, i.e., $\lambda \in \text{spec}(A) \cup \text{spec}(\hat{M}_A)$. The modes $\lambda \in \text{spec}(\hat{M}_A)$ are FMs of (8.2), as they cause a rank deficiency of M_{λ,S_1,S_2}. This is also obvious from (8.7), interpreting the structure as a Kalman decomposition and noting that the entries in $\hat{B}^d$ and $\hat{C}^d$ that correspond to the modes of $\hat{M}_A$ are all zero. However, these FMs result from augmenting the system and do not affect stability nor performance of the original system. The choice of M_A which determines these FMs is therefore important only for the controller synthesis, i.e., M_A needs to be chosen such that the pairs $(A_\xi, B_{\xi u})$ and $(A_\xi, C_{\xi y})$ are stabilizable and reachable and such that $\lambda \in \hat{M}_A$ do not limit the achievable control performance. Therefore, only eigenvalues of A will be considered as potential FMs for the original system. Furthermore, as only unobservable and uncontrollable channels can cause a rank deficiency of M_{λ,S_1,S_2}, only the partitions of these channels need to be considered.

FMs of $\mathcal{A}_\xi$ in (8.2), the closed-loop of (7.4) under controller (8.1), are thus the eigenvalues of $\hat{M}_A$, and the FMs of system (5.25) in the original state space which would occur under static output feedback ${D^K}^d$.

In [48], the result was stated that FMs under decentralized static feedback are equivalent to FMs under decentralized dynamic feedback of the same structure. Lemma 8.1 shows that this set of FMs is also a subset of FMs under the augmented dynamic controller (in addition to the FMs introduced by M_A).

8.2 Elimination of Fixed Modes by Communication

We assume that the input-output structure of the system is fixed. FMs will therefore be eliminated by changing the controller structure through communication.

8.2.1 Communication of Measurements and Controller States

In the following, it is shown how to remove the FMs by introducing communication between the subcontrollers. In particular, we consider the cases of communicating only controller states, or only measurements. Depending on the application, it can of course be reasonable to minimize the number of communication links, and to communicate both, controller states and measurements per link.

We define the sets $\mathcal{E}^y$ and $\mathcal{E}^{\xi^K}$, which comprise all existing measurement and controller state communication links, respectively. This means that if the measurement communication topology contains the link (i,j), i.e., if $(i,j) \in \mathcal{E}^y$, then the measurements of j are communicated to i. In this case, the controller gains ${B^K}^i_{\xi ij}$ and ${D^K}^i_{ij}$ will be used. The set $\mathcal{E}^{\xi^K}$ is defined accordingly and enables the use of the gains ${A^K}^i_{\xi ik}$ and ${C^K}^i_{\xi ik}$ for a link $(i,k) \in \mathcal{E}^{\xi^K}$. The sets $\mathcal{E}^y$ and $\mathcal{E}^{\xi^K}$ are subsets of the link set $\mathcal{E}_{\text{full}} = \{(1,2), ..., (N, N-1)\}$ of all $N(N-1)$ possible directed links.

Remark 8.1. Note that in Chapters 5 and 6, we defined the set of controller interconnection links $\mathcal{E}^K$ as the set of all links to communicate both controller states ξ_i^K and measurements y_i, i.e., $\mathcal{E}^K = \mathcal{E}^{\xi^K} = \mathcal{E}^y$.

In order to characterize the FMs of the system with communication, as in Proposition 8.1, we formulate the controller gains of K_ξ in (8.1) as

$$\begin{aligned} A_\xi^K &= {A^K}_\xi^d + \mathbb{B}_A \, {A^K}_\mathcal{E}^i \, \mathbb{C}_A, \\ B_\xi^K &= {B^K}_\xi^d + \mathbb{B}_B \, {B^K}_\mathcal{E}^i \, \mathbb{C}_B, \\ C_\xi^K &= {C^K}_\xi^d + \mathbb{B}_C \, {C^K}_\mathcal{E}^i \, \mathbb{C}_C, \\ D^K &= {D^K}^d + \mathbb{B}_D \, {D^K}_\mathcal{E}^i \, \mathbb{C}_D, \end{aligned} \tag{8.10}$$

with

$$\begin{aligned} {A^K}_\mathcal{E}^i &= \mathrm{diag}_{(i,k)\in\mathcal{E}^{\xi^K}} \left({A^K}_{\xi_{ik}}^i \right), \\ {B^K}_\mathcal{E}^i &= \mathrm{diag}_{(i,j)\in\mathcal{E}^{y}} \left({B^K}_{\xi_{ij}}^i \right), \\ {C^K}_\mathcal{E}^i &= \mathrm{diag}_{(i,k)\in\mathcal{E}^{\xi^K}} \left({C^K}_{\xi_{ik}}^i \right), \\ {D^K}_\mathcal{E}^i &= \mathrm{diag}_{(i,j)\in\mathcal{E}^{y}} \left({D^K}_{ij}^i \right). \end{aligned} \tag{8.11}$$

The structure of the communication is captured in $\mathbb{B}_{\{A,B,C,D\}}$ and $\mathbb{C}_{\{A,B,C,D\}}$, which are defined as for example $\mathbb{B}_A = \mathrm{concat}_{(i,j)\in\mathcal{E}^{\xi^K}} \left(\mathbb{B}_{A,ij}^\top \right)^\top$, where $\mathbb{B}_{A,ij}$ accounts for the link $(i,j) \in \mathcal{E}^{\xi^K}$ and is given by

$$\mathbb{B}_{A,ij} = \begin{bmatrix} 0_{n_{\xi i} \times n_{\xi 1}} & \dots & 0_{n_{\xi i} \times n_{\xi i-1}} & I_{n_{\xi i}} & 0_{n_{\xi i} \times n_{\xi i+1}} & \dots & 0_{n_{\xi i} \times n_{\xi N}} \end{bmatrix}^\top,$$

and $\mathbb{B}_{\{B,C,D\}}$ and $\mathbb{C}_{\{A,B,C,D\}}$ are defined analogously. With these definitions, the closed-loop system in (8.7) , extended by communication as in (8.10), has the closed-loop matrix $\hat{A}_{clp} = \hat{A} + \hat{B}\,\tilde{K}\,\hat{C}$ with block-diagonal controller gain

$$\tilde{K} = \mathrm{diag}({D^K}^d, {C^K}^d{}_\xi, {B^K}_\xi^d, {A^K}_\xi^d, {D^K}^i{}_\mathcal{E}, {C^K}^i{}_\mathcal{E}, {B^K}^i_\mathcal{E}, {A^K}^i_\mathcal{E}),$$

and corresponding $\hat{B}$ and $\hat{C}$ given as

$$\hat{B} = \left[\begin{array}{cccccccc} B_u & B_u & 0 & 0 & B_u\,\mathbb{B}_D & B_u\,\mathbb{B}_C & 0 & 0 \\ 0 & 0 & 0 & 0 & 0 & 0 & 0 & 0 \\ \hdashline 0 & 0 & I_{n_\xi} & I_{n_\xi} & 0 & 0 & \mathbb{B}_B & \mathbb{B}_A \end{array}\right], \quad \hat{C} = \left[\begin{array}{ccc} C_y & 0 & 0 \\ 0 & 0 & I_{n_\xi} \\ C_y & 0 & 0 \\ 0 & 0 & I_{n_\xi} \\ \mathbb{C}_D C_y & 0 & 0 \\ 0 & 0 & \mathbb{C}_C \\ \mathbb{C}_B C_y & 0 & 0 \\ 0 & 0 & \mathbb{C}_A \end{array}\right]. \tag{8.12}$$

Full Communication of Measurements or Controller States

In the case of all-to-all communication of measurements or controller states, i.e., $\mathcal{E}^y = \mathcal{E}_{\text{full}}$ or $\mathcal{E}^{\xi^K} = \mathcal{E}_{\text{full}}$, the expression in (8.12) can be simplified. The closed-loop can be written as in (8.7), but with the respective controller gains

$$K^y = \text{diag}(D^K, C^{K^d}_{\ \xi}, B^K{}_\xi, A^{K^d}_{\ \xi}), \quad \text{or} \quad K^{\xi^K} = \text{diag}(D^{K^d}, C^K{}_\xi, B^{K^d}_{\ \xi}, A^K{}_\xi), \tag{8.13}$$

where $A^K{}_\xi$, $B^K{}_\xi$, $C^K{}_\xi$ and D^K are full gains as defined before. Using the definition in (8.10), they are recovered as

$$\begin{aligned} A^K{}_\xi &:= A^{K^d}_{\ \xi} + \mathbb{B}_A\, A^{K^i}_{\ \mathcal{E}_{\text{full}}}\, \mathbb{C}_A, \\ B^K{}_\xi &:= B^{K^d}_{\ \xi} + \mathbb{B}_B\, B^{K^i}_{\ \mathcal{E}_{\text{full}}}\, \mathbb{C}_B, \\ C^K{}_\xi &:= C^{K^d}_{\ \xi} + \mathbb{B}_C\, C^{K^i}_{\ \mathcal{E}_{\text{full}}}\, \mathbb{C}_C, \\ D^K &:= D^{K^d}_{\ \xi} + \mathbb{B}_D\, D^{K^i}_{\ \mathcal{E}_{\text{full}}}\, \mathbb{C}_D, \end{aligned} \tag{8.14}$$

with the all-to-all communication in $\mathcal{E}_{\text{full}}$. In the following, either the case of communicating only controller states or only measurements is considered.

8.2.2 Existence of Communication Topologies to Eliminate FMs

In the following, it is shown that there always exists a communication topology of only measurements or controller states, such that all FMs are eliminated.

Lemma 8.2. *The augmented closed-loop system* (8.7) *with all-to-all communication:*

a) of only measurements, i.e., $\mathcal{E}^y = \mathcal{E}_{\text{full}}$, $\mathcal{E}^{\xi^K} = \varnothing$, *and* K^y *as in* (8.13) *, has no FMs.*

b) of only controller states, i.e., $\mathcal{E}^{\xi^K} = \mathcal{E}_{\text{full}}$, $\mathcal{E}^y = \varnothing$ *and* K^{ξ^K} *as in* (8.13) *has no FMs, if and only if the following condition on the overlapping structure is satisfied:* $n_x - \text{rank}\left(\begin{bmatrix} \lambda I_{n_x} - A & B_{u,S_1} \\ C_{y,S_2} & 0 \end{bmatrix}\right) \leq \sum_{i\in S_1} n_{\xi i}$, $\forall$ S_1, S_2 *being disjoint partitions of* S *as defined before, and for all FM canditates* λ.

Proof: a) As $B^K{}_\xi$ and D^K are full blocks, $\hat{B}_{S_1}$ in Proposition 8.1 becomes

$$\hat{B}_{S_1} = \left[\begin{array}{cccc} B_{u,S_{D_1}} & B_{u,S_1} & 0 & 0 \\ 0 & 0 & 0 & 0 \\ \hdashline 0 & 0 & \hat{I}_{S_{B_1}} & \hat{I}_{S_1} \end{array}\right],$$

with $S_{B_1} = S$ or $S_{B_1} = \varnothing$ and $S_{D_1} = S$ or $S_{D_1} = \varnothing$. Accordingly, $\hat{C}_{S_2}$ is given by

$$\hat{C}_{S_2} = \left[\begin{array}{cc:c} C_{y,S_{D_2}} & 0 & 0 \\ 0 & 0 & \hat{I}_{S_2} \\ C_{y,S_{B_2}} & 0 & 0 \\ 0 & 0 & \hat{I}_{S_2} \end{array}\right], \tag{8.15}$$

with S_{B_2} and S_{D_2} being equal to S or $\varnothing$, such that they form disjoint partitions of S with S_{B_1} and S_{D_1}, respectively. The necessary rank checks thus reduce to the four possible combinations of $S_{B_1} = S$ and $S_{B_2} = \varnothing$ and vice versa, combined with the analogous two possible choices for S_{D_1} and S_{D_2}. In all cases, for the remaining entries in $\hat{B}_{S_1}$ and $\hat{C}_{S_2}$, all possible disjoint partitions of S into S_1 and S_2 need to be considered. In all cases, it is easy to check that $\operatorname{rank}(M_{\lambda,S_1,S_2}) \geq 2n_\xi$. It suffices to note that the first block has always rank greater or equal to n_x, as in all possible cases, either $B_{u,S_{D_1}}$ or $C_{y,S_{B_2}}$ are full blocks, and the pairs (A, B_u) and (A, C_y) are assumed to be controllable and observable.

b) Since the blocks ${A^K}_\xi$ and ${C^K}_\xi$ are full, $\hat{B}_{S_1}$ in Proposition 8.1 becomes

$$\hat{B}_{S_1} = \left[\begin{array}{cccc} B_{u,S_1} & B_{u,S_{C_1}} & 0 & 0 \\ 0 & 0 & 0 & 0 \\ \hdashline 0 & 0 & \hat{I}_{S_1} & \hat{I}_{S_{A_1}} \end{array}\right],$$

and the corresponding entries $\hat{I}_{S_2}$ in $\hat{C}_{S_2}$ become $\hat{I}_{S_{A_2}}$ and $\hat{I}_{S_{C_2}}$, i.e.,

$$\hat{C}_{S_2} = \left[\begin{array}{cc:c} C_{y,S_2} & 0 & 0 \\ 0 & 0 & \hat{I}_{S_{C_2}} \\ C_{y,S_2} & 0 & 0 \\ 0 & 0 & \hat{I}_{S_{A_2}} \end{array}\right]. \tag{8.16}$$

Similarly to a), the four possible combinations of these blocks being full or empty and the corresponding blocks forming disjoint partitions over S need to be checked. In the two cases, where $B_{u,S_{C_1}}$ is a full block, the first block in (8.9) has rank n_x, because of the controllability of (A, B_u). In the case where $\hat{I}_{S_{A_1}}$ and $\hat{I}_{S_{C_2}}$ are full blocks, the third block in (8.9) is of rank $2n_\xi$. In the remaining case, it holds that $\operatorname{rank}(M_{\lambda,S_1,S_2}) = \operatorname{rank}\left(\begin{bmatrix} \lambda I_{n_x} - A & B_{u,S_1} \\ C_{y,S_2} & 0 \end{bmatrix}\right) + 2n_\xi - n_x + \sum_{i\in S_1} n_{\xi_i}$, which has to be $\geq 2n_\xi$ for the system to have no FMs, and the given condition follows.

□

Instead of an augmented DOF controller, the controller in (8.1) can be interpreted as a decentralized augmented SSF controller that is based on an overlapping estimator. In that case, $D^K = 0$, and interconnected terms are considered only in ${A^K}^i_\xi$ and ${B^K}^i_\xi$, and thus ${C^K}^i_\xi = 0$. The following result gives some mild conditions, under which there always exists a communication topology of measurements, $\mathcal{E}^y$, or controller states, $\mathcal{E}^{\xi^K}$, that removes all FMs.

Corollary 8.1. *The augmented closed-loop system* (8.7) *with* $D^K = 0$ *and with all-to-all communication, which is introduced through* ${A^K}^i_\xi$ *and* ${B^K}^i_\xi$*:*

a) *of only measurements, i.e.,* $\mathcal{E}^y = \mathcal{E}_{\text{full}}$, $\mathcal{E}^{\xi^K} = \varnothing$, *and* $K^y = \text{diag}(0, {C^K}_\xi^d, {B^K}_\xi, {A^K}_\xi^d)$, *has no FMs, if and only if the following condition on the overlapping structure is satisfied:* $n_x - \text{rank}(\lambda I_{n_x} - A,\ B_{u,S_1}) \leq \sum_{i \in S_2} n_{\xi i},\ \forall\ S_1,\ S_2$ *as defined before, and for all FM canditates* λ.

b) *of only controller states, i.e.,* $\mathcal{E}^{\xi^K} = \mathcal{E}_{\text{full}}$, $\mathcal{E}^y = \varnothing$ *and* $K^{\xi^K} = \text{diag}(0, {C^K}_\xi^d, {B^K}_\xi^d, {A^K}_\xi)$, *has no FMs, if and only if the following condition on the overlapping structure is satisfied:* $n_x - \text{rank}\left(\begin{bmatrix} \lambda I_{n_x} - A & B_{u,S_1} \\ C_{y,S_2} & 0 \end{bmatrix}\right) \leq \min\left(\sum_{i \in S_2} n_{\xi i},\ \ \sum_{i \in S_1} n_{\xi i}\right),\ \forall\ S_1,\ S_2$ *as defined before, and for all FM canditates* λ.

Proof: a) As ${B^K}_\xi$ is a full block, $\hat{B}_{S_1}$ in Proposition 8.1 becomes

$$\hat{B}_{S_1} = \left[\begin{array}{ccc} B_{u,S_1} & 0 & 0 \\ 0 & 0 & 0 \\ \hdashline 0 & \hat{I}_{S_{B_1}} & \hat{I}_{S_1} \end{array}\right],$$

with $S_{B_1} = S$ or $S_{B_1} = \varnothing$. Accordingly, the entry C_{y,S_2} in $\hat{C}_{S_2}$ becomes $C_{y,S_{B_2}}$ since S_{B_2} and S_{B_1} form disjoint partitions of S. The necessary rank checks thus reduce to the two cases $S_{B_1} = \varnothing$ and $S_{B_2} = S$ and vice versa. In both cases, for the remaining entries in $\hat{B}_{S_1}$ and $\hat{C}_{S_2}$, all possible disjoint partitions of S into S_1 and S_2 need to be considered. In the first case with $C_{y,S_{B_2}} = C_y$, it always holds that $\text{rank}(M_{\lambda,S_1,S_2}) \geq 2n_\xi$, as (A, C_y) is observable. In the second case, from (8.9) with $C_{y,S_{B_2}} = \varnothing$ and $\hat{I}_{S_{B_1}} = I_{n_\xi}$, for all possible S_1 and S_2, it holds that $\text{rank}\left(M_{\lambda,S_1,S_2}\right) = \text{rank}([\lambda I_{n_x} - A, B_{u,S_1}]) + 2n_\xi - n_x + \sum_{i \in S_2} n_{\xi_i}$, which has to be $\geq 2n_\xi$ for no FMs, and the given conditions follow.

b) Because the block ${A^K}_\xi$ is full, $\hat{I}_{S_1}$ and $\hat{I}_{S_2}$ of the third block columns and rows in $\hat{B}_{S_1}$ and $\hat{C}_{S_2}$ become $\hat{I}_{S_{A_1}}$ and $\hat{I}_{S_{A_2}}$. The two cases to be checked are $S_{A_1} = S$ and $S_{A_2} = \varnothing$ and vice versa. The result follows with similar reasoning as in a).

□

8.3 Minimum Set of Communication Links to Remove FMs

We consider the problem of determining a minimal communication link set to remove all FMs. The communication of either measurements or controller states is considered. In the following, for the ease of presentation, we will denote the communication topology that is to be minimized by T, which can stand for both $\mathcal{E}^{\xi^K}$ or $\mathcal{E}^y$. First, all FMs are identified, which by Lemma 8.1, is done by the rank checks of $\tilde{M}_{\lambda,S_1,S_2}$. All rank-deficient

cases are denoted by $r = 1, ..., R$ of rank-deficiency $d_r = \tilde{d}_r = n_x - \text{rank}(\tilde{M}_{\lambda_r, S_{1,r}, S_{2,r}})$, with the fixed modes λ_r, and with the partitions $S_{1,r}$ and $S_{2,r}$.

We propose to formulate the problem of finding a minimal set of communication links to eliminate all FMs as the following minimum cost coverage problem with submodular constraints [26],

$$\begin{aligned} T^* = &\underset{T}{\text{argmin}} \ |T| \\ &\text{s.t. } f_r(T) \geq d_r, \quad \forall r \in \{1, ..., R\}, \end{aligned} \tag{8.17}$$

with

$$f_r(T) = \min_{\hat{S}_1, \hat{S}_2} \left(\text{rank}(M_{\lambda_r, S_{1,r}, S_{2,r}, \mathbb{B}_{T,\hat{S}_1}, \mathbb{C}_{T,\hat{S}_2}}) \right) - \text{rank}(M_{\lambda_r, S_{1,r}, S_{2,r}}), \tag{8.18}$$

where $M_{\lambda_r, S_{1,r}, S_{2,r}}$ is defined as in (8.4) with the partitions $S_{1,r}$ and $S_{2,r}$. The set function $f_r(T)$ indicates the rank increase of $M_{\lambda_r, S_{1,r}, S_{2,r}}$ for implementing the link set T. All possible disjoint partitions $\hat{S}_1$ and $\hat{S}_2$ of T need to be checked. They are concatenated through the corresponding $\mathbb{B}_T$ and $\mathbb{C}_T$, comprising the $\mathbb{B}_{\{A,B,C,D\}}$ and $\mathbb{C}_{\{A,B,C,D\}}$, to $\hat{B}$ and $\hat{C}$, as in (8.12). The matrix $M_{\lambda_r, S_{1,r}, S_{2,r}}$ with these concatenated partitions of T is denoted by $M_{\lambda_r, S_{1,r}, S_{2,r}, \mathbb{B}_{T,\hat{S}_1}, \mathbb{C}_{T,\hat{S}_2}}$.

Minimum cost coverage problems are known to be NP-hard [120]. But the submodularity of the constraints is exploited to give a guaranteed suboptimality bound for the greedy algorithm and for efficient cuts in a decision tree based algorithm. To show submodularity of the constraints in (8.17), we reformulate them as

$$g(T) \geq \sum_{r=1}^{R} d_r, \tag{8.19}$$

with

$$g(T) = \sum_{r=1}^{R} \min(f_r(T), d_r). \tag{8.20}$$

The submodularity of the constraints of (8.17) in (8.18) intuitively means that the increase in information between the subsystems is larger for adding a communication link to a sparser communication topology than adding the same communication link to a denser communication topology. Now, we state the following preliminary result, in order to then prove submodularity of $g(T)$ in (8.20).

Lemma 8.3. *The set function $f_r(T)$ in (8.17) is submodular and monotone.*

Proof: First, we show monotonicity of $f_r(T)$. A direct application of Definition 3.4 in Section 3.1 leads to

$$\forall\, T_1 \subseteq T_2 \subseteq \mathcal{E}_{\text{full}}, \quad f_r(T_1) \leq f_r(T_2).$$

Inserting the definition of $f_r(T)$ from (8.18) results in

$$\min_{\hat{S}_1,\hat{S}_2}\left(\operatorname{rank}(M_{\lambda_r,S_{1,r},S_{2,r},\mathbb{B}_{T_1,\hat{S}_1},\mathbb{C}_{T_1,\hat{S}_2}})\right) \leq \min_{\hat{S}_1,\hat{S}_2}\left(\operatorname{rank}(M_{\lambda_r,S_{1,r},S_{2,r},\mathbb{B}_{T_2,\hat{S}_1},\mathbb{C}_{T_2,\hat{S}_2}})\right), \tag{8.21}$$

which is clear from the property of the rank and the fact that the minimum on the right-hand side (RHS) is searched over the partitions $\hat{S}_1, \hat{S}_2$ of T_2, which are strict supersets of the partitions of T_1 of the left-hand side (LHS). Therefore, the RHS cannot have a lower rank.

To show submodularity of the function $f_r(T)$, the following definition, which is equivalent to Definition 3.5 from Section 3.1, with $T = T_1 \cap T_2$, $T \cup \{e_1, e_2\} = T_1 \cup T_2$, $T \cup \{e_1\} = T_1$, $T \cup \{e_2\} = T_2$, is verified. Applying the definition to the function $f_r(T)$ leads to the following result. $\forall\, T \subseteq \mathcal{E}_{\text{full}}, e_1, e_2 \in \mathcal{E}_{\text{full}} \setminus T$,

$$\begin{aligned}
&f_r(T \cup \{e_1\}) + f_r(T \cup \{e_2\}) \geq f_r(T \cup \{e_1, e_2\}) + f_r(T) \\
\iff &\min_{\hat{S}_1,\hat{S}_2}\left(\operatorname{rank}(M_{r,T\cup\{e_1\},\hat{S}_1,\hat{S}_2})\right) + \min_{\hat{S}_1,\hat{S}_2}\left(\operatorname{rank}(M_{r,T\cup\{e_2\},\hat{S}_1,\hat{S}_2})\right) \geq \\
&\min_{\hat{S}_1,\hat{S}_2}\left(\operatorname{rank}(M_{r,T\cup\{e_1,e_2\},\hat{S}_1,\hat{S}_2})\right) + \min_{\hat{S}_1,\hat{S}_2}\left(\operatorname{rank}(M_{r,T,\hat{S}_1,\hat{S}_2})\right),
\end{aligned} \tag{8.22}$$

where we used $M_{r,T,\hat{S}_1,\hat{S}_2} := M_{\lambda_r,S_{1,r},S_{2,r},\mathbb{B}_{T,\hat{S}_1},\mathbb{C}_{T,\hat{S}_2}}$ for the ease of presentation. This means that the sum of rank increases of $M_r := M_{\lambda_r,S_{1,r},S_{2,r}}$ for concatenating the corresponding rows and columns of $\mathbb{B}_T$ and $\mathbb{C}_T$ separately is larger than for adding them simultaneously. For simplicity of the argument, we first consider the case, where $T = \varnothing$. The inequality has to hold for the minimum over the partitions $\hat{S}_1, \hat{S}_2$ in each term. Let us denote the rank increases for the two possible partitions $\hat{S}_1, \hat{S}_2$ for adding $\{e_1\}$ by

$$b_1 := \operatorname{rank}(M_{r,\{e_1\},\hat{S}_1=\{e_1\},\hat{S}_2=\varnothing}),$$

$$c_1 := \operatorname{rank}(M_{r,\{e_1\},\hat{S}_1=\varnothing,\hat{S}_2=\{e_1\}}),$$

and b_2, c_2 accordingly for adding $\{e_2\}$. Similarly, for the rank increase of adding $\{e_1, e_2\}$, let us denote

$$b_{12} := M_{r,\{e_1,e_2\},\hat{S}_1=\{e_1,e_2\},\hat{S}_2=\varnothing},$$
$$c_{12} := M_{r,\{e_1,e_2\},\hat{S}_1=\varnothing,\hat{S}_2=\{e_1,e_2\}}.$$

Then, (8.22) becomes

$$\begin{aligned}
\min(b_1, c_1) + \min(b_2, c_2) &= \min(b_1 + b_2, b_1 + c_2, b_2 + c_1, c_1 + c_2) \\
&\geq \min(b_{12}, c_{12}, b_1 + c_2, b_2 + c_1) + 0\,,
\end{aligned} \tag{8.23}$$

where the equality holds since $b_1, b_2, c_1, c_2 \geq 0$. The inequality in (8.23) holds as $b_1 + b_2 \geq b_{12}$, which holds with equality in the case where the matrices $\mathbb{B}_{T,\hat{S}_1=\{e_1\}}$ and $\mathbb{B}_{T,\hat{S}_1=\{e_2\}}$ only contain linearly independent vectors and strict inequality can hold if they contain linearly dependent ones. The same holds for c_{12}, which completes the proof for $T = \varnothing$.

If $T \neq \varnothing$, it is easy to show that the same argument holds. In this case, again, the LHS of (8.22) can be written as one minimum function, and for each of its arguments, the minimum function on the RHS contains an argument of equal or smaller value, with the same reasoning as before. □

With this, we can now state the following result.

Lemma 8.4. *The function* $g(T) = \sum_{r=1}^{R} \min(f_r(T), d_r)$ *is submodular and monotone.*

Proof: By construction, the function $g(T)$ is monotone, as by Lemma 8.3 , $f_r(T)$ is monotone, and thus enlarging the argument set cannot decrease the function value. The function $g(T)$ is submodular as f_r is submodular and monotone, and thus their truncation $\min(f_r(T), d_r)$ is submodular. Finally, the sum of submodular functions is also submodular [26]. □

8.3.1 Greedy Algorithm

Depending on the application, it may not be critical to find the minimal communication, but a suboptimal solution might be acceptable. Then, a greedy algorithm can be used [111]. It starts from the empty link set $T^1 = \varnothing$ and the search set $S^1 = \mathcal{E}_{\text{full}}$ of all possible communication links. In each iteration n, a link $(i,j)^*$ from the search set that causes the largest increase of $g(T^n \cup (i,j))$ with respect to $g(T^n)$ in (8.20) is added to the link set until the rank deficiency is removed. These steps are given in Algorithm 8.1. The submodularity of $g(T)$ implies a suboptimality bound of a factor H by which the

Algorithm 8.1 Greedy algorithm to determine suboptimal solution of (8.17): minimal sets of communication links to eliminate all FMs.

1: **Input:** A, B_u, C_y, K_ξ, V, FMs and rank deficient cases $r = 1, ..., R$ identified as in Lemma 8.1 for $g(T)$,
2: **Initialization:** $n = 1$, $T^1 = \varnothing$, Search set $S^1 = \mathcal{E}_{\text{full}}$,
3: **while** $g(T^n) \leq \sum_r d_r$ **do**
4: Compute rank increase $\Delta g_{(i,j)} = g(T^n \cup (i,j)) - g(T^n), \quad \forall\ (i,j) \in S^n$,
5: Update $T^{n+1} = T^n \cup (i,j)^*$, with $(i,j)^* = \underset{(i,j)\in S^n}{\arg\max}\, \Delta g_{(i,j)}$,
6: Update $S^{n+1} = S^n \setminus (i,j)^*$,
7: $n = n + 1$,
8: **end**
9: $T^* = T^n$,
10: **Output:** Suboptimal solution of sets of communication links T^*.

optimal value is not exceeded. This factor is given by

$$H(\max_j g(\{j\})),$$

where $H(d) = \sum_{i=1}^{d} \frac{1}{i}$ [111], and thus $H(\max_j g(\{j\})) = \sum_{i=1}^{\max_j g(\{j\})} \frac{1}{i} = 1 + \frac{1}{2} + ... + \frac{1}{\max_j g(\{j\})}$, with j being the element from the universe set with the maximum value of $g(\cdot)$. As the greedy algorithm has a polynomial complexity and no other polynomial algorithm can have better suboptimality guarantees [121], the greedy algorithm is the best choice if the amount of communication is not critical.

8.3.2 Tree Search Algorithm

If it is critical to find the minimum set of communication links, i.e., the optimal solution, then we propose Algorithm 8.2 , a branch and bound algorithm with efficient cuts and reductions of the search sets. A search tree is built such that each node contains a set of communication links. From one level to the next one, the link set, T^n, of the node, n, grows by one link. The root contains no links, i.e., $T^{n=1} = \varnothing$. In addition to the link set, each node also contains a search set of potential links $\mathcal{E}^n$. These links are possibly added to the link set to create the children of the node, $n+$, for the next level of the tree. For the root, the search set $\mathcal{E}^{n=1} = \mathcal{E}_{\text{full}}$ contains all $N\,(N-1)$ possible links. To branch a node, all links of its search set are separately added to its link set. If a link (i,j) increases the rank of $g(T)$, i.e., $g(T^{n+}) > g(T^n)$, then a child with link set $T^{n+} = T^n \cup (i,j)$ is created, if the same link set does not already exist in a different node. The search set of the child is $\mathcal{E}^{n+} = \mathcal{E}^n \setminus (i,j)$. All the links, (k,l) which have not been added for creating a child, i.e., with $g(T^n \cup (k,l)) \not> g(T^n)$, are then cut from all search sets of the created children $n+$. The tree is finished at the level where at least one node has a set T with $g(T) \geq \sum_r d_r$. This level is at most $\sum_r d_r$. All link sets T^n of this last level of the tree with $g(T^n) \geq \sum_r d_r$ are minimal sets of communication links, which eliminate all FMs. Instead of the number of links, also the number of signals to be communicated can be minimized. In this case, the corresponding single columns and rows of $\mathbb{B}_T$ and $\mathbb{C}_T$ are added to branch the nodes.

Theorem 8.1. *Algorithm 8.2 finds all optimal solutions T^* of Problem* (8.17) .

Proof: In each iteration, only the links e are cut, which do not increase the function $g(T)$ in this level of the tree. Because of the submodularity of $g(T)$, they cannot increase the value of $g(T)$ when added later on, i.e., if $g(T \cup \{e\}) - g(T) = 0$, then also $g(\hat{T} \cup \{e\}) - g(\hat{T}) = 0$ at a node with link set $\hat{T}$ with $\hat{T} \supseteq T$. Therefore, the links that are cut do not belong to potential optimal link sets and all optimal link sets, i.e., with minimal cardinality, are found by Algorithm 8.2 . □

Compared to testing all combinations of links, the computational effort of Algorithm 8.2 is reduced by exploiting the submodularity of $g(T)$. The efficiency is determined by how many nodes are cut and how much the search sets are shrunk. Let p_j^i be the ratio of the

Algorithm 8.2 Search tree algorithm to determine the minimal sets of communication links to eliminate all FMs.

Data: A, B_u, C_y, K_ξ, V, FMs and rank deficient cases $r = 1, ..., R$ identified as in Lemma 8.1 for $g(T)$,
Result: Minimal set of communication links T^*,
Initialization: Tree root: $T^{n=1} = \varnothing$, $\mathcal{E}^{n=1} = \mathcal{E}_{\text{full}}$, $n = 1$,
while $\nexists\, T^n$, with $g(T^n) \geq \sum_r d_r$ **do**
    1) Branch nodes by creating children with
        $T^{n+} = T^n \cup (i, j)$ and $\mathcal{E}^{n+} = \mathcal{E}^n \setminus (i, j)$
        if $g(T^{n+}) > g(T^n)$ and $\nexists\, m \neq n+ \mid T^m = T^n \cup (i, j)$,
    2) Cut links (k, l) from search sets of created nodes
        if $g(T^n \cup (k, l)) \not> g(T^n)$,
    $T^{n+1} = T^{n+}, \quad n = n + 1$,
end
$T^* = T^n$,

number of children created by node j in level i with respect to $m := |T|$, and let $\bar{R}$ be the number of links required to remove all FMs. In the worst-case, $\bar{R} = \sum_{r=1}^{R} d_r$, but it can be lower in practical examples. The number of nodes to be checked in Algorithm 8.2 is then

$$m + (p_1^0 m)^2 + \sum_{i=1}^{p_1^0 m} \left((p_i^1 m)^2 + \sum_{j=1}^{p_i^1 m} \left((p_j^2 m)^2 + \ldots + \sum_{k=1}^{p_t^{\bar{R}-3} m} (p_k^{\bar{R}-2} m)^2 \right) \right).$$

Thus, its complexity is $O(m^{\bar{R}})$, but reduced by a linear factor of up to $\prod_{i=0}^{\bar{R}-1} (\bar{p}^i) \bar{p}^{\bar{R}-1}$, with $\bar{p}^i = \max_j p_j^i$, compared to the exhaustive approach of checking all combinations. With exponential complexity Algorithm 8.2 is clearly less efficient than the polynomial-time greedy algorithm. However, Algorithm 8.2 finds the optimum, which unless $P = NP$ cannot be guaranteed for any polynomial algorithm [121].

8.4 Numerical Example

The results are illustrated by a numerical example of a system with $N = 3$ subsystems and $n_x = 4$ states, with

$$A = \begin{bmatrix} 0.25 & 0 & 0 & 0 \\ 2 & 1.5 & 0 & 0 \\ 1 & 0 & 1.5 & 0 \\ 1 & 0 & 0 & 4 \end{bmatrix}, \quad B = [B_1, B_2, B_3], \quad C = [C_1^\top, C_2^\top, C_3^\top]^\top,$$

with

$$B_1 = \begin{bmatrix} 1 & 0 & 0 & 0 \end{bmatrix}^\top, \quad B_2 = \begin{bmatrix} 0 & 1 & 2 & 0 \\ 0 & 3 & 1 & 0 \end{bmatrix}^\top, \quad B_3 = \begin{bmatrix} 0 & 0 & 0 & 1 \end{bmatrix}^\top,$$

$$C_1 = \begin{bmatrix} 1 & 1 & 0 & 0 \\ 1 & 0 & 1 & 0 \end{bmatrix}, \quad C_2 = \begin{bmatrix} 1 & 0 & 0 & 0 \end{bmatrix}, \quad C_3 = \begin{bmatrix} 0 & 0 & 0 & 1 \end{bmatrix}.$$

The augmented states of the subsystems are

$$\xi_1 = x_1, \quad \xi_2 = \begin{bmatrix} x_1 & x_2 & x_3 \end{bmatrix}^\top, \quad \xi_3 = \begin{bmatrix} x_1 & x_4 \end{bmatrix}^\top,$$

and the mapping V is given by

$$V = \begin{bmatrix} V_1^\top & V_2^\top & V_3^\top \end{bmatrix}^\top,$$

with

$$V_1 = \begin{bmatrix} 1 & 0 & 0 & 0 \end{bmatrix}, \quad V_2 = \begin{bmatrix} I_3 & 0_{3\times 1} \end{bmatrix}, \quad V_3 = \begin{bmatrix} 1 & 0 & 0 & 0 \\ 0 & 0 & 0 & 1 \end{bmatrix}.$$

The augmented controller gains have the structure $C^{K^d}_{\xi} = \operatorname{diag}_{i=1}^{3}\left(C^{K^d}_{\xi i}\right)$ with $C^{K^d}_{\xi i} \in \mathbb{R}^{n_{ui}\times n_{\xi i}}$ and D^K is chosen to be zero, i.e., $D^K = 0$. The objective is to find a minimal communication topology of measurements, which means that an interconnected structure in B^K_ξ is introduced.

To find all FMs, the ranks of matrices $\tilde{M}_{\lambda,S_1,S_2}$, given in Lemma 8.1, are checked for all partitions S_1 of uncontrollable and S_2 of unobservable channels for $\lambda \in \{0.25, 1.5, 4\}$. For $\lambda = 1.5$, two rank-deficient cases of rank-deficiencies $d_1 = d_2 = 1$ are found. The corresponding partitions are $S_{1,1} = \{1, 3\}$, $S_{2,1} = \{2\}$ and $S_{1,2} = \{1\}$, $S_{2,2} = \{2, 3\}$. Thus, $\lambda = 1.5$ is an unstable FM and $R = 2$. To remove the FM $\lambda = 1.5$, Algorithm 8.2 is used to find a minimal communication link set of measurements, which is guaranteed to exist as the condition in Corollary 8.1 a) holds. Figure 8.1 illustrates the search tree. Starting from the root with $T^{n=1} = \varnothing$ and $\mathcal{E}^{n=1} = \mathcal{E}_{\text{full}} = \{(1,2),(1,3),(2,1),(2,3),(3,1),(3,2)\}$, each link $(i,j) \in \mathcal{E}^{n=1}$ is tested separately for whether $g(T^{n+}) > g(T^n)$ holds. If so, a child is created, as in Figure 8.1 for $(2,1)$, $(2,3)$ and $(3,1)$. Otherwise, the link is removed from the search set of the children. As $(2,1)$ removes both rank-deficiencies, it is the optimal solution of (8.17). In this simple example, as $d_1 = d_2 = 1$, the same number of nodes is checked for both the search tree algorithm and the greedy algorithm, and the greedy algorithm also finds the optimum. However, the procedure of cutting links by exploiting submodularity is illustrated.

8.5 Conclusions

We have shown how FMs within the overlapping framework introduced in Chapter 7 can be identified. The communication of both measurements and controller states is

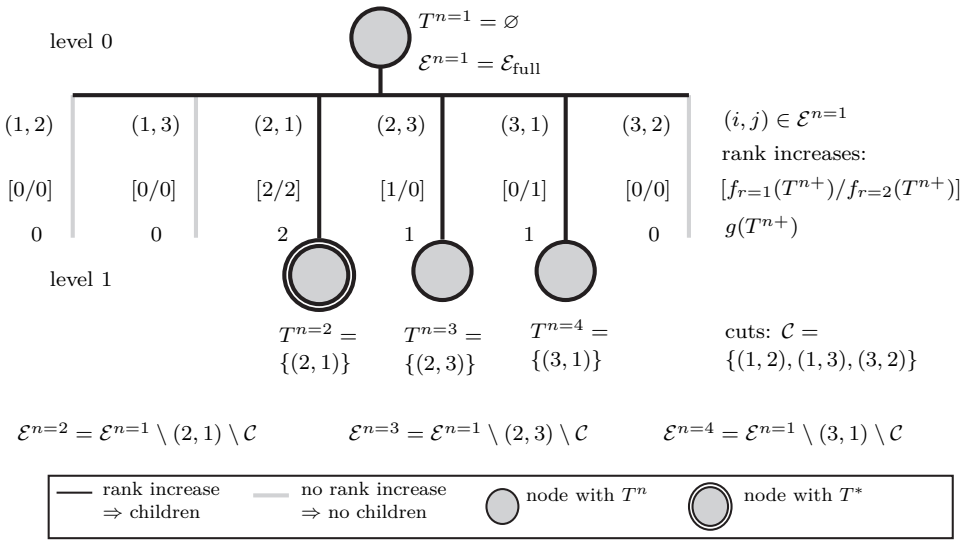

Figure 8.1: Search tree to remove $d_{r=1} = 1$ and $d_{r=2} = 1$.

considered, and the existence of a communication topology to remove all FMs has been proved. The objective of finding the minimal communication topology to remove all FMs is formulated as a minimum cost coverage problem with constraints that were shown to be submodular. Therefore, a polynomial-time greedy algorithm that has a guaranteed suboptimality bound is applicable. An alternative algorithm, based on a tree search with efficient cuts, which finds the minimal communication link sets, can be used. Although we used overlapping state space representations, the results can be transferred to systems with non-overlapping structures.

Part III

Control of an Architectural Cable Net Geometry

CHAPTER 9

Introduction to Cable Net Formwork

This part of the thesis presents methods for controlling the form of a tensioned cable net structure. These cable net structures can be used as components in a flexible formwork for the construction of lightweight building elements, such as thin concrete shells, and enable efficient construction. Controlling the form of the cable net is required in order to precisely achieve the desired design which guarantees to satisfy the mechanical stability and other important mechanical properties of the shell structures. Thus, the control enables the use of the cable net based formwork in construction.

9.1 Flexible Formwork in Construction

Doubly-curved thin concrete shells can be designed with a high stiffness and structural stability due to their curvatures [122]. Therefore, shell elements can span large areas using comparatively little material [123]. Through requiring less concrete, a significant amount of energy can be saved compared to conventional building structures. In addition to their structural advantages, shells are also interesting from an architectural point of view as their doubly-curved form enables new design concepts and aesthetic expression in buildings [124].

9.1.1 Cable Net Based Formwork

In the construction process of thin concrete shells a formwork is needed as a supporting structure on which to pour or spray the concrete. Conventional formwork is very labor-, material- and time-intensive, as it consists of a large number of non-reusable customized timber elements. Examples of traditional shell construction processes are illustrated in Figure 9.1.

To overcome these drawbacks of traditional construction, a flexible formwork, which consists of a net of cables or rods and a fabric layer on top, can be used [123], [125] . The tension forces and the weight of both the net and the concrete are supported by a rigid frame at the boundaries of the net. This new kind of formwork is beneficial in many

(a) Chapel Lomas de Cuernavaca, Mexico, Felix Candela, 1959

(b) Rolex Learning Center, EPFL, Switzerland, SANAA, 2010

Figure 9.1: Traditional formwork for concrete shell construction.

aspects. Through the standardization and recycling of elements, the amount of material required and the waste are reduced. Furthermore, the construction of the formwork is faster and less expensive than traditional formwork, which may enable the construction of more lightweight structures in the future. An example of the cable net based formwork is shown in Figure 9.2.

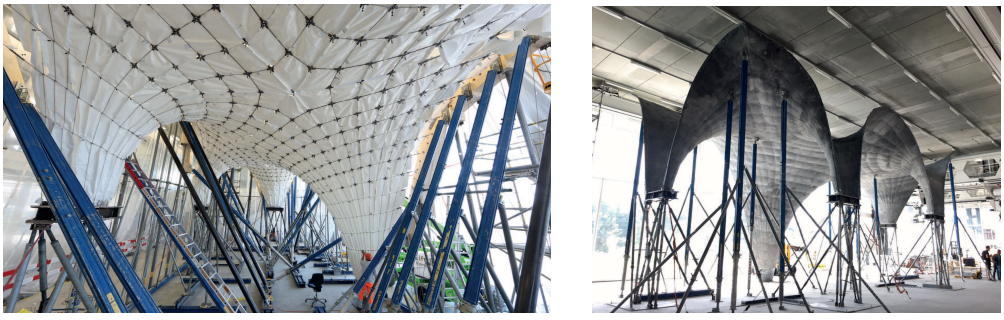

Figure 9.2: Prototype HiLo-Roof, Block Research Group, ETH, 2017.

Figure 9.3: HiLo roof on top of the NEST building [126] .

9.1.2 HiLo Research and Innovation Unit for NEST

A motivating application for the research presented in this part of the thesis is given by the shell roof which is planned for the so-called HiLo (High performance, low energy) Research and Innovation Unit. It is an ultra-lightweight thin concrete shell which will be built on a demonstrator building called NEST (Next Evolution in Sustainable Building Technologies), on the EMPA campus in Dübendorf, Switzerland [126], [127]. For its construction, a flexible formwork will be used. Figure 9.3 depicts the planned HiLo roof on the NEST building.

9.1.3 Shell Design and Construction

The design process of the shell comprises several steps. A detailed description can be found in [125], [128], [129] . First, the form of the shell is designed, taking into account multiple criteria such as boundary conditions, head clearance, aesthetic and design aspects, buckling stability and other mechanical properties. Then the cable net topology is chosen and mapped onto the designed surface of the shell. Via an optimization, the desired force distribution of the cable net loaded by the concrete is obtained [128]. This is called the form finding problem and will be explained in more detail in Section 9.2.2. From this final desired state of the tensioned and loaded cable net, the initial state of the unloaded pre-stressed cable net, i.e., without the concrete, can be calculated. This initial state is referred to as the target form in the cable net construction.

The building process starts with the assembly of the cable net on-site. The net is then tightened to a pre-stressed state. If traditional methods were to be used, the cable net construction would be finished after this pre-stressing step. Then, the fabric membrane is laid on top of the pre-stressed form of the cable net, and the concrete is sprayed on top. However, because of uncertainties in the material behavior and fabrication tolerances of

the cable net and frame, model mismatch occurs and the desired pre-stressed form of the cable net is in general not precisely achieved using typical construction methods. This has been demonstrated in [129] in an experiment for a small-scale simple shell prototype. Therefore, control of the cable net form is required.

In this work, a feedback loop to minimize the deviations from the desired form of the cable net is proposed. It is based on measurements of the nodal position coordinates of the cable net representing its form, and adjustments of the cable lengths of the boundary edges.

9.1.4 Challenges and Open Problems

The structural properties of the concrete shell depend critically on its form. Deviations from the optimized form can lead to instabilities, buckling behavior, or reduced stability under loads. Furthermore, in some construction applications, it may be desired to have high accuracy in specific areas of the structure that connect to other building elements, for example a glass window underneath a shell roof. To satisfy the accuracy requirements of the shell, the tolerances in the cable net form are very tight.

Due to the flexibility of the cable net and the possibly large fabrication and construction errors, the built form of the cable net is likely to deviate from the nominal design. Therefore, it must be adjusted to get closer to the designed form. Because of model mismatch, an approach purely based on a nominal model is not satisfactory. Time-invariant dynamic or static control of the cable net form could potentially be applied. However, this would in general involve a large number of measurement iterations and cable lengths adjustments, which are time-consuming to implement on the construction site.

In the form finding problem, the lengths and forces of all cables are free variables. A linearizing variable substitution can be applied to follow the linear force density method that results in a linear optimization problem [130]. In contrast, for the control problem, only the lengths of the boundary edges are free variables, the system is highly underactuated, and the linear force density method is not applicable.

9.2 Related Work

This section provides an overview of the state-of-the-art methods related to the topics of Part III. A literature review on modeling and control of cable net structures as a special class of tensegrity structures is provided. This overview is not exhaustive but sets the contributions of this part of the thesis into context with related literature.

9.2.1 Tensegrity Structures

The cable net formwork belongs to the class of so-called tensegrity structures, which is an active field of research [131]–[135]. Prominent early examples of tensegrity structures are the pre-stressed cable net structure for the roof of the Olympic Games facilities in Munich in 1972 [136] and the cable dome constructions for the Korean Olympic Games in 1986 [137].

Tensegrity structures are pin-jointed networks of cables, bars or struts, which can support tension forces, compression forces, or both, respectively. Tensegrity structures can be modeled by an underlying graph which encodes the connectivity of the network. Relevant questions that have been explored in [138]–[141], are related to equilibrium configurations, structural stability, rigidity and deployability of tensegrity structures. Static equilibrium configurations result from force balances. This has been presented in the seminal work of [130] and has extensively been applied in later works [142], [143]. In the early work of [144] a so-called spider web is analyzed. It is a cable net, and thus belongs to a special class of tensegrity structures. Energy arguments are used to make conclusions about its rigidity. In more recent work, energy minimization approaches have been proposed to find equilibrium configurations [145], [146].

9.2.2 Form Finding Problem

The so-called form finding problem is the problem of designing the cable net parameters in terms of unstressed edge lengths given the topology and the desired form of the net structure, possibly considering self-stress and loads. An overview of form finding methods is provided in [147], [148]. In the work of [130], the linear force density method, based on force equilibrium equations, is introduced. A linearizing variable substitution renders the problem linear in the force densities. Other form finding methods are based on solving the nonlinear equations. An example is the so-called dynamic relaxation which is an iterative algorithm based on virtual movements in the structure [149].

9.2.3 Control of Tensegrity Structures

Different applications of the lightweight, and possibly deployable, tensegrity structures have been investigated in the fields of aerospace, biology, architecture or robotics. In [150], [151], the topic of shape change, such as deployment, of tensegrity structures is addressed. Feedforward reference trajectories as sequences of quasi-static equilibrium configurations are designed. As no model uncertainties are considered, the designed reference states along the trajectory are feasible, and feedback is not needed for the control of the static state configuration. In [150] feedback is only used to attenuate vibrations of the structure during the deployment process. In [152], [153], open-loop quasi-static

trajectories of admissible static equilibrium configurations are designed for the reconfiguration of tensegrity structures. Again, no model uncertainties are accounted for. Using a dynamical model, the authors in [154] design a passivity-based closed-loop control law that depends on the coordinate position error. The initial and desired configurations are assumed to be feasible equilibrium configurations. In [155], uncertainties in actuated model parameters are considered.

Because of their low mass and high flexibility, tensegrity elements have also been used in robotics, see e.g., [156]–[158], and references therein. In [157], the linear force density method [130] can be used to compute an open-loop trajectory of quasi-static equilibria configurations for locomotion because all cables are actuated. Full actuatability of all cables, allowing for a transformation of the model to affine control inputs, is also assumed in [141]. In [159], knowledge about the rigidity of tensegrity structures is exploited for the application of multi-agent formation control. By assigning a virtual rigid tensegrity network to the formation, distributed controllers can be derived from the forces of the virtual stress matrix and stabilize the formation.

9.3 Scope of Part III

This part of the thesis presents a feedback-based construction method which iteratively brings the form of the cable net to within a prescribed tolerance of the target configuration. The focus lies on sparse inputs and an efficient method that requires few measurement and control iterations.

9.3.1 Precision Form Control

The form of the cable net is characterized by its nodal position coordinates. The terms of form, shape or configuration will be used synonymously in the following. Precision in the form of the cable net is crucial for the mechanical properties of the shell. Therefore, the goal of the proposed control algorithm is to minimize the error of the static cable net configuration with respect to the desired form in the presence of mismatch in the model and uncertainty in the boundary conditions. The free variables available as control inputs are the unstressed lengths or tensions of the cables at the boundary of the net.

As only the boundary edge lengths are free variables, the linear force density method is not applicable. Therefore, nonlinear optimization techniques are invoked. We derive a control problem formulation that allows for penalization of deviations in the x, y and z-coordinates of each node of the cable net. This is useful in construction applications, for example, in order to fit other building elements in specific places in proximity of the structure.

9.3.2 Minimum Number of Control Iterations

The control iterations on the construction site involve manual processes of measuring a potentially large number of nodal positions and adjusting a large number of cable edge lengths at the boundary of the net. The measurements and actuation are therefore time-consuming and expensive, and the required number of iterations is to be minimized. We therefore propose a two-step model-based control method, where 1) the model is re-identified in each iteration, and 2) a new control input is computed and applied. We propose an algorithm to identify important uncertain parameters of the cable net based on the updated set of measurements. The remeasuring also takes care of unmodeled changes in the boundary conditions. The measured data and the model knowledge are thus combined for efficient identification and control of the cable net. The iterations are stopped when the cable net reaches the desired tolerance or no further improvement is possible. A diagram of this control structure is given in Figure 9.4.

9.3.3 Efficient Control Input Computations with Guaranteed Feasibility

For a fixed identified model from step 1) in Figure 9.4, an efficient algorithm for the control input calculation in step 2) is presented. In particular, a sequential quadratic programming (SQP) variant is proposed to solve a reformulation of the form optimization problem, which is a non-convex constrained optimization problem. In each SQP iteration, a descent direction for the reformulated problem is efficiently computed by solving a quadratic program (QP). A line search over feasible points along this descent direction is performed. The feasible points are computed by solving second-order cone programs (SOCP). The resulting feasible SQP iterates prevent the algorithm from converging to a stationary point of local infeasibility, which is a common issue for other nonlinear solvers. We prove that the SQP algorithm on the reformulated optimization problem generates iterates that are equal to the ones of a Gauss-Newton iteration on the original problem, for which convergence is proved.

9.3.4 Sparse Actuation and Experimental Validation

To compute sparse actuation, we introduce an extension to the control input calculation, which is based on an iterative reweighting scheme of the l_1-norm of the input vector. This is practically relevant in applications where the actuation is not automated and therefore time-consuming. Our experimental prototype provides such an example where manual adjustments of a potentially large number of cable lengths are required.

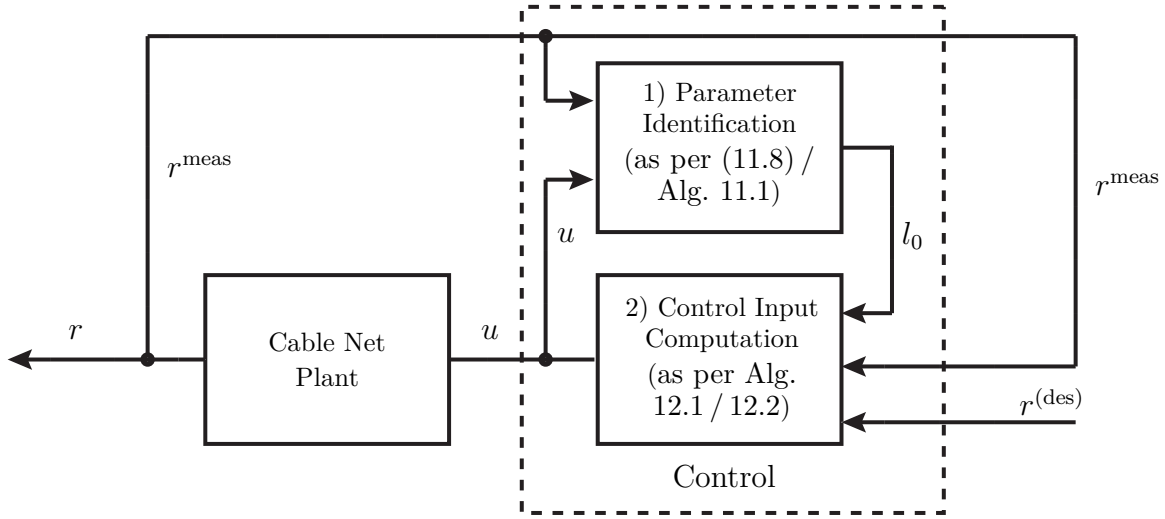

Figure 9.4: Illustration of the closed loop control structure for the cable net reconfiguration.

9.4 Summary of the Contributions of Part III

The contributions of Part III are summarized as follows.

1. We present two approaches to characterize the static equilibrium of the cable net structure. One is based on force balances and characterizes the equilibrium point through nonlinear implicit equations. The other one is an energy minimization approach which can be formulated as a second-order cone program for a fixed input vector. The advantages of both models are combined in an efficient control algorithm.

2. We propose a control loop that consists of iterations of 1) re-identifying the parameters of the cable net based on the updated set of measurements, and 2) computing and applying new control inputs to the plant.

3. For step 1) of the control loop, methods based on the force balance model and at least two form measurements are proposed for the identification of important uncertain parameters of the cable net. A parameter identification method based on distributed optimization achieves good results for large-scale structures and when measurement noise is present.

4. For step 2) of the control loop, we present an efficient control input calculation for minimizing the form error of the cable net. As the original form optimization problem is intractable, we present a tractable reformulation, which is a constrained non-convex optimization problem. To solve the reformulated problem, we propose

an SQP variant with feasible iterates, which is equivalent to a Gauss-Newton iteration on the original problem. The feasible iterates are efficiently computed by convex programming based on the energy minimization model. We prove that the iterates of the proposed algorithm converge to a stationary point of the original optimization problem.

5. An extension for sparse input computation based on an l_1-norm regularization term in the cost is proposed for efficient actuation in practice.

6. The proposed methods are validated in experiments on a quarter-scale cable net system prototype of a doubly-curved roof shell.

9.5 Outline of Part III of the Thesis

This part of the thesis is structured as follows. Chapter 10 is dedicated to the modeling of the cable net structure. A force based and an energy based modeling approach are presented. Chapter 11 presents methods for the identification of important model parameters of the cable net. In Chapter 12, the control input calculation based on an SQP variant is introduced and an extension for sparse input calculation is proposed. An experimental validation of the presented methods on a cable net system prototype are presented in Chapter 13. Section 14.2 in Part IV provides conclusions and an outlook related to Part III.

CHAPTER 10

Model of the Cable Net System

This chapter presents the mathematical description of the cable net. We will use tools from graph theory to describe the topology of the net. In order to express the form of the cable net in terms of the states, parameters and inputs, two modeling approaches of the static equilibria of the cable net are presented: One is based on force balance equations and the other one is based on an energy minimization. Both of these approaches will be combined in Chapter 12 to derive an efficient algorithm to compute control inputs.

This chapter is structured as follows. Sections 10.1 and 10.2 introduce a graph-theoretical description of the cable net and define the states, parameters and inputs. Section 10.3 presents some assumptions on the cable net system. The models of the static equilibrium configurations, based on force balances and on energy minimization, are presented in Sections 10.4 and 10.5, respectively, before Section 10.6 concludes the chapter.

10.1 Graph-Theoretical Description

The cable net is associated with an underlying graph $\mathcal{G} = (\mathcal{N}, \mathcal{E})$. Its n nodes in the node set $\mathcal{N}$ represent the connection points of the cable net, and its m edges in the edge set $\mathcal{E} \subseteq \mathcal{N} \times \mathcal{N}$ correspond to the cable segments of the net. The node set is divided into the two disjoint subsets, $\mathcal{N}_I$ of n_I nodes that lie in the interior of the cable net, and $\mathcal{N}_B$ of n_B boundary nodes that are attached to the rigid frame. The edge set is composed of the two disjoint sets $\mathcal{E}_I$ of m_I interior edges between interior nodes, and $\mathcal{E}_B$ of m_B boundary edges which connect the boundary nodes on the rigid frame to interior nodes in the interior of the net. It holds that $\mathcal{N} = \mathcal{N}_I \cup \mathcal{N}_B$, $\mathcal{N}_I \cap \mathcal{N}_B = \varnothing$ and $\mathcal{E} = \mathcal{E}_I \cup \mathcal{E}_B$, $\mathcal{E}_I \cap \mathcal{E}_B = \varnothing$. By a slight abuse of notation, we use both the edge set and an index set for the edges, i.e., the index $e \in \{1, ..., m\}$ or equivalently the index $(s, t) \in \mathcal{E}$ denotes the edge e connecting nodes s and t. A top view of the cable net is depicted in Figure 10.1 with the interior nodes s_a and t_a connected by the interior edge (s_a, t_a) and with the interior node s_b connected by the boundary edge (s_b, t_b) to the boundary node t_b.

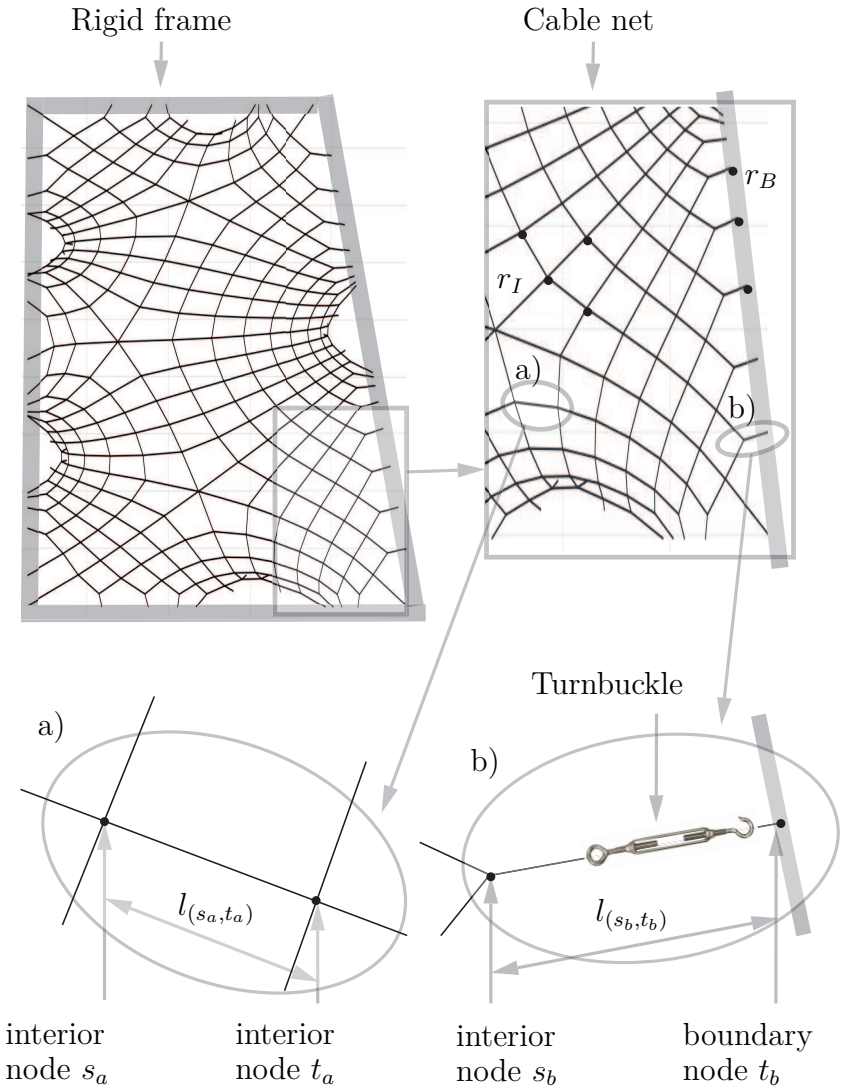

Figure 10.1: Top view of the cable net system. a) Interior edge $(s_a, t_a) \in \mathcal{E}_I$ connecting nodes $s_a \in \mathcal{N}_I$ and $t_a \in \mathcal{N}_I$ with edge length $l_{(s_a,t_a)}$. b) Boundary edge $(s_b, t_b) \in \mathcal{E}_B$ with edge length $l_{(s_b,t_b)}$ connecting the interior node $s_b \in \mathcal{N}_I$ and the boundary node $t_b \in \mathcal{N}_B$.

In order to describe the topology of the net, we will use the incidence matrix $M \in \mathbb{R}^{m\times n}$, which is defined as

$$[M]_{(s,t),\,s} := \begin{cases} 1\,, & \text{if edge } (s,t) \text{ is starting at node } s\,, \\ -1\,, & \text{if edge } (s,t) \text{ is ending at node } s\,, \\ 0\,, & \text{if edge } (s,t) \text{ is not connected to node } s\,. \end{cases} \tag{10.1}$$

For later use, we arrange the columns of M to

$$M := [M_I, M_B]\,, \tag{10.2}$$

such that the first part, $M_I \in \mathbb{R}^{m\times n_I}$, describes the topology of the interior edges and the second part, $M_B \in \mathbb{R}^{m\times n_B}$, the one of the boundary edges.

10.2 States, Parameters and Inputs

The geometric form of the net is described by the states, which are the position coordinates of the cable net nodes, defined as

$$x = [x_I^\top\,, x_B^\top]^\top\,, \quad y = [y_I^\top\,, y_B^\top]^\top\,, \quad z = [z_I^\top\,, z_B^\top]^\top \ \in \mathbb{R}^n\,, \tag{10.3}$$

where the subscripts distinguish between the interior and boundary nodes. For individual nodes, $s \in \{1, ..., n\}$, we define the vector of their coordinates as

$$r_s = [x_s\,,\, y_s\,,\, z_s]^\top \in \mathbb{R}^3.$$

We also define the stacked vectors of the coordinates of all interior, all boundary and the collection of all the nodes as

$$r_I = [r_1^\top\,, \ldots\,, r_{n_I}^\top]^\top, \quad r_B = [r_{n_I+1}^\top\,, \ldots\,, r_n^\top]^\top \text{ and } r = [r_I^\top\,, r_B^\top]^\top.$$

The term configuration is used as a synonym for the form or shape of the cable net defined through the nodal position coordinates. The actual length of an edge (s,t) is denoted by $l_{(s,t)}$ and is given by the Euclidean distance between the two nodes, given as

$$l_{(s,t)} := \|r_s - r_t\|_2. \tag{10.4}$$

The materials and dimensions of the edges in the cable net are described by the following fixed parameters. The Young's modulus E indicates the relation between stress and strain in the material. The constant $EA_{(s,t)}$ is used to denote the product of the Young's modulus E and the cross section area A of the edge (s,t) and defines its elastic properties. Other important parameters of the system influencing the forces within the net are the unstressed lengths of the edges, which are denoted by

$$l_0 = \left[l_{0,1}, ..., l_{0,(s,t)}, ..., l_{0,m}\right]^\top \in \mathbb{R}^m, \tag{10.5}$$

with $l_{0,(s,t)}$ the parameter of the edge (s,t). In the interior of the net, these parameters are fixed and cannot be changed once the cable net has been constructed. The boundary edges connect the cable net to the rigid frame via turnbuckles, as can be seen in Figure 10.1. These turnbuckles can introduce a defined change in the unstressed length of the boundary edges, which are used as inputs to the system in order to control the form. The possible input vector is thus defined as the vector collecting all the changes in unstressed lengths for all boundary edges

$$u := [u_1\,,\,\ldots\,,\,u_{(s,t)}\,,\,\ldots\,,\,u_{m_B}]^\top \in \mathbb{R}^{m_B}, \quad \forall (s,t) \in \mathcal{E}_B, \tag{10.6}$$

with $u_{(s,t)}$ being the change in unstressed length $l_{0,(s,t)}$ for the boundary edge (s,t). Here, the assumption is made that the turnbuckles are not elastic. The unstressed length of edge (s,t) after applying the input $u_{(s,t)}$ is defined as

$$\overline{l}_{0,(s,t)} = l_{0,(s,t)} - u_{(s,t)}\,,\ \forall (s,t) \in \mathcal{E}_B. \tag{10.7}$$

We also use the notation

$$\overline{l}_{0,(s,t)} = l_{0,(s,t)}\,,\ \forall (s,t) \in \mathcal{E}_I, \tag{10.8}$$

if (s,t) is a non-adjustable interior edge. In Figure 10.1, the interior edge (s_a,t_a) is of constant unstressed length $\overline{l}_{0,(s_a,t_a)} = l_{0,(s_a,t_a)}$, and the boundary edge (s_b,t_b) is of adjustable unstressed length $\overline{l}_{0,(s_b,t_b)} = l_{0,(s_b,t_b)} - u_{(s_b,t_b)}$, with possible $u_{(s_b,t_b)} \neq 0$. With (10.4) and (10.7), (10.8), the actual elongation of the edge (s,t) is given by

$$\Delta l_{(s,t)} = l_{(s,t)} - \overline{l}_{0,(s,t)}\,. \tag{10.9}$$

Configurations that have no slack cables avoid sagging of the concrete and are preferred. This means that the edges of the cable net are desired to be in zero or positive tension. Therefore, the following constraints can be introduced

$$g_{(s,t)}(r_I, r_B, u) := -\Delta l_{(s,t)} \leq 0\,, \quad \forall (s,t) \in \mathcal{E}. \tag{10.10}$$

We summarize these constraints for all edges in the vector

$$g(r_I, r_B, u) := [g_1, ..., g_m]^\top\,. \tag{10.11}$$

However, there may be slack cables in the net because of construction imprecision. These slack edges may or may not be removable by the control, depending on the parameters of the edges. In other words, there may or may not exist a configuration with no slack edges for the given parameters. Depending on the construction, there might be physical limitations on the possible change in the unstressed lengths of the boundary edges. Then, input constraints in the form of

$$\begin{aligned} u &\leq u_{ub}, \\ -u &\leq -u_{lb}, \end{aligned} \tag{10.12}$$

need to be introduced, with $u_{ub} \in \mathbb{R}^{m_B}$ and $u_{lb} \in \mathbb{R}^{m_B}$ being upper and lower bounds on the possible inputs, respectively.

10.3 Assumptions on the Cable Net System

The cable net is a pre-stressed, pin-jointed structure consisting of only cables and no rigid elements. The boundary edges of the net are attached to a rigid frame. This kind of tensegrity structure [141], [142], was introduced as a spider-web in [138]. In the model-based control of the cable-net form, static equilibrium configurations are considered. In order to model these equilibrium configurations, we define the reduced graph $\bar{\mathcal{G}}$ generated by removing all slack edges. Thus, the graph $\bar{\mathcal{G}}$ is defined as $\bar{\mathcal{G}} = \{\mathcal{N}, \bar{\mathcal{E}}\}$ with $\bar{\mathcal{E}}$ being the set of all tensioned edges of the cable net. Here, it is assumed that nodes that have only slack adjacent edges have already been removed from the node set $\mathcal{N}$. A further assumption is that the cable net is designed in such a way that $\bar{\mathcal{G}}$ does not contain 2-cycles or self-loops. Moreover, no interior node is connected to more than three boundary nodes, and if there is more than one boundary edge connected to the same interior node, then the directions of this set of boundary edges are linearly independent.

We assume that $\bar{\mathcal{G}}$ is known and that it stays constant for the series of equilibrium configurations considered during the control, i.e., cables do not change from being slack to being tensioned or vice versa. In the design phase, the desired force distribution in the cable net is designed in such a way that all cables are in positive tension. In practice, checking these conditions in the real system can be done by force measurements, by manual examination, or by measuring whether the actual edge lengths, l, are longer in the pre-stressed state than the initial edge lengths, l_0.

Furthermore, we assume that the material parameters, EA, and the self-weight of the net are known and are constant. The unstressed lengths of the edges, l_0, are identified and thus updated within each iteration of the control algorithm as in Figure 9.4. The coordinates of the boundary nodes at the rigid frame are measured and updated in each iteration of the control algorithm. This feedback is important since the frame is not perfectly rigid and thus introduces uncertainties on the boundary conditions.

10.4 Force Balance Equations

A static equilibrium of the cable net can be characterized by a state where all net forces are zero. This concept is introduced in the following.

10.4.1 Nonlinear Elastic Force Balance Equations

The net force at each interior node s is the sum over the tension forces of all its adjacent edges $(s,t) \in \bar{\mathcal{E}}_s$, where we denote by $\bar{\mathcal{E}}_s$ the set of all adjacent edges of node s which are

in tension, i.e., $\forall(s,t)$, such that $\Delta l_{(s,t)} \geq 0$. Thus, the net force at node s is given by

$$\begin{aligned} h_s &= \sum_{(s,t)\in\bar{\mathcal{E}}_s} EA_{(s,t)} \left(\frac{l_{(s,t)} - \overline{l}_{0,(s,t)}}{\overline{l}_{0,(s,t)}} \right) d_{(s,t)} - p_s \\ &= \sum_{(s,t)\in\bar{\mathcal{E}}_s} EA_{(s,t)} l_{(s,t)} \left(\frac{1}{\overline{l}_{0,(s,t)}} - \frac{1}{l_{(s,t)}} \right) d_{(s,t)} - p_s \\ &= \sum_{(s,t)\in\bar{\mathcal{E}}_s} EA_{(s,t)} \left(r_s - r_t \right) \left(\frac{1}{\overline{l}_{0,(s,t)}} - \frac{1}{l_{(s,t)}} \right) - p_s, \end{aligned} \tag{10.13}$$

where $d_{(s,t)} = (r_s - r_t)/l_{(s,t)}$ is the direction vector of the edge (s,t) along which the corresponding force is acting, and $p_s = \begin{bmatrix} p_{s,x} & p_{s,y} & p_{s,z} \end{bmatrix}^\top$ accounts for external point loads in x-, y- and z-directions at the interior node $s \in \mathcal{N}_I$.

For a fixed input vector u, the static equilibrium of the cable net can be characterized by the configuration r_I for which all the net forces at all interior nodes are zero, i.e., which is the solution of the equations

$$h_s = \sum_{(s,t)\in\bar{\mathcal{E}}_s} EA_{(s,t)} \left(\begin{bmatrix} x_s \\ y_s \\ z_s \end{bmatrix} - \begin{bmatrix} x_t \\ y_t \\ z_t \end{bmatrix} \right) \left(\frac{1}{\overline{l}_{0,(s,t)}} - \frac{1}{l_{(s,t)}} \right) - \begin{bmatrix} p_{s,x} \\ p_{s,y} \\ p_{s,z} \end{bmatrix} = 0, \quad \forall s \in \mathcal{N}_I. \tag{10.14}$$

If no external forces are acting on the net, then $p_s = \begin{bmatrix} p_{s,x} & p_{s,y} & p_{s,z} \end{bmatrix}^\top = 0$. Note that summing the forces of only the tensioned adjacent edges in (10.14) prevents the accounting of the contribution of slack edges as compression forces.

The function $h : \mathbb{R}^{3n} \times \mathbb{R}^{m_B} \mapsto \mathbb{R}^{3n_I}$ is the vector of all force equilibrium equations for all interior nodes, i.e.,

$$h(r,u) = \begin{bmatrix} h_1^\top & \dots & h_{n_I}^\top \end{bmatrix}^\top. \tag{10.15}$$

For fixed boundary values, $r_B = \bar{r}_B$, the notation is simplified to $h : \mathbb{R}^{3n_I} \times \mathbb{R}^{m_B} \mapsto \mathbb{R}^{3n_I}$ with

$$h(r_I,u) = \begin{bmatrix} h_1^\top & \dots & h_{n_I}^\top \end{bmatrix}^\top. \tag{10.16}$$

10.4.2 Matrix Form of the Force Balance Equations

We will now formulate the set of force balance equations in (10.14) in a matrix form. This will be beneficial in the parameter identification in Section 11.2, because it allows for a linearizing variable substitution.

We define the vectors w_x, w_y and $w_z \in \mathbb{R}^m$ which contain the pairwise differences in position coordinates of all adjacent nodes, projected onto the x- , y- and z-directions,

respectively, i. e. , $w_x = Mx$, $w_y = My$, $w_z = Mz \in \mathbb{R}^m$. For later use, we define the diagonal matrices W_x , W_y and W_z, which contain the elements of these vectors, i. e. ,

$$W_x = \mathrm{diag}(w_x)\,,\ W_y = \mathrm{diag}(w_y)\,,\ W_z = \mathrm{diag}(w_z)\,. \tag{10.17}$$

After reordering and stacking the components of (10.14) into

$$h := [h_{1,x}, ...h_{n_I,x}, h_{1,y}, ...h_{n_I,y}, h_{1,z}, ...h_{n_I,z}]^\top \in \mathbb{R}^{3n_I},$$

and with the incidence matrix M in (10.1) in Section 10.1, we can formulate the force balance equations of (10.14) in the following matrix form

$$h = \begin{bmatrix} M_I^\top & 0 & 0 \\ 0 & M_I^\top & 0 \\ 0 & 0 & M_I^\top \end{bmatrix} \begin{bmatrix} W_x \\ W_y \\ W_z \end{bmatrix} EA \left(\overline{l}_{0,\mathrm{inv}} - l_{\mathrm{inv}}\right) - p = 0\,, \tag{10.18}$$

where the diagonal matrix $EA \in \mathbb{R}^{m\times m}$ contains the stiffness constants $EA_e \in \mathbb{R}$ for all edges, $e \in \mathcal{E}$, the vector $\overline{l}_{0,\mathrm{inv}}$ contains the inverses of the unstressed edge lengths after applying inputs, as in (10.7), i.e.,

$$\overline{l}_{0,\mathrm{inv}} := \begin{bmatrix} \frac{1}{l_{0,1}-u_1} & \cdots & \frac{1}{l_{0,m}-u_m} \end{bmatrix}^T \in \mathbb{R}^m \tag{10.19}$$

and l_{inv} contains the inverses of the actual edge lengths, l_e, as in (10.4), i.e.,

$$l_{\mathrm{inv}} := \begin{bmatrix} \frac{1}{l_1} & \dots & \frac{1}{l_m} \end{bmatrix}^T \in \mathbb{R}^m. \tag{10.20}$$

The vector p contains all external forces p_s on all interior nodes s. The diagonal matrix $EA \in \mathbb{R}^{m\times m}$ contains the material constants $EA_e \in \mathbb{R}$ for all edges, e.

We illustrate these definitions in the following example.

Example 10.1. Let us consider the following topology of $n_I = 1$ interior node, 1, and $n_B = 3$ boundary nodes, 2, 3 and 4, connected by the boundary edges $(1, 2)$, $(1, 3)$ and $(1, 4)$. The topology is depicted in Figure 10.2. In this example, we have $r_I = r_1 = [x_1, y_1, z_1]^\top$, $r_B = [r_2^\top, r_3^\top, r_4^\top]^\top = [x_2, ..., z_4]^\top$. The collected interior and boundary x-coordinates are given by $x_I = x_1$ and $x_B = [x_2, x_3, x_4]^\top$, and equivalently for y_I, y_B, z_I and z_B. The incidence matrix, M, and the vector of distances in x-direction between the connected nodes, w_x, e.g., are given by

$$w_x = \underbrace{\begin{bmatrix} 1 & -1 & 0 & 0 \\ 1 & 0 & -1 & 0 \\ 1 & 0 & 0 & -1 \end{bmatrix}}_{M} \underbrace{\begin{bmatrix} x_1 \\ x_2 \\ x_3 \\ x_4 \end{bmatrix}}_{x} = \begin{bmatrix} x_1 - x_2 \\ x_1 - x_3 \\ x_1 - x_4 \end{bmatrix}.$$

For this simple example topology, only one force balance (with x-, y- and z-components) can be formulated, as $n_I = 1$, i.e., $h = [h_{1,x}, h_{1,y}, h_{1,z}]^\top$. The set of neighboring nodes

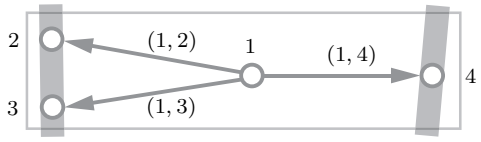

Figure 10.2: Example topology in 3D of one interior node 1 and three boundary nodes 2, 3 and 4, connected by three edges $(1,2)$, $(1,3)$ and $(1,4)$.

for node 1 is $\mathcal{N}_s = \{2,3,4\}$. Assuming that no external forces are acting on the interior node, i.e., $p_1 = 0$, the resulting force $h_{1,x}$ at node 1 is the sum of the three neighboring edge forces in x-direction and is given by

$$h_{1,x} = \underbrace{\begin{bmatrix}1\\1\\1\end{bmatrix}^\top}_{M_I^\top} \underbrace{\begin{bmatrix}x_1-x_2 & 0 & 0\\ 0 & x_1-x_3 & 0\\ 0 & 0 & x_1-x_4\end{bmatrix}}_{W_x} \underbrace{\begin{bmatrix}EA_{(1,2)}(\frac{1}{l_{0,(1,2)}-u_{(1,2)}}-\frac{1}{l_{(1,2)}})\\ EA_{(1,3)}(\frac{1}{l_{0,(1,3)}-u_{(1,3)}}-\frac{1}{l_{(1,3)}})\\ EA_{(1,4)}(\frac{1}{l_{0,(1,4)}-u_{(1,4)}}-\frac{1}{l_{(1,4)}})\end{bmatrix}}_{EA(\bar{l}_{0,\mathrm{inv}}-l_{\mathrm{inv}})} = 0.$$

Note that the topology is in 3D and that the linear independence assumption of the three boundary edges as stated in Section 10.3 must be satisfied.

10.4.3 Comparison to Linear Force Density Method

Given the desired shape of the shell in terms of x, y, and z coordinates, the design of the nominal cable net parameters l_0 is called the form-finding problem [130]. In this design problem, all the lengths l_0 and forces, $h_{(s,t)}$, of the edges of the net are free variables. This allows for the variable substitution $\rho_{(s,t)} := \frac{h_{(s,t)}}{l_{(s,t)}}$, where $\rho_{(s,t)}$ is the force density of the edge (s,t), [130]. With the elastic force in edge (s,t) being equal to

$$h_{(s,t)} = EA_{(s,t)}\frac{\Delta l_{0,(s,t)}}{l_{0,(s,t)}} = EA_{(s,t)}\frac{l_{(s,t)}-l_{0,(s,t)}}{l_{0,(s,t)}},$$

the force density of edge (s,t) is given as

$$\rho_{(s,t)} = \frac{EA_{(s,t)}}{l_{(s,t)}}\frac{l_{(s,t)}-l_{0,(s,t)}}{l_{0,(s,t)}}.$$

The matrix equation in 10.18 can be reformulated as

$$\begin{bmatrix}M_I^\top & 0 & 0\\ 0 & M_I^\top & 0\\ 0 & 0 & M_I^\top\end{bmatrix}\begin{bmatrix}W_x\\W_y\\W_z\end{bmatrix}\rho = \begin{bmatrix}p_x\\p_y\\p_z\end{bmatrix}, \tag{10.21}$$

where the vector of force densities $\rho \in \mathbb{R}^m$ is given as

$$\rho = EA\left(\bar{l}_{0,\mathrm{inv}} - l_{\mathrm{inv}}\right),$$

with the entries $\rho_{(s,t)}$ of all edges (s,t), i.e., $\rho = \text{concat}_{(s,t)\in\bar{\mathcal{E}}}\big(\rho_{(s,t)}\big)$. The equation in (10.21) is linear in the force densities ρ. For known (desired) coordinates x, y, z, (10.21) can be solved for the force densities ρ, and the parameters l_0 can be obtained from the definition of ρ with known lengths l.

Because in our cable-net application, the unstressed edge lengths in the interior of the net ($l_{0,e},\ \forall\ e \in \mathcal{E}_I$) are fixed, the corresponding force densities are not free variables, and therefore the linear force density approach is not applicable. We will, however, make use of the formulation in (10.18) in the identification problem in Section 11.2.

10.5 Energy Minimization

In order to find the static equilibrium of the system, an approach of minimizing its total energy can be taken. In the following, we assume that the elastic tension forces versus elongation functions of the edges are linear and increasing. Note that this can easily be generalized to piecewise linear and increasing functions. Under this assumption, for a given fixed vector of inputs u in (10.6) , this energy minimization problem is equivalent to a convex second-order cone program (SOCP), [16], [28].

The total energy of the cable net is expressed as

$$V(r,u) = -p_z z_I + \sum_{(s,t)\in\mathcal{E}} \frac{EA_{(s,t)}}{2\bar{l}_{0,(s,t)}}(l_{(s,t)} - \bar{l}_{0,(s,t)})^2, \tag{10.22}$$

which is the sum of the potential energies of all nodes (first term) and the sum of the elastic energies of all tensioned edges (second term). The vector p_z in (10.22) accounts for point loads due to self-weight and any other loads in z-direction such as the weight of the fabric and, if applicable, the concrete on all interior nodes. The problem of finding the equilibrium of the cable net can be solved by minimizing the total energy (10.22),

$$\begin{aligned} R(u) = \underset{r}{\text{argmin}}\ \ & V(r,u) \\ \text{s.t.}\quad & r_B = \overline{r}_B\,, \end{aligned} \tag{10.23}$$

where $\overline{r}_B$ are the fixed positions at the rigid frame where the boundary edges are connected. The function $R(u)$ denotes the mapping of the inputs u to the coordinates r. We will show in Section 12.2 that this function is well-defined and that it is equivalently defined by the implicit force balance equations $h(\cdot,u) = 0$ in (10.14). The function $R(u)$ is however not explicitly defined.

For a fixed input vector u, i.e. constant $\bar{l}_0$, it is possible to rewrite the problem given in (10.23) as a convex optimization problem. We introduce a variable v and vector q.

The entry $q_{(s,t)}$ of q for the edge (s,t) is defined as

$$q_{(s,t)} = \left(\frac{\sqrt{EA_{(s,t)}}}{\sqrt{\overline{l}_{0,(s,t)}}} \left(l_{(s,t)} - \overline{l}_{0,(s,t)} \right) \right)_+ , \tag{10.24}$$

with the notation $(\cdot)_+ = \max(0, \cdot)$. The upper bound v on the term $\|q\|_2^2$ satisfies the following hyperbolic constraint

$$\|q\|_2^2 \leq v \iff \left\| \begin{pmatrix} 2q \\ 1 - v \end{pmatrix} \right\|_2 \leq 1 + v.$$

Rewriting the problem in terms of the variables q and v, we find that the coordinates r_I of the interior nodes in a static equilibrium configuration can be obtained as the minimizers to the following SOCP.

Problem $\mathcal{P}_{\text{minE}}$:

$$\begin{aligned} \min_{r_I, v, q} \quad & -p_z z_I + \frac{1}{2} v \\ \text{s.t.} \quad & \frac{\sqrt{EA_{(s,t)}}}{\sqrt{\overline{l}_{0,(s,t)}}} \left(\|r_s - r_t\|_2 - \overline{l}_{0,(s,t)} \right) \leq q_{(s,t)}, \\ & 0 \leq q_{(s,t)}, \quad \forall\ (s,t) \in \mathcal{E}, \\ & r_B = \overline{r}_B, \\ & \left\| \begin{pmatrix} 2q \\ 1 - v \end{pmatrix} \right\|_2 \leq 1 + v\,, \end{aligned} \tag{10.25}$$

for a fixed input vector u, i.e. constant lengths $\overline{l}_{0,(s,t)}$.

Note that the definition of $q_{(s,t)}$ in (10.24) allows for only positive tension forces to contribute to the energy V of the system. This is consistent with the model assumption that in the case where $l_{(s,t)} < l_{0,(s,t)}$, the cable is not in compression, but it is a slack cable under zero force. However, the solution of Problem $\mathcal{P}_{\text{minE}}$ does not guarantee that there are no slack cables in the equilibrium state of the cable net.

10.6 Conclusions

We presented a mathematical description of the cable net system in terms of its inputs, parameters, states and the topology. Based on these definitions, two approaches can be used in order to formulate equilibrium points of the cable net. While the force balance approach results in implicit equations that are nonlinear in the states and inputs, the minimum energy approach is formulated as a second-order cone program for fixed inputs, which can be efficiently solved with convex programming. Both these properties will be exploited in Chapter 12 to formulate an efficient control algorithm. The force balance approach is furthermore used for parameter identification in Chapter 11.

CHAPTER 11

Parameter Identification

The stiffnesses, the forces and the form of the cable net are sensitive to the unstressed edge lengths. However, the unstressed lengths are likely to deviate from the nominal values of the design model, because they are subject to fabrication tolerances and uncertainties. In general, the cable net is constructed in its stressed state. Therefore, only the stressed lengths of the edges can be measured. Thus, the unstressed edge lengths represent the model parameters with the largest amount of uncertainty.

This chapter presents the first step in the iterations of the complete control algorithm, illustrated in Figure 9.4. This first step consists of the identification of the unstressed lengths of the cable net. In each iteration of the overall control algorithm, a new measurement is taken. Based on the updated measurement data, the model parameters are re-identified and the cable net model is updated. The updated model is then used in the second step of the iterations of the complete control algorithm, where a new control input is computed and applied to the system. We present two identification methods based on measurements of at least two different cable net configurations. The results presented in this chapter have been published in [17].

The chapter is structured as follows. Sections 11.2 and 11.3 present two parameter identification methods that are based on linear regression and distributed optimization, respectively. Section 11.4 provides simulation results for both methods and Section 11.5 concludes the chapter.

11.1 Problem Setting

For the identification of the parameters l_0, we assume that the material parameters, i.e., Young's modulus and the cross section, EA, of the edges, are known. In the experiment, the coordinates of the nodes will be measured by tacheometry and are assumed to be corrupted by normal distributed additive measurement noise, δ_I. We denote the noisy coordinate measurements by

$$\hat{r}_I := r_I + \delta_I \,. \tag{11.1}$$

The coordinates, r_I, belonging to one equilibrium configuration do not provide enough information to uniquely identify the parameters $l_{0,(s,t)}$. Therefore, we need to base the identification on the measurement of $p \geq 2$ different configurations. Different configurations of the cable net are obtained by changing the boundary edges by applying inputs u, as defined in (10.6). We use a superscript $(\cdot)^{(i)}$ to denote the variables related to the i-th configuration of the cable net. We define p inputs for p different configurations with $0 \neq u^{(i)} \neq u^{(j)} \neq 0$, $i, j \in \{2, ..., p\}$ and w. l. o. g. we choose $u^{(1)} = 0$. For later use, we define the index set $\mathcal{U}^{(i)}$, which collects all indices of $u^{(i)}$ being different from $u^{(1)}$, i.e., different from zero, as

$$\mathcal{U}^{(i)} = \bigcup \text{ indices } k, \text{ with } u_k^{(i)} \neq u_k^{(1)}, \text{ i.e., } u_k^{(i)} \neq 0. \tag{11.2}$$

We denote the resulting configurations by $r^{(i)}$, and it is assumed that $r^{(i)} \neq r^{(j)}$, $i \neq j$, $i, j \in \{1, ..., p\}$.

11.2 Linear Regression

In this section, we formulate a set of equations, which are linear in the inverses of the unstressed lengths of the edges. This allows for linear least squares regression, which performs well for precise measurements. However, it is not straightforward to exactly account for measurement noise on the nodal coordinates.

Problem Formulation

For the i-th configuration of the cable net, we define the matrices $W_x^{(i)}$, $W_y^{(i)}$ and $W_z^{(i)}$ as in (10.17), and the vectors $\overline{l}_{0,\text{inv}}^{(i)}$ and ${l_{\text{inv}}}^{(i)}$ are as defined in (10.19) and (10.20), respectively. We rewrite the force balance equations (10.18) for configuration i as

$$h^{(i)} = \underbrace{\left(I_3 \otimes \begin{pmatrix} M_I^\top & S_I^{(i)} \end{pmatrix}\right) \begin{bmatrix} W_x^{(i)} \\ W_y^{(i)} \\ W_z^{(i)} \end{bmatrix} EA\, C_I^{(i)}}_{=:\, T_I^{(i)} \in \mathbb{R}^{3n_I \times m}} \left(\overline{l}_{0,\text{inv}}^{(i)} - l_{\text{inv}}^{(i)}\right) = 0. \tag{11.3}$$

In (11.3), $S_I^{(i)}$ and $C_I^{(i)}$ are identities of appropriate sizes. In the following, we define $S_U^{(i)}$, $C_U^{(i)}$ and $S_0^{(i)}$, $C_0^{(i)}$ as selection matrices to obtain the matrices $T_U^{(i)}$ and $T_0^{(i)}$, equivalently to $T_I^{(i)}$ in (11.3).

There are m unknown unstressed lengths $l_{0,1}$, ..., $l_{0,m}$ to be identified, and there are $3n_I$ equations for each configuration of the cable net with $3n_I > m$. However, the resulting system of equations (11.3) for one single configuration has infinitely many solutions, as the incidence matrix M, and therefore $T_I^{(i)}$, is rank-deficient. Even in the noise-free case, one configuration does not give enough information to determine

the parameters $l_{0,e}$. In the following, we will use bold symbols to denote vectors and matrices containing information about the different configurations, $1, \dots, p$. In order to formulate the right-hand side of the force balance equations, we define

$$\mathbf{l}_{\text{inv}} := \left[l_{\text{inv}}^{(1)\top}, \dots, l_{\text{inv}}^{(p)\top} \right]^\top \in \mathbb{R}^{pm}, \tag{11.4}$$

$$\mathbf{T}_I := \begin{bmatrix} T_I^{(1)} & & 0 \\ & \ddots & \\ 0 & & T_I^{(p)} \end{bmatrix}. \tag{11.5}$$

In the following, we bring the force balance equations into a linear regression form, where the parameter vector contains the inverses of the unstressed edge lengths. We define

$$\bar{\mathbf{l}}_{0,\text{inv}} := \left[l_{0,\text{inv}}^\top, (\bar{l}_{0,\text{inv}}^{(2)} C_U^{(2)})^\top, \dots, (\bar{l}_{0,\text{inv}}^{(p)} C_U^{(p)})^\top \right]^\top, \tag{11.6}$$

with

$$l_{0,\text{inv}} := \left[\tfrac{1}{l_{0,1}}, \dots, \tfrac{1}{l_{0,m}} \right]^\top,$$

and where the selection matrix $C_U^{(i)}$ consists of the unit vectors e_k for all $k \in \mathcal{U}^{(i)}$, with $\mathcal{U}^{(i)}$ as defined in (11.2), i. e.,

$$C_U^{(i)} := [e_{k_1}, e_{k_2}, \dots], \text{ with } k_1 < k_2 < \dots \in \mathcal{U}^{(i)}. \tag{11.7}$$

The vector $\bar{l}_{0,\text{inv}}^{(i)} C_U^{(i)}$ thus collects all unstressed edge lengths of configuration i, with $i \in \{2, \dots, p\}$, which are different from those in configuration 1 because of the applied inputs $u^{(i)} \neq 0$. The linear regression problem for the identification of $\bar{\mathbf{l}}_{0,\text{inv}}$ is then given by

$$Y\, \bar{\mathbf{l}}_{0,\text{inv}} = b. \tag{11.8}$$

In (11.8), Y and b are referred to as the observation matrix and the measurement vector, and are given by

$$\begin{aligned} Y &:= \begin{bmatrix} T_I^{(1)} & 0 & \cdots & 0 \\ T_0^{(2)} & T_U^{(2)} & \ddots & \vdots \\ \vdots & 0 & \ddots & 0 \\ T_0^{(p)} & 0 & 0 & T_U^{(p)} \end{bmatrix}, \\ b &:= \mathbf{T}_I\, \mathbf{l}_{\text{inv}}, \end{aligned} \tag{11.9}$$

where $T_I^{(1)}$ is as given in (11.3) with $S_I^{(1)} = C_I^{(1)} = I$. To obtain the matrices $T_0^{(i)}$ and $T_U^{(i)}$, equivalently as $T_I^{(i)}$ in (11.3), we define

$$\left[S_0^{(i)}\right]_{k,l} := \begin{cases} 1, & k \notin \mathcal{U}^{(i)},\ k = l, \\ 0, & \text{otherwise}, \end{cases} \qquad \left[S_U^{(i)}\right]_{k,l} := \begin{cases} 1, & k \in \mathcal{U}^{(i)},\ k = l, \\ 0, & \text{otherwise}, \end{cases}$$

$C_0^{(i)} = I$, and $C_U^{(i)}$ as defined in (11.7). As the system of equations (11.8) is linear in $\overline{\mathbf{l}}_{0,\text{inv}}$, we solve it in the least squares sense and obtain l_0 as $l_0 = \left[\frac{1}{l_{0,\text{inv},1}}, \dots, \frac{1}{l_{0,\text{inv},m}}\right]^\top$.

In the noise-free case, $p = 2$ is sufficient to give the exact parameters l_0. If the measurement noise is significant, the method does not give an unbiased estimate as the expected measurement noise is additive Gaussian on the coordinates, but not on the measurement vector b, and the noise also enters the observation matrix Y.

Note that the configurations can in theory be chosen arbitrarily, under the mild condition that Y has full rank. However, simulations show that the choice is rather important as the precision of the solution can differ. Good choices of different configurations are those which make the observation matrix well-conditioned. To this end, the inputs should be sparse and produce large differences in the coordinates.

11.3 Distributed Parameter Identification Based on ADMM

In this section, we formulate the parameter identification as an optimization problem, where we take into account the Gaussian additive measurement noise on the x-, y- and z-coordinates of the interior nodes, as introduced in (11.1). We first formulate the optimization problem for the parameter identification of the overall system. As solving the resulting nonlinear optimization problem is computationally expensive, especially if large scale systems are considered, we split it into local subproblems and solve it by a distributed consensus ADMM algorithm [32], as introduced in Section 3.5.

11.3.1 Parameter Identification Problem

The measurements of $p \geq 2$ different configurations are again required for the identification. We define a vector of optimization variables for the measurement noise $\delta_I^{(i)}$ of configuration i. The stacked vector for the different configurations is denoted by

$$\boldsymbol{\delta}_I := \left[\delta_I^{(1)\top}, ..., \delta_I^{(p)\top}\right]^\top. \tag{11.10}$$

The objective of the optimization is to minimize $||\boldsymbol{\delta}_I||_2^2$ and the constraints are the force balances on the interior nodes of all configurations of the net. The coordinates $\mathbf{r}_I$ are expressed as

$$\mathbf{r}_I = \hat{\mathbf{r}}_I - \boldsymbol{\delta}_I, \tag{11.11}$$

using (11.1) and bold symbols for stacked vectors as introduced before. The identification problem for the overall system is given as

$$\begin{aligned} \min_{l_0, \boldsymbol{\delta}_I} \quad & ||\boldsymbol{\delta}_I||_2^2 \\ \text{s. t.} \quad & h(\hat{\mathbf{r}}_I, \boldsymbol{\delta}_I, \mathbf{u}, l_0) = 0, \\ & g(\hat{\mathbf{r}}_I, \boldsymbol{\delta}_I, \mathbf{u}, l_0) \leq 0. \end{aligned} \tag{11.12}$$

The equality constraints, $h(\hat{\mathbf{r}}_I, \boldsymbol{\delta}_I, \mathbf{u}, l_0) = 0$, are the force balance equations as before, and the m inequality constraints, $g(\hat{\mathbf{r}}_I, \boldsymbol{\delta}_I, \mathbf{u}, l_0) \leq 0$, impose non-negative tension in all edges, and are given by

$$g(\hat{\mathbf{r}}_I, \boldsymbol{\delta}_I, \mathbf{u}, l_0) := \bar{\mathbf{l}}_0 - \mathbf{l} \leq 0. \tag{11.13}$$

Both equality and inequality constraints are again formulated in terms of the noisy measurements, $\hat{\mathbf{r}}_I$, and the uncertain measurement noise, $\boldsymbol{\delta}_I$, i.e., the coordinates $\mathbf{r}_I$ are expressed by $\mathbf{r}_I = \hat{\mathbf{r}}_I - \boldsymbol{\delta}_I$. In order to solve this nonlinear optimization problem efficiently, we separate it into local subproblems, which are easier to solve in a distributed manner.

11.3.2 Decomposed Identification Problem

We separate the overall optimization problem (11.12) into one local optimization problem per interior node, which involves optimization variables corresponding only to the node itself, its neighboring nodes and the connected edges.

This is possible as the cost function of (11.12) is separable and the constraints of the local subproblems can be formulated in terms of local variables, which are copies of the global ones. Neighboring nodes thus have local optimization variables representing the same physical parameters, which are constrained to be equal at the solution. We call the interior nodes s, with $s \in \{1, ..., n_I\}$. Each interior node has v neighboring nodes, denoted by $t_q \in \mathcal{N}_s$, with $q = 1, ..., v$. They can be divided into v_I interior and v_B boundary neighboring nodes of node s, i.e., $v = v_I + v_B$. In order to formulate the local subproblem of node s, we introduce the vector of local optimization variables for the parameters to be identified, i.e., for the unstressed lengths $l_{0,(s,t_q)}$ connecting node s with its neighboring nodes $t_q \in \mathcal{N}_s$ as $l_{0,s} \in \mathbb{R}^v$. Additional optimization variables for each local problem are the measurement uncertainties of the coordinates of node s and its neighbors t_q in all configurations, which are contained in the vector $\boldsymbol{\delta}_s \in \mathbb{R}^{3p(1+v_I)}$. The problem is then given as

$$\min_{l_{0,s}, \boldsymbol{\delta}_s} \quad \sum_{s \in \mathcal{N}_I} \left(f_s(\boldsymbol{\delta}_s) + k_s(\hat{\mathbf{r}}_s, \hat{\mathbf{r}}_{t_q}, \boldsymbol{\delta}_s, \mathbf{u}_s, l_{0,s}) \right),$$

with

$$\begin{aligned} f_s(\boldsymbol{\delta}_s) &= ||\boldsymbol{\delta}_s||_2^2, \\ k_s(\hat{\mathbf{r}}_s, \hat{\mathbf{r}}_{t_q}, \boldsymbol{\delta}_s, \mathbf{u}_s, l_{0,s}) &= \mathcal{I}_{h_s}(\hat{\mathbf{r}}_s, \hat{\mathbf{r}}_{t_q}, \boldsymbol{\delta}_s, \mathbf{u}_s, l_{0,s}) \\ &\quad + \sum_{t_q \in \mathcal{N}_s} \mathcal{I}_{g_{(s,t_q)}}(\hat{\mathbf{r}}_s, \hat{\mathbf{r}}_{t_q}, \boldsymbol{\delta}_s, \mathbf{u}_s, l_{0,s}), \\ &\quad \forall s \in \mathcal{N}_I, \end{aligned} \tag{11.14}$$

where $\mathcal{I}_a(b)$ is the indicator function of b satisfying (a), defined as

$$\mathcal{I}_{(a)}(b) := \begin{cases} 0 \text{ if } b \text{ satisfies } (a), \\ \infty \text{ otherwise.} \end{cases} \tag{11.15}$$

Local Identification Problems

The vectors $l_{0,s}$ and $\boldsymbol{\delta}_s$ of local optimization variables contain copies of parts of the global optimization variables. In order to have the local problems converge to the global solution, the neighboring nodes need to agree on these variables, i.e., come to a consensus. We introduce the global consensus variables $\mu_{l_0} \in \mathbb{R}^{3m}$ and $\boldsymbol{\mu}_\delta \in \mathbb{R}^{3p\,n_I}$, with μ_{l_0} containing the consensus variables of the unstressed lengths of all edges and $\boldsymbol{\mu}_\delta$ containing the consensus variables for the uncertainties on the interior nodal coordinates in the different configurations. We denote the vectors $\mu_{l_{0,s}} \in \mathbb{R}^v$ and $\boldsymbol{\mu}_{\delta_s} \in \mathbb{R}^{3p\,(1+v_I)}$ as the parts of μ_{l_0} and $\boldsymbol{\mu}_\delta$ containing the global variables corresponding to the local copies $l_{0,s}$ and $\boldsymbol{\delta}_s$, respectively. Therefore, the consensus constraints can be formulated as

$$\left[l_{0,s}^\top, \boldsymbol{\delta}_s^\top\right]^\top - \left[\mu_{l_{0,s}}^\top, \boldsymbol{\mu}_{\delta_s}^\top\right]^\top = 0, \quad \forall s \in \mathcal{N}_I. \tag{11.16}$$

The local optimization problem of node s, including the consensus constraints, is given as

$$\begin{aligned} \min_{l_{0,s}, \boldsymbol{\delta}_s} \quad & f_s(\boldsymbol{\delta}_s) + k_s(\hat{\mathbf{r}}_s, \hat{\mathbf{r}}_{t_q}, \boldsymbol{\delta}_s, \mathbf{u}_s, l_{0,s}) \\ \text{s.t.} \quad & \left[l_{0,s}^\top, \boldsymbol{\delta}_s^\top\right]^\top - \left[\mu_{l_{0,s}}^\top, \boldsymbol{\mu}_{\delta_s}^\top\right]^\top = 0, \\ & \forall s \in \mathcal{N}_I. \end{aligned} \tag{11.17}$$

In the following, we form the augmented Lagrangians for the local problems by integrating the consensus constraints into the cost function. We define the penalty parameter ρ and the dual multipliers $\lambda_s := [\lambda_{l_{0,s}}^\top, \boldsymbol{\lambda}_{\delta_s}^\top]^\top$, where $\lambda_{l_{0,s}} \in \mathbb{R}^v$ and $\boldsymbol{\lambda}_{\delta_s} \in \mathbb{R}^{3p(1+v_I)}$. The augmented Lagrangian of each local optimization problem is

$$\begin{aligned} \mathcal{L}_{\rho,s}(l_{0,s}, \boldsymbol{\delta}_s, \lambda_{l_{0,s}}, \boldsymbol{\lambda}_{\delta_s}, \mu_{l_{0,s}}, \boldsymbol{\mu}_{\delta_s}) = \; & f_s(\boldsymbol{\delta}_s) + k_s(\hat{\mathbf{r}}_s, \hat{\mathbf{r}}_{t_q}, \boldsymbol{\delta}_s, \mathbf{u}_s, l_{0,s}) \\ & + \begin{bmatrix} \lambda_{l_{0,s}} \\ \boldsymbol{\lambda}_{\delta_s} \end{bmatrix}^\top \left(\begin{bmatrix} l_{0,s} \\ \boldsymbol{\delta}_s \end{bmatrix} - \begin{bmatrix} \mu_{l_{0,s}} \\ \boldsymbol{\mu}_{\delta_s} \end{bmatrix} \right) + \frac{\rho}{2} \left(\begin{bmatrix} l_{0,s} \\ \boldsymbol{\delta}_s \end{bmatrix} - \begin{bmatrix} \mu_{l_{0,s}} \\ \boldsymbol{\mu}_{\delta_s} \end{bmatrix} \right)^2, \\ & \forall s \in \mathcal{N}_I. \end{aligned} \tag{11.18}$$

11.3.3 Distributed ADMM Algorithm

In order to solve optimization problem (11.17) for all interior nodes, we use a distributed consensus ADMM algorithm [32], as introduced in Section 3.5. This method iterates between minimizing the augmented Lagrangians (11.18) with respect to the local optimization variables, minimizing them with respect to the consensus variables, and updating the dual multipliers for the consensus constraints. Convergence criteria to a fixed point can be defined in terms of the primal and dual residuals [32], as introduced in Section 3.5. For the parameter identification problem, the steps of the resulting ADMM algorithm are given in Algorithm 11.1. The first and third steps in lines 6 and 10 of Algorithm 11.1,

Algorithm 11.1 Distributed Consensus ADMM for the Identification of l_0.

1: **Input:** Penalty parameter ρ, measurements $\hat{\mathbf{r}}_I$, inputs $\mathbf{u}$,
2: **Initialization**: $l_{0,s}^0, \boldsymbol{\delta}_s^0, \lambda_{l_{0,s}}^0, \boldsymbol{\lambda}_{\delta_s}^0, \mu_{l_{0,s}}^0, \boldsymbol{\mu}_{\delta_s}^0$, set iteration $\kappa = 1$,
3: **while** *Primal, dual residuals not converged* **do**
4: **for** $s = 1$ **to** n_I **do**
5: $$\begin{bmatrix} l_{0,s}^\top & \boldsymbol{\delta}_s^\top \end{bmatrix}^{\kappa+1\top} = \underset{l_{0,s}, \boldsymbol{\delta}_s}{\operatorname{argmin}} \mathcal{L}_{\rho,s}(l_{0,s}, \boldsymbol{\delta}_s, \lambda_{l_{0,s}}^\kappa, \boldsymbol{\lambda}_{\delta_s}^\kappa, \mu_{l_{0,s}}^\kappa, \boldsymbol{\mu}_{\delta_s}^\kappa),$$
6: **end**
7: $$\begin{bmatrix} \mu_{l_0}^\top & \boldsymbol{\mu}_\delta^\top \end{bmatrix}^{\kappa+1\top} = \underset{\mu_{l_{0,s}}, \boldsymbol{\mu}_{\delta_s}}{\operatorname{argmin}} \sum_{s=1}^{n_I} \mathcal{L}_{\rho,s}(l_{0,s}^{\kappa+1}, \boldsymbol{\delta}_s^{\kappa+1}, \lambda_{l_{0,s}}^\kappa, \boldsymbol{\lambda}_{\delta_s}^\kappa, \mu_{l_{0,s}}, \boldsymbol{\mu}_{\delta_s}),$$
8: **for** $s = 1$ **to** n_I **do**
9: $$\begin{bmatrix} \lambda_{l_{0,s}} \\ \boldsymbol{\lambda}_{\delta_s} \end{bmatrix}^{\kappa+1} = \begin{bmatrix} \lambda_{l_{0,s}} \\ \boldsymbol{\lambda}_{\delta_s} \end{bmatrix}^{\kappa} + \rho \left(\begin{bmatrix} l_{0,s} \\ \boldsymbol{\delta}_s \end{bmatrix}^{\kappa+1} - \begin{bmatrix} \mu_{l_0,s} \\ \boldsymbol{\mu}_{\delta_s} \end{bmatrix}^{\kappa+1} \right),$$
10: **end**
11: $\kappa \leftarrow \kappa + 1$,
12: **end**
13: **Output:** Parameter estimate l_0.

respectively, can be completely distributed. The second step requires communication between adjacent nodes.

In the presence of measurement noise, the optimization variables $\boldsymbol{\mu}_\delta$ are required for a feasible solution of (11.12) . The formulation involves $m+3p\,n_I$ unknown variables and $3p\,n_I$ equality constraints and therefore does not define a unique solution. Increasing the number of configurations, p, does not give a unique parameter vector l_0, as each different configuration introduces additional measurement noise variables. In general, there can be multiple fixed points of the above optimization problem, which have an error with respect to the real parameters. The converged solution depends on the starting point and on the experimental configurations. We observe in simulations that the maximum estimation error of l_0 is in the range of the measurement noise, which is sufficiently accurate for this application.

11.4 Simulation Results

We present simulation results for a $1:4$ model of the HiLo roof, described in Chapter 9 and visualized in Figure 11.1. This system has $n_I = 295$ interior and $n_B = 75$ boundary nodes. The number of edges, and therefore parameters to be identified, is $m = 606$. The material parameters correspond to polyamid $PA6$ with $E = 3000\,\mathrm{Nmm}^2$ and $A = \pi \cdot (3.8\,\mathrm{mm})^2$. Under the applied tension, the edges stretch in the range of $1 \times 10^{-3}\,\mathrm{m}$ to $1 \times 10^{-1}\,\mathrm{m}$.

Remark 11.1. For the parameter identification, the material property is not relevant in absolute terms, as it is a constant factor in the force equilibrium equations. Only the ratios between the different edge stiffnesses are important, which we choose to be one in this example for all edges. However, the material stiffness, together with the range of forces which can be applied, determine how easily the configuration can be reconfigured into a measurably different form.

In the following simulations, we compare the performance of the linear regression as well as the distributed ADMM algorithm for the parameter identification. We consider the noise-free case and a case with additive white Gaussian noise with a standard deviation of 0.1 mm on the node coordinates, which corresponds to the expected measurement noise by tacheometry. We simulate the identification process of the parameters, l_0, using different configurations, which are obtained as the solution to $\mathcal{P}_{\mathrm{minE}}$ in (10.25). Gaussian noise is added to give the simulated measurement. The noise-free reference parameters are denoted by l_0^{SOCP}.

11.4.1 Simulation Results for Least Squares Identification

We solve the linear regression problem in (11.8) and compare three cases, where we solve (11.8) based on $p = 1$, $p = 2$ and $p = 3$ configurations. The three different configurations are obtained by applying the inputs $u^{(1)} = 0$, $u^{(2)}$ with $u_k^{(2)} = 0.1\, l_{0,k}$, $\forall\, k \in \bar{\mathcal{E}}_B$, and $u^{(3)}$ with $u_k^{(3)} = 0.05\,\mathrm{m}$ for six different boundary edges, k. The different input locations and the resulting configurations can be seen in Figure 11.1. The identified parameters are denoted by l_0^{LS}. Table 11.1 shows the results, where $\mathrm{cond}(\cdot)$ denotes the condition number, $\|\cdot\|_\infty$ is the maximum absolute value and $\mathrm{RMS}(\cdot)$ is the root-mean-square-error $\sqrt{\|\cdot\|_2^2 / m}$. The results confirm that one configuration alone does not define a unique solution. For the noise-free case, $p \geq 2$ gives the (numerically) exact solution. In the presence of noise, the solution is no longer exact. Increasing p provides some averaging of the noise, but the exact solution is not found.

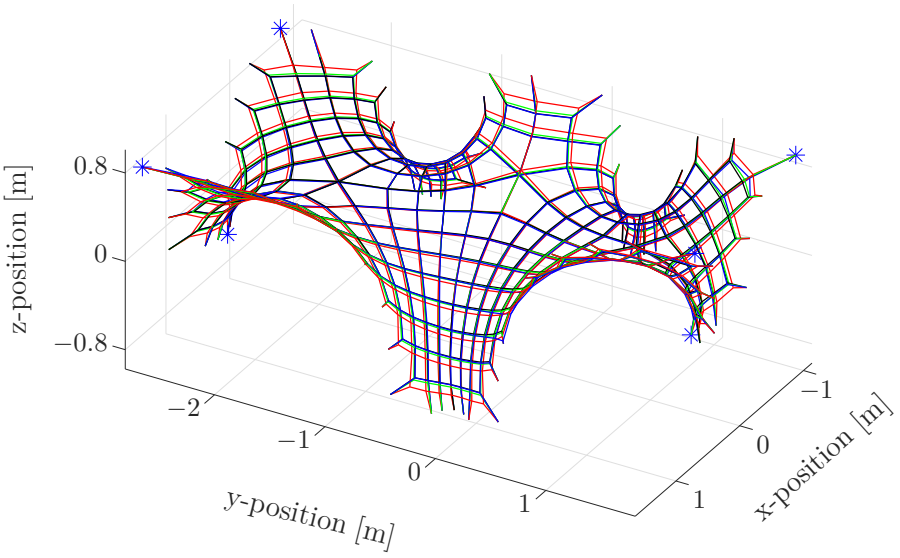

Figure 11.1: Simulation model (1 : 4) of the cable net geometry for the HiLo roof. — $r^{(1)}$, — $r^{(2)}$ (for LS), — $r^{(3)}$ (for LS), — $r^{(4)}$ (for ADMM), * Input locations of $u^{(3)}$.

Table 11.1: Results of the LS-approach.

p	noise (std σ)	cond(Y)	$\|l_0^{\mathrm{LS}} - l_0^{\mathrm{SOCP}}\|_\infty$	RMS ($l_0^{\mathrm{LS}} - l_0^{\mathrm{SOCP}}$)
1	0	3.3×10^5	1.9×10^{-1} m	6.9×10^{-2} m
2	0	1.3×10^3	2.2×10^{-5} m	1.0×10^{-5} m
3	0	3.3×10^2	2.8×10^{-5} m	4.4×10^{-6} m
1	0.1 mm	1.5×10^3	1.9×10^{-1} m	6.9×10^{-2} m
2	0.1 mm	1.0×10^3	1.1×10^{-1} m	4.2×10^{-2} m
3	0.1 mm	3.3×10^2	8.8×10^{-3} m	3.1×10^{-3} m

11.4.2 Simulation Results for ADMM Algorithm

We now use the distributed ADMM algorithm for the identification. Again, one configuration does not define a unique solution for the parameters l_0. We choose $p = 2$, which defines a unique solution in the noise-free case. For the simulation, we choose the first configuration as before, with inputs $u^{(1)} = 0$ and the second one is obtained by applying the input $u^{(4)}$ with $u_k^{(4)} = 0.4\, l_{0,k}$, $\forall\, k \in \bar{\mathcal{E}}_B$. This configuration is shown as $r^{(4)}$ in Figure 11.1 .

We initialize Algorithm 11.1 with $l_0^{(0)}$, where each parameter has an error with respect to the reference l_0^{SOCP} of 0.001 m in the noise-free case and of 0.005 m in the case with added measurement noise. This represents realistic values for the fabrication tolerances. The ADMM penalty parameter is set to $\rho = 1$.

Figure 11.2 shows the convergence plots for both the noise-free and the noisy case. Figures 11.2 (a) and 11.2 (b) show the RMS-error from the identified parameters l_0^{ADMM} to the reference l_0^{SOCP} and the maximum absolute value of the error, $\|l_0^{\mathrm{LS}} - l_0^{\mathrm{SOCP}}\|_\infty$, respectively. Figures 11.2 (c) and 11.2 (d) show the convergence of the consensus variables and the convergence of the consensus multipliers of the ADMM algorithm, respectively. One can see that the algorithm converges to a fixed point, which has a small error in the noisy case, as described before. In our example, the maximum absolute value of the error, $\|l_0^{\mathrm{ADMM}} - l_0^{\mathrm{SOCP}}\|_\infty$, is 1×10^{-4} m in the noise-free case and 2×10^{-4} m in the noisy case and the RMS-error is 2×10^{-5} m in the noise-free case and 6×10^{-5} m in the noisy case. This represents an accurate solution for our application and is in the range of the added measurement noise. Other simulation examples show qualitatively similar results. In examples of anticlastic shells with fewer nodes and a bigger ratio of boundary nodes to interior nodes, the algorithm converges faster and more monotonically.

11.5 Conclusions

Two methods have been presented for the identification of the important unknown parameters, l_0, of the cable net. While the first method is a linear regression, which is easy to implement and fast to solve, it can become imprecise if the measurement noise is significant. The second method is a distributed ADMM approach, which ensures feasibility of the solution. Simulations show that the algorithm converges to a precise solution, even in the presence of measurement noise.

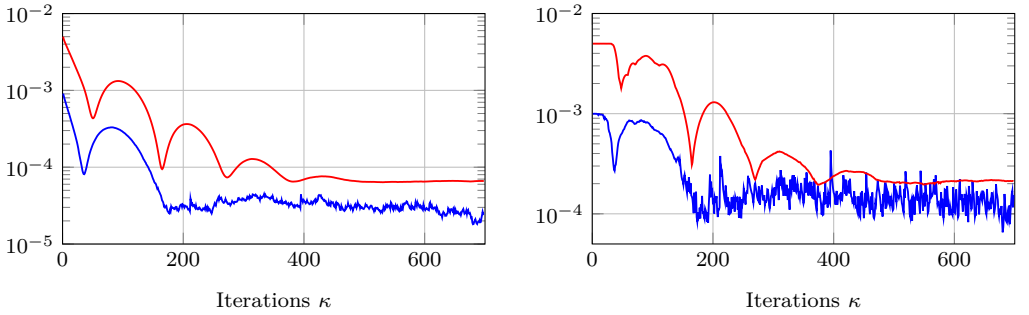

(a) RMS ($l_0^{\mathrm{ADMM}} - l_0^{\mathrm{SOCP}}$)

(b) $\|l_0^{\mathrm{ADMM}} - l_0^{\mathrm{SOCP}}\|_\infty$

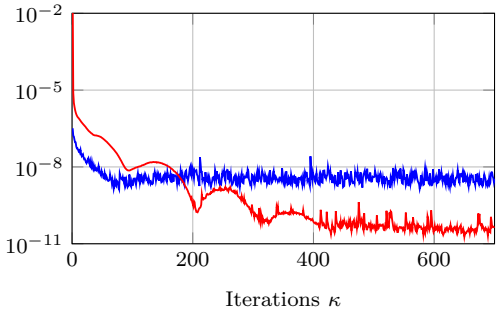

(c) $\|\mu_{l_0}^{\kappa} - \mu_{l_0}^{(\kappa-1)}\|_2 / \sqrt{m}$

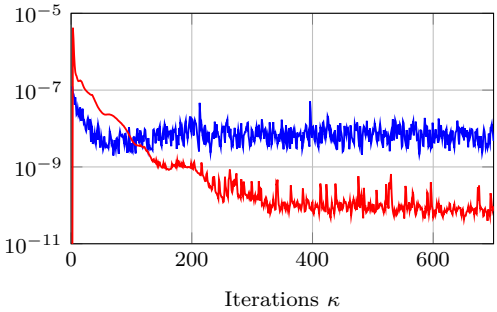

(d) $\|\lambda_{l_0}^{\kappa} - \lambda_{l_0}^{(\kappa-1)}\|_2 / \sqrt{m}$

Figure 11.2: Convergence plots of the distributed ADMM algorithm. — noise-free measurements — noisy measurements.

CHAPTER 12

Control Input Computations and Complete Cable Net Reconfiguration Procedure

This chapter presents the second part of the complete control algorithm, illustrated in Figure 9.4, which is the computation of control inputs for a fixed model of the cable net. The last section of the chapter then summarizes the complete control algorithm of both the identification and the control computation steps. For the control input computation, an SQP variant is presented, where in each iteration an approximation of the optimal control problem as a QP is solved. A line search is performed along the part of the minimizer corresponding to the control input. Along this direction, feasible points are generated by convex programming. The convergence of this control input calculation to a stationary point of the optimal control problem is proved by showing equivalence of the iterations of the algorithm to a Gauss-Newton iteration performed on the original optimal control problem. For practical applicability to systems where actuation is time-consuming, we present a variant of the algorithm which is based on an l_1-norm regularization and which results in sparse control inputs. The work presented in this chapter has been published in [16] and [19].

This chapter is structured as follows. Section 12.1 presents the optimal control algorithm which is an SQP variant with feasible iterates. Section 12.2 gives the convergence proof of the algorithm. We propose a variant of the algorithm for sparse input calculation in Section 12.3. Section 12.4 presents the complete control algorithm consisting of the parameter identification from Chapter 11 and the control input calculations from Sections 12.1 or 12.3. Sections 12.5 and 12.6 present numerical experiments and a conclusion to this chapter, respectively.

12.1 Control Input Computation

In this section, we first state the form optimization problem. Then, we present a Sequential Quadratic Programming (SQP) variant to compute a Gauss-Newton (GN) descent direction, followed by a line search to find an appropriate step size. Finally, we present

the algorithm, and compare it to general purpose nonlinear solvers.

12.1.1 Optimal Control Problem for a Fixed Model

Given a set of model parameters of the cable net $l_0^{(k)}$, and fixed boundary nodes $\bar{r}_B = \bar{r}_B^{\text{meas},(k)}$ for the fixed measured configuration (k), an optimal control problem (OCP) minimizes the weighted l_2-norm of the distance between the desired coordinates $r^{(\text{des})}$ and the model coordinates as a function of the input u and is thus given as

$$\begin{aligned} &\text{Problem} \quad \mathcal{P}_{\text{ocp,u}} : \\ &\min_{u} \quad f_{\text{ocp,u}}(u) = \frac{1}{2} \left\| R(u) - r_I^{(\text{des})} \right\|_{Q_r}^2 , \end{aligned} \tag{12.1}$$

with Q_r being a positive semi-definite weighting matrix. The function $R(u)$ was introduced in Section 10.5 as the mapping of the inputs u to the coordinates r, which is not explicitly known and is only implicitly defined through the energy minimization in (10.23) or through the force balance equations $h(\cdot, u) = 0$ in (10.14). However, the problem can be reformulated by introducing additional optimization variables r_I for the interior node coordinates together with constraints to guarantee that the minimizer $p = [r_I^\top,\ u^\top]^\top$ of the problem represents a static equilibrium of the cable net. The reformulated problem is the following

$$\begin{aligned} &\text{Problem} \quad \mathcal{P}_{\text{ocp}} : \\ &\min_{r_I, u} \quad f_{\text{ocp}}(r_I) = \frac{1}{2} \left\| r_I - r_I^{(\text{des})} \right\|_{Q_r}^2 \\ &\text{s.t.} \quad h([r_I^\top, \bar{r}_B^\top]^\top, u) = 0. \end{aligned} \tag{12.2}$$

The $3n_I$ equality constraints in (10.14), $h([r_I^\top, \bar{r}_B^\top]^\top, u) = 0$, represent the force balances at the interior nodes and implicitly express the function $R(u)$. We will show in Section 12.2, that the function $R(u)$ is well defined and that problem $\mathcal{P}_{\text{ocp}}$ is an exact reformulation of $\mathcal{P}_{\text{ocp,u}}$.

In contrast to using the force-density method in Section 10.4.3, the cost functions $f_{\text{ocp,u}}(u)$ or $f_{\text{ocp}}(r_I)$, in (12.1) or (12.2), respectively, penalize the individual nodal coordinates x, y, and z. In construction applications this is beneficial as specific regions of the geometry can be penalized with larger weight if more precision is needed to fit other elements to these areas of the structure.

Remark 12.1. The m inequality constraints in (10.10), $g(r_I, \bar{r}_B, u) \leq 0$, which represent non-negative elongations of the edges, can be added. If the problem is feasible, they guarantee the absence of slack cables. If there are physical limitations on the inputs, then the constraints in (10.12) need to be added. In the following, we do not consider any constraints on the inputs. The underlying assumption is that the design provides all the actuation that is needed for the control task.

12.1.2 Control Calculation: GN Iteration Based on an SQP Variant

We propose solving Problem $\mathcal{P}_{\text{ocp,u}}$ in (12.1) efficiently by a Gauss Newton (GN) iteration, as introduced in Section 3.7. The GN descent directions for $\mathcal{P}_{\text{ocp,u}}$ are computed in SQP iterations [34], [160], as introduced in Section 3.8, on $\mathcal{P}_{\text{ocp}}$ in (12.2). Then, a line search along the GN direction on $f_{\text{ocp,u}}$ is implemented, where $\mathcal{P}_{\text{minE}}$ is solved to evaluate $R(u)$.

Problem $\mathcal{P}_{\text{ocp}}$ is iteratively approximated as a Quadratic Program (QP) around a sequence of points $p^\kappa = [r_I^{\kappa\top},\ u^{\kappa\top}]^\top$ of nodal position coordinates and inputs at iterations κ. In standard SQP methods, the cost function of the QP is obtained by a quadratic approximation of the Lagrangian, which involves the Hessian of the Lagrangian. Instead, we take the constrained GN approach [34], [161], where we exploit the least-squares structure of the cost function $f_{\text{ocp}}(r_I)$ in $\mathcal{P}_{\text{ocp}}$. The GN iteration uses only the first-order term for the approximate Hessian H, as described in (3.18) in Section 3.7, i.e.,

$$\begin{aligned} H &= \nabla_{(r_I,u)}((r_I^\kappa - r_I^{(\text{des})})Q_r^{\frac{1}{2}})^\top \nabla_{(r_I,u)}((r_I^\kappa - r_I^{(\text{des})})Q_r^{\frac{1}{2}}) \\ &= \text{diag}(Q_r, 0). \end{aligned} \tag{12.3}$$

This approximation has significant computational advantages if the system is large, because no second order information needs to be computed. It is a good approximation if the residuals $r_I^\kappa - r_I^{(\text{des})}$ are small or nearly affine. With $\Delta p^\kappa = [\Delta r_I^{\kappa\top},\ \Delta u^{\kappa\top}]^\top$, the QP in iteration κ is given by

$$\begin{aligned} &\text{Problem } \mathcal{P}_{\text{SQP}}^\kappa: \\ &\min_{\Delta p^\kappa} \quad f_{\text{ocp}}^{\text{GN}}(\Delta r_I^\kappa) = \frac{1}{2}\Delta p^{\kappa\top} H \Delta p^\kappa + \nabla_{(r_I,u)} f_{\text{ocp}}^\top \Delta p^\kappa \\ &\text{s.t.} \quad h([r_I^{\kappa\top}, \bar{r}_B^\top]^\top, u^\kappa) + \nabla_{(r_I,u)} h([r_I^{\kappa\top}, \bar{r}_B^\top]^\top, u^\kappa)\Delta p^\kappa = 0. \end{aligned} \tag{12.4}$$

The equality constraints of $\mathcal{P}_{\text{SQP}}^\kappa$ in (12.4) are the linearized constraints of $\mathcal{P}_{\text{ocp}}$. With H in (12.3) and f_{ocp} in (12.2), $f_{\text{ocp}}^{\text{GN}}$ in (12.4) can be simplified to

$$\begin{aligned} f_{\text{ocp}}^{\text{GN}}(\Delta r_I^\kappa) &= \frac{1}{2}\|r_I^\kappa - r_I^{(\text{des})} + \nabla_{(r_I,u)}(r_I^\kappa - r_I^{(\text{des})})\Delta p^\kappa\|_{Q_r}^2 \\ &= \frac{1}{2}\|r_I^\kappa - r_I^{(\text{des})} + \Delta r_I^\kappa\|_{Q_r}^2. \end{aligned} \tag{12.5}$$

Given $\Delta p^\kappa = [\Delta r_I^{\kappa\top},\ \Delta u^{\kappa\top}]^\top$, which is the minimizer of $\mathcal{P}_{\text{SQP}}^\kappa$, then Δu^κ is the GN descent direction of $\mathcal{P}_{\text{ocp,u}}$. This is proved in Section 12.2.

12.1.3 Line Search

An inexact backtracking line search, as described in Section 3.7, along the direction Δu^κ, is performed for the cost function $f_{\text{ocp,u}}$ to find a step length α^κ satisfying the

Wolfe conditions

$$\begin{aligned} f_{\mathrm{ocp,u}}(u^\kappa + \alpha^\kappa \Delta u^\kappa) \;&\leq\; f_{\mathrm{ocp,u}}(u^\kappa) + c_1 \alpha^\kappa \nabla_u f_{\mathrm{ocp,u}}(u^\kappa)^\top \Delta u^\kappa, \\ \nabla_u f_{\mathrm{ocp,u}}(u^\kappa + \alpha^\kappa \Delta u^\kappa)^\top \Delta u^\kappa \;&\geq\; c_2 \nabla_u f_{\mathrm{ocp,u}}(u^\kappa)^\top \Delta u^\kappa, \end{aligned} \tag{12.6}$$

where $c_1 \in \mathbb{R}$ and $c_2 \in \mathbb{R}$ are constants satisfying $0 < c_1 < c_2 < 1$. For the evaluation of the cost function $f_{\mathrm{ocp,u}}(u)$, we compute $R(u)$ as the part r_I of the minimizer of $\mathcal{P}_{\mathrm{minE}}$ in (10.25), and the computation of the gradient in (12.6) is performed by

$$\nabla_u f_{\mathrm{ocp,u}}(u) = Q_r (R(u) - r_I^{(\mathrm{des})})^\top (-\nabla_{r_I} h(R(u), u)^{-1} \nabla_u h(R(u), u). \tag{12.7}$$

The related proofs are given in Section 12.2.

To find α^κ, the backtracking line search takes trial steps along the direction Δu^κ. It is initialized with $\alpha^\kappa = 1$. If the Wolfe conditions are satisfied, the unit step length is accepted. Otherwise, the next step length $\alpha^\kappa \leftarrow \rho\, \alpha^\kappa$ is tested, where $0 < \rho < 1$, until a suitable step length is found. The Wolfe conditions guarantee that the step lengths are not too small and that sufficient decrease of the cost function $f_{\mathrm{ocp,u}}$ is achieved at the next iterate, which is given by

$$p^{(\kappa+1)} = [R(u^\kappa + \alpha^\kappa \Delta u^\kappa)^\top, \;\; u^{\kappa\top} + \alpha^\kappa \Delta u^{\kappa\top}]^\top, \tag{12.8}$$

where $R(u)$ is the component r_I of the minimizer of $\mathcal{P}_{\mathrm{minE}}$ in (10.25).

The variant of SQP applied to $\mathcal{P}_{\mathrm{ocp}}$ in (12.2), which solves the GN iteration of $\mathcal{P}_{\mathrm{ocp,u}}$ in (12.1) to compute the control input $u^{(k+1)}$ for the current measured configuration $r^{\mathrm{meas},(k)}$, results in Algorithm 12.1. Global convergence to a KKT point of $\mathcal{P}_{\mathrm{ocp}}$, which is equal to a stationary point of $\mathcal{P}_{\mathrm{ocp,u}}$ is shown in Section 12.2.

Note that the standard SQP methods generate iterates $p^{\kappa+1} = p^\kappa + \alpha^\kappa \Delta p^\kappa$, with $\Delta p^\kappa = [\Delta r_I^{\kappa\top}, \; \Delta u^{\kappa\top}]^\top$ being the minimizer of $\mathcal{P}^\kappa_{\mathrm{SQP}}$. Before convergence, all of these iterates may be infeasible. Therefore, a line search for guaranteeing global convergence would need to be performed on a merit function that accounts for both the decrease in the cost as well as the constraint violations [34]. This requires design parameters that can be difficult to tune. In the SQP variant proposed here, we use the GN direction Δu^κ, which is a component of the minimizer of $\mathcal{P}^\kappa_{\mathrm{SQP}}$, to perform GN iterations on $\mathcal{P}_{\mathrm{ocp,u}}$. Since $\mathcal{P}_{\mathrm{ocp,u}}$ is unconstrained and thus all iterates are feasible, the cost function $f_{\mathrm{ocp,u}}$ can be chosen as the merit function in the line search. Note that this is enabled by the efficient computation of $R(u)$ as the part r_I of the minimizer of $\mathcal{P}_{\mathrm{minE}}$.

12.1.4 Comparison to Other Solvers

There are many "general-purpose" solvers available that are applicable to general non-convex optimization problems. However, the more general these solvers are, the less they are able to exploit specific problem structure. An example of an efficient open-source

Algorithm 12.1 Algorithm to compute $u^{(k+1)}$ for current measured configuration $r^{\text{meas},(k)}$ solving GN iterations on $\mathcal{P}_{\text{ocp,u}}$ via SQP variant on $\mathcal{P}_{\text{ocp}}$.

Input: Measured configuration $r_I^{\text{meas},(k)}, r_B^{\text{meas},(k)}, u^{(k)}$,
Target coordinates $r_I^{(\text{des})}$, convergence bound c_{c},
Model parameters EA, $l_0^{(k)}$ (in $\mathcal{P}_{\text{minE}}$, $\mathcal{P}_{\text{SQP}}^{\kappa}$),
Line search parameters c_1, c_2, ρ,
Initialization: Set $p^0 = \infty, \quad p^1 = [r_I^{\text{meas},(k)\top}, u^{(k)\top}]^\top, \quad \kappa = 1$,
Set $\bar{r}_B = r_B^{\text{meas},(k)}$ in $\mathcal{P}_{\text{minE}}$ and $\mathcal{P}_{\text{SQP}}^{\kappa}$,
while $\|p^\kappa - p^{\kappa-1}\| \geq c_c$ **do**
    Solve $\mathcal{P}_{\text{SQP}}^{\kappa}$ to obtain Δu^κ,
    Perform backtracking line search with (12.6) to find α^κ,
    Set next feasible iterate $p^{\kappa+1}$ as per (12.8),
end
Set $p = p^\kappa$,
Set $u^{(k+1)} = u^\kappa$,
Output: Control input $u^{(k+1)}$ belonging to KKT point $p = [R(u^{(k+1)})^\top, u^{(k+1)\top}]^\top$ of $\mathcal{P}_{\text{ocp}}$.

solver, which is suitable for large-scale nonlinear problems is IPOPT [162]. This solver is applicable to the optimal control problem $\mathcal{P}_{\text{ocp}}$ in (12.2). However, for this problem, a feasible solution is not guaranteed to be found. Simulations confirm that the iterates of IPOPT often converge to a point of local infeasibility.

Algorithm 12.1 and IPOPT are local methods, i.e., they find a local stationary point given an initial point. In contrast, global methods aim at finding the global minimum by considering multiple local minima and choosing the best one. An example of such global methods are evolutionary (genetic) algorithms. They can also be used to solve problem $\mathcal{P}_{\text{ocp}}$. However, they are generally very inefficient and scale badly with the problem dimension, which results in very slow convergence. For the cable net application, the measurement of the initial pre-stressed form provides a good starting point for the solver. Therefore, global methods such as genetic algorithms are considered to be unnecessary and do not provide any advantage over the algorithm proposed in this work.

In summary, compared to other more general nonlinear solvers, Algorithm 12.1 exploits the knowledge of the given problem structure. In particular, this is achieved through the GN approximation in $\mathcal{P}_{\text{SQP}}^{\kappa}$ as well as through the computation of feasible iterates by convex programming in $\mathcal{P}_{\text{minE}}$. This renders Algorithm 12.1 very efficient and guarantees convergence to a stationary feasible point.

12.2 Convergence Proof of Algorithm 12.1

This section proves the following result.

Theorem 12.1. *For fixed model parameters and under the cable net assumptions in Section 10.3, Algorithm 12.1 converges to a stationary point of* $\mathcal{P}_{\text{ocp,u}}$ *in* (12.1).

First, we present results, which are used in the proof of Theorem 12.1.

12.2.1 Well-posedness of $\mathcal{P}_{\text{ocp}}$, $\mathcal{P}_{\text{ocp,u}}$ and $\mathcal{P}_{\text{minE}}$

Proposition 12.1. *Under the cable net assumptions in Section 10.3, the mapping* $R(u) : u \mapsto r_I$ *defined through the equations* $h(r_I, u) = 0$ *in* (10.14) *is injective, i.e., for a given* u *(and a fixed* r_B*), there exists a unique* r_I *that solves* $h(r_I, u) = 0$.

Proof of Proposition 12.1: Under the cable net assumptions in Section 10.3, and for a fixed input vector u, the cable net is a so-called spider web, for which the following holds: Any configuration r_I of a spider web such that all edges in $\bar{\mathcal{E}}$ are in positive tension, and such that every interior node in $\mathcal{N}_I$ is connected to a boundary node in $\mathcal{N}_B$ by edges in $\bar{\mathcal{E}}$, is unique and r_I is the minimum point for the associated quadratic energy function $V(r_I)$. For the proof of this result, we refer to Proposition 5.5.2 in [163]. Similar results can be found in [138] and [144]. □

Proposition 12.2. *Under the cable net assumptions in Section 10.3, and for a constant input* u*, the partial Jacobian* $\nabla_{r_I} h(r_I, u)$ *at an equilibrium configuration* r_I *is non-singular.*

Proof of Proposition 12.2: Using the statement of Proposition 12.1 that the equilibrium configuration r_I corresponding to a proper self-stress of a spider web is the unique minimum of the associated energy function $V(r_I)$, implies that the Hessian of $V(r_I)$ with respect to r_I is positive definite at that point. Furthermore, it is easy to show that the partial Jacobian of the force balance equations, $\nabla_{r_I} h(r_I, u)$, at an equilibrium is equal to the Hessian of the energy function with respect to r_I [138], which completes the proof. □

In the following, we make use of the Implicit Function Theorem and therefore briefly restate it here.

Theorem 12.2 (Implicit Function Theorem [34])**.** *Let* $h : \mathbb{R}^{3n_I} \times \mathbb{R}^{m_B} \mapsto \mathbb{R}^{3n_I}$ *be a function such that*

(i) $h(\hat{r}_I, \hat{u}) = 0$ *for some* $\hat{r}_I \in \mathbb{R}^{3n_I}$,

(ii) the function $h(\cdot,\cdot)$ *is continuously differentiable in some neighborhood of* $(\hat{r}_I, \hat{u})$,

(iii) $\nabla_{r_I} h(r_I, u)$ *is nonsingular at the point* $(r_I, u) = (\hat{r}_I, \hat{u})$.

Then there exist open sets $\mathcal{N}_{r_I} \subset \mathbb{R}^{3n_I}$ *and* $\mathcal{N}_u \subset \mathbb{R}^{m_B}$ *containing* $\hat{r}_I$ *and* $\hat{u}$, *respectively, and a unique continuous function* $R(u) : \mathcal{N}_u \mapsto \mathcal{N}_{r_I}$ *such that* $\hat{r}_I = R(\hat{u})$ *and* $h(r_I, u) = 0$ *for all* $u \in \mathcal{N}_u$. *If* $h(r_I, u)$ *is p-times continuously differentiable with respect to both* r_I *and* u *for some* $p > 0$, *then* $R(u)$ *is also p-times continuously differentiable with respect to* u, *and we have*

$$\nabla_u R(u) = -[\nabla_{r_I} h(r_I, u)]^{-1} \nabla_u h(r_I, u),$$

for all $u \in \mathcal{N}_u$.

With this result, we can now state the following.

Proposition 12.3. *Under the cable net assumptions in Section 10.3, the function* $R(u) : u \mapsto r_I$ *in* $\mathcal{P}_{\text{ocp,u}}$ *is well-defined, i.e., at any equilibrium point, locally it exists uniquely and is continuously differentiable.*

Proof of Proposition 12.3: We apply the Implicit Function Theorem in Theorem 12.2 to $h(r_I, u)$ in (10.14). This is valid as $h(r_I, u)$ satisfies (i) because we assume that for the given parameters and a given $\hat{u}$ and under the cable net assumptions in Section 10.3, there exists an equilibrium configuration $\hat{r}_I$. Condition (ii) holds due to the function definition of $h(\cdot,\cdot)$ in (10.14). Condition (iii) is satisfied because of Proposition 12.2. Therefore, the Implicit Function Theorem can be applied and $R(u)$ exists and is unique and continuously differentiable with $\nabla_u R(u) = -[\nabla_{r_I} h(r_I, u)]^{-1} \nabla_u h(r_I, u)$ (locally at any equilibrium point). □

Corollary 12.1. *Problems* $\mathcal{P}_{\text{ocp}}$ *and* $\mathcal{P}_{\text{ocp,u}}$ *in* (12.2) *and* (12.1), *respectively, are equivalent reformulations in the sense that* $(r_I^*, u^*) = \arg\min \mathcal{P}_{\text{ocp}}$ *if and only if* $u^* = \arg\min \mathcal{P}_{\text{ocp,u}}$.

Proof of Corollary 12.1: With Propositions 12.1 and 12.3, $h(\cdot, u) = 0$ and $R(u)$ describe the mapping from a given u to the same r_I. The minimizer of $\mathcal{P}_{\text{ocp}}$, (r_I^*, u^*), needs to be feasible, i.e., it needs to satisfy $h(r_I^*, u^*) = 0$, and therefore $R(u^*) = r_I^*$, and $\mathcal{P}_{\text{ocp}}$ and $\mathcal{P}_{\text{ocp,u}}$ are exact reformulations. □

Furthermore, the following result shows that the iteration in (12.8) is well-defined, where $R(u)$ corresponds to r_I^* in the minimizer of $\mathcal{P}_{\text{minE}}$ for fixed u.

Proposition 12.4. *The part r_I^* of the minimizer of $\mathcal{P}_{\text{minE}}$ in (10.25) for a fixed input u is equal to the value of r_I^* defined through $h(r_I^*, u) = 0$ in (10.14).*

Proof of Proposition 12.4: We note that the minimizer r_I^* of Problem $\mathcal{P}_{\text{minE}}$ for a fixed u is unique. This is stated and proved in Lemma 5.3 in [146]. The uniqueness of the minimizer r_I^* of $\mathcal{P}_{\text{minE}}$ together with the unique value of r_I^* solving $h(\cdot, u) = 0$ from Proposition 12.1 implies the equality. □

The following property of the Jacobian $\nabla_u h(r_I, u)$ will be of further use in the following.

Proposition 12.5. *At each equilibrium point (r_I, u), the Jacobian $\nabla_u h(r_I, u)$ has full column rank.*

Proof of Proposition 12.5. With the definition of $h(r_I, u)$ in (10.14), the partial Jacobian $\nabla_u h(r_I, u)$ is given by

$$\nabla_u h(r_I, u) = \begin{bmatrix} \frac{\partial h_1}{\partial u_1} & \dots & \frac{\partial h_1}{\partial u_{m_B}} \\ \vdots & & \vdots \\ \frac{\partial h_{3n_I}}{\partial u_1} & \dots & \frac{\partial h_{3n_I}}{\partial u_{m_B}} \end{bmatrix}, \tag{12.9}$$

with

$$\frac{\partial h_i}{\partial u_{(s,t)}} = \begin{cases} EA_{(s,t)} \begin{bmatrix} x_s - x_t \\ y_s - y_t \\ z_s - z_t \end{bmatrix} \frac{1}{\left(l_{0,(s,t)} - u_{(s,t)}\right)^2}, & \text{if } i = s \text{ or } i = t, \text{ and } (s,t) \in \mathcal{E}_B, \\ 0 & \text{if } i \neq s \text{ and } i \neq t, \text{ or } (s,t) \in \mathcal{E}_I. \end{cases} \tag{12.10}$$

Only the force change in the boundary edges, i.e., for $(s,t) \in \mathcal{E}_B$, in the sum of (10.14) are non-zero. The entries of $\nabla_u h(r_I, u)$ in (12.10) are always non-zero (first case), except if $x_s = x_t$, $y_s = y_t$ or $z_s = z_t$ (second case), where the latter means alignment of the edge (s,t) with a coordinate axis, which can happen at most for two of the coordinates. Therefore, in each column of $\nabla_u h(r_I, u)$, we have at least one nonzero entry. Every row has as many non-zero entries as the number of connected boundary edges to the corresponding node. Under the cable net assumptions in Section 10.3 at most three boundary nodes are connected to the same node and the corresponding boundary edges have linearly independent directions, and thus the corresponding columns and rows of $\nabla_u h(r_I, u)$ are linearly independent. Therefore, there is always a submatrix of $\nabla_u h(r_I, u)$ of size $m_B \times m_B$ of full rank. □

The following example illustrates the idea used for the proof of Proposition 12.5.

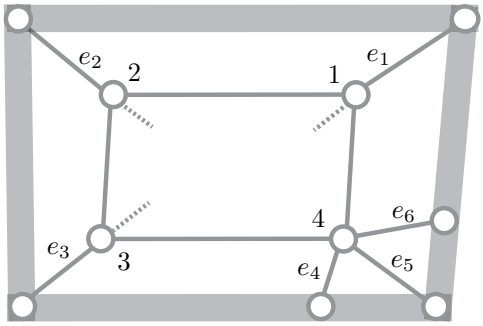

Figure 12.1: Example topology in 3D with interior nodes 1, 2, 3, 4, and boundary edges e_1, e_2, e_3, e_4, e_5 and e_6.

Example 12.1. Let us consider the 3D net topology that is illustrated in Figure 12.1. The interior nodes 1, 2 and 3 are connected by the boundary edges e_1, e_2, and e_3, respectively. Interior node 4 is connected by the boundary edges e_4, e_5 and e_6, which have linearly independent direction vectors, which satisfies the cable net assumptions in Section 10.3.

We use the definition of the edge-node incidence matrix M of the net topology, as defined in (10.2) in Section 10.1. We further partition the matrix M_I according to $M_I = [M_{II}^\top \; M_{IB}^\top]^\top$, where the part $M_{IB} \in \mathbb{R}^{m_B \times n_I}$ describes the topology of boundary edges which are connected to interior nodes. The sparsity structure of the partial Jacobian $\nabla_u h(r_I, u)$ is then given by $[0^\top \; \hat{M}_{IB}^\top]^\top \otimes [1 \; 1 \; 1]^\top$, where $\hat{M}_{IB}$ denotes the sparsity structure of M_{IB}, i.e., it has ones in the places of non-zero entries.

Let us consider a cable net topology as illustrated in Figure 12.1. The sparsity structure of the partial Jacobian $\nabla_u h(r_I, u)$ for this topology corresponds to

$$\begin{bmatrix} 0 \\ \hat{M}_{IB} \end{bmatrix} \otimes \begin{bmatrix} 1 \\ 1 \\ 1 \end{bmatrix} = \left[\begin{array}{cccccc} 0 & 0 & 0 & 0 & 0 & 0 \\ & & \vdots & & & \\ 0 & 0 & 0 & 0 & 0 & 0 \\ \hdashline 1 & 0 & 0 & 0 & 0 & 0 \\ 0 & 1 & 0 & 0 & 0 & 0 \\ 0 & 0 & 1 & 0 & 0 & 0 \\ 0 & 0 & 0 & 1 & 1 & 1 \end{array}\right] \otimes \begin{bmatrix} 1 \\ 1 \\ 1 \end{bmatrix}.$$

The zero rows describe the interior nodes that do not have a direct connection to any boundary edge. Because of the linear independence of the edges e_4, e_5 and e_6, the block in $\nabla_u h(r_I, u)$, corresponding to the block of $[1 \; 1 \; 1] \otimes [1 \; 1 \; 1]^\top$ in this example, has no linearly independent directions, and thus $\nabla_u h(r_F, u)$ has full column rank.

12.2.2 Existence of a Unique Search Direction Δu^κ

With Propositions 12.2 and 12.5, we can choose the weighting matrix Q_r, such that

$$\operatorname{rank}\left(Q_r^{\frac{1}{2}}\left(\nabla_{r_I} h\right)^{-1}\nabla_u h\right) = m_B. \tag{12.11}$$

Note that any positive definite weighting matrix Q_r trivially satisfies (12.11).

We can now state the following.

Lemma 12.1. *If Q_r is chosen such that (12.11) is satisfied, then $\mathcal{P}^\kappa_{\text{SQP}}$ in (12.4) has a unique solution, $\Delta p^\kappa = [\Delta r_I^{\kappa\top},\ \Delta u^{\kappa\top}]^\top$, in each iteration of Algorithm 12.1. Furthermore, LICQ of $\mathcal{P}_{\text{ocp}}$ is fulfilled in each iteration of Algorithm 12.1.*

Proof of Lemma 12.1: To see that Lemma 12.1 holds, we show that:

a) In each iteration, the Jacobian of the equality constraints $h(r_I^\kappa, u^\kappa) = 0$, i.e., $\nabla_{(r_I,u)} h(r_I^\kappa, u^\kappa) \in \mathbb{R}^{3n_I \times 3n_I + m_B}$ has full row rank.

b) The matrix H is positive definite on the tangent space of the constraints, i.e., $\Delta p^{\kappa\top} H \Delta p^\kappa > 0$, $\forall \Delta p^\kappa \neq 0$, s.t. $\nabla_{(r_I,u)} h(r_I, u)\Delta p^\kappa = 0$.

The partial Jacobian $\nabla_{r_I} h(r_I) \in \mathbb{R}^{3n_I \times 3n_I}$ has full rank at any equilibrium configuration r_I, and thus at any feasible iterate, see Proposition 12.2, and therefore a) holds. It implies the linear independence constraint qualification (LICQ) [164], as defined in Section 3.6. To see that b) holds, we note that $\Delta p^{\kappa\top} H\ \Delta p^\kappa = [\Delta r_I^{\kappa\top}\ \Delta u^{\kappa\top}]\text{diag}(Q_r, 0)[\Delta r_I^{\kappa\top}\ \Delta u^{\kappa\top}]^\top = \Delta r_I^\kappa Q_r \Delta r_I^{\kappa\top}$. For all Δp^κ, s.t. $\nabla_{(r_I,u)} h(r_I, u)\Delta p^\kappa = 0$, this is equal to $\Delta u^{\kappa\top} H_u \Delta u^\kappa$, with

$$H_u = \nabla_u h^\top (\nabla_{r_I} h)^{-\top} Q_r (\nabla_{r_I} h)^{-1} \nabla_u h.$$

As Q_r is chosen such that it satisfies (12.11), and with Propositions 12.2 and 12.5, it holds that $H_u > 0$ and thus b) holds. It implies that $\mathcal{P}^\kappa_{\text{SQP}}$ is strictly convex and has a unique solution. □

12.2.3 GN Descent Direction

We show the relationship between the GN directions of $\mathcal{P}_{\text{ocp}}$ and $\mathcal{P}_{\text{ocp,u}}$. Let us denote the GN direction of $\mathcal{P}_{\text{ocp,u}}$ by $\Delta u^\kappa_{\mathcal{P}_{\text{ocp,u}}}$ and the GN direction of $\mathcal{P}_{\text{ocp}}$ by $[\Delta r_I^{\kappa\top},\ \Delta u^{\kappa\top}]^\top$. With the GN approximation of the Hessian, as introduced in Section 3.7.2,

$$\nabla_u^2 f_{\text{ocp,u}}(u^\kappa) \approx (Q_r^{\frac{1}{2}} \nabla_u R(u^\kappa))^\top (Q_r^{\frac{1}{2}} \nabla_u R(u^\kappa)), \tag{12.12}$$

the GN search direction $\Delta u^\kappa_{\mathcal{P}_{\text{ocp,u}}}$ is obtained by solving

$$\begin{aligned} \nabla_u R(u^\kappa)^\top Q_r \nabla_u R(u^\kappa) \Delta u^\kappa_{\mathcal{P}_{\text{ocp,u}}} &= -\nabla_u f_{\text{ocp,u}}(u^\kappa) \\ &= -\nabla_u R(u^\kappa)^\top Q_r (R(u^\kappa) - r_I^{(\text{des})}), \end{aligned} \tag{12.13}$$

which is well-defined because of Theorem 12.2.

We can now state the following.

Lemma 12.2. *In each iteration κ of Algorithm 12.1, the GN search direction $\Delta u^{\kappa}_{\mathcal{P}_{\mathrm{ocp,u}}}$ for $\mathcal{P}_{\mathrm{ocp,u}}$ in* (12.1) *is equal to the Δu^{κ} component of the GN search direction for $\mathcal{P}_{\mathrm{ocp}}$ in* (12.2)*, which is computed by solving $\mathcal{P}^{\kappa}_{\mathrm{SQP}}$ in* (12.4) *in Algorithm 12.1.*

Proof of Lemma 12.2: First, we have to show that $[\Delta r_I^{*\top},\ \Delta u^{*\top}]^{\top} = \arg\min(\mathcal{P}^{\kappa}_{\mathrm{SQP}}) \iff \Delta u^* = \Delta u_{\mathcal{P}_{\mathrm{ocp,u}}} = \arg\min(f^{\mathrm{GN}}_{\mathrm{ocp,u}})$, where $f^{\mathrm{GN}}_{\mathrm{ocp,u}}$ is the optimization problem of obtaining the GN direction of $f_{\mathrm{ocp,u}}$, which is given as

$$f^{\mathrm{GN}}_{\mathrm{ocp,u}}(\Delta u^{\kappa}_{\mathcal{P}_{\mathrm{ocp,u}}}) = \frac{1}{2}\left\| R(u^{\kappa}) - r_I^{(\mathrm{des})} + \nabla_u R(u^{\kappa})\Delta u^{\kappa}_{\mathcal{P}_{\mathrm{ocp,u}}} \right\|^2_{Q_r}. \tag{12.14}$$

With the constraints of $\mathcal{P}^{\kappa}_{\mathrm{SQP}}$, i.e., $\nabla_u h(r_I^{\kappa}, u^{\kappa})\,\Delta u^{\kappa} + \nabla_{r_I} h(r_I^{\kappa}, u^{\kappa})\,\Delta r_I^{\kappa} = 0$, we have

$$\Delta r_I^{\kappa} = -\left(\nabla_{r_I} h(r_I^{\kappa}, u^{\kappa})\right)^{-1} \nabla_u h(r_I^{\kappa}, u^{\kappa})\,\Delta u^{\kappa}.$$

Together with the Implicit Function Theorem, it holds that $\Delta r_I^{\kappa} = \nabla_u R(u^{\kappa})\,\Delta u^{\kappa}$, and together with $R(u^{\kappa}) = r_I^{\kappa}$, the cost functions $f^{\mathrm{GN}}_{\mathrm{ocp,u}}(\Delta u^{\kappa}_{\mathcal{P}_{\mathrm{ocp,u}}})$ in (12.14) and $f^{\mathrm{GN}}_{\mathrm{ocp}}(\Delta r_I^{\kappa})$ in (12.5) are exact reformulations. Therefore, the component Δu^{κ} of the GN direction for $\mathcal{P}_{\mathrm{ocp}}$ is equal to the GN direction $\Delta u^{\kappa}_{\mathcal{P}_{\mathrm{ocp,u}}}$ for $\mathcal{P}_{\mathrm{ocp,u}}$.

Furthermore, because of Lemma 12.1 a), as the constraints of $\mathcal{P}^{\kappa}_{\mathrm{SQP}}$ satisfy the LICQ, the tangent cone of the nonlinear constraints $h(r_I, u) = 0$ and the set of feasible linearized directions of $\mathcal{P}^{\kappa}_{\mathrm{SQP}}$ are equal at the current point, and thus the minimizer of $\mathcal{P}^{\kappa}_{\mathrm{SQP}}$ is the same as the GN direction of $\mathcal{P}_{\mathrm{ocp}}$. □

12.2.4 Main Proof

We have proved that the Δu^{κ} component of the minimizer of $\mathcal{P}^{\kappa}_{\mathrm{SQP}}$ is equal to the GN direction of $\mathcal{P}_{\mathrm{ocp,u}}$. With this result, the remainder of the proof reduces to showing convergence of the GN-iteration on the unconstrained problem $\mathcal{P}_{\mathrm{ocp,u}}$.

Proof of Theorem 12.1: Lemma 12.2 states that Δu^{κ}, obtained from the solution of $\mathcal{P}^{\kappa}_{\mathrm{SQP}}$ in (12.4), is a GN descent direction for the unconstrained $\mathcal{P}_{\mathrm{ocp,u}}$ optimization in (12.1). The line search in Algorithm 12.1 guarantees feasibility of $R(u^{\kappa}+\alpha^{\kappa}\Delta u^{\kappa})$ and satisfaction of the Wolfe conditions in (12.6). The convergence to a critical point of $\mathcal{P}_{\mathrm{ocp,u}}$ follows from Theorem 10.1 in [34]. □

Corollary 12.2. *For fixed model parameters and under the cable net assumptions in Section 10.3, Algorithm 12.1 converges to a KKT point of $\mathcal{P}_{\mathrm{ocp}}$ in* (12.2).

Proof of Corollary 12.2: At the point of convergence, $p = [r_I^\top,\ u^\top]^\top$, the constraints of $\mathcal{P}_{\text{ocp}}$ are satisfied, because $r_I = R(u)$ in (12.8), and therefore $h(r_I, u) = 0$. Under constraint satisfaction, $\mathcal{P}_{\text{ocp}}(r_I, u)$ and $\mathcal{P}_{\text{ocp,u}}(u)$ are equivalent reformulations. Therefore, at the point of convergence, stationarity conditions and constraint satisfaction for $\mathcal{P}_{\text{ocp}}$ hold, and as stated in Lemma 12.1, LICQ for $\mathcal{P}_{\text{ocp}}$ holds, which means that the point of convergence is a KKT-point of $\mathcal{P}_{\text{ocp}}$. □

12.3 Sparse Control Input Computation

Depending on the construction application and the site conditions, the actuation may not be fully automated, or may even be completely manual. For large-scale structures with a large number of boundary edges the process of manually applying inputs can be very time- and labor-intensive. Depending on the deviations in the form that need to be corrected, it can be efficient to apply inputs to only a (possibly small) subset of the boundary edges rather than to adjust all of them. Simulation results suggest that this might not significantly compromise the performance.

Motivated by the goal of making the actuation practically feasible, a sparse input vector is computed. To do so, an additional term is introduced in the cost function to account for the cardinality of the input vector. As proposed in [165] and used in [166], we use the weighted l_1-norm as a convex regularizer for the cardinality. The resulting sparse input vector is denoted by u_{l_1} in the following, and the corresponding cable net configuration $R(u_{l_1})$ is denoted by r_{I,l_1}. The weighted l_1-norm is given by $\|W\, u_{l_1}\|_{l_1} = \sum_i w_i |u_{i,l_1}|$, with W being a diagonal matrix of the weights w_i. The cost function is convex and given by

$$f_{l_1} = f_{\text{ocp}}(r_{I,l_1}, u_{l_1}) + \gamma \, \|W\, u_{l_1}\|_{l_1}, \tag{12.15}$$

with γ a weighting factor. If $\gamma = 0$, the fully actuated solution is achieved, and as γ is increased, the solution becomes more and more sparse. If the weights w_i are chosen to be the inverses of the entries of u_{i,l_1}, then this weighted l_1-norm is equal to the cardinality of u_{l_1}. As the entries u_{i,l_1} are not known a priori, these particular weights cannot be chosen a priori. Therefore, an iterative reweighting scheme is implemented [165], [167]. In the first iteration the initial problem with $\gamma = 0$ is solved. Then, the weights w_i are updated to penalize smaller entries more and more, approximating the cardinality of u_{l_1}.

The sparse OCP, denoted by $\mathcal{P}_{\text{ocp},l_1}$, consists of minimizing f_{l_1} subject to the constraints of $\mathcal{P}_{\text{ocp}}$ and is given as follows

$$\begin{aligned} \text{Problem} \quad & \mathcal{P}_{\text{ocp},l_1} : \\ & \min_{r_{I,l_1}, u_{l_1}} \quad f_{l_1} = f_{\text{ocp}}(r_{I,l_1}, u_{l_1}) + \gamma \, \|W u_{l_1}\|_{l_1} \\ & \text{s.t.} \quad\ \ h(r_{I,l_1}, u_{l_1}) = 0\,. \end{aligned} \tag{12.16}$$

In order to solve Problem $\mathcal{P}_{\text{ocp},l_1}$ by the SQP variant in Section 12.1, we transform it into the following QP.

$$\begin{aligned}
&\text{Problem} \quad \mathcal{P}^{\kappa}_{\text{SQP},l_1}: \\
&\min_{\Delta r^{\kappa}_{I,l_1}, \Delta u^{\kappa}_{l_1}, \beta} \quad f^{\text{GN}}_{l_1} = \frac{1}{2}\left\| r^{\kappa}_{I,l_1} + \Delta r^{\kappa}_{I,l_1} - r^{(\text{des})}_{I} \right\|^2_{Q_r} + \gamma\ (w^{\top}\beta) \\
&\quad \text{s.t.} \qquad (u^{\kappa}_{l_1} + \Delta u^{\kappa}_{l_1}) \leq \beta, \\
&\qquad\qquad -(u^{\kappa}_{l_1} + \Delta u^{\kappa}_{l_1}) \leq \beta, \\
&\qquad\qquad \nabla_{(r_I,u)} h(r^{\kappa}_{I,l_1}, u^{\kappa}_{l_1}) \Delta p^{\kappa} + h(r^{\kappa}_{I,l_1}, u^{\kappa}_{l_1}) = 0,
\end{aligned} \tag{12.17}$$

with w being the vector of the weights w_i. Algorithm 12.2 summarizes the steps for solving $\mathcal{P}_{\text{ocp},l_1}$ using Algorithm 12.1 together with an iterative reweighting scheme of the l_1-norm in the cost function. The result is a sparse input vector u_{l_1}.

Algorithm 12.2 Computation of sparse input vector $u^{(k+1)} = u_{l_1}$ for current measured configuration $r^{\text{meas},(k)}$ corresponding to feasible point $p = [r^{\top}_{I,l_1},\ u^{\top}_{l_1}]^{\top}$, which solves the iteratively reweighted problem $\mathcal{P}_{\text{ocp},l_1}$.

Input: Parameters $\tau > 0$, $\epsilon > 0$, convergence bound c_{w},
Data as in Algorithm 12.1 with initial point $r^{\text{meas},(k)}, u^{(k)}$,
Initialize: Set $\nu = 0$, $\gamma > 0$, $w^0 = 0$,
Perform Algorithm 12.1 for SQP variant on $\mathcal{P}_{\text{ocp},l_1}$ for $r^{\text{meas},(k)}, u^{(k)}$ to obtain initial fully actuated solution u^0,
while $\nu < 1$ **or** $\|w^{\nu} - w^{\nu-1}\| \geq c_w$ **do**
    Set $\nu = \nu + 1$,
    Update weights: $w^{\nu}_i = \frac{\tau}{|u^{\nu-1}_{i,l_1}| + \epsilon}$,
    Algorithm 12.1 for SQP variant on $\mathcal{P}_{\text{ocp},l_1}$ for $r^{\text{meas},(k)}, u^{(k)}$ with w^{ν}
    to obtain $p^{\nu} = [r^{\nu\top}_{I,l_1},\ u^{\nu\top}_{l_1}]^{\top}$,
end
Set $p = p^{\nu}$,
Set $u^{(k+1)} = u^{\nu}$,
Output: Sparse input $u^{(k+1)} = u_{l_1}$.

Remark 12.2. This sparsity-promoting algorithm is possible because the inputs u are optimization variables. This is not the case for a force-density formulation.

12.4 Complete Cable Net Reconfiguration Procedure

The complete control algorithm combines the parameter identification from Chapter 11 and the control input calculation from this chapter. It was introduced in Chapter 9 and illustrated in Figure 9.4. The steps are summarized in Algorithm 12.3.

Remark 12.3. It would be possible to carry out the line search along Δu^κ directly on the cable net by replacing the solution of $\mathcal{P}_{\text{minE}}$ via an actuation and measurement step on the physical cable net. However, such an approach is considered to be too expensive in the construction application. Instead, the combination of parameter identification and model-based optimal control exploits the measurement information and the model knowledge and thus the number of expensive measurements and cable length actuations on the construction site can be reduced.

Algorithm 12.3 Complete control algorithm: Re-identification of the model and computation of (sparse) control inputs in Algorithm 12.1 (12.2).

Input: Target coordinates $r_I^{(\text{des})}$, material parameters EA, convergence bound $c_{\text{c},1}$,
Initialization: Set $k = 1$, $r_I^{\text{meas},(0)} = \infty$, $u^{(1)} = 0$, take first measurement $r^{\text{meas},(1)}$,
while $|\|r_I^{\text{meas},(k)} - r_I^{(\text{des})}\|_{Q_r} - \|r_I^{\text{meas},(k-1)} - r_I^{(\text{des})}\|_{Q_r}| \geq c_{\text{c},1}$ **do**
    Identify $l_0^{(k)}$ as per Algorithm 11.1,
    Update $l_0^{(k)}$ and $\bar{r}_B = r_B^{\text{meas},(k)}$ in $\mathcal{P}_{\text{SQP}}^\kappa$ ($\mathcal{P}_{\text{SQP},l_1}^\kappa$) and $\mathcal{P}_{\text{minE}}$,
    Compute $u^{(k+1)}$ ($u_{l_1}^{(k+1)}$) as per Algorithm 12.1 (12.2)
    with updated models in $\mathcal{P}_{\text{SQP}}^\kappa$ ($\mathcal{P}_{\text{SQP},l_1}^\kappa$) and $\mathcal{P}_{\text{minE}}$,
    Apply $u^{(k+1)}$ ($u_{l_1}^{(k+1)}$),
    Take measurement $r^{\text{meas},(k+1)}$,
    Update measurement data set,
    $k = k + 1$,
end
Output: r_I^{meas}, stationary point of $\|r_I^{\text{meas}} - r_I^{(\text{des})}\|_{Q_r}$.

12.5 Simulation Results

We consider again the model of a 1:4 prototype of the HiLo roof, which will be described in detail in Section 13.1. Simulation results for the control of its geometry from a perturbed configuration with chosen reference inputs to a desired one are presented in the following. For the simulation, feasible desired target coordinates are chosen, i.e., they can exactly be achieved by the cable net. This is a choice, which is not necessary for the control, but which is useful for the validation of the algorithm in simulation, as the global optimal solution to the control problem is thus known.

The parameters used in the simulation are the same as in Section 11.4: The material of the cable net is polyamid $PA6$ with $E = 3000\,\text{Nmm}^2$ and $A = \pi \cdot (3.8\,\text{mm})^2$ for all edges. The cable net has $n_I = 295$ interior nodes and $n_B = 75$ boundary nodes, a total of $m = 606$ edges, whereof $m_B = 75$ boundary edges. The number of boundary edges, m_B, equals the dimension of the input vector, as defined in (10.6). The dimensions of the system are approximately $3\,\text{m} \times 4\,\text{m} \times 2\,\text{m}$.

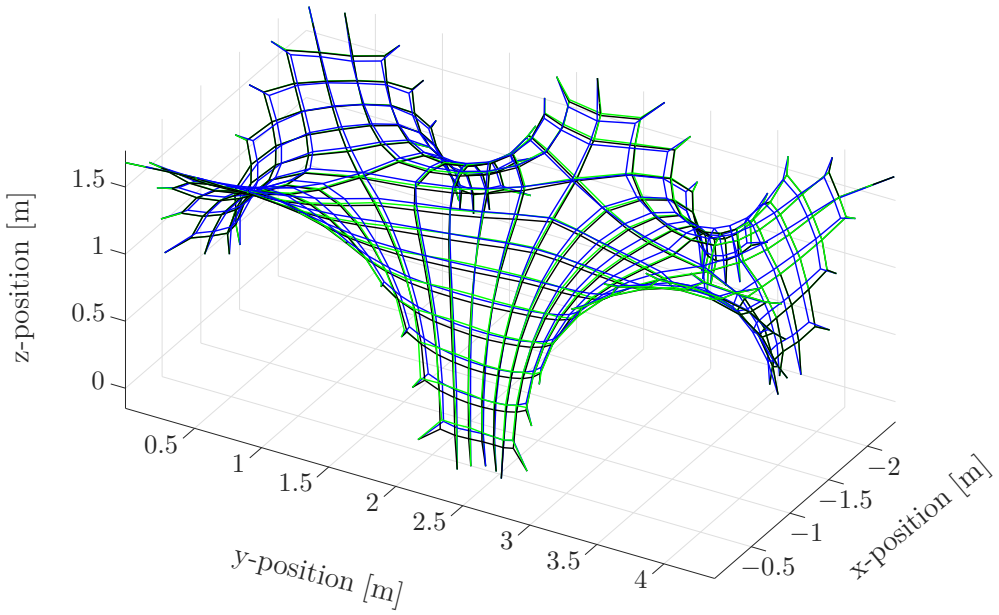

Figure 12.2: — Desired target configuration, — Initial configuration, — Optimal configuration resulting from control input computed in 20 iterations of Algorithm 12.1.

Control Input Computation

We start from an initial perturbed configuration, $r^{(\mathrm{ini})}$, which is obtained by shortening all boundary lengths by 0.05 m with respect to the desired configuration, $r^{(\mathrm{des})}$. This would actually represent a very large deviation for the real application. We assume the parameters of the system are known, as they can be identified. We then perform 20 iterations of Algorithm 12.1 with target coordinates $r_I^{(\mathrm{des})}$ corresponding to the desired unperturbed configuration of the design model. Figure 12.2 shows the initial perturbed configuration, the desired one as well as the one resulting under the applied control input. In Figure 12.3, the decrease of the cost function value is plotted over 20 iterations of Algorithm 12.1. We observe exponential convergence to the global optimum with cost function value zero. Other simulation examples with random perturbations on the boundary edges qualitatively show the same result.

Sparse Control Input Computation

For the sparse input calculations in Algorithm 12.2, the sparsity of the solution and the cost depend on the parameters τ, ϵ and γ. They also depend on the initial solution $u^{(1)}$ of the first iteration $\nu = 1$, with $\gamma = 0$, of Algorithm 12.2. If the vector $u^{(1)}$ contains many small entries compared to other entries and the weights $w_i^{(2)}$ are therefore not all

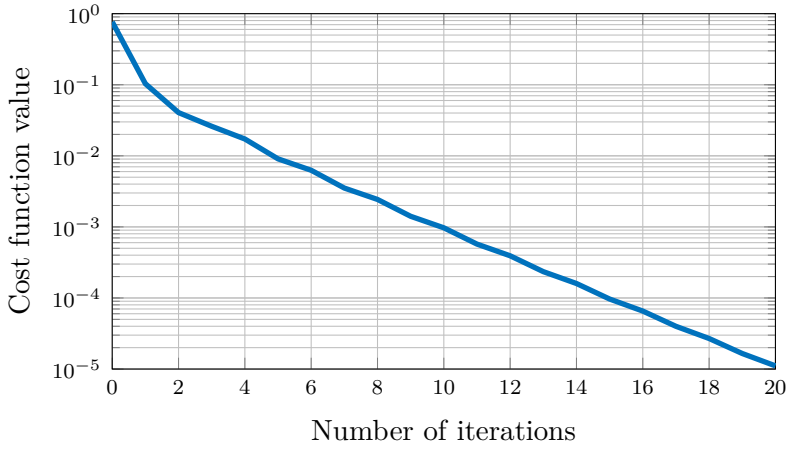

Figure 12.3: Cost function values $\|r_I - r_I^{(\mathrm{des})}\|_2^2$ for 20 iterations of Control Algorithm 12.1

equal, simulations show that Algorithm 12.2 converges to a sparse solution within a few reweighting iterations.

We show a simulation example, where the reference input is randomly chosen from a uniform distribution in the range of 2 cm for all boundary edges. The reference input is illustrated in Figure 12.5 in blue. Four iterations of Algorithm 12.2 are performed, and within each iteration, 10 iterations of Algorithm 12.1 are performed (as described in step 10 of Algorithm 12.2). The cost function values in the iterations of Algorithm 12.2 are shown in Figure 12.4. In the first iteration, a dense input is obtained. At the beginning of iterations 2, 3, and 4, the reweighting in Algorithm 12.2 takes place. The number of edges with zero input at the end of iterations 1, 2, 3 and 4 are 0, 21, 38, and 40, respectively. The resulting sparse input, u_{l_1}, is shown in Figure 12.5 in red.

12.6 Conclusions

For a fixed (re-identified) model of the cable net system, a control algorithm has been presented that is guaranteed to converge to a stationary point of the optimal control problem. An SQP variant has been presented, where the problem structure is exploited in a Gauss-Newton approximation to compute a descent direction, and in a line search for computing the next feasible iterate by convex programming. An extension of the algorithm to compute sparse inputs has been presented.

The control input computation represents the second step in each iteration of the complete cable net reconfiguration. This complete control algorithm has been presented to combine the two steps of model identification and control input computation. An experimental validation of the proposed control algorithm will be presented in Chapter 13.

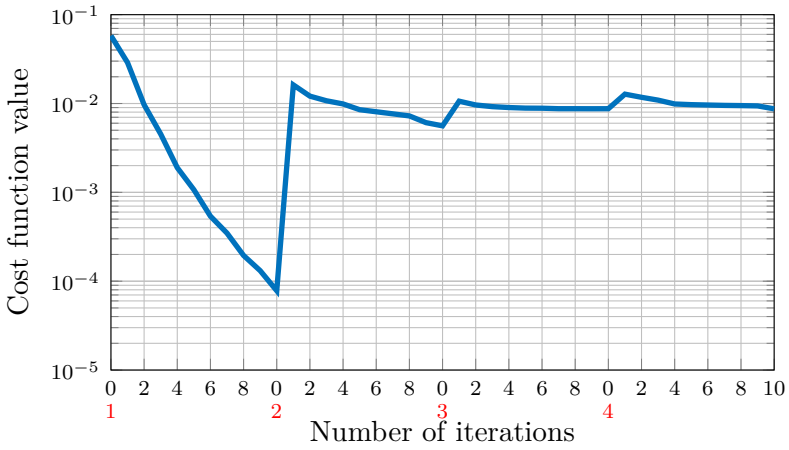

Figure 12.4: Cost function values $\|r_I - r_I^{(\text{des})}\|_2^2$ for 4 iterations of Algorithm 12.2 (indicated with the red labels). Within each of them 10 iterations of Algorithm 12.1 are performed (as shown with the black labels).

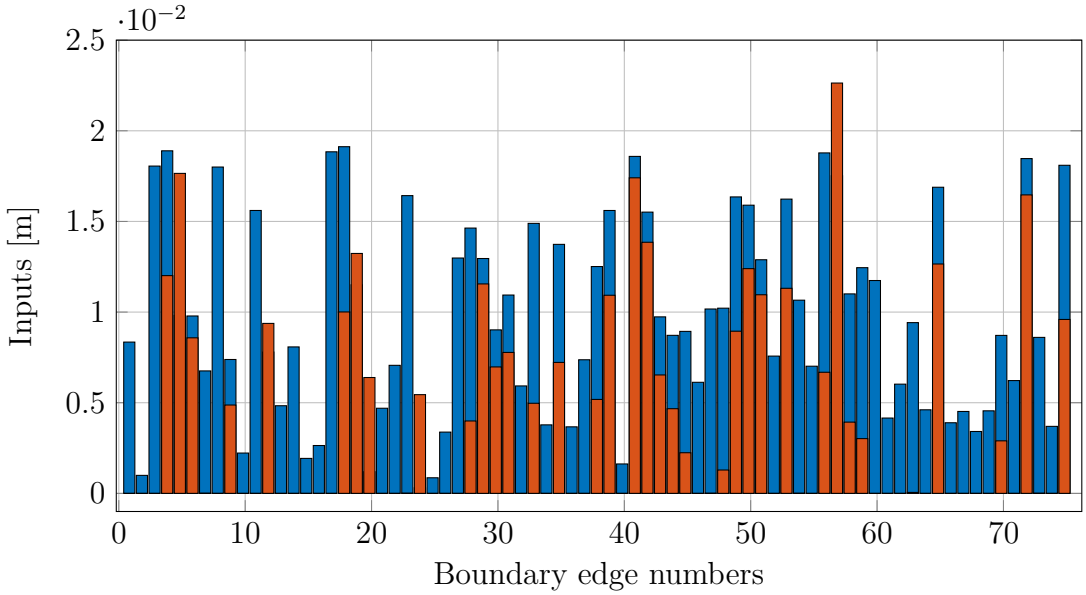

Figure 12.5: Reference input (blue) and sparse solution (red) at the end of 4 iterations of Algorithm 12.2. Boundary edge numbers correspond to a consecutive edge numbering.

CHAPTER 13

Experiments

This chapter presents experimental results on a prototype of the cable net system for the HiLo roof, which was described in Section 9.1.2. The objective is an experimental validation of the complete control loop as presented in Section 9.3.2. The results in this chapter have been published in [18] and [19].

The chapter is structured as follows. Section 13.1 describes the experimental cable net system prototype. In Section 13.2 the measurement process is described. The experimental results are presented in Section 13.3, before Section 13.4 concludes this chapter.

13.1 Prototype Cable Net System

The experimental prototype is based on the design of the HiLo Roof, which will be built on the NEST building [126] as introduced in Section 9.1.2 and illustrated in Figure 9.3. The model has been used in the simulation results in Sections 11.4 and 12.5. It is on a scale of 1:4 with dimensions of approximately $4\,\mathrm{m} \times 3\,\mathrm{m} \times 2\,\mathrm{m}$. The frame supporting the pre-stressed net structure is built as a timber housing. A top view of this prototype is shown in Figure 13.1.

The net is realized using plastic and metal rods rather than wire cables. This however is compatible with our cable net assumptions as the configurations are chosen such that all edges are in tension. In simulation and from measurements, this can be verified by computing Δl for each edge. The edges are connected via steel connectors to steel rings that are the nodes of the net. The net has a total of $n = 295$ nodes, and $m = 606$ edges, including $m_B = 75$ boundary edges, which are connected via turnbuckles to the anchored boundary points on the wooden frame. The realization of the net and the connection to the frame can be seen in Figures 13.2 and 13.3. The edges are constructed from rods of plastic material, PA6. From material tests and connected load cells in the four upper corner edges of the net system, an approximately linear elastic behavior of the material was confirmed during the experiments, with a Young's modulus of $E = 1650\,\mathrm{MPa}$ up until $25\,\mathrm{MPa}$, which is equivalent to a force of $860\,\mathrm{N}$ in the rods. The initial corner rod

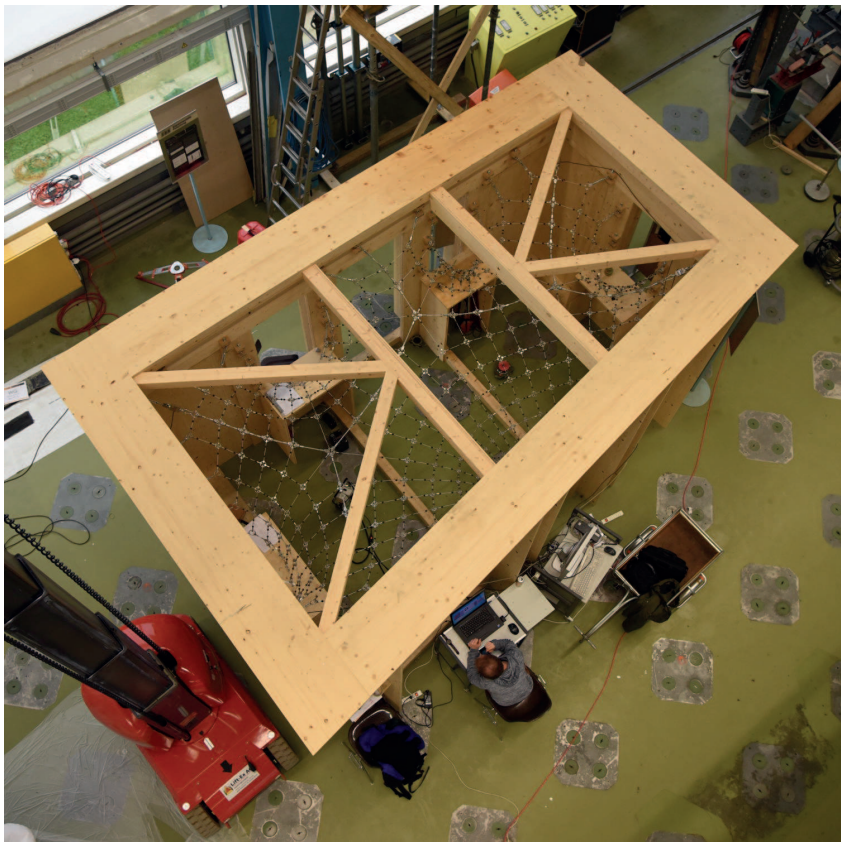

Figure 13.1: Top view of the prototype with stiff wooden frame and cable net structure.

Figure 13.2: Turnbuckle connecting the cable net structure to the boundary node at the wooden frame and realization of a node in the net as ring construction with attached rods and with markers for the image-based measurements.

forces were between 130 N and 170 N, and remained below 415 N, which is less than half of the yield load.

13.2 Measurement Process

While the ideal model of the net consists of lines and ideal intersection points, the nodes of the prototype are realized as ring elements, shown in Figure 13.2. This makes the estimation of the nodal positions of the net more challenging. The nodes of the ideal model in Chapter 10 are defined as the points, where the forces of the adjacent edges balance. For the prototype, these points lie close to the center of the ring elements.

For the experiments, the measurement method is based on image processing. The prototype is equipped with black spherical markers, which can be seen in Figure 13.2. Because of the construction, they cannot be directly attached to the nodes in the center of the rings. Therefore, instead of directly measuring the nodal positions, the measured marker positions are used to estimate the nodal positions. The nodal positions of the k-th measurement are denoted by a superscript $(\cdot)^{\mathrm{meas},(k)}$, i.e., $r_I^{\mathrm{meas},(k)}$, or by $r^{\mathrm{meas},(k)}$.

In order to measure the marker positions, the spatial directions from known reference positions to the markers are measured. Based on these measurements, the positions of the markers are calculated via triangulation. For the measurements of the directions to the markers the vision-based theodolite system QDaedalus [168]–[171], is used in a

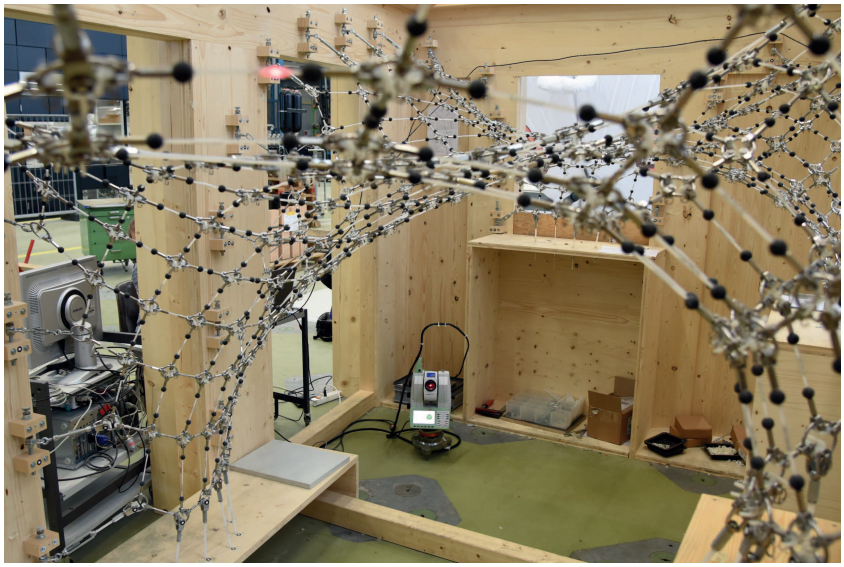

Figure 13.3: Theodolite station underneath the net structure pointing towards a marker.

semi-automated way. In Figure 13.3, the theodolite station which is used to measure the marker positions is shown under the prototype cable net structure. For more details about the measurement method, we refer to [18]. The measured marker positions have sub-millimeter accuracy. We estimate the nodal positions by interpolating the marker positions around each node. The accuracy of this interpolation depends on the locations and number of markers around each node. Near the boundary of the net, the estimated nodal positions were found to be less accurate due to a smaller number of markers and non-uniform marker placement around the nodes.

13.3 Experimental Results

The objective of the experiments is the validation of the control strategy in Algorithm 12.3. In the experiments, we performed only one identification step and one control actuation step, as the control performance was already very good. The details of the identification step and the control step are described in the following.

Parameter Identification

Because of the ring construction, and the necessary interpolation of the measured marker positions, we can estimate the nodal displacements precisely, but the estimated absolute nodal positions are not as accurate. Therefore, we use a simplified approach for determining the l_0 values, instead of the methods proposed in Chapter 11. A simple model is chosen, where the same material properties are assumed for all edges. The first

configuration of the net, $r^{\text{meas},(1)}$, is chosen such that its stress state is approximately uniform. The forces of the edges are at the lower range of possible forces for linear-elastic behavior of the material, however still sufficient to avoid slack edges in the net. This was verified by force measurements at the upper corners of the net and by manual inspection of the edges. We define $u^{(1)} = 0$ and from the measured nodal coordinates of this initial configuration the parameters of the unstressed lengths of the edges, $r^{\text{meas},(1)}$, are determined to be

$$\begin{aligned} l_{0,(s,t)} &= 0.990\ l^{(1)}_{(s,t)}, \quad \text{if } (s,t) \text{ is an elastic edge (plastic rod)}, \\ l_{0,(s,t)} &= 0.999\ l^{(1)}_{(s,t)}, \quad \text{if } (s,t) \text{ is a stiff edge (metal rod)}, \end{aligned} \tag{13.1}$$

where $l^{(1)}_{(s,t)} = \|r^{\text{meas},(1)}_s - r^{\text{meas},(1)}_t\|_2$ is the actual measured length of the edge (s,t) in the initial configuration, denoted by the superscript (1). The stiff edges of the prototype are made of metal because of construction constraints. The choice of the scalings for l_0 in (13.1) is based on the following relation, which holds for the plastic rods,

$$\begin{aligned} f^{\text{elast}}_{(s,t)} &= EA_{(s,t)} \frac{\Delta l_{(s,t)}}{l_{0,(s,t)}} \iff \\ \frac{\Delta l_{(s,t)}}{l_{0,(s,t)}} &= \frac{f^{\text{elast}}_{(s,t)}}{EA_{(s,t)}} = \frac{150\,\text{N}}{1.65 \times 10^9 \frac{\text{N}}{\text{m}^2} \pi (32.4\,\text{mm})^2} \approx 0.01, \end{aligned}$$

where $EA_{(s,t)} = 1.65 \times 10^9 \frac{\text{N}}{\text{m}^2} \pi (32.4\,\text{mm})^2$ is given and $f^{\text{elast}}_{(s,t)} = 150\,\text{N}$ was measured. The strain $\Delta l / l_0$ of the plastic rod edges is therefore $\approx 1\%$. Based on the assumption of a uniform stress state in the initial measured configuration, a uniform strain is assumed for all plastic edges. For the metal edges, the Young's modulus is higher by approximately a factor of 100. Precisely accounting for this would lead to a model for which the derivatives of the edge forces would have values in significantly different ranges and the optimization problem in (12.2) would become harder to solve numerically. Therefore, the parameters of $l_{0,(s,t)}$ for the stiff edges are chosen as in (13.1). For comparison, the model with higher values of stiffness for the metal rods was used in a simulation study with a small step size and required many more iterations to converge. It was confirmed that the simplified model assumptions do not compromise the precision of the simulation results.

After this initial measurement for determining the unstressed lengths $l^{(1)}_0$, several additional configurations were used to validate the identified model behavior. Nodal positions were computed from the model, the identified parameters, the measured boundary coordinates, and the inputs of the configurations. These nodal positions were then compared to the measured positions. The comparison showed a good match between the computed model behavior and the behavior of the experimental prototype in terms of the displacement of the nodes under the applied inputs. However, the match between the simulated and estimated absolute position coordinates was not very accurate for some nodes and had a large variation over the net. Possible reasons for this are the inaccuracies

in the nodal position estimates introduced by interpolating the measured marker positions from a small number of markers, and from non-uniformly placed markers around the nodes. This appears especially at the boundary regions of the net due to construction limitations. To reduce the effect of this estimation error in the absolute nodal positions, the weighting matrix Q_r is chosen such that it gives more weight to the coordinates that more precisely match the simulated nodal coordinates. This leads to control inputs that correct for the control error rather than correcting for the measurement interpolation errors.

Control of the Nodal Positions

In the second phase of the experiments, the goal was to compute and apply (dense and sparse) control inputs, corresponding to the second part of the control algorithm, and to evaluate the resulting control performance. We use the superscripts (ini), (des), and (con) to denote the initial, desired and controlled configurations. As before, the controlled configuration resulting from a sparse input vector u_{l_1} is denoted by $r_{l_1}^{(\mathrm{con})}$.

We present the results of one of several control experiments, as it is representative of the observed control performance. Figure 13.4 shows the manual process of applying the computed control inputs to the prototype system and a motivation for computing sparse input vectors. The turnbuckles are manually actuated to adjust the unstressed lengths of the corresponding boundary edges, while measuring the change in unstressed lengths via calipers. In Figure 13.5, the three measured configurations of the 1:4 HiLo roof prototype are shown. Blue depicts the initial configuration, $r^{(\mathrm{ini})}$. Black shows the desired target configuration, $r^{(\mathrm{des})}$, and green shows the resulting controlled configuration, $r_{l_1}^{(\mathrm{con})}$, after applying the computed sparse inputs. The red triangles ▲, and black diamonds ♦, show the actuated boundary edges, which are lengthened and shortened, respectively.

In order to be able to evaluate the control performance, the target configuration $r^{(\mathrm{des})}$ is defined by measuring an actual configuration. This has the advantage of knowing that the target is achievable, and also specifies the inputs required to achieve it. Furthermore, we know that the stress state corresponding to this configuration lies within the range of the linear material behavior of the edges, and that no slack edges are present. The control experiment is then started from an initial configuration, $r^{(\mathrm{ini})}$, which is achieved by perturbing the target configuration, $r^{(\mathrm{des})}$. The inputs that would then result in the target configuration are depicted in Figure 13.6 as a reference. Their input locations correspond to the ones shown in Figure 13.5 by red triangles ▲, and black diamonds ♦. Note that $r^{(\mathrm{ini})}$ and $r^{(\mathrm{con})}$ correspond to $r^{\mathrm{meas},(1)}$ and $r^{\mathrm{meas},(2)}$, respectively, in Algorithm 12.3, since only one iteration is performed. However, in the experiments, we chose the starting configuration to be different from the $r^{\mathrm{meas},(1)}$, as explained before. For comparison, both the fully actuated and the sparse input vectors are computed and their performance is compared in terms of the error norms $\|r^{(\mathrm{des})} - r^{(\mathrm{con})}\|_{Q_r}^2$ and $\|r^{(\mathrm{des})} - r_{l_1}^{(\mathrm{con})}\|_{Q_r}^2$, respectively.

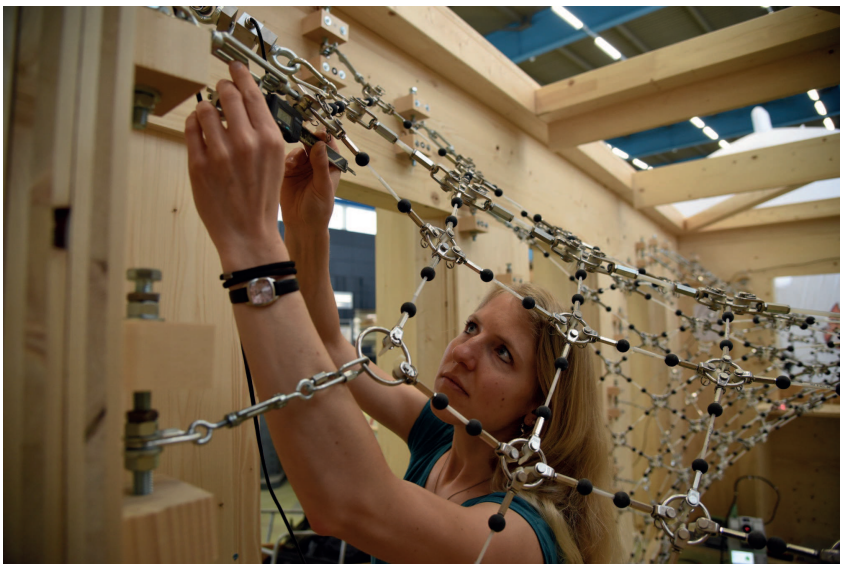

Figure 13.4: Manual application of control actions: Measuring the changes in lengths of the boundary edges by calipers and adjusting the turnbuckles to apply the computed control inputs.

Note that in this case the solution is known to be sparse because of the chosen configuration of the initial condition and the target. Figure 13.6 shows the fully actuated control input vector u computed by Algorithm 12.1 with parameters $c_1 = 10^{-4}$, $c_2 = 0.9$ and $\rho = 0.8$ in the line search in (12.6) and in the backtracking. Figure 13.7 shows the sparse input vector u_{l_1} resulting from Algorithm 12.2 with parameters $\tau = 10^{-4}$, $\epsilon = 10^{-8}$ and $\gamma = 0.3$. In the experiment, only the sparse input vector is applied to the prototype leading from the initial perturbed (blue) configuration, $r^{(\mathrm{ini})}$, to the controlled (green) one, $r_{l_1}^{(\mathrm{con})}$. Because of the very good control performance, only one control iteration was performed on the prototype. The fully actuated control input vector u is not experimentally applied to the prototype system. However, in simulation, both u and the sparse u_{l_1} can be compared. With $r^{(\mathrm{con})}$ and $r_{l_1}^{(\mathrm{con})}$ being the minimizers of Problem $\mathcal{P}_{\mathrm{minE}}$ for the fully actuated u and the sparse u_{l_1}, the error norms are $\|r^{(\mathrm{des})} - r^{(\mathrm{con})}\|_{Q_r}^2 = 1.669 \times 10^{-3}\,\mathrm{m}^2$ and $\|r^{(\mathrm{des})} - r_{l_1}^{(\mathrm{con})}\|_{Q_r}^2 = 1.883 \times 10^{-3}\,\mathrm{m}^2$, respectively.

The experiments on the prototype show the following control performance. The measured data reveal that the error norm is decreased by 98.8%, from $\|r^{(\mathrm{des})} - r^{(\mathrm{ini})}\|_{Q_r}^2 = 1.55{\times}10^{-2}\,\mathrm{m}^2$ to $\|r^{(\mathrm{des})} - r_{l_1}^{(\mathrm{con})}\|_{Q_r}^2 = 1.82{\times}10^{-4}\,\mathrm{m}^2$. The unweighted error norm of the deviations is decreased by 98.7% from $\|r^{(\mathrm{des})} - r^{(\mathrm{ini})}\|_2^2 = 2.21 \times 10^{-2}\,\mathrm{m}^2$ to $\|r^{(\mathrm{des})} - r_{l_1}^{(\mathrm{con})}\|_2^2 = 2.81 \times 10^{-4}\,\mathrm{m}^2$. The RMS-error, defined by $\|r^{(\mathrm{des})} - r_{l_1}^{(\mathrm{con})}\|_2/n$, decreased by 88.5% from 0.134 mm to 0.0154 mm. Figure 13.8 shows the spatial distribution of the initial nodal position errors over the net. The spatial distribution of the controlled nodal position errors is shown in Figure 13.9. Figure 13.10 shows the histogram of the distribution

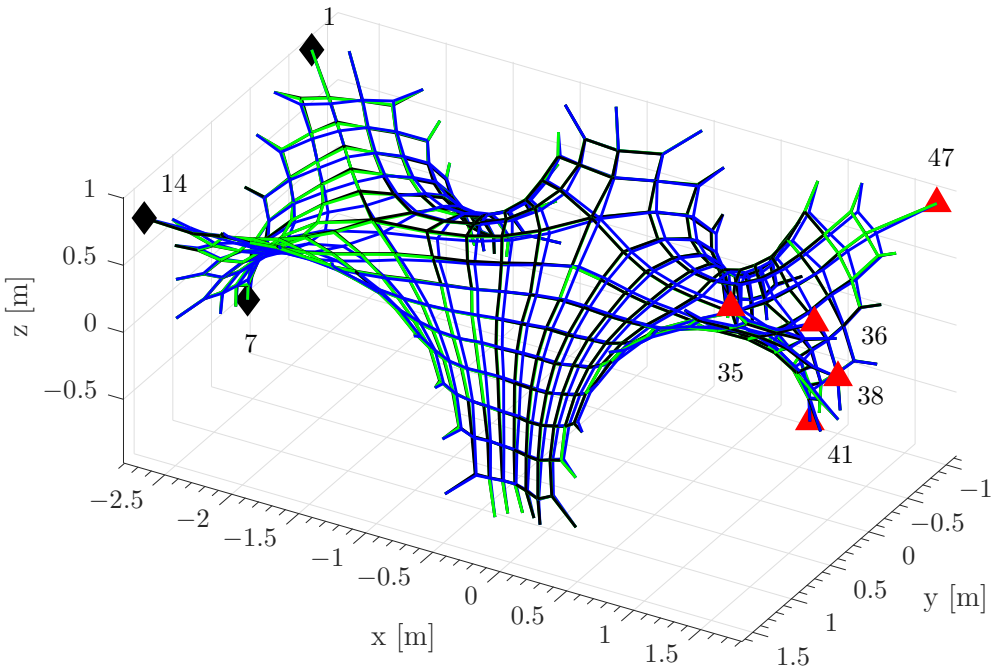

Figure 13.5: Measured configurations: — Initial configuration $r^{(\mathrm{ini})}$, — Desired configuration $r^{(\mathrm{des})}$, — Controlled configuration $r_{l_1}^{(\mathrm{con})}$. Displacements of configurations $r^{(\mathrm{des})}$ and $r_{l_1}^{(\mathrm{con})}$ relative to initial configuration $r^{(\mathrm{ini})}$ are shown scaled by a factor of five for better visualization. ▲ Lengthened edges, ♦ Shortened edges. The displayed numbers of the actuated edges correspond to a consecutive edge numbering.

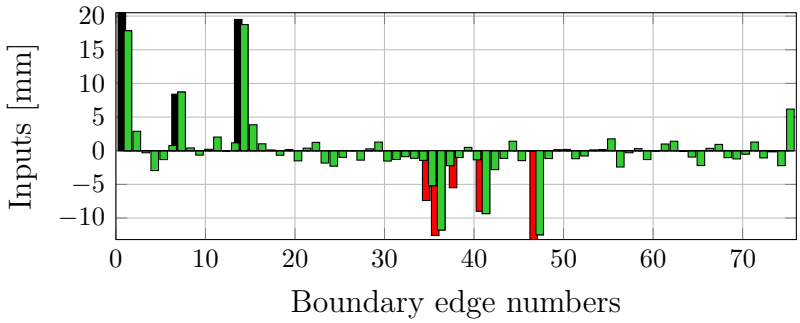

Figure 13.6: Reference inputs for shortening and for lengthening to steer the initial perturbed configuration $r^{(\mathrm{ini})}$ to the desired target configuration $r^{(\mathrm{des})}$, Computed fully actuated control inputs from Algorithm 12.1.

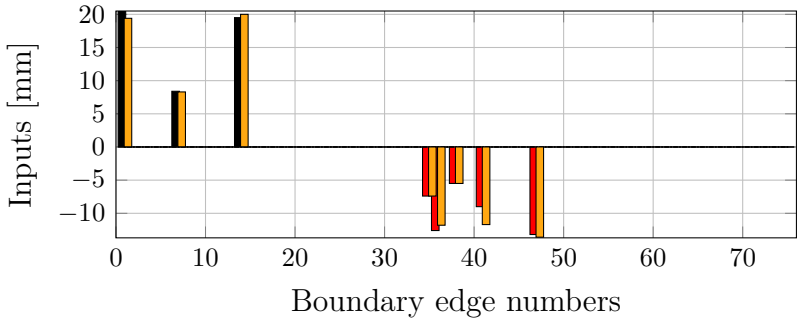

Figure 13.7: Reference inputs for shortening and for lengthening to steer the initial perturbed configuration $r^{(\mathrm{ini})}$ to the desired target configuration $r^{(\mathrm{des})}$, Computed sparse control inputs by Algorithm 12.2.

of the measured deviation before and after the control on the prototype in terms of the Euclidean distances. The highest deviations can be seen in the z-coordinates, which are corrected from initial errors of more than 15 mm to final errors of approximately 2 mm.

13.4 Conclusions

This chapter presented experimental results conducted on a cable net system prototype for a lightweight concrete shell structure. Some details in the construction elements, such as the ring and marker design should be modified to reduce errors in the measurement of the nodal positions. Despite these inaccuracies, the experiments showed a very good control performance. With only one control iteration and a sparse input actuation, the control is very efficient to implement in practice.

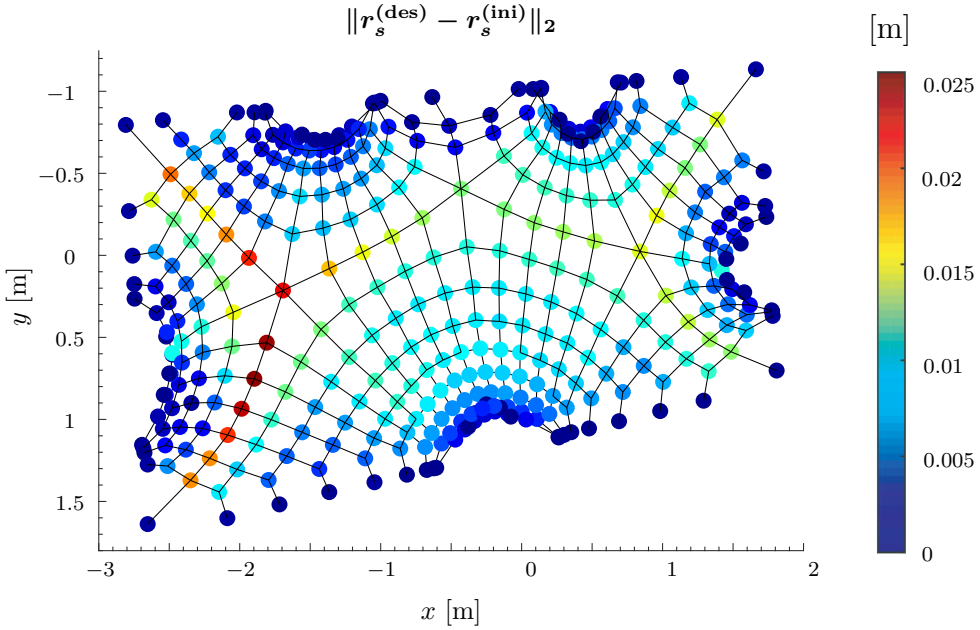

Figure 13.8: Control scenario with sparse actuation. Initial errors $\|r_s^{(\mathrm{des})} - r_s^{(\mathrm{ini})}\|_2$, the distance between the initial configuration $r_s^{(\mathrm{ini})}$ and the desired coordinates $r_s^{(\mathrm{des})}$, for each node.

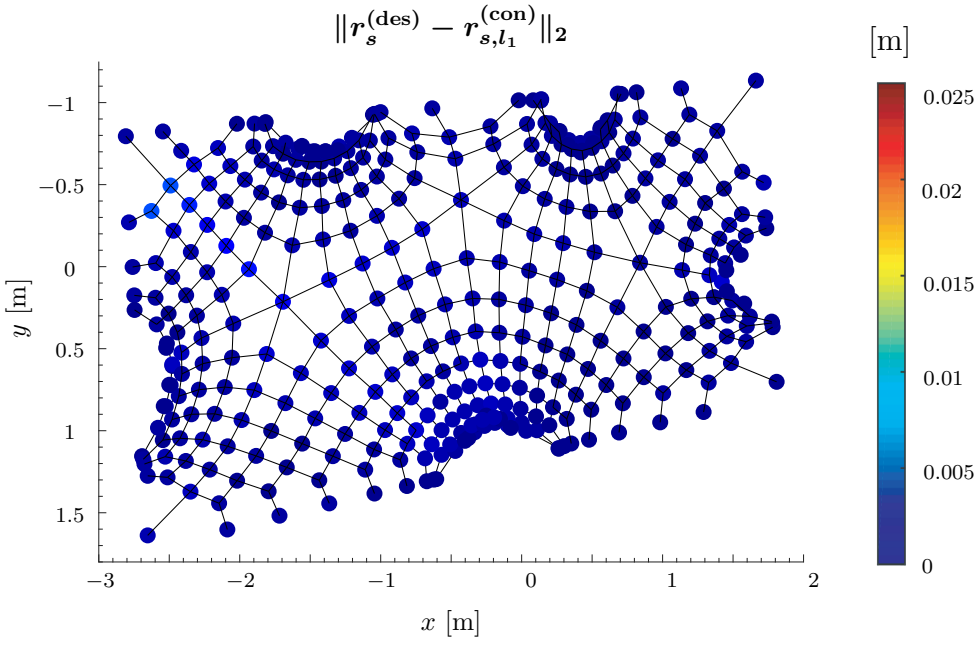

Figure 13.9: Control scenario with sparse actuation. Controlled errors $\|r_s^{(\mathrm{des})} - r_{s,l_1}^{(\mathrm{con})}\|_2$, the distance between the controlled coordinates, $r_{s,l_1}^{(\mathrm{con})}$, and the desired coordinates, $r_s^{(\mathrm{des})}$, for each node.

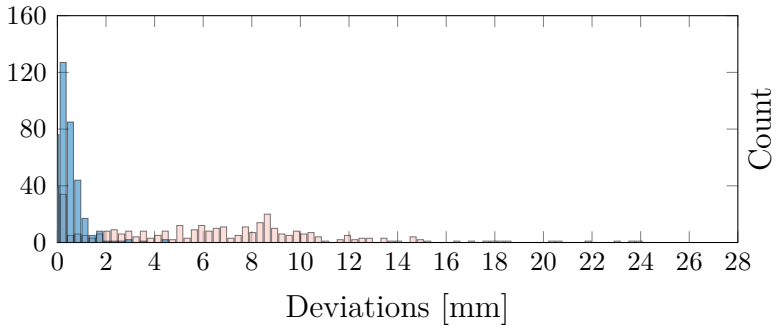

Figure 13.10: Histograms of the distances from the initial coordinates to the desired ones: $\|r_s^{(\mathrm{des})} - r_s^{(\mathrm{ini})}\|_2$ from the controlled coordinates to the desired ones: $\|r_s^{(\mathrm{des})} - r_{s,l_1}^{(\mathrm{con})}\|_2$, for all nodes $s = 1, ..., n$.

Part IV

Conclusions

CHAPTER 14

Conclusions and Outlook

The work presented in this thesis focuses on different aspects of digital fabrication. This chapter summarizes the results, draws conclusions and provides an outlook on possible future research directions.

14.1 Conclusions of Part II: Control of Interconnected Systems

Automating construction processes, which are mostly performed manually to date, would allow for more efficiency and precision in building construction. Because construction tasks are typically complex, the potential that multiple cooperating robots provide can be leveraged. Such multi-agent systems can be modeled as heterogeneous interconnected systems with communication restrictions. Part II presents methods and results for dealing with key challenges that arise when controlling such systems.

14.1.1 Conclusions

In order to overcome the computational challenges related to the controller design for large-scale interconnected systems, a scalable method was proposed. Scalability is achieved in two aspects. First, applying the full block S-Procedure (FBSP) allowed us to decompose the controller synthesis matrix inequalities into smaller ones that are in the order of the individual subsystems. Second, we proposed a distributed synthesis method based on an ADMM scheme with only nearest neighbor communication and without a central coordinator. While these methods are applicable to general heterogeneous systems, we introduced a new class of systems that describes systems for which the subsystems and interconnections can be grouped. This class of so-called α-β-heterogeneous systems thus consists of α groups of homogeneous subsystems with β different interconnection types. We showed how the model for heterogeneous systems is transformed into a more compact form in the case of small values of α and β. This also implies an

improved scalability of the decomposed controller synthesis. Furthermore, the methods allow for different interconnection topologies of the plant and the controller.

In order to increase the achievable control performance in the case of a decentralized control architecture, an augmented overlapping control scheme was proposed. Through the augmentation of the state space representation with copies of states of neighboring subsystems, the local model knowledge of the individual subsystems is increased. Thus the performance is improved without introducing explicit communication. The augmented overlapping controller can be interpreted as a higher order decentralized controller or as a controller with less structure, i.e., a distributed instead of a decentralized structure, when contracted back to the original state space.

The problem of decentralized fixed modes (DFMs), which can destabilize the system or limit the performance, was addressed. Methods to find a minimum communication topology that eliminates all DFMs were proposed. Based on the formulation as a submodular set cover problem, either a polynomial-time but suboptimal greedy algorithm or an efficient tree search algorithm that finds the minimal sets of communication links, can be applied.

14.1.2 Outlook

The presented results lead to further potential research directions. Some ideas are presented in the following.

Reduction of Conservatism

The structural assumptions on the Lyapunov matrix and multiplier matrices, which are necessary to decompose the synthesis equations, introduce conservatism. A detailed analysis of this source of conservatism is required in order to increase the achievable performance by relaxing the corresponding structural constraints. Relaxing these constraints implies less structured Lyapunov and multiplier matrices, and thus potentially more coupling between the decomposed synthesis conditions. In preliminary work we have explored a direction of extending the controller synthesis conditions with an instrumental variable which avoids terms containing products of the Lyapunov matrix and controller gains. This approach allows a free choice of the structure of the Lyapunov matrix and the multiplier matrices. In particular, choosing them with the same structure as the interconnection matrix allows again for an efficient decomposition of the synthesis equations. Preliminary results show the potential of improving the control performance and thus reducing the conservatism.

More General System Classes and Interconnections

Although not considered in this thesis, the modeling framework allows for an extension to more general system classes and interconnections. In particular, the modeling framework based on a linear fractional representation (LFR) of the system can represent interconnected systems with linear parameter varying (LPV) subsystems. This provides the possibility to model uncertain, time-varying, or nonlinear dynamics of subsystems. The interconnection operator can also capture uncertainties, such as parametric or time-varying uncertainties, or switching topologies. Based on the FBSP, a robust or gain-scheduled controller design can be performed. Further extensions, such as time-delayed interconnections, are possible within the broader framework of integral quadratic constraints (IQCs), of which the FBSP can be seen as a special case.

Elimination of FMs through Sensing or Actuatuation

The methods presented for the elimination of FMs in Chapter 8 focus on introducing communication links between the subcontrollers. The minimum cost coverage problem formulation with submodular constraints can easily be extended to include the addition of sensors or actuators. Both the greedy algorithm as well as the tree search algorithm can be applied. However, the complexity in each iteration grows with the degrees of freedom.

14.2 Conclusions of Part III: Control of a Cable Net Structure

Part III of the thesis introduced a feedback-based form control of a tensioned cable net which enables a novel construction method for lightweight structures.

14.2.1 Conclusions

A new control application was presented which enables a precise construction of lightweight building structures such as thin concrete shells. Feedback-based form control is introduced in order to precisely achieve the designed form of a cable net formwork. Precision in the form of the pre-stressed cable net is necessary to guarantee the desired mechanical properties of the thin concrete shell structures. The proposed form control is therefore essential for enabling this novel construction method with flexible formwork. The benefits of the cable net based formwork include a reduction of material and waste, which is partially due to the possibility of re-using the cable net elements. This also leads to a reduction in cost. These benefits can favor a broader use of lightweight thin concrete shell elements in future constructions.

The form control is based on measurements of nodal positions of the cable net and adjustments of the boundary edge lengths. For an efficient control, the number of expensive measurements and actuations on-site is minimized. This is achieved through an iterative two-step control algorithm which exploits model knowledge as well as measurement data. Based on the form measurements, the algorithm iteratively updates the model parameters and then computes control inputs to minimize the error norm between the measured and desired form of the cable net. The parameter identification is based on a distributed optimization algorithm. The control input calculation is an SQP variant where all iterates are feasible. This prevents the algorithm from converging to stationary points of local infeasibility. The feasible iterates are efficiently computed by convex programming. Convergence of the algorithm to a feasible stationary point of the optimal control problem was proved. For practical application, sparse input vectors can be enforced by adding an l_1-norm regularization term to the cost. The sparse input further reduces the time and cost of actuations. A prototype of a cable net based formwork for the construction of a lightweight roof was used for an experimental assessment of the method. The experiments showed very good control performance.

14.2.2 Outlook

The results of this work can be extended to consider the following research questions.

Stress Bounds

If the structural design is optimized for minimal material use, the structural robustness with respect to possible control inputs can be compromised. In this case, additional constraints, which account for possible bounds on the maximum allowable stresses within the cable net elements, should be introduced. A design which is structurally robust against all necessary control actuations, and can thus tolerate all forces caused by the control, would, however, be a more desirable approach with respect to the achievable control performance.

Uncertainties and Robust Approaches

In addition to errors in the unstressed cable lengths, there are other uncertainties and sources of model mismatch, such as nonlinear material behavior or uncertainties in the load distribution. They could be incorporated in the proposed model identification. In this work, two steps of identifying an exact model and applying control inputs computed based on the identified model, were proposed. Alternatively, a robust control approach, which is robust against possible model mismatch and uncertainties, could be implemented. This could however compromise the achievable precision of the cable net form. Some first results in this direction will be published in [172].

Furthermore, the initial design problem of the cable net could be modified. Instead of solving a nominal form design problem, which defines the topology of the net and the force distribution within the cable elements without taking into account any uncertainties, the fabrication tolerances could be directly included in a robust design problem. This would lead to a robustness of the cable net form with respect to pre-specified uncertainties in the model or load.

Controllability and Actuation

The cable net is highly underactuated because all nodal positions in the interior of the net are controlled by possible adjustments at the few boundary edges of the net. Therefore, not any desired form of the net is achievable. Relating the ratio between the number of boundary edges and the number of interior nodes to some notion of controllability would be an interesting analysis.

The controllability could be improved by introducing more possibilities of actuation, which are not limited to the boundary edges. Changing the lengths of interior edges may be possible but would not be very practical. Alternatively, interior nodal positions could directly be controlled by different methods of actuation, for example by strings that are attached to interior nodes and anchored to the ground.

More General Forms

The presented cable net system is a very efficient structure. It gains stability and rigidity from the prestressing forces, which allows for a reduction of the required material. However, the forms of the cable net are limited to doubly-curved surfaces. The use of different structural elements in addition to cables is a possible approach to extend the types of forms that can be considered. Bending elements, such as gridshells [173], gain stiffness through internal moments and are another class of efficient structural elements that are interesting in this context. However, with an increased complexity in the form comes an increased difficulty in analytical modeling. As a possible direction to mitigate this challenge, a data-driven approach for parameter identification will be presented in [174].

Part V

Appendices

APPENDIX A

Appendices

In the following, details about the linearizing variable transformations and the iterative solution method for dynamic output feedback control in (5.34) are presented. They will be used in Chapter 7 in a numerical example. For the case of static state feedback control, the convexifying variable substitution of (5.34) is given. Then, the derivation of the consensus ADMM update steps in Algorithm 5.1 is presented.

A.1 Dynamic Output Feedback Controller Synthesis

The multiplier condition in (5.33) is convex, however, the nominal condition in (5.34) with the closed-loop matrices in (5.23) is not convex. This is due to the terms that involve products of the Lyapunov matrix with controller matrices and products of the controller matrices with themselves and with multiplier matrices. Therefore, first a linearizing variable transformation is applied, which eliminates the product terms with the Lyapunov matrix. However, the transformed equations still involve bilinear terms of the multipliers and the interconnection output matrix, which need to be solved in an iterative way.

Variable Transformation

In the following, we perform the variable transformation [68] from the Lyapunov matrix $\mathcal{X}$ and the controller gains, given as

$$\begin{aligned}&(A^{Kd},\ A^{Ki},\ B^{Kd},\ B^{Ki},\ C^{Kd},\ C^{Ki},\ D^{Kd},\ D^{Ki},\ \mathcal{X})\\ \text{to }&(\boldsymbol{A^{Kd}},\ \boldsymbol{A^{Ki}},\ \boldsymbol{B^{Kd}},\ \boldsymbol{B^{Ki}},\ \boldsymbol{C^{Kd}},\ \boldsymbol{C^{Ki}},\ \boldsymbol{D^{Kd}},\ \boldsymbol{D^{Ki}},\ Z,\ Y),\end{aligned} \tag{A.1}$$

with the symmetric matrices Z, Y, and the transformed controller gains in bold. As proposed in [68], the following congruence transformation is applied to the nominal condition in (5.34). Defining

$$T_Y = \begin{bmatrix} Y & I \\ V^\top & 0 \end{bmatrix}, \quad T_Z = \begin{bmatrix} I & Z \\ 0 & U^\top \end{bmatrix}, \tag{A.2}$$

with $\mathcal{X}T_Y = T_Z$, and $Z, Y > 0$ and U, V such that $I - ZY = UV^\top$, this leads to the following transformed nominal condition

$$\left[\star\right]^\top \left[\begin{array}{cc:cc:cc} 0 & I & 0 & 0 & 0 & 0 \\ I & 0 & 0 & 0 & 0 & 0 \\ \hdashline 0 & 0 & -\gamma^2 I & 0 & 0 & 0 \\ 0 & 0 & 0 & I & 0 & 0 \\ \hdashline 0 & 0 & 0 & 0 & \tilde{Q}_i & \tilde{S}_i \\ 0 & 0 & 0 & 0 & \tilde{S}_i^\top & \tilde{R}_i \end{array}\right] \left[\begin{array}{ccc} I & 0 & 0 \\ T_Z^\top \mathcal{A}_i T_Y & T_Z^\top \mathcal{B}_{1,i} & T_Z^\top \mathcal{B}_{2,i} \\ \hdashline 0 & I & 0 \\ \mathcal{C}_{1,i} T_Y & \mathcal{D}_{11,i} & \mathcal{D}_{12,i} \\ \hdashline 0 & 0 & I \\ \mathcal{C}_{2,i} T_Y & \mathcal{D}_{21,i} & \mathcal{D}_{22,i} \end{array}\right] < 0, \tag{A.3}$$

with the following transformed closed-loop matrices in bold

$$\left[\begin{array}{c:c:c} T_Z^\top \mathcal{A}_i T_Y & T_Z^\top \mathcal{B}_{1,i} & T_Z^\top \mathcal{B}_{2,i} \\ \hdashline \mathcal{C}_{1,i} T_Y & \mathcal{D}_{11,i} & \mathcal{D}_{12,i} \\ \hdashline \mathcal{C}_{2,i} T_Y & \mathcal{D}_{21,i} & \mathcal{D}_{22,i} \end{array}\right] = \left[\begin{array}{c:c:c} \boldsymbol{\mathcal{A}}_i & \boldsymbol{\mathcal{B}}_{1,i} & \boldsymbol{\mathcal{B}}_{2,i} \\ \hdashline \boldsymbol{\mathcal{C}}_{1,i} & \boldsymbol{\mathcal{D}}_{11,i} & \boldsymbol{\mathcal{D}}_{12,i} \\ \hdashline \boldsymbol{\mathcal{C}}_{2,i} & \boldsymbol{\mathcal{D}}_{21,i} & \boldsymbol{\mathcal{D}}_{22,i} \end{array}\right]. \tag{A.4}$$

With the closed-loop matrices from (5.23), the expressions in (A.4) can be factorized into

$$\left[\begin{array}{cc:c:cc} A_i Y & A_i & B_{w_i} & B_{p_i} & 0 \\ 0 & Z A_i & Z B_{w_i} & Z B_{p_i} & 0 \\ \hdashline C_{z_i} Y & C_{z_i} & D_{zw_i} & D_{zp_i} & 0 \\ \hdashline C_{q_i} Y & C_{q_i} & D_{qw_i} & 0 & 0 \\ V^\top & 0 & 0 & 0 & 0 \\ C_{y_i} Y & C_{y_i} & D_{yw_i} & 0 & I \end{array}\right] + \left[\begin{array}{cc} 0 & B_{u_i} \\ I & 0 \\ 0 & D_{zu_i} \\ 0 & D_{qu_i} \\ 0 & 0 \\ 0 & 0 \end{array}\right] \left[\begin{array}{cccc} \boldsymbol{A}^{\boldsymbol{K}^d}_i & \boldsymbol{A}^{\boldsymbol{K}^i}_i & \boldsymbol{B}^{\boldsymbol{K}^d}_i & \boldsymbol{B}^{\boldsymbol{K}^i}_i \\ \boldsymbol{C}^{\boldsymbol{K}^d}_i & \boldsymbol{C}^{\boldsymbol{K}^i}_i & \boldsymbol{D}^{\boldsymbol{K}^d}_i & \boldsymbol{D}^{\boldsymbol{K}^i}_i \end{array}\right] \left[\begin{array}{cc:c:ccc} I & 0 & 0 & 0 & 0 & 0 \\ 0 & 0 & 0 & 0 & I & 0 \\ 0 & C_{y_i} & D_{yw_i} & 0 & 0 & 0 \\ 0 & 0 & 0 & 0 & 0 & I \end{array}\right], \tag{A.5}$$

with

$$\left[\begin{array}{cc} \boldsymbol{A}^{\boldsymbol{K}^d}_i & \boldsymbol{A}^{\boldsymbol{K}^i}_i \\ \boldsymbol{C}^{\boldsymbol{K}^d}_i & \boldsymbol{C}^{\boldsymbol{K}^i}_i \end{array}\right.\left.\begin{array}{cc} \boldsymbol{B}^{\boldsymbol{K}^d}_i & \boldsymbol{B}^{\boldsymbol{K}^i}_i \\ \boldsymbol{D}^{\boldsymbol{K}^d}_i & \boldsymbol{D}^{\boldsymbol{K}^i}_i \end{array}\right] = \left[\begin{array}{cccc} Z A_i Y & 0 & 0 & 0 \\ 0 & 0 & 0 & 0 \end{array}\right] + \left[\begin{array}{cc} U & Z B_{u_i} \\ 0 & I \end{array}\right] \left[\begin{array}{cc} A^{K^d}_i & A^{K^i}_i \\ C^{K^d}_i & C^{K^i}_i \end{array}\right.\left.\begin{array}{cc} B^{K^d}_i & B^{K^i}_i \\ D^{K^d}_i & D^{K^i}_i \end{array}\right] \left[\begin{array}{cccc} V^\top & 0 & 0 & 0 \\ 0 & I & 0 & 0 \\ C_{y_i} Y & 0 & I & 0 \\ 0 & 0 & 0 & I \end{array}\right]. \tag{A.6}$$

As defined before, the controller matrices denoted by a superscript $(\cdot)^d$ are the block-diagonal, decentralized parts, i.e., $A^{K^d}_i = A^K_{ii}$, $B^{K^d}_i = B^K_{ii}$, $C^{K^d}_i = C^K_{ii}$, $D^{K^d}_i = D^K_{ii}$. For the ease of presentation, the interconnected controller gains are given as $A^{K^i}_i = A^K_{ik}$, $B^{K^i}_i = B^K_{ik}$, $C^{K^i}_i = C^K_{ik}$, $D^{K^i}_i = D^K_{ik}$, where it is assumed that the subcontroller i is interconnected to only one neighboring subcontroller k. This is easily extended to more interconnections per subcontroller by extending the interconnection channels.

The transformed nominal condition to solve thus becomes

$$\begin{aligned}
&\left[\star\right]^\top \left[\begin{array}{cc:cc:cc} 0 & I & 0 & 0 & 0 & 0 \\ I & 0 & 0 & 0 & 0 & 0 \\ \hdashline 0 & 0 & -\gamma^2 I & 0 & 0 & 0 \\ 0 & 0 & 0 & I & 0 & 0 \\ \hdashline 0 & 0 & 0 & 0 & \tilde{Q}_i & \tilde{S}_i \\ 0 & 0 & 0 & 0 & \tilde{S}_i^\top & \tilde{R}_i \end{array}\right] \left[\begin{array}{ccc} I & 0 & 0 \\ \boldsymbol{\mathcal{A}}_i & \boldsymbol{\mathcal{B}}_{1,i} & \boldsymbol{\mathcal{B}}_{2,i} \\ \hdashline 0 & I & 0 \\ \boldsymbol{\mathcal{C}}_{1,i} & \boldsymbol{\mathcal{D}}_{11,i} & \boldsymbol{\mathcal{D}}_{12,i} \\ \hdashline 0 & 0 & I \\ \boldsymbol{\mathcal{C}}_{2,i} & \boldsymbol{\mathcal{D}}_{21,i} & \boldsymbol{\mathcal{D}}_{22,i} \end{array}\right] < 0, \\
&\begin{bmatrix} Y & I \\ I & Z \end{bmatrix} > 0,
\end{aligned} \tag{A.7}$$

where the last inequality ensures that the Lyapunov matrix is positive definite. The terms $\boldsymbol{\mathcal{A}}_i$, $\boldsymbol{\mathcal{B}}_{1,i}$ and $\boldsymbol{\mathcal{B}}_{2,i}$ are affine in the transformed variables and the product terms with the Lyapunov matrix are thus eliminated. However, (A.7) yields now product terms of multiplier variables with $\boldsymbol{\mathcal{C}}_{2,i}$, which depend on V and Y. Therefore, (A.7) needs to be solved iteratively as briefly sketched in the following.

Iterative Solution Steps

The iterative solution, similar as proposed in [68], is based on the fixing of a set of optimization variables and solving for the other ones and vice versa. In the first part, the goal is to find a feasible solution without minimizing the performance bound. To do so, first, a decentralized controller for the plant without interconnections, i.e., with $\mathcal{P}$ being set to zero, is found. In the subsequent iterations, the interconnections of the plant are scaled as $r\,\mathcal{P}$, with r between 0 and 1. The factor r is iteratively maximized by bisection, and the goal is to compute an interconnected controller for the interconnected system. This is achieved by iteratively keeping one of the sets of variables Q, R, S, K^i, or Y, V, U, K^d fixed and optimizing over the other one, and vice versa.

Departing from this stabilizing controller, in the second part, the performance bound γ is optimized. The same iterations of fixing optimization variables and solving for the other ones, as described before, can be performed.

A.2 Static State Feedback Controller Synthesis

In the case of state feedback, i.e., $C_y = I$ and $D_{yw} = 0$ and $D_{yu} = 0$, a variable transformation can be applied which yields a convex controller synthesis. We assume now local control inputs, i.e., $B_{u_{ik}} = 0$, such that the controller can be interconnected. For example, for static state feedback (SSF), the linearizing variable substitution from $\mathcal{X}$ to $\mathcal{Y} = \mathcal{X}^{-1}$ and from the controller gains ${D^{K^d}}_i$ and ${D^{K^i}}_i$ to the transformed ones $\boldsymbol{D}^{\boldsymbol{K}^d}_i$

and $\boldsymbol{D^{K}}_{i}^{i}$ can be performed. The transformed closed-loop matrices can be factorized as

$$\left[\begin{array}{cc:c:c} A_i\mathcal{Y} & B_{w_i} & B_{p_i} & B_{u_i} \\ \hdashline C_{z_i}\mathcal{Y} & D_{zw_i} & D_{zp_i} & D_{zu_i} \\ \hdashline C_{q_i}\mathcal{Y} & 0 & 0 & D_{qw_i} \\ 0 & 0 & 0 & 0 \end{array}\right] + \left[\begin{array}{cc} B_{u_i} & 0 \\ \hdashline D_{zu_i} & 0 \\ \hdashline 0 & 0 \\ 0 & I \end{array}\right] \left[\begin{array}{c} \boldsymbol{D^{K}}_{i}^{d} \\ \boldsymbol{D^{K}}_{i}^{i} \end{array}\right] \left[\begin{array}{c:c:c:c} I & 0 & 0 & 0 \end{array}\right], \tag{A.8}$$

with

$$\begin{bmatrix} \boldsymbol{D^{K}}_{i}^{d} \\ \boldsymbol{D^{K}}_{i}^{i} \end{bmatrix} = \begin{bmatrix} D^{K}{}_{i}^{d} \\ D^{K}{}_{i}^{i} \end{bmatrix} \mathcal{Y}, \tag{A.9}$$

which is affine in the new variables $\boldsymbol{D^{K}}_{i}^{\boldsymbol{d}}$, $\boldsymbol{D^{K}}_{i}^{\boldsymbol{i}}$ and $\mathcal{Y}$. The synthesis conditions have thus been transformed to LMIs which can be solved by convex programming.

A.3 Derivation of Algorithm 5.1

The derivation of Algorithm 5.1 is presented as follows. We start by formulating the consensus ADMM problem as in [32], where global coordination is required. By introducing a specific set of local variables, the problem is decomposed. Finally, the update steps of Algorithm 5.1 are derived.

Distributed Synthesis With Global Coordination

Let us define the selection matrices H_i and E_i such that the entries of $H_i\, l$ correspond to the copies of local variables of $E_i s_i$. With this definition, and with the global variable l and the local variables s_i, for subsystems i, as defined in Section 5.5.2, we formulate the following global consensus constraints

$$E_i\, s_i = H_i l, \quad \forall i \in \mathcal{N}.$$

The decomposed synthesis problem with global consensus is formulated as

$$\begin{aligned} &\min_{s_i} \sum_{i=1}^{N} \Big(f_i(s_i) + g_i(s_i) \Big), \\ &\text{s.t.} \quad E_i s_i = H_i\, l, \quad \forall i \in \mathcal{N}, \end{aligned} \tag{A.10}$$

with $f_i(\cdot)$ as defined before and with

$$g_i(s_i) = \mathcal{I}_{(5.33)}(s_i) + \mathcal{I}_{(5.34)}(s_i), \quad \forall i \in \mathcal{N}.$$

The local augmented Lagrangian of subsystem i for the synthesis problem is given as

$$\begin{aligned} \mathcal{L}_{\rho,i} =& f_i(s_i) + g_i(s_i) \\ &+ \lambda_i^{\top} \left(E_i s_i - H_i\, l\right) + \frac{\rho}{2} \| E_i s_i - H_i\, l \|_2^2. \end{aligned} \tag{A.11}$$

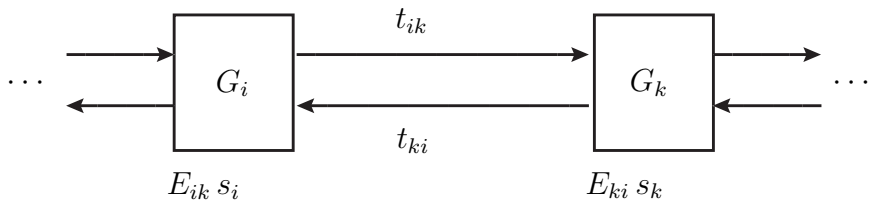

Figure A.1: Local variables per subsystem (here: i and $k \in \mathcal{N}$) and global variables per edge (here: (i,k) and $(k,i) \in \mathcal{E}$).

Subsystem i		Subsystem k	
Consensus constraints	Dual variables	Consensus constraints	Dual variables
$E_{ik}\, s_i = t_{ik}$	u_{ik}	$E_{ki}\, s_k = t_{ki}$	u_{ki}
$E_{ki}\, s_k = t_{ik}$	v_{ik}	$E_{ik}\, s_i = t_{ki}$	v_{ki}

Table A.1: Consensus constraints and corresponding dual variables per subsystem with neighboring subsystems (here i with k).

The consensus ADMM as in [32] involves the following update steps.

$$
\begin{aligned}
s_i^{(\kappa+1)} &= \underset{s_i}{\operatorname{argmin}}\ \mathcal{L}_{\rho,i}(\lambda_i^{(\kappa)}, l^{(\kappa)}, s_i),\ \forall i \in \mathcal{N},\\
l^{(\kappa+1)} &= \underset{l}{\operatorname{argmin}}\ \sum_{\mathcal{N}} \mathcal{L}_{\rho,i}(s_i^{(\kappa+1)}, \lambda_i^{(\kappa)}, l),\\
\lambda_i^{(\kappa+1)} &= \lambda_i^{(\kappa)} + \rho\ (E_i s_i^{(\kappa+1)} - H_i\, l^{(\kappa+1)}),\ \forall i \in \mathcal{N}.
\end{aligned}
$$

This formulation involves a global consensus of all local variables $E_i s_i$ with the corresponding parts of the global variable $H_i\, l$. If a central instance is available and broadcasting is assumed, these global consensus steps can directly be implemented.

Decomposed Synthesis Problem With Local Consensus Variables

In order to avoid a global coordinator, we aim to eliminate the global consensus variable l. Therefore, we introduce the local consensus variables t_{ik}, and t_{ki} per interconnections (i,k) and (k,i), and corresponding dual multipliers u_{ik}, v_{ik}, u_{ki}, and v_{ki} for subsystems i and k, respectively, which allows us to form the consensus constraints as shown in Figure A.1 and Table A.1.

We formulate the decomposed synthesis problem for all subsystems i with local consensus variables as

$$
\begin{aligned}
\min_{s_i, t_{ik}}\quad & \sum_{i=1}^{N} f_i(s_i) + g_i(s_i)\\
\text{s.t.}\quad & \left.\begin{aligned} E_{ik}\, s_i &= t_{ik},\\ E_{ki}\, s_k &= t_{ik}. \end{aligned}\right\} \forall i \in \mathcal{N}, k \in \mathcal{N}_i.
\end{aligned}
\tag{A.12}
$$

Derivation of the ADMM Iterations in Algorithm 5.1

Because of the symmetry of the undirected communication graph $\mathcal{T}$, problem (A.12) can be transformed into the simplified two-step ADMM algorithm, as given in Algorithm 5.1. The derivation follows the steps in [114] and is presented in the following.

For the optimization problem in (A.12), we formulate the augmented Lagrangian as

$$\begin{aligned}\mathcal{L}_\rho(s,t,(u,v)) = \sum_{i=1}^{N} \Big(& f_i(s_i) + g_i(s_i) \\ & + \sum_{k\in\mathcal{N}_i} \Big(u_{ik}^\top (E_{ik}\, s_i - t_{ik}) + \frac{\rho}{2}\|E_{ik}\, s_i - t_{ik}\|_2^2 \\ & \qquad + v_{ik}^\top (E_{ki}\, s_k - t_{ik}) + \frac{\rho}{2}\|E_{ki}\, s_k - t_{ik}\|_2^2 \Big) \Big),\end{aligned} \tag{A.13}$$

where s, t, u, and v are defined as the stacked vectors $s = \text{concat}_{i\in\mathcal{N}}(s_i)$, $t = \text{concat}_{(i,k)\in\mathcal{E}}(t_{ik})$, $u = \text{concat}_{(i,k)\in\mathcal{E}}(u_{ik})$, and $v = \text{concat}_{(i,k)\in\mathcal{E}}(v_{ik})$.

The standard consensus ADMM iterations as in [32] with respect to $\mathcal{L}_\rho(s,t,(u,v))$ are the following.

$$\begin{aligned} s_i^{(\kappa+1)} \leftarrow \underset{s_i}{\text{argmin}} \Big\{ & f_i(s_i) + g_i(s_i) \\ & + \sum_{k\in\mathcal{N}_i} \Big((u_{ik}^{(\kappa)} + v_{ki}^{(\kappa)})^\top (E_{ik}\, s_i) \\ & + \frac{\rho}{2}\|E_{ik}\, s_i - t_{ik}^{(\kappa)}\|_2^2 + \frac{\rho}{2}\|E_{ik}\, s_i - t_{ki}^{(\kappa)}\|_2^2 \Big) \Big\}, \\ t_{ik}^{(\kappa+1)} \leftarrow \underset{t_{ik}}{\text{argmin}} \Big\{ & - t_{ik}^\top (u_{ik}^{(\kappa)} + v_{ik}^{(\kappa)}) \\ & + \frac{\rho}{2}\|t_{ik} - E_{ik}\, s_i^{(\kappa+1)}\|_2^2 + \frac{\rho}{2}\|t_{ik} - E_{ki}\, s_k^{(\kappa+1)}\|_2^2 \Big\}, \\ u_{ik}^{(\kappa+1)} \leftarrow & \; u_{ik}^{(\kappa)} + \rho \left(E_{ik}\, s_i^{(\kappa+1)} - t_{ik}^{(\kappa+1)} \right), \\ v_{ik}^{(\kappa+1)} \leftarrow & \; v_{ik}^{(\kappa)} + \rho \left(E_{ki}\, s_k^{(\kappa+1)} - t_{ik}^{(\kappa+1)} \right). \end{aligned} \tag{A.14}$$

The minimization step of $t_{ik}^{(\kappa+1)}$ admits the closed-form solution

$$t_{ik}^{(\kappa+1)} = \frac{1}{2}\left(E_{ik}\, s_i^{(\kappa+1)} + E_{ki}\, s_k^{(\kappa+1)} \right) + \frac{1}{2\rho}\left(u_{ik}^{(\kappa)} + v_{ik}^{(\kappa)} \right). \tag{A.15}$$

Summing the update equations of $u_{ik}^{(\kappa+1)}$ and $v_{ik}^{(\kappa+1)}$, and replacing $t_{ik}^{(\kappa+1)}$ with the explicit solution in (A.15) leads to

$$u_{ik}^{(\kappa)} + v_{ik}^{(\kappa)} = 0, \tag{A.16}$$

and thus, the minimization step of $t_{ik}^{(\kappa+1)}$ simplifies to the following update

$$t_{ik}^{(\kappa+1)} = \frac{1}{2}\left(E_{ik}\, s_i^{(\kappa+1)} + E_{ki}\, s_k^{(\kappa+1)} \right). \tag{A.17}$$

Furthermore, the update step of $u_{ik}^{(\kappa+1)}$ becomes

$$u_{ik}^{(\kappa+1)} \leftarrow u_{ik}^{(\kappa)} + \frac{\rho}{2}\left(E_{ik}\, s_i^{(\kappa+1)} + E_{ki}\, s_k^{(\kappa+1)}\right). \tag{A.18}$$

Note that for initial conditions $t_{ik}^{(0)} = t_{ki}^{(0)}$, it follows from (A.17) that $t_{ik}^{(\kappa)} = t_{ki}^{(\kappa)}$ for all $\kappa > 0$. Also, it follows from (A.16) and (A.18) that for initial conditions $u_{ik}^{(0)} = v_{ik}^{(0)} = 0$ and $u_{ik}^{(0)} = u_{ki}^{(0)} = 0$, then $u_{ik}^{(\kappa)} = -v_{ik}^{(\kappa)}$ and $u_{ik}^{(\kappa)} = -u_{ki}^{(\kappa)}$, for all $\kappa > 0$. If we define

$$\lambda_i = u_{ik} - v_{ik} = 2u_{ik},$$

this leads to the update

$$\lambda_i^{(\kappa+1)} = \lambda_i^{(\kappa)} + \rho \sum_{k\in\mathcal{N}_i}\left(T_{ik}\, s_i^{(\kappa)} - T_{ki}\, s_k^{(\kappa)}\right),$$

and we arrive at the ADMM iterations in Algorithm 5.1, with T_{ik} as defined in Section 5.5.2.

Remark A.1. In the case of the consensus over ν_i over all subsystems i, and the pairwise consensus over the multipliers defined per undirected edge of two neighboring subsystems, the dual multipliers are defined by

$$\begin{aligned}\lambda_i &= \left[\sum_{k\in\mathcal{N}_i}(u_{\nu_{ik}} - v_{\nu_{ik}}), \mathrm{concat}_{k\in\mathcal{N}_i}\left(\left[u_{m_{ik}}^\top - v_{m_{ik}}^\top,\ u_{m_{ki}}^\top - v_{m_{ki}}^\top\right]\right)\right]^\top \\ &= 2\left[\sum_{k\in\mathcal{N}_i} u_{\nu_{ik}}, \mathrm{concat}_{k\in\mathcal{N}_i}\left(\left[u_{m_{ik}}^\top,\ u_{m_{ki}}^\top\right]\right)\right]^\top,\end{aligned} \tag{A.19}$$

where the first sum takes care of the consensus over γ_i and the remaining parts account for the pairwise consensus over the multipliers of the edges.

A.4 Derivation of the Residuals in ADMM

The following presents the derivation of the residuals in (5.42). Starting from the definition of the primal and dual residuals [32], we have

$$\begin{aligned} r^{(\kappa+1)} &= \mathrm{concat}_{i=1}^{N}\left(\mathrm{concat}_{k\in\mathcal{N}_i}\left(r_{ik}^{(\kappa+1)}\right)\right), \\ d^{(\kappa+1)} &= \mathrm{concat}_{i=1}^{N}\left(\mathrm{concat}_{k\in\mathcal{N}_i}\left(d_{ik}^{(\kappa+1)}\right)\right), \end{aligned} \tag{A.20}$$

with

$$\begin{aligned} r_{ik}^{(\kappa+1)} &= E_{ik} s_i^{(\kappa+1)} - t_{ik}^{(\kappa+1)}, \\ d_{ik}^{(\kappa+1)} &= t_{ik}^{(\kappa+1)} - t_{ik}^{(\kappa)}. \end{aligned} \tag{A.21}$$

Replacing $t_{ik}^{(\kappa+1)}$ and $t_{ik}^{(\kappa)}$ by the expressions in (A.17), we obtain

$$\begin{aligned} r_{ik}^{(\kappa+1)} &= E_{ik}s_i^{(\kappa+1)} - \frac{1}{2}(E_{ik}s_i^{(\kappa+1)} + E_{ki}s_k^{(\kappa+1)}), \\ d_{ik}^{(\kappa+1)} &= \frac{1}{2}(E_{ik}s_i^{(\kappa+1)} + E_{ki}s_k^{(\kappa+1)}) - \frac{1}{2}(E_{ik}s_i^{(\kappa)} + E_{ki}s_k^{(\kappa)}), \end{aligned} \tag{A.22}$$

which leads to the primal and dual residuals in (5.42) in Section 5.5.2 which can be considered as convergence criteria.

Bibliography

[1] I. Agusti-Juan, "Sustainability assessment and development of guidelines for digital fabrication in construction," PhD thesis, Swiss Federal Institute of Technology, Switzerland, 2018.

[2] G. P. Lydon, S. Caranovic, I. Hischier, and A. Schlueter, "Coupled simulation of thermally active building systems to support a digital twin," *Energy Build.*, vol. 202, 2019.

[3] A. Sawhney, M. Riley, and J. Irizarry, *Construction 4.0: An innovation platform for the built environment*. London: Routledge, 2019.

[4] M. Giftthaler, "Towards a unified framework of efficient algorithms for numerical optimal robot control," PhD thesis, Swiss Federal Institute of Technology, Switzerland, 2018.

[5] A. Gawel, R. Siegwart, M. Hutter, T. Sandy, H. Blum, J. Pankert, K. Kramer, L. Bartolomei, S. Ercan, F. Farshidian, M. Chli, and F. Gramazio, "A fully-integrated sensing and control system for high-accuracy mobile robotic building construction," 2019. arXiv: `1912.01870`.

[6] F. Furrer, M. Wermelinger, H. Yoshida, F. Gramazio, M. Kohler, R. Siegwart, and M. Hutter, "Autonomous robotic stone stacking with online next best object target pose planning," *IEEE Int. Conf. Robot. Autom.*, pp. 2350–2356, 2017.

[7] S. J. Keating, J. C. Leland, L. Cai, and N. Oxman, "Toward site-specific and self-sufficient robotic fabrication on architectural scales," *Sci. Robot.*, vol. 2, no. 5, 2017.

[8] C. Robeller, Y. Weinand, V. Helm, A. Thoma, F. Gramazio, and M. Kohler, "Robotic integral Attachment," in *Fabricate*, A. Menges, B. Sheil, R. Glynn, and M. Skavara, Eds., UCL Press, 2017, pp. 92–97.

[9] S. Parascho, A. Gandia, A. Mirjan, F. Gramazio, and M. Kohler, "Cooperative fabrication of spatial metal structures," in *Fabricate*, UCL Press, 2017, pp. 24–29.

[10] N. Hack, W. V. Lauer, F. Gramazio, and M. Kohler, "Mesh Mould: Robotically fabricated metal meshes as concrete formwork and reinforcement," in *Int. Conf. Text. Reinf. Concr.* RILEM Publications SARL, 2015, pp. 347–359.

[11] P. Valeri, R. M. Fernandez, and A. Muttoni, "New perspectives for design of lightweight structures by using textile reinforced concrete," *fib Symp.*, 2019.

[12] Y. R. Stürz, A. Eichler, and R. S. Smith, "A framework for distributed control based on overlapping estimation for cooperative tasks," *IFAC-PapersOnLine*, vol. 50, no. 1, pp. 14 296–14 301, 2017.

[13] ——, "Fixed mode elimination by minimum communication within an estimator-based framework for distributed control," *IEEE Control Syst. Lett.*, vol. 1, no. 2, pp. 346–351, 2017.

[14] ——, "Scalable controller synthesis for heterogeneous interconnected systems applicable to an overlapping control framework," *Eur. Control Conf.*, vol. 1, pp. 2561–2568, 2018.

[15] Y. R. Stürz, A. Eichler, and R. S. Smith, "Distributed control design for heterogeneous interconnected systems," 2020. arXiv: 2004.04876.

[16] Y. R. Stürz, M. Morari, and R. S. Smith, "Sequential quadratic programming for the control of an architectural cable net geometry," *Am. Control Conf.*, pp. 3503–3508, 2016.

[17] ——, "Two methods for the identification of uncertain parameters of an architectural cable net geometry," *IEEE Conf. Control Appl.*, pp. 804–809, 2016.

[18] A. Liew, Y. R. Stürz, S. Guillaume, T. Van Mele, R. S. Smith, and P. Block, "Active control of a rod-net formwork system prototype," *Autom. Constr.*, vol. 96, pp. 128–140, 2018.

[19] Y. R. Stürz, M. Morari, and R. S. Smith, "Control of an architectural cable net geometry," *IEEE Trans. Control Syst. Technol.*, 2019.

[20] Y. R. Stürz, L. M. Affolter, and R. S. Smith, "Parameter identification of the KUKA LBR iiwa robot including constraints on physical feasibility," *IFAC-PapersOnLine*, vol. 50, no. 1, pp. 6863–6868, 2017.

[21] A. Romero, P. N. Beuchat, Y. R. Stürz, R. S. Smith, and J. Lygeros, "Nonlinear control of quadcopters via approximate dynamic programming," *IEEE Eur. Control Conf.*, pp. 3752–3759, 2019.

[22] P. N. Beuchat, Y. R. Stürz, and J. Lygeros, "A teaching system for hands-on quadcopter control," *IFAC PapersOnLine*, vol. 52, no. 9, pp. 36–41, 2019.

[23] S. Skogestad and I. Postlethwaite, *Multivariable feedback control: Analysis and design*. New York, USA: Wiley, 1997.

[24] C. Scherer and S. Weiland, "Linear matrix inequalities in control," in *Control Syst. Handbook, Second Ed. Control Syst. Adv. Methods*, CRC Press, 2011, pp. 24/1–24/30.

[25] C. Scherer, *Theory of robust control*. TU Delft, Faculty of Mechanical Engineering and Marine Technology (3mE), 2006, pp. 1–160.

[26] A. Krause and D. Golovin, "Submodular function maximization," in *Tractability Pract. Approaches to Hard Probl.* Cambridge, UK: Cambridge University Press, 2014, pp. 71–104.

[27] S. Boyd and L. Vandenberghe, *Convex optimization*. Cambridge, UK: Cambridge University Press, 2010.

[28] M. S. Lobo, L. Vandenberghe, S. Boyd, and H. Lebret, "Applications of second-order cone programming," *Linear Algebra Appl.*, vol. 284, no. 1, pp. 193–228, 1998.

[29] Y. Nesterov and A. Nemirovskii, *Interior point polynomial time methods in convex programming*. Philadelphia, USA: SIAM Studies in Applied and Numerical Mathematics, 1994.

[30] S. Boyd, L. El Ghaoui, E. Feron, and V. Balakrishnan, *Linear matrix inequalities in system and control theory*. Philadelphia, USA: SIAM Studies in Applied and Numerical Mathematics, 1994, vol. 15.

[31] D. P. Bertsekas and J. N. Tsitsiklis, *Parallel and distributed computation: Numerical methods*. New York, USA: Prentice Hall, Inc., 1989.

[32] S. Boyd, N. Parikh, E. Chu, P. Borja, and J. Eckstein, "Distributed optimization and statistical learning via the alternating direction method of multipliers," *Found. Trends Mach. Learn.*, vol. 3, no. 1, pp. 1–122, 2010.

[33] L. Chen, D. Sun, and K. C. Toh, "A note on the convergence of ADMM for linearly constrained convex optimization problems," *Comput. Optim. Appl.*, vol. 66, no. 2, pp. 327–343, 2017.

[34] J. Nocedal and S. J. Wright, *Numerical optimization*, Second Edi. New York, USA: Springer, 2006.

[35] P. E. Gill, W. Murray, M. A. Saunders, and M. H. Wright, "Some theoretical properties of an augmented Lagrangian merit function," in *Adv. Optim. parallel Comput.* New York, USA: North-Holland, 1992, pp. 101–128.

[36] J. A. Fax and R. M. Murray, "Information flow and cooperative control of vehicle formations," *IEEE Trans. Automat. Contr.*, vol. 49, no. 9, pp. 1465–1476, 2004.

[37] R. M. Murray, "Recent research in cooperative control of multivehicle systems," *J. Dyn. Syst. Meas. Control*, vol. 129, no. 5, pp. 571–583, 2007.

[38] B. Siciliano, L. Sciavicco, L. Villani, and G. Oriolo, *Robotics modelling, planning and control*, ser. Advanced Textbooks in Control and Signal Processing. London, UK: Springer, 2009.

[39] R. Featherstone, *Rigid body dynamics algorithms*. New York, USA: Springer, 2008.

[40] N. Hogan, "Impedance control: An approach to manipulation," in *Am. Control Conf.*, 1985, pp. 304–313.

[41] L. Bakule, "Decentralized control: An overview," *Annu. Rev. Control*, vol. 32, no. 1, pp. 87–98, 2008.

[42] D. D. Šiljak, *Decentralized control of complex systems*, ser. Mathematics in Science and Engineering. Boston, USA: Academic Press, 2015.

[43] R. D'Andrea and G. E. Dullerud, "Distributed control design for spatially interconnected systems," *IEEE Trans. Automat. Contr.*, vol. 48, no. 9, pp. 1478–1495, 2003.

[44] C. Langbort and R D'Andrea, "Distributed control of heterogeneous systems interconnected over an arbitrary graph," in *IEEE Conf. Decis. Control*, 2003, pp. 2835–2840.

[45] G. Como, B. Bernhardsson, and A. Rantzer, Eds., *Information and control in networks*. Cham, Switzerland: Springer, 2014.

[46] F. L. Lewis, H. Zhang, K. Hengster-Movric, and A. Das, *Cooperative control of multi-agent systems: Optimal and adaptive design approaches*. London, UK: Springer, 2014.

[47] M. Rotkowitz and S. Lall, "A characterization of convex problems in decentralized control," *IEEE Trans. Automat. Contr.*, vol. 50, no. 12, pp. 1984–1996, 2005.

[48] S.-H. Wang and E. J. Davison, "On the stabilization of decentralized control systems," *IEEE Trans. Automat. Contr.*, vol. 18, no. 5, pp. 473–478, 1973.

[49] E. J. Davison and A. G. Aghdam, "Characterization and calculation of approximate decentralized fixed modes (ADFMs)," in *Adv. Stat. Control. Algebr. Syst. Theory, Dyn. Syst. Charact.* Boston, USA: Birkhäuser, 2008, pp. 223–244.

[50] C. Conte, C. N. Jones, M. Morari, and M. N. Zeilinger, "Distributed synthesis and stability of cooperative distributed model predictive control for linear systems," *Automatica*, vol. 69, pp. 117–125, 2016.

[51] M. A. Müller, M. Reble, and F. Allgöwer, "A general distributed MPC framework for cooperative control," *IFAC Proc. Vol.*, vol. 44, no. 1, pp. 7987–7992, 2011.

[52] R. S. Smith and F. Y. Hadaegh, "Closed-loop dynamics of cooperative vehicle formations with parallel estimators and communication," *IEEE Trans. Automat. Contr.*, vol. 52, no. 8, pp. 1404–1414, 2007.

[53] J. Lavaei and A. G. Aghdam, "Control of continuous-time LTI systems by means of structurally constrained controllers," *Automatica*, vol. 44, no. 1, pp. 141–148, 2008.

[54] P. Gahinet, "A convex characterization of gain-scheduled $\mathcal{H}_\infty$ controllers," *IEEE Trans. Automat. Contr.*, vol. 40, no. 5, pp. 853–864, 1995.

[55] G. Scorletti and G. Duc, "A convex approach to decentralized $\mathcal{H}_\infty$ control," *Am. Control Conf.*, pp. 2390–2394, 1997.

[56] C. Langbort, R. S. Chandra, and R. D'Andrea, "Distributed control design for systems interconnected over an arbitrary graph," *IEEE Trans. Automat. Contr.*, vol. 49, no. 9, pp. 1502–1519, 2004.

[57] P. Viccione, C. W. Scherer, and M. Innocenti, "LPV synthesis with integral quadratic constraints for distributed control of interconnected systems," in *IFAC Proc. Vol.*, vol. 42, 2009, pp. 13–18.

[58] G. E. Dullerud and R. D'Andrea, "Distributed control of heterogeneous systems," *IEEE Trans. Automat. Contr.*, vol. 49, no. 12, pp. 2113–2128, 2004.

[59] P. Massioni and M. Verhaegen, "Distributed control for identical dynamically coupled systems: A decomposition approach," *IEEE Trans. Automat. Contr.*, vol. 54, no. 1, pp. 124–135, 2009.

[60] ——, "A full block S-Procedure application to distributed control," *Am. Control Conf.*, pp. 2338–2343, 2010.

[61] P. Massioni, "Distributed control for alpha-heterogeneous dynamically coupled systems," *Syst. Control Lett.*, vol. 72, pp. 30–35, 2014.

[62] C. Hoffmann, A. Eichler, and H. Werner, "Control of heterogeneous groups of systems interconnected through directed and switching topologies," *IEEE Trans. Automat. Contr.*, vol. 60, no. 7, pp. 1904–1909, 2015.

[63] C. Hoffmann and H. Werner, "Convex distributed controller synthesis for interconnected heterogeneous subsystems via virtual normal interconnection matrices," *IEEE Trans. Automat. Contr.*, vol. 62, no. 10, pp. 5337 –5342, 2017.

[64] A. Rantzer and A. Megretski, "System analysis via integral quadratic constraints," *IEEE Trans. Automat. Contr.*, vol. 42, no. 6, pp. 819–830, 1997.

[65] G. Meinsma, T. Iwasaki, and M. Fu, "When is (D,G)-scaling both necessary and sufficient," *IEEE Trans. Automat. Contr.*, vol. 45, no. 9, pp. 1755–1759, 2000.

[66] Z. Li, Z. Duan, and G. Chen, "Consensus of multiagent systems and synchronization of complex networks: A unified viewpoint," *IEEE Trans. Circuits Syst.*, vol. 57, no. 1, pp. 213–224, 2010.

[67] Y. Zheng, R. P. Mason, and A. Papachristodoulou, "Scalable design of structured controllers using chordal decomposition," *IEEE Trans. Automat. Contr.*, vol. 63, no. 3, pp. 752–767, 2018.

[68] C. Scherer, "Robust mixed control and LPV control with full block scalings," in *Adv. Linear Matrix Inequal. Methods Control*, Philadelphia, USA: SIAM, 1999, pp. 187–207.

[69] C. Langbort, R. D'Andrea, and S. Boyd, "A decomposition approach to distributed analysis of networked systems," *IEEE Conf. Decis. Control*, pp. 3980–3985, 2004.

[70] S. Schuler, U. Münz, and F. Allgöwer, "Decentralized state feedback control for interconnected systems with application to power systems," *J. Process Control*, vol. 24, no. 2, pp. 379–388, 2014.

[71] F. Lin, M. Fardad, and M. R. Jovanovic, "Design of optimal sparse feedback gains via the alternating direction method of multipliers," *IEEE Trans. Automat. Contr.*, vol. 58, no. 9, pp. 2426–2431, 2013.

[72] X. Wu and M. R. Jovanović, "Sparsity-promoting optimal control of systems with symmetries, consensus and synchronization networks," *Syst. Control Lett.*, vol. 103, pp. 1–8, 2017.

[73] F. Dorfler, M. R. Jovanovic, M. Chertkov, and F. Bullo, "Sparse and optimal wide-area damping control in power networks," *Am. Cont. Conf.*, pp. 4289–4294, 2013.

[74] B. K. Poolla, S. Bolognani, and F. Dorfler, "Optimal Placement of Virtual Inertia in Power Grids," *IEEE Trans. Aut. Contr.*, vol. 62, no. 12, pp. 6209–6220, 2015.

[75] C. Conte, "Stability and computations in cooperative distributed model predictive control," PhD thesis, Swiss Federal Institute of Technology, Switzerland, 2014.

[76] J. Köhler, M. A. Müller, and F. Allgöwer, "Distributed model predictive control: Recursive feasibility under inexact dual optimization," *Automatica*, vol. 102, 2019.

[77] S. Riverso and G. Ferrari-Trecate, "Tube-based distributed control of linear constrained systems," *Automatica*, vol. 48, no. 11, pp. 2860–2865, 2012.

[78] M. Farina and R. Scattolini, "Distributed non-cooperative MPC with neighbor-to-neighbor communication," *IFAC-PapersOnline*, pp. 404–409, 2011.

[79] M. N. Zeilinger, Y. Pu, G. Ferrari-Trecate, S. Riverso, and C. N. Jones, "Plug and play distributed model predictive control based on distributed invariance and optimization," *IEEE Conf. Decis. Control*, pp. 5770–5776, 2013.

[80] S. Riverso, M. Farina, and G. Ferrari-Trecate, "Plug-and-play decentralized model predictive control," *IEEE Conf. Decis. Control*, pp. 4193–4198, 2013.

[81] ——, "Plug-and-play model predictive control based on robust control invariant sets," *Automatica*, vol. 50, no. 8, pp. 2179–2186, 2014.

[82] J. Anderson, J. C. Doyle, S. H. Low, and N. Matni, "System level synthesis," *Annu. Rev. Control*, vol. 47, pp. 364–393, 2019.

[83] Y. S. Wang, N. Matni, and J. C. Doyle, "Separable and localized system-level synthesis for large-scale systems," *IEEE Trans. Automat. Contr.*, vol. 63, no. 12, pp. 4234–4249, 2018.

[84] M. Ikeda and D. D. Šiljak, "Overlapping decompositions, expansions and contractions of dynamic systems," *Large Scale Syst.*, vol. 1, no. 1, pp. 29–38, 1980.

[85] A. Iftar, "Overlapping decentralized dynamic optimal control," *Int. J. Control*, vol. 58, no. 1, pp. 187–209, 1993.

[86] ——, "Overlapping decentralized dynamic optimal control," *Int. J. Control*, vol. 58, no. 1, pp. 187–209, 1993.

[87] A. Mitra and S. Sundaram, "An approach for distributed state estimation of LTI systems," *Annu. Allert. Conf.*, pp. 1088–1093, 2016.

[88] U. A. Khan, S. Kar, A. Jadbabaie, and J. M. F. Moura, "On connectivity, observability, and stability in distributed estimation," *IEEE Conf. Decis. Control*, pp. 6639–6644, 2010.

[89] S. Park and N. C. Martins, "Necessary and sufficient conditions for the stabilizability of a class of LTI distributed observers," *Conf. Decis. Control*, pp. 7431–7436, 2012.

[90] M. Farina, G. Ferrari-Trecate, and R. Scattolini, "Distributed moving horizon estimation for linear constrained systems," *IEEE Trans. Automat. Contr.*, vol. 55, no. 11, pp. 2462–2475, 2010.

[91] S. Riverso, M. Farina, R. Scattolini, and G. Ferrari-Trecate, "Plug-and-play distributed state estimation for linear systems," *IEEE Conf. Decis. Control*, pp. 4889–4894, 2013.

[92] B. D. O. Anderson and D. J. Clements, "Algebraic characterization of fixed modes in decentralized control," *Automatica*, vol. 17, no. 5, pp. 703–712, 1981.

[93] E. J. Davison and T. N. Chang, "Decentralized stabilization and pole assignment for general proper systems," *IEEE Trans. Automat. Contr.*, vol. 35, no. 6, pp. 652–664, 1990.

[94] A. Alavian and M. C. Rotkowitz, "On a Hankel-based measure of decentralized controllability and observability," *IFAC-PapersOnLine*, vol. 28, no. 22, pp. 227–232, 2015.

[95] A. Alavian and M. Rotkowitz, "Stabilization of decentralized systems with arbitrary information structure," in *Conf. Decis. Control*, 2014, pp. 4032–4038.

[96] P. R. Sahoo, A. Patel, S. Ghosh, and A. K. Naskar, "Selection of overlapping interaction through approximate decentralized fixed mode measure," 2019. arXiv: `1904.05273`.

[97] V. A. Armentano and M. G. Singh, "A procedure to eliminate decentralized fixed modes with reduced information exchange," *IEEE Trans. Automat. Contr.*, vol. 27, no. 1, pp. 258–260, 1982.

[98] J. Lavaei and A. G. Aghdam, "Overlapping control design for multi-channel systems," *Automatica*, vol. 45, no. 5, pp. 1326–1331, 2009.

[99] K. Ünyelioğlu and M. E. Sezer, "Optimum feedback patterns in multivariable control systems," *Int. J. Control*, vol. 49, no. 3, pp. 791–808, 1989.

[100] S. Sojoudi and A. G. Aghdam, "Overlapping control systems with optimal information exchange," *Automatica*, vol. 45, no. 5, pp. 1176–1181, 2009.

[101] S. Pequito, S. Kar, and A. P. Aguiar, "A framework for structural input/output and control configuration selection in large-scale systems," *IEEE Trans. Automat. Contr.*, vol. 61, no. 2, pp. 303–318, 2016.

[102] M. V. Subbotin and R. S. Smith, "Elimination of fixed modes of a decentralized distributed estimator with inter-agent communication," *IEEE Conf. Decis. Control*, pp. 2545–2550, 2008.

[103] D. K. Molzahn, F. Dörfler, H. Sandberg, S. H. Low, S. Chakrabarti, R. Baldick, and J. Lavaei, "A survey of distributed optimization and control algorithms for electric power systems," *IEEE Trans. Smart Grid*, vol. 8, no. 6, pp. 2941–2962, 2017.

[104] P. Braun, T. Faulwasser, L. Grüne, C. M. Kellett, S. R. Weller, and K. Worthmann, "Hierarchical distributed ADMM for predictive control with applications in power networks," *IFAC J. Syst. Control*, vol. 3, pp. 10–22, 2018.

[105] J. Guo, G. Hug, and O. Tonguz, "Impact of communication delay on asynchronous distributed optimal power flow using ADMM," *Int. Conf. Smart Grid*, pp. 177–182, 2017.

[106] A. Hansson and M. Verhaegen, "Distributed system identification with ADMM," *IEEE Conf. Decis. Control*, pp. 290–295, 2015.

[107] Q. Ba, K. Savla, and G. Como, "Distributed optimal equilibrium selection for traffic flow over networks," *IEEE Conf. Decis. Control*, pp. 6942–6947, 2015.

[108] N. K. Dhingra, M. R. Jovanovic, and Z. Q. Luo, "An ADMM algorithm for optimal sensor and actuator selection," *IEEE Conf. Decis. Control*, pp. 4039–4044, 2015.

[109] P. Graf, J. Annoni, C. Bay, D. Biagioni, D. Sigler, M. Lunacek, and W. Jones, "Distributed reinforcement learning with ADMM-RL," *Am. Control Conf.*, pp. 4159–4166, 2019.

[110] C. A. Alonso and N. Matni, "Distributed and localized model predictive control via system level synthesis," 2019.

[111] L. A. Wolsey, "An analysis of the greedy algorithm for the submodular set covering problem," *Combinatorica*, vol. 2, pp. 385 –393, 1982.

[112] G. Mateos, J. A. Bazerque, and G. B. Giannakis, "Distributed sparse linear regression," *IEEE Trans. Signal Process.*, vol. 58, no. 10, pp. 5262–5276, 2010.

[113] T. H. Chang, M. Hong, and X. Wang, "Multi-agent distributed optimization via inexact consensus ADMM," *IEEE Trans. Signal Process.*, vol. 63, no. 2, pp. 482–497, 2015.

[114] G. Banjac, F. Rey, P. Goulart, and J. Lygeros, "Decentralized resource allocation via dual consensus ADMM," *Amer. Contr. Conf.*, pp. 2789–2794, 2019.

[115] M. S. Darup, G. Book, and P. Giselsson, "Towards real-time ADMM for linear MPC," *Eur. Control Conf.*, pp. 4276–4282, 2019.

[116] R. A. Horn and C. R. Johnson, *Matrix analysis*, Second Edi. New York, USA: Cambridge University Press, 2013.

[117] M. Ikeda, D. D. Šiljak, and D. E. White, "An inclusion principle for dynamic systems," *IEEE Trans. Automat. Contr.*, vol. 29, no. 3, pp. 244–249, 1984.

[118] S. S. Stanković and D. D. Šiljak, "Stabilization of fixed modes in expansions of LTI systems," *Syst. Control Lett.*, vol. 57, no. 4, pp. 365–370, 2008.

[119] J. Szewczyk, F. Plumet, and P. Bidaud, "Planning and controlling cooperating robots through distributed impedance," *J. Robot. Syst.*, vol. 19, no. 6, pp. 283–297, 2002.

[120] U. Feige, "A threshold of ln n for approximating set cover," *J. ACM*, vol. 45, no. 4, pp. 634–652, 1998.

[121] G. L. Nemhauser and L. A. Wolsey, "Maximizing submodular set functions: Formulations and analysis of algorithms," *Stud. Graphs Discret. Program.*, vol. 59, pp. 279–301, 1981.

[122] W. J. Lewis, *Tension structures: Form and behaviour*. London, UK: Thomas Telford Publishing, 2003.

[123] R. Torsing, J. Bakker, R. Jansma, and D. Veenendaal, "Large-scale designs for mixed fabric and cable net formed structures," *Int. Conf. Flex. formwork*, pp. 346–355, 2012.

[124] T. d'Estree Sterk, "Shape change in responsive architectural structures: Current reasons & challenge," *Annu. Conf. Assoc. Comput. Des. Archit.*, pp. 251–260, 2006.

[125] D. Veenendaal and P. Block, "Design process for prototype concrete shells using a hybrid cable-net and fabric formwork," *Eng. Struct.*, vol. 75, pp. 39–50, 2014.

[126] https://www.empa.ch/web/nest, *Next Evolution in Sustainable Building Technologies (NEST)*, 2019.

[127] http://hilo.arch.ethz.ch, *HiLo Research and Innovation Unit for NEST*, 2019.

[128] T. Van Mele and P. Block, "A novel form finding method for fabric formwork for concrete shells," *J. Int. Assoc. Shell Spat. Struct.*, vol. 52, no. 4, pp. 217–224, 2010.

[129] D. Veenendaal, M. Bezbradica, D. Novák, and P. Block, "Controlling the geometry and forces of a hybrid cable-net and fabric formwork for thin concrete shells," *IASS-SLTE Symp.*, pp. 170–177, 2014.

[130] H.-J. Schek, "The force density method for form finding and computation of general networks," *Comput. Methods Appl. Mech. Eng.*, vol. 3, no. 1, pp. 115–134, 1974.

[131] C. R. Calladine, "Buckminster Fuller's tensegrity structures and Clerk Maxwell's rules for the construction of stiff frames," *Int. J. Solids Struct.*, vol. 14, no. 2, pp. 161–172, 1978.

[132] R. Motro, "Tensegrity systems: The state of the art," *Int. J. Sp. Struct.*, vol. 7, no. 2, pp. 75–83, 1992.

[133] H. Furuya, "Concept of deployable tensegrity structures in space application," *Int. J. Sp. Struct.*, vol. 7, no. 2, pp. 143–151, 1992.

[134] S. Pellegrino, "A class of tensegrity domes," *Int. J. Sp. Struct.*, vol. 7, no. 2, pp. 127–142, 1992.

[135] K. Snelson, "Snelson on the tensegrity invention," *Int. J. Sp. Struct.*, vol. 11, no. 1-2, pp. 43–48, 1996.

[136] K. Linkwitz and H.-J. Schek, "Über eine Methode zur Berechnung vorgespannter Seilnetze und ihre praktische Anwendung auf die Olympiadächer München," *IABSE Congr. Rep.*, vol. 9, 1972.

[137] D. H. Geiger, A. Stefaniuk, and D. Chen, "The design and construction of two cable domes for the Korean Olympics," *IASS Symp. Shells, Membr. Sp. Fram.*, vol. 2, pp. 265–272, 1986.

[138] R. Connelly and W. Whiteley, "Second-order rigidity and prestress stability for tensegrity frameworks," *SIAM J. Discret. Math.*, vol. 9, no. 3, pp. 453–491, 1996.

[139] R. Connelly, "Stress and stability," *Chapter an Unpubl. B.*, pp. 1–28, 2001.

[140] S. Guest, "The stiffness of prestressed frameworks: A unifying approach," *Int. J. Solids Struct.*, vol. 43, no. 3, pp. 842 –854, 2006.

[141] R. E. Skelton and M. C. De Oliveira, *Tensegrity systems*. New York, USA: Springer, 2009.

[142] S. Hernandez Juan and J. M. Mirats Tur, "Tensegrity frameworks: Static analysis review," *Mech. Mach. Theory*, vol. 43, pp. 859–881, 2008.

[143] D. Williamson and R. E. Skelton, "Equilibrium conditions of a tensegrity structure," *Int. J. Solids Struct.*, vol. 40, pp. 6347–6367, 2003.

[144] R. Connelly, "Rigidity and energy," *Invent. Math.*, vol. 66, no. 1, pp. 11–33, 1982.

[145] Y. Kanno, M. Ohsaki, and J. Ito, "Large-deformation and friction analysis of non-linear elastic cable networks by second-order cone programming," *Int. J. Numer. Methods Eng.*, vol. 55, no. 9, pp. 1079–1114, 2002.

[146] Y. Kanno and M. Ohsaki, "Minimum principle of complementary energy of cable networks by using second-order cone programming," *Int. J. Solids Struct.*, vol. 40, no. 17, pp. 4437–4460, 2003.

[147] A. G. Tibert and S. Pellegrino, "Review of form-finding methods for tensegrity structures," *Int. J. Sp. Struct.*, vol. 18, no. 4, pp. 209–223, 2003.

[148] T. Tran, H. T. Nguyen, and Q. P. Ha, "Stability of complex systems with mixed connection configurations under shared control," *Int. Conf. Control. Autom. Robot. Vis.*, pp. 512–517, 2010.

[149] M. R. Barnes, "Form finding and analysis of tension structures by dynamic relaxation," *Int. J. Sp. Struct.*, vol. 14, no. 2, pp. 89–104, 1999.

[150] J. Van de Wijdeven and B. De Jager, "Shape change of tensegrity structures: Design and control," *Am. Control Conf.*, pp. 2522–2527, 2005.

[151] C. Sultan and R. Skelton, "Deployment of tensegrity structures," *Int. J. Solids Struct.*, vol. 40, no. 18, pp. 4637–4657, 2003.

[152] J.-P. Pinaud, M. Masic, and R. E. Skelton, "Path planning for the deployment of tensegrity structures," *Smart Struct. Mater. Model. Signal Process. Control*, vol. 5049, pp. 436–447, 2003.

[153] J.-P. Pinaud, S. Solari, and R. E. Skelton, "Deployment of a class 2 tensegrity boom," *Smart Struct. Mater. Smart Struct. Integr. Syst.*, vol. 5390, pp. 155–162, 2004.

[154] A. S. Wroldsen, M. C. De Oliveira, and R. E. Skelton, "Modelling and control of non-minimal non-linear realisations of tensegrity systems," *Int. J. Control*, vol. 82, no. 3, pp. 389–407, 2009.

[155] N. Kanchansaratool, "Control of flexible structures," PhD thesis, The Australian National University, Canberra, Australia, 2003.

[156] J. B. Aldrich, R. E. Skelton, and K. Kreutz-Delgado, "Control synthesis for a class of light and agile robotic tensegrity structures," *Am. Control Conf.*, pp. 5245–5251, 2003.

[157] J. Friesen, A. Pogue, T. Bewley, M. D. Oliveira, R. Skelton, and V. Sunspiral, "DuCTT : A tensegrity robot for exploring duct systems," *Int. Conf. Robot. Autom.*, pp. 4222–4228, 2014.

[158] K. Caluwaerts, J. Despraz, A. Işçen, A. P. Sabelhaus, J. Bruce, B. Schrauwen, and V. SunSpiral, "Design and control of compliant tensegrity robots through simulation and hardware validation," *J. R. Soc. Interface*, vol. 11, no. 98, 2014.

[159] Q. Yang, M. Cao, H. Fang, and J. Chen, "Constructing universally rigid tensegrity frameworks with application in multi-agent formation control," *IEEE Trans. Automat. Contr.*, vol. 64, no. 1, pp. 381 –388, 2019.

[160] P. T. Boggs and J. W. Tolle, "Sequential quadratic programming," *Acta Numer.*, vol. 4, pp. 1–51, 1995.

[161] H. Schwetlick, Y. Tilleb, and W. Schellong, "Gauss-Newton-like methods for nonlinear least squares with equality constraints - Local convergence and applications," *Statistics*, vol. 16, no. 2, pp. 167–178, 1985.

[162] A. Wächter and L. T. Biegler, "On the implementation of an interior-point filter line-search algorithm for large-scale nonlinear programming," *Math. Program.*, vol. 106, no. 1, pp. 25–57, 2006.

[163] R. Connelly and S. D. Guest, "Frameworks, tensegrities and symmetry: Understanding stable structures," 2015.

[164] S. J. Wright and M. J. Tenny, "A feasible trust-region sequential quadratic programming algorithm," *SIAM J. Optim.*, vol. 14, no. 4, pp. 1074–1105, 2004.

[165] E. J. Candes, M. B. Wakin, and S. P. Boyd, "Enhancing sparsity by reweighted l_1 minimization," *J. Fourier Anal. Appl.*, vol. 14, no. 5, pp. 877–905, 2008.

[166] X. Wu and M. R. Jovanović, "Sparsity-promoting optimal control of systems with symmetries, consensus and synchronization networks," *Syst. Control Lett.*, vol. 103, pp. 1–8, 2017.

[167] M. S. Asif and J. Romberg, "Fast and accurate algorithms for re-weighted l_1-norm minimization," *IEEE Trans. Signal Process.*, vol. 61, no. 23, pp. 5905–5916, 2013.

[168] S. Guillaume, C. Muller, and P. H. Cattin, *TRINET+, logiciel de compensation 3D version 6.1, Mode d'emploi, HEIG-VD*, Yverdon, Switzerland, 2008.

[169] S. Guillaume, B. Bürki, S. Griffet, and H. Mainand Durand, "QDaedalus: Augmentation of total stations by CCD sensor for automated contactless high-precision metrology," in *FIG Work. Week*, 2012, pp. 6–10.

[170] S. Guillaume, J. Clerc, J. Ray, and M. Kistler, "Contribution of the image-assisted theodolite system QDaedalus to geodetic static and dynamic deformation monitoring," *Jt. Int. Symp. Deform. Monit.*, pp. 66–74, 2016.

[171] B. Bürki, S. Guillaume, P. Sorber, and H. P. Oesch, "DAEDALUS: A versatile usable digital clip-on measuring system for total stations," *Int. Conf. Indoor Position. Indoor Navig.*, pp. 1–10, 2010.

[172] Y. R. Stürz, A. Iannelli, and R. S. Smith, "Robust control of an architectural cable net geometry," in *IFAC World Congr.*, [to appear], 2020.

[173] S. Schleicher, A. Rastetter, R. La Magna, A. Schönbrunner, N. Haberbosch, and J. Knippers, "Form-finding and design potentials of bending-active plate structures," in *Modelling Behaviour: Design Modelling Symposium*, M. R. Thomsen, M. Tamke, C. Gengnagel, B. Faircloth, and F. Scheurer, Eds. Springer International Publishing, 2015, pp. 53–63.

[174] Y. R. Stürz, M. Khosravi, and R. S. Smith, "Parameter identification for digital fabrication: A Gaussian process learning approach," in *IFAC World Congr.*, [to appear], 2020.